DTIC FILE COPY

SECURITY CLASSIFICATION OF THIS PAGE

REPORT DOCUMENTATION PAGE

Form Approved OMB No. 0704-0188

1a. REPORT SECURITY CLASSIFICATION UNCLASSIFIED	1b. RESTRICTIVE MARKINGS NONE
2a. SI[illegible] CLASSIFICATION AUTHORITY	3. DISTRIBUTION/AVAILABILITY OF REPORT APPROVED FOR PUBLIC RELEASE; DISTRIBUTION UNLIMITED.
2b. D	
4. PE AD-A217 953	5. MONITORING ORGANIZATION REPORT NUMBER(S) AFIT/CI/CIA- 89-099
6a. NAME OF PERFORMING ORGANIZATION AFIT STUDENT AT TX A&M Univ	6b. OFFICE SYMBOL (If applicable)
	7a. NAME OF MONITORING ORGANIZATION AFIT/CIA
6c. ADDRESS (City, State, and ZIP Code)	7b. ADDRESS (City, State, and ZIP Code) Wright-Patterson AFB OH 45433-6583
8a. NAME OF FUNDING/SPONSORING ORGANIZATION	8b. OFFICE SYMBOL (If applicable)
	9. PROCUREMENT INSTRUMENT IDENTIFICATION NUMBER
8c. ADDRESS (City, State, and ZIP Code)	10. SOURCE OF FUNDING NUMBERS

PROGRAM ELEMENT NO.	PROJECT NO.	TASK NO.	WORK UNIT ACCESSION NO.

11. TITLE (Include Security Classification) (UNCLASSIFIED)
ELECTTONIC PROPERTIES OF HIGH-TEMPERATURE SUPERCONDUCTORS

12. PERSONAL AUTHOR(S)
BRENT ARMAND RICHERT

13a. TYPE OF REPORT	13b. TIME COVERED	14. DATE OF REPORT (Year, Month, Day)	15. PAGE COUNT
THESIS/DISSERTATION	FROM _____ TO _____	1989	180

16. SUPPLEMENTARY NOTATION
APPROVED FOR PUBLIC RELEASE IAW AFR 190-1
ERNEST A. HAYGOOD, 1st Lt, USAF
Executive Officer, Civilian Institution Programs

17. COSATI CODES			18. SUBJECT TERMS (Continue on reverse if necessary and identify by block number)
FIELD	GROUP	SUB-GROUP	

19. ABSTRACT (Continue on reverse if necessary and identify by block number)

90 02 12 005

20. DISTRIBUTION/AVAILABILITY OF ABSTRACT	21. ABSTRACT SECURITY CLASSIFICATION
☒ UNCLASSIFIED/UNLIMITED ☐ SAME AS RPT. ☐ DTIC USERS	UNCLASSIFIED

22a. NAME OF RESPONSIBLE INDIVIDUAL	22b. TELEPHONE (Include Area Code)	22c. OFFICE SYMBOL
ERNEST A. HAYGOOD, 1st Lt, USAF	(513) 255-2259	AFIT/CI

DD Form 1473, JUN 86 — Previous editions are obsolete. — SECURITY CLASSIFICATION OF THIS PAGE

AFIT/CI "OVERPRINT"

ELECTRONIC PROPERTIES OF HIGH-TEMPERATURE SUPERCONDUCTORS

A Dissertation

by

BRENT ARMAND RICHERT

Submitted to the Office of Graduate Studies of
Texas A&M University
in partial fulfillment of the requirements for the degree of

DOCTOR OF PHILOSOPHY

August 1989

Major Subject: Physics

ELECTRONIC PROPERTIES OF HIGH-TEMPERATURE SUPERCONDUCTORS

A Dissertation

by

BRENT ARMAND RICHERT

Approved as to style and content by:

Roland E. Allen
(Chair of Committee)

Donald G. Naugle
(Member)

Marko V. Jarić
(Member)

Michael B. Hall
(Member)

Richard L. Arnowitt
(Head of Department)

August 1989

ABSTRACT

Electronic Properties of High-Temperature Superconductors. (August 1989)

Brent Armand Richert, B.S., U. S. Air Force Academy;

M.S., University of New Mexico

Chair of Advisory Committee: Dr. Roland E. Allen

We have developed a semiempirical tight-binding model for the electronic energy bands, the local and total densities of states, and the atomic valences in the high-temperature superconductors $La_{1.85}Sr_{0.15}CuO_4$, $YBa_2Cu_3O_7$, $Bi_2Sr_2CuO_6$, $Bi_2CaSr_2Cu_2O_8$, $Tl_2Ba_2CuO_6$, $Tl_2CaBa_2Cu_2O_8$, $Tl_2Ca_2Ba_2Cu_3O_{10}$, $TlCa_3Ba_2Cu_4O_{11}$, $BaPb_{0.75}Bi_{0.25}O_3$, and $Ba_{0.6}K_{0.4}BiO_3$. A single tight-binding model, with fully transferable parameters, provides a good description of the electronic structures of all these materials.

Calculations of the changes in electronic properties associated with atomic substitutions in $YBa_2Cu_3O_7$, $Bi_2CaSr_2Cu_2O_8$, and $Tl_2CaBa_2Cu_2O_8$ give results in agreement with expected chemical trends and consistent with observed changes in the superconducting properties. For example, substitution of Pb for Bi in $Bi_2CaSr_2Cu_2O_8$ increases the concentration of hole carriers within the CuO_2 planes. Similarly, doping with Hg or Pb in $Tl_2CaBa_2Cu_2O_8$ also affects the carrier concentration, with Hg creating holes and Pb destroying them.

Oxygen vacancies in both $La_{1.85}Sr_{0.15}CuO_{4-y}$ and $YBa_2Cu_3O_{7-y}$ act as electron donors. This is consistent with the observations that oxygen vacancies degrade the superconductivity and metallic conductivity in these materials. Lanthanum vacancies in $La_{2-x}CuO_4$ donate holes, giving the same electronic effect

as doping with divalent metal atoms or excess oxygen in initially stoichiometric La_2CuO_4.

We propose a specific excitonic mechanism for high-temperature superconductivity, which requires insulating metal-oxide layers adjacent to the superconducting planes. The attractive pairing interaction between carriers is mediated by two-dimensional excitons in the insulating region. No specific magnetic properties in the metallic region are needed for this mechanism, which is applicable to all currently-known high-T_c materials. Reasonable estimates of the physical parameters lead to a pairing interaction that is sufficient to give high-T_c superconductivity. The theory predicts a metal-oxide (e.g., BaO) exciton that may be observable. In addition, the theory predicts that high-temperature superconductivity will not be found in materials such as $Ca_{1-x}K_xCuO_2$ or $Ca_{1-x}Y_xCuO_2$, since these materials lack the insulating metal-oxide layers necessary to support the excitons.

To Silvia

ACKNOWLEDGMENTS

I would like to express my sincere appreciation and thanks to Dr. Roland Allen. His guidance and knowledge provided direction to this work. I also acknowledge the support of many faculty and fellow students, including Dr. Roger Smith, Dr. Donald Naugle, Dr. Marko Jarić, and Dr. Greg Rose. I acknowledge support from the U. S. Air Force, the Office of Naval Research, and the Robert A. Welch Foundation. Finally, I thank my wife Silvia, who provided constant encouragement and love.

TABLE OF CONTENTS

TABLE OF CONTENTS (Continued)

LIST OF TABLES

LIST OF FIGURES

LIST OF FIGURES (Continued)

LIST OF FIGURES (Continued)

CHAPTER I

INTRODUCTION

The discovery of high-temperature superconductivity by Bednorz and Müller[1] has been followed by an intense search for new materials, and an equally intense investigation of their structural and electronic properties. Numerous systems have been discovered, with a current record superconducting transition temperature, T_c, of 125 K. The discovery of high-temperature superconductors without copper, principally $Ba_{1-x}K_xBiO_3$ with $T_c \approx 34$ K, has placed stringent constraints on the development of a comprehensive theory for high-temperature superconductivity. As described in the following chapters, we have addressed four theoretical problems: (1) the basic electronic structure of high-T_c superconductors; (2) the effects of atomic substitutions; (3) the effects of atomic vacancies; and (4) the mechanism of high-temperature superconductivity.

Chapter II provides an overview of the literature detailing the experimental discoveries and characterizations of high-temperature superconductors. We attempt to give proper credit for original discoveries, but much of the literature includes concurrent research and confirmatory results which are also important. Emphasis is placed on those experiments that are directly related to our own research, but results that are needed to appreciate the complexity of these materials are also included.

Chapter III describes the development of a semiempirical tight-binding model which has been used to calculate electronic energy bands, local and total densities of states, and atomic valences. We find that a single model,

---

The journal model used is *Physical Review B*.

with fully transferable parameters, provides a good description of the electronic structure of every material examined, in the sense that results in the local-density approximation are satisfactorily reproduced.

The results of electronic structure calculations based on this model are presented in Chapter IV. The copper-oxide superconductors $La_{1.85}Sr_{0.15}CuO_4$, $YBa_2Cu_3O_7$, $Bi_2Sr_2CuO_6$, $Bi_2CaSr_2Cu_2O_8$, $Tl_2Ba_2CuO_6$, $Tl_2CaBa_2Cu_2O_8$, $Tl_2Ca_2Ba_2Cu_3O_{10}$, and $TlCa_3Ba_2Cu_4O_{11}$, and the bismuth-oxide superconductors $BaPb_{0.75}Bi_{0.25}O_3$ and $Ba_{0.6}K_{0.4}BiO_3$, have been examined. Although these materials have very different crystal and magnetic structures, common features in the electronic structures provide strong clues regarding the mechanism of superconductivity.

We present in Chapter V a study of atomic substitutions in $YBa_2Cu_3O_7$, $Bi_2CaSr_2Cu_2O_8$, and $Tl_2CaBa_2Cu_2O_8$, to determine the modifications in the electronic structure. Substitutions on the Ba, Cu, and O sites were considered for the case of $YBa_2Cu_3O_7$. In the remaining materials, we studied doping on the Bi or Tl site. The results are compared with the experimentally-observed changes in the superconductivity of these materials.

A critically important factor in these superconductors is the oxygen content. Calculations of the electronic effects of oxygen vacancies in $La_{1.85}Sr_{0.15}CuO_{4-y}$ and $YBa_2Cu_3O_{7-y}$ are reported in Chapter VI. The modification of the density of states and the shift in the Fermi energy were calculated for $0 < y < 1.0$. The effect of lanthanum vacancies in undoped La_2CuO_4 is also presented.

The most important theoretical question is the specific mechanism of high-T_c superconductivity. In Chapter VII we propose a mechanism that involves two-dimensional excitons in the insulating metal-oxide layers (e.g., LaO, BaO,

or SrO) adjacent to the superconducting layers (e.g., CuO_2 or BiO_2). This mechanism requires no specific magnetic properties for the conduction region, and is applicable to all currently-known high-temperature superconductors. We have calculated matrix elements for the interaction between charge carriers and the metal-oxide excitons, and have estimated the attractive interaction leading to superconductivity.

CHAPTER II

REVIEW OF EXPERIMENTS

Stoichiometry and Crystal Structure

The discovery of superconductivity in the La–Ba–Cu–O system by Bednorz and Müller[1] in 1986 initiated an explosion of research activity in high-temperature superconductivity. Their polycrystalline samples, of nominal composition $Ba_xLa_{5-x}Cu_5O_{15-y}$, indicated an onset of superconductivity at $T_c \approx 30$ K in resistivity measurements.[1] The superconducting phase with $T_c = 35$ K was identified as the solid solution $La_{2-x}Ba_xCuO_4$, $x \approx 0.15$, which has the tetragonal K_2NiF_4 structure at room temperature.[2] This oxygen-defect perovskite is characterized by CuO_2 planes surrounded by layers of LaO, giving two formula units per bct cell. The transition temperature was optimized by replacing Ba with Sr, giving $T_c = 38$ K for $La_{1.85}Sr_{0.15}CuO_4$.[3,4] Neutron diffraction studies of this phase indicate a transition to an orthorhombic crystal structure below 200 K, associated with a buckling of the CuO_2 planes and a doubling of the unit cell.[5] The corner-sharing, tilted CuO_6 octahedra have an in-plane copper-oxygen bond length of 1.89 Å and an out-of-plane bond length of 2.41 Å.[5]

Stoichiometry has been found to play a critical role in several different respects. The superconducting properties are highly sensitive to the oxygen content, with the highest T_c resulting from full oxygen occupancy.[3,4] Excess Sr doping with $x > 0.15$ apparently leads to charge compensation through the formation of oxygen vacancies, with a depression of T_c.[3,6,7] Annealing under high oxygen pressure suppresses the formation of oxygen vacancies, and allows superconductivity at $T_c \approx 36$ K in $La_{2-x}Sr_xCuO_4$ up to $x = 0.24$.[8] However,

the transition temperature decreases for $x > 0.24$, with no superconductivity observed beyond $x = 0.32$, although metallic conductivity persists.[8]

The undoped material La_2CuO_4 has an orthorhombic structure at room temperature,[9] with a possible monoclinic distortion reported below 10 K.[10] This parent compound exhibits superconductivity of a filamentary nature. The small volume fraction (much less than 1%) of superconducting region was attributed to either excess oxygen or lanthanum vacancies within the material.[11] The lanthanum-deficient material $La_{2-x}CuO_4$ shows a sharper resistive transition and a greater diamagnetic susceptibility than the nominal La_2CuO_4 superconductor,[12] indicating that La vacancies can indeed contribute to the superconductivity.

The discovery of superconductivity in the Y–Ba–Cu–O system[13] with a T_c of 93 K surpassed the previous theoretical limits on T_c and broke the temperature barrier of 77 K, the boiling point of liquid nitrogen. The superconducting phase was rapidly isolated[14–16] as $YBa_2Cu_3O_7$, often called the 1:2:3 phase to refer to the metal stoichiometry. This material has an orthorhombic crystal structure ($a = 3.856$ Å, $b = 3.870$ Å, and $c = 11.666$ Å) characterized by double layers of CuO_2, separated by Y ions and surrounded by BaO layers, stacked with one-dimensional chains of CuO.[17–21] The chains form a linear coordination of copper and oxygen atoms along the b axis of the crystal, with a bond length of 1.93 Å.[18] The CuO_2 layers are distorted from perfect planes by displacements of the oxygen atoms along the c axis toward the Y ion.[17] The plane copper sites are five-coordinated with oxygen, with an average in-plane interatomic distance of 1.95 Å and an out-of-plane distance of 2.38 Å.[18] These bond lengths are comparable to the Cu–O distances in $La_{1.85}Sr_{0.15}CuO_4$. The small difference in

the a and b lattice parameters allows the formation of twin boundaries along the [110] direction in the orthorhombic phase.[22]

A high-temperature orthorhombic-to-tetragonal phase transition near 700 °C in $YBa_2Cu_3O_7$ is found to be an order-disorder transition in which the oxygen atoms in the CuO chains are disordered onto the normally vacant adjacent sites.[23] Oxygen is lost from $YBa_2Cu_3O_7$ under ambient atmosphere at temperatures over 400 °C, and the orthorhombic-to-tetragonal transition occurs near an oxygen content of 6.5.[23] The decrease in oxygen stoichiometry introduces vacancies on the oxygen chain sites.[24] Other structural effects are also associated with oxygen vacancies, such as an increase in the c lattice parameter and an increase in the Cu–O out-of-plane interatomic distance with decreasing oxygen content.[25]

Oxygen vacancies in $YBa_2Cu_3O_{7-y}$ have a dramatic effect on the superconductivity. The oxygen vacancies lead to a depression of T_c from above 90 K to about 55 K for $0.1 \leq y \leq 0.5$, and a loss of the superconductivity and even metallic conductivity for $y > 0.5$.[26,27] The plateau in T_c near 55 K for $0.3 \leq y \leq 0.5$ is associated with a long-range ordering of the oxygen vacancy sites along the b axis, parallel to the chains, and a short correlation length along the a axis.[28,29] Speculation on the importance of the integrity of the CuO chains for high-temperature superconductivity centered on such issues as one-dimensional superconductivity along the chains,[30] oxygen-defect enhancement of pairing for superconductivity,[31] and coupling between the CuO_2 planes and CuO chains.[23,25] However, further experiments have indicated that the one-dimensional nature of the CuO chains is unimportant for high-temperature superconductivity. Experiments with the systems $YBa_{2-x}La_xCu_3O_{7-y}$ and

$Y_{1-x}Ca_xBa_2Cu_3O_{7-y}$ demonstrate that the transition temperature may be varied *without* changing the oxygen content.[32,33] The T_c is correlated with the carrier density within the CuO_2 planes, while charges associated with the CuO chains are localized and do not contribute to superconductivity.[32] In particular, the material $Y_{0.85}Ca_{0.15}Ba_2Cu_3O_6$ is superconducting with $T_c = 50$ K, but has a tetragonal structure and complete oxygen vacancies in the chain region.[34] The oxygen in the chains thus serves primarily as an electron reservoir for the rest of the structure.[35] In the same manner that a saturation and decrease in T_c is seen in $La_{2-x}Sr_xCuO_4$ for $x > 0.24$,[8] doping with Ca in $Y_{1-x}Ca_xBa_2Cu_3O_7$ leads to a depression of T_c from 93 K to $\approx$ 80 K as the carrier concentration increases.[34]

A second superconducting phase in the Y–Ba–Cu–O system was first observed as a defect structure in $YBa_2Cu_3O_7$ that increased the c axis from 11.7 Å to 13.6 Å.[36,37] This phase, with $T_c = 81$ K, was isolated in thin film samples[38,39] as $YBa_2Cu_4O_8$, with an orthorhombic unit cell and a doubled c axis of 27.2 Å. The structure includes two CuO chains, linked together in an edge-sharing, square-planar CuO_4 coordination.[40] The remaining structure is unchanged from that of $YBa_2Cu_3O_7$. Intergrowths of single-chain $YBa_2Cu_3O_7$ and double-chain $YBa_2Cu_4O_8$ can also form, resulting in a $Y_2Ba_4Cu_7O_{15}$ phase.[41]

Bulk samples of $YBa_2Cu_4O_8$ have been formed,[41,42] along with a series of samples with rare earths replacing Y.[42] These samples all exhibit high-temperature superconductivity with T_c ranging from 57 to 81 K. The oxygen stoichiometry of this phase is relatively constant compared to the $YBa_2Cu_3O_7$ phase, perhaps because of the additional copper coordination of the oxygens in the double chains.[40–42] The oxygen content is thermally stable up to a

temperature of 850 °C, beyond which the structure decomposes.[41] Thus, it is difficult to study the variation of T_c with oxygen content in $YBa_2Cu_4O_8$.

The next series of discoveries raised the record transition temperature for the copper-oxide superconductors to over 100 K. Michel *et al.*[43] reported that partial substitution of bismuth on the La/Sr site in $La_{2-x}Bi_zSr_{x-z}CuO_4$ increased the transition temperature T_c from 38 K to 42 K. They also reported[44] a new family of superconductors in the Bi–Sr–Cu–O system with T_c from 7 to 22 K. The absence of rare earth elements distinguished this system from the other cuprate superconductors. The superconducting phase was tentatively identified as $Bi_2Sr_2Cu_2O_{7-y}$, with a substructure of Bi_2O_2 units stacked with the copper-oxide perovskite substructures.[44] The discovery of superconductivity with onset T_c's up to 114 K in the Bi–Ca–Sr–Cu–O system[45,46] extended this system into true high-temperature superconductivity.

The phase with T_c = 85 K was identified[47,48] as $Bi_2CaSr_2Cu_2O_8$. Intergrowths of a higher-T_c phase gave magnetic and resistive onset temperatures above 110 K, but the resistance of the mixed-phase sample did not go to zero above 85 K. The 85 K phase was found to have a layered structure.[48–52] There are two CuO_2 planes, separated by a Ca ion and surrounded by SrO layers. This substructure is then layered with two BiO planes, giving the stacking sequence BiO–SrO–CuO_2–Ca–CuO_2–SrO–BiO along the c axis. A solid solution for Sr and Ca allows mutual substitution on these sites, with T_c optimized for the indicated stoichiometry.[47–50] The crystal structure is pseudotetragonal,[49] with a = 3.81 Å and c = 30.52 Å, but with a long-range incommensurate modulation of approximately $5\sqrt{2}$ cells ($\approx$ 27 Å) along the [110] direction.[48–50] Instead of the twinning observed in $YBa_2Cu_3O_7$, 90° twist boundaries are observed as

stacking faults perpendicular to the c axis.[53,54] The relatively large separation ($\approx$ 3.3 Å) between the BiO double layers gives a micaceous nature to the bulk material.[48,49]

The incommensurate structural modulation is associated with disorder within the BiO layers,[48–52,54] although additional disorder is observed in the SrO and CuO_2 layers.[55] Electron microscope[51,56] and scanning tunneling microscope[57] images detail the Bi atom superstructure, giving some support to a structural model that requires a vacant Bi site every nine or ten unit cells to fit the modulation.[55,57] However, a model for excess oxygen atoms within the BiO bilayer can account for the superstructure[58] and the excess oxygen stoichiometry (measured by thermogravimetric analysis as 8.25 per formula unit[49]). This model compares $Bi_2CaSr_2Cu_2O_8$ with the isostructural material $Bi_2Sr_3Fe_2O_9$, which has a *commensurate* modulation. This isostructural compound accommodates an extra oxygen every ten cells to stabilize the strained BiO bilayer. In $Bi_2CaSr_2Cu_2O_8$, one extra oxygen for every 9.52 bismuth atoms only approximately fits the copper-oxygen sublattice, leading to the incommensurate distortion.[58]

$Bi_2CaSr_2Cu_2O_8$ is relatively insensitive to oxygen loss compared to $YBa_2Cu_3O_7$. Heating in argon leads to an oxygen loss of 0.1 per formula unit, but superconductivity persists.[49] Annealing in oxygen leads to a slight excess in the oxygen stoichiometry,[49] perhaps associated with the incommensurate modulation.[58]

The T_c = 114 K phase proved to be difficult to isolate. Although clear resistive and magnetic onsets of superconductivity are observed near 114 K, a zero-resistance state above 100 K could not initially be found. The finite

resistance was attributed to incomplete grain connectivity for the higher-T_c phase, which grew in thin shells around the 85 K phase.[59] Annealing the samples in oxygen at 885 °C for several days enhanced the Meissner effect of the higher-T_c phase,[59] and produced zero resistance at 107 K. Addition of Pb to this material also allowed zero resistance up to 107 K.[50,60,61] Pb substitutes for Bi and stabilizes the higher-T_c structure.[50,61,62]

$Bi_2Ca_2Sr_2Cu_3O_{10}$ was identified as the 114 K superconductor.[63,64] The structure of this phase is the same as for $Bi_2CaSr_2Cu_2O_8$, but with an additional $CaCuO_2$ slab, giving a c axis of 37.1 Å and a stacking sequence of BiO–SrO–CuO_2–Ca–CuO_2–Ca–CuO_2–SrO–BiO.[64] Stacking faults in this phase occur by intergrowths of the 85 K phase, which have double rather than triple CuO_2 layers. These intergrowths have prevented a definitive determination of the atomic substructure and possible incommensurate modulation in $Bi_2Ca_2Sr_2Cu_3O_{10}$. However, disorder in the BiO layers is expected to occur in this phase.[64]

A third phase $Bi_2Sr_2CuO_6$ has a T_c of only 6 K.[64–66] This phase is similar to that proposed by Michel *et al.*[44] The bct structure with a = 3.81 Å and c = 24.61 Å has a single CuO_2 plane per unit cell,[65] similar to $La_{2-x}Sr_xCuO_4$. The plane is sandwiched by SrO layers and stacked with double BiO layers to give the c axis ordering BiO–SrO–CuO_2–SrO–BiO. The CuO_6 octahedra are tilted as in $La_{2-x}Sr_xCuO_4$, distorting the copper-oxide region from a perfect plane.[66] A small orthorhombic or monoclinic distortion is observed along with 90° twist boundaries about [001].[66] An incommensurate superstructure is found in $Bi_2Sr_2CuO_6$, which is again related to disorder in the BiO layers.[64,66] Vacancies on the Sr site have been observed,[65] which may account for some variations in T_c reported for this phase.[64–66]

Another set of copper-oxide materials containing Tl has yielded the highest T_c's. Superconductivity in the Tl–Ba–Cu–O system was seen above 80 K.[67] The phase with T_c = 83 K was identified as $Tl_2Ba_2CuO_6$, and is structurally very similar to $Bi_2Sr_2CuO_6$, although the CuO_2 layers are planar.[66] The addition of Ca to this system increases T_c over 110 K.[68,69] The structure of the phase $Tl_2CaBa_2Cu_2O_8$ (with T_c = 112 K) is similar to that of $Bi_2CaSr_2Cu_2O_8$, but with no evidence of a long-range modulation.[70,71] The phase $Tl_2Ca_2Ba_2Cu_3O_{10}$ has T_c = 125 K, and has a triple layer of CuO_2 planes.[71–73]

All these materials are body-centered tetragonal and have one, two, or three layers of CuO_2 planes separated by Ca ions, sandwiched by BaO layers, and stacked with double TlO layers.[66,70–73] The TlO layers are separated by $\approx$ 2.0 Å, significantly smaller than the distance between the BiO planes in the analogous bismuth cuprates, so that the Tl materials are more plate-like than micaceous.[66,70–72] For $Tl_2CaBa_2Cu_2O_8$ and $Tl_2Ca_2Ba_2Cu_3O_{10}$, the copper-oxygen planes are separated by $\approx$ 3.2 Å, similar to the multiple-layer Bi cuprates.[70–73] A solid solution for Tl and Ca has been observed for these materials.[66,70,72] Although there is displacement of the Tl and O atoms from their ideal positions, no long-range modulation occurs in these phases.[66,70–73] Short-range correlations (less than 5 Å) in the thallium and oxygen disorder have been observed in neutron diffraction data.[74,75]

Another series of phases in the Tl–Ca–Ba–Cu–O system has only a single TlO layer per unit cell. The stoichiometries $TlCaBa_2Cu_2O_7$ (with T_c = 85 K) and $TlCa_2Ba_2Cu_3O_9$ (with T_c = 110 K) have a primitive tetragonal structure with double or triple CuO_2 layers stacked with a TlO monolayer.[76,77] The single-layer CuO_2 phase $TlBa_2CuO_5$ does not exhibit superconductivity.[76] The phase

$TlCa_3Ba_2Cu_4O_{11}$ was discovered to contain four consecutive CuO_2 layers[78,79] and has $T_c = 122$ K.

Under certain fabrication conditions, all of the Tl phases are observed to have intergrowths of different numbers of CuO_2 layers and either double or single TlO layers, resulting in a change in the transition temperature compared with the pure phase.[80] The materials with TlO monolayers generally have increased T_c's with an increase of intergrowths, while the TlO bilayer systems have lower T_c's with more intergrowths.

The increase in T_c with additional copper-oxide layers observed for the Bi and Tl cuprates led to speculation that even higher T_c's could be found by increasing the number of adjacent CuO_2 layers. However, the discovery of $Tl_2Ca_3Ba_2Cu_4O_{12}$ (with $T_c = 119$ K) and $TlCa_4Ba_2Cu_5O_{13}$ (with $T_c = 110$ K) shows a breakdown of the simple increase in T_c with the number of copper-oxide planes.[78,81] Instead, a saturation (and decrease) in T_c is seen for additional layers of CuO_2. Also, the material $Ca_{0.86}Sr_{0.14}CuO_2$ has been synthesized.[82] This tetragonal structure is the limit of a very large number of adjacent CuO_2 planes. However, the material is semiconducting, even when doped with alkali metals such as Na or K, or with trivalent elements such as Y or La, so that T_c is not simply dependent on adjacent copper-oxide planes.[82]

A series of high-temperature superconductors was discovered in the system $Pb_2ASr_2Cu_3O_8$, where A = Y, La, Pr, Nd, Sm, Eu, Gd, Dy, Ho, Tm, Yb, or Lu.[83] Doping with Ca or excess Sr induces superconductivity in these materials. In particular, the phase $Pb_2Y_{0.5}Ca_{0.5}Sr_2Cu_3O_8$ has $Tc = 68$ K. The orthorhombic structure consists of double CuO_2 planes separated by the Ca or rare earth element, as in $YBa_2Cu_3O_7$. The copper perovskite structure

is sandwiched by SrO layers, then stacked with a PbO–Cu–PbO structure. The copper layer separating the PbO planes is completely deficient in oxygen, but changes in the oxygen stoichiometry are accommodated by inserting oxygen in this layer.[83] However, the oxidation of this copper layer is not necessary in order for superconductivity to exist. The double CuO_2 planes are separated by ≈ 3.5 Å, somewhat larger than the 3.2 Å typically found in the Bi and Tl cuprates. A superconducting phase with the rare earth Tb has also been formed in this system.[84]

The copper-oxide superconductors containing Bi, Tl, and Pb all have layers of CuO_2 stacked with metal-oxide layers. There are no one-dimensional CuO chains in any of these materials, structurally distinguishing them from $YBa_2Cu_3O_7$.[17] The existance of high-temperature superconductivity without the chains indicates that this one-dimensional CuO structure is not necessary. However, the common feature of CuO_2 planes within these layered materials is thought to play a major role in the specific mechanism of superconductivity.

The newest set of cuprate superconductors is closely related to the La_2CuO_4 system. The rare earth cuprates R_2CuO_4 with R = Pr, Nd, Sm, Eu, or Gd have a structure very similar to La_2CuO_4, but with the out-of-plane oxygens rotated 45° to face-centered positions. These materials are not metallic or superconducting, even with substitution of divalent Sr on the rare earth site.[85] However, partial substitution of Ce (with a formal valence of four) in $R_{2-x}Ce_xCuO_{4-y}$ (R = Pr, Nd, or Sm) dopes the system with electrons and allows superconductivity over 24 K.[86] In particular, the stoichiometry $Nd_{1.85}Ce_{0.15}CuO_4$ has $T_c = 30$ K, is strictly tetragonal, and has undistorted CuO_2 planes.[87] Annealing under a reducing atmosphere to introduce oxygen vacancies ($y \approx 0.07$) enhances the

formation of a bulk superconductor in this phase.[86]

Prior to the discovery of superconductivity in the La–Ba–Cu–O system, the highest transition temperature in an oxide superconductor was 13 K for $BaPb_{1-y}Bi_yO_3$ at $y = 0.25$.[88] This material was studied extensively after its discovery in 1975, particularly since its transition temperature was unusually high compared with other oxide materials of that time period. The superconductivity persists in $BaPb_{1-y}Bi_yO_3$ from 9 to 13 K for the solid solution range $0.05 \leq y \leq 0.30$.[88] The end member $BaPbO_3$ is metallic,[89] while $BaBiO_3$ is semiconducting.[88] All these materials have the basic cubic perovskite structure, but with distortions that change the symmetry of the unit cell:[90] $BaPbO_3$ is orthorhombic, $BaPb_{0.75}Bi_{0.25}O_3$ is tetragonal, and $BaBiO_3$ is monoclinic. The transition from semiconductor to superconductor to metal with Pb doping in $BaPb_{1-y}Bi_yO_3$ somewhat parallels the behavior of Sr-doped $La_{2-x}Sr_xCuO_4$.[8]

Initial attempts to increase the transition temperature of $BaPb_{1-y}Bi_yO_3$ by addition of alkali metals such as Na or K were unsuccessful, but sharper transitions were seen for these materials.[88,91] However, high-temperature superconductivity with T_c up to 22 K was found in the $Ba_{1-x}(K,Rb)_xBiO_3$ system.[92] The single phase $Ba_{0.6}K_{0.4}BiO_3$ has $T_c = 30$ K,[93,94] and with annealing can exhibit $T_c = 34$ K.[95] This material is strictly cubic[93,94,96] with $a = 4.29$ Å. No ordering of Ba and K is observed in the superconducting phase,[96] and the structure remains cubic in the temperature range 14 – 300 K.[97]

The similarity in structure and composition of $BaPb_{0.75}Bi_{0.25}O_3$ and $Ba_{0.6}K_{0.4}BiO_3$ suggests that these materials should share the same properties of superconductivity. In addition, the maximum T_c in these copper-free materials is at least comparable to that of the copper oxides (particularly $La_{2-x}Sr_xCuO_4$),

indicating that the specific properties of copper and its d electrons are not required for high-temperature superconductivity.

In summary, Table 2.1 lists the stoichiometry, superconducting transition temperature, and layered structure of the high-temperature superconductors. The diversity of these systems is remarkable, yet many similarities are seen in the physical properties. This places strong constraints on theoretical models that must describe all of these systems.

Superconductivity and Transport Properties

The characterization of the high-temperature superconductors revealed many similarities among the superconducting and normal state properties of these materials, along with several distinct differences. Some of the results are consistent with the standard Bardeen, Cooper, and Schrieffer (BCS) theory of superconductivity,[98] but with notable exceptions. The superconducting T_c of the bulk materials was found to increase slightly with pressure for the materials $La_{2-x}(Ba,Sr)_xCuO_4$,[99] $YBa_2Cu_3O_7$,[100] $Bi_2CaSr_2Cu_2O_8$,[46] and $Tl_2CaBa_2Cu_2O_8$,[69] while $BaPb_{1-y}Bi_yO_3$ has a negative pressure effect.[91] Hall coefficient measurements in the normal state indicate p-type conductivity (so that the charge carriers are holes) in $La_{2-x}Sr_xCuO_4$,[101,102] $YBa_2Cu_3O_7$,[103] $Bi_2CaSr_2Cu_2O_8$,[104] and $Tl_2Ca_2Ba_2Cu_3O_{10}$.[105] The Hall "constant" $R_H = -1/nec$ actually varies with temperature (roughly as T^{-1}) in these materials.[101-105] The bismuth-oxide superconductors $BaPb_{1-y}Bi_yO_3$ and $Ba_{1-x}K_xBiO_3$ also have hole carriers.[106,107] The trend of an initial increase in T_c with hole concentration, n, is generally correlated to doping with lower valent elements (such as Sr^{2-} replacing La^{3-} and K^{1-} replacing Ba^{2+}) or to directly

TABLE 2.1. Structures of high-temperature superconductors.

Stoichiometry	T_c (K)	Metal stacking sequence	Reference
$La_{1.85}Sr_{0.15}CuO_4$	38	La-Cu-La	1
$YBa_2Cu_3O_7$	93	Ba-Cu-Y-Cu-Ba-Cu	13
$YBa_2Cu_4O_8$	81	Ba-Cu-Y-Cu-Ba-Cu-Cu	38,39
$Bi_2Sr_2CuO_6$	6	Bi-Bi-Sr-Cu-Sr	44,65
$Bi_2CaSr_2Cu_2O_8$	85	Bi-Bi-Sr-Cu-Ca-Cu-Sr	45
$Tl_2Ba_2CuO_6$	83	Tl-Tl-Ba-Cu-Ba	67
$Tl_2CaBa_2Cu_2O_8$	112	Tl-Tl-Ba-Cu-Ca-Cu-Ba	68
$Tl_2Ca_2Ba_2Cu_3O_{10}$	125	Tl-Tl-Ba-Cu-Ca-Cu-Ca-Cu-Ba	69
$Tl_2Ca_3Ba_2Cu_4O_{12}$	119	Tl-Tl-Ba-Cu-Ca-Cu-Ca-Cu-Ca-Cu-Ba	78
$TlCaBa_2Cu_2O_7$	85	Tl-Ba-Cu-Ca-Cu-Ba	76
$TlCa_2Ba_2Cu_3O_9$	110	Tl-Ba-Cu-Ca-Cu-Ca-Cu-Ba	76
$TlCa_3Ba_2Cu_4O_{11}$	122	Tl-Ba-Cu-Ca-Cu-Ca-Cu-Ca-Cu-Ba	78,79
$TlCa_4Ba_2Cu_5O_{13}$	110	Tl-Ba-Cu-Ca-Cu-Ca-Cu-Ca-Cu-Ca-Cu-Ba	81
$Pb_2Y_{0.5}Ca_{0.5}Sr_2Cu_3O_8$	68	Pb-Cu-Pb-Sr-Cu-(Y,Ca)-Cu-Sr	83
$Nd_{1.85}Ce_{0.15}CuO_4$	30	Nd-Cu-Nd	86,87
$BaPb_{0.75}Bi_{0.25}O_3$	13	Ba-(Pb,Bi)	88
$Ba_{0.6}K_{0.4}BiO_3$	34	(Ba,K)-Bi	92-95

increasing n through the addition of more charge-carrying planes (as in the Bi and Tl cuprates). However, the materials $R_{2-x}Ce_xCuO_4$ become superconducting by doping Ce^{4+} on the trivalent rare earths R, so that electron carriers are added, as confirmed by the negative Hall coefficient[86]

The anisotropic crystal structure of the copper-oxide superconductors is clearly demonstrated in resistivity measurements for in-plane and out-of-plane conduction. The resistivity along the c axis (perpendicular to the CuO_2 planes) is generally several orders of magnitude larger than the in-plane resistivity just above T_c, with anistropy values of 10^3 in $La_{2-x}Sr_xCuO_4$,[108] 100 to 250 in $YBa_2Cu_3O_7$,[109,110] and 10^5 in $Bi_2CaSr_2Cu_2O_8$.[111] The in-plane resistivity shows a linear decrease with temperature down to T_c for those samples with sharp superconducting transitions, while the resistivity parallel to the c axis indicates an onset of localization at temperatures just above T_c. For cubic $Ba_{1-x}K_xBiO_3$, resistivity data show hopping conductivity at all stoichiometries,[107] in contrast to the metallic behavior seen in the cuprates.

The pairing of charge carriers in the superconducting state was demonstrated in flux quantization measurements.[112,113] Flux vortices trapped within $YBa_2Cu_3O_7$ are quantized to the value $hc/2e$, consistent with $2e$ pairs. Voltage steps observed in the ac Josephson effect in $La_{2-x}Sr_xCuO_4$ and $YBa_2Cu_3O_7$ are integral multiples of $h/2e$ times the frequency of the applied microwave radiation, confirming the $2e$ pairing in these materials.[114-116] The pair wave function appears to be a singlet BCS-like state, with no nodes observed in the magnetic penetration depth as determined by muon-spin-relaxation measurements[117] and dc magnetization.[118] The observation of the dc Josephson effect in tunneling between the singlet-paired superconductors Pb, Sn, and Al and the high-

temperature superconductors $La_{2-x}Sr_xCuO_4$ and $YBa_2Cu_3O_7$ indicates that the pairs must be of the same symmetry in all these materials.[114-116] Also, dc Josephson tunneling has been observed in all heterojunctions of the superconductors Pb, $YBa_2Cu_3O_7$, $Bi_2CaSr_2Cu_2O_8$, and $Tl_2Ca_2Ba_2Cu_3O_{10}$, confirming that all these materials have singlet pairing.[119]

The characteristic energy gap Δ (at $T = 0$) of BCS superconductivity has proven difficult to determine in the high-temperature superconductors. The BCS ratio $2\Delta / k_B T_c = 3.53$ represents the weak-coupling ratio of the energy gap to the transition temperature.[98] Initial measurements in tunneling and infrared reflectivity experiments gave a range of values from 2 to 10 for this ratio, at least partially attributable to sample inhomogeneity.[120] Recent tunneling[121] and infrared reflectivity[122] measurements on $YBa_2Cu_3O_7$ yield a ratio between 3 and 4, consistent with weak coupling. Tunneling measurements[123] of $BaPb_{1-y}Bi_yO_3$ give a ratio of 3.5, while reflectivity measurements[124] give the ratio 3.2, again consistent with the BCS value. However, the energy gap measurements in the other materials are still controversial, with tunneling,[125,126] infrared reflectivity,[127] and high-resolution photoemission[128] experiments yielding a ratio $2\Delta/k_BT_c$ in the strong-coupling range $4.5 - 8$ for $Bi_2CaSr_2Cu_2O_8$.

Another disputed measurement for these materials is the change in the specific heat, ΔC_v, at the transition temperature. A small change of ≈ 4 percent in C_v for $YBa_2Cu_3O_7$ has recently been measured.[129] Combined with a free-electron estimate of the Sommerfeld constant γ, this gives a ratio $\Delta C_v / \gamma T_c$ near the weak-coupling value of 1.43.[98,129]

The coherence length, ξ, is anisotropic and quite short in these materials. Estimates of ξ are made from measurements of the upper critical field, H_{c2}, in

these type II superconductors by using the approximation $H_{c2} \approx hc/2e\pi\xi^2$ for one flux quantum per area $\pi\xi^2$. For example, in $Bi_2CaSr_2Cu_2O_8$ an in-plane coherence length of $\xi_{ab} = 31$ Å was found, while along the c axis, $\xi_c = 4$ Å.[130] The coherence length in the c direction is thus shorter than the intercell spacing ($\approx$ 12 Å) of the double CuO_2 layers in this phase. Interpretation of these estimates is severely limited if H_{c2} is determined by resistivity measurements, since a melting of the flux lattice is observed well below T_c at all fields greater than the lower critical field, H_{c1}, resulting in finite flux-flow resistivity.[131,132] Only magnetization measurements of H_{c2} may be considered accurate.

A particular property of BCS superconductivity is the isotope effect, which predicts that the transition temperature is proportional to $M^{-\alpha}$, where M is the mass of the atom and $\alpha = 0.5$ for single-element superconductors.[98] Substitution of ^{18}O for ^{16}O was studied to determine the partial α_{ox} in the multicomponent high-temperature superconductors. Results for $La_{2-x}Sr_xCuO_4$ gave α_{ox} in the range $0.16 - 0.37$, smaller than the BCS value but significant.[133,134] Measurements for $YBa_2Cu_3O_7$ gave a much smaller value $\alpha_{ox} < 0.02$.[135–138] A small but nonzero isotope shift has been reported for ^{18}O substitution in multiphase Bi–Ca–Sr–Cu–O materials.[139] In the bismuth-oxide superconductors $BaPb_{1-y}Bi_yO_3$ and $Ba_{1-x}K_xBiO_3$, the ^{18}O isotope effect has been reported[140] as $\alpha_{ox} = 0.2 - 0.25$, but a value as large as 0.4 for $Ba_{1-x}K_xBiO_3$ has been suggested.[141] Although in general the isotope effect results from electron-phonon interactions, the specific value of α can vary significantly from the BCS value even in well-characterized low-temperature superconductors, so that small (or large) isotopic shifts in T_c do not necessarily limit the specific mechanism of high-temperature superconductivity.

Magnetic Properties

Magnetic ordering has been observed in the non-superconducting phases of the copper oxides. The oxygen-deficient material La_2CuO_{4-y} exhibits three-dimensional antiferromagnetic ordering on the Cu sites,[142-145] with the spins of magnitude $\approx 0.4\,\mu_B$ aligned in the copper planes. A canting of the spins by 0.17° from the planes gives rise to a weak local ferromagnetic moment, which vanishes at long range since the canting is opposite in alternate copper layers.[146] The Néel temperature, T_N, is very sensitive to y, ranging from $T_N = 295$ K for $y = 0.03$ to $T_N \approx 0$ K for $y = 0$.[142] At temperatures well above T_N, a two-dimensional quantum spin-fluid state is observed, with instantaneous correlations extending over distances of 200 Å.[147] No superconductivity has been observed in samples exhibiting antiferromagnetism. However, local magnetic moments have been observed *in superconducting phases of* $La_{2-x}Sr_xCuO_4$ ($0.07 \leq x \leq 0.15$) at temperatures below 3 K, with fields at least an order of magnitude smaller than those associated with long-range antiferromagnetic order in the insulating state.[148,149]

The parent compound $YBa_2Cu_3O_6$ is an antiferromagnetic insulator. The Néel temperature of $YBa_2Cu_3O_{7-y}$ is again sensitive to the oxygen stoichiometry, with a maximum $T_N \approx 500$ K for $y = 1.0$, dropping to $T_N = 0$ K for $y \approx 0.6$.[150] An indication of magnetic ordering at temperatures below 10 K was observed in superconducting phases of $YBa_2Cu_3O_{7-y}$, possibly associated with local antiferromagnetic order.[151] Two distinct three-dimensional antiferromagnetic orderings are found in $YBa_2Cu_3O_6$. The high-temperature ordering is associated with the copper plane sites only, while a $T_N = 210$ K transition occurs for ordering on the copper plane and chain sites.[152] A two-dimensional

spin-wave excitation is seen in the non-superconducting material above the Néel temperature.[153]

The bismuth and thallium cuprates do not have non-superconducting parent compounds as do $La_{2-x}Sr_xCuO_4$ and $YBa_2Cu_3O_7$, in the sense that the stoichiometric, undoped materials are superconducting. However, these materials can be made non-superconducting by various atomic substitutions. In particular, replacement of Ca by Y gives the phase $Bi_2YSr_2Cu_2O_8$, which is insulating.[154–156] This phase exhibits antiferromagnetic order on the copper sites with $T_N \approx 210$ K.[157,158] Substitution of Y for Ca to form the insulating phase $TlYBa_2Cu_2O_7$ also results in three-dimensional antiferromagnetic order with $T_N > 350$ K.[159] Presumably other phases in the Bi and Tl cuprate systems will exhibit this antiferromagnetic behavior with similar dopants; however, such measurements have not yet been reported.

The rare-earth cuprates R_2CuO_4, R = Pr, Nd, Sm, Eu, or Gd, are antiferromagnetic insulators. For example, the Néel temperature of Pr_2CuO_4 is 270 K.[85] Doping with Ce to create the superconducting phase destroys the antiferromagnetic order.[85]

No magnetic structure has been seen in $BaBiO_3$, $BaPb_{1-y}Bi_yO_3$, or $Ba_{1-x}K_xBiO_3$.[160] This is as expected, since magnetism is not generally associated with valence s states such as those of Pb and Bi. The set of bismuth oxide high-temperature superconductors is thus unique in its lack of magnetic ordering.

CHAPTER III

TIGHT-BINDING MODEL

In this chapter we present the details of the tight-binding model used to calculate the electronic structure of the high-temperature superconductors. The details of the electronic structure provide a critically important foundation for understanding both the normal-state and superconducting properties. In Chapter IV, the electronic structure results of this model are compared with other calculations and with experiment. In Chapter V, this model is used to examine the effect of atomic substitutions, while vacancy effects on the electronic structure are presented in Chapter VI.

The validity of any model for the electronic structure is determined by its agreement with experimental results. The tight-binding model has a distinct advantage in this respect over other techniques, since one can obtain a better representation of the electronic structure by using a semiempirical fit to the experimental measurements. Also, the parameters of the model have a strong chemical meaning, representing effective atomic energies and bond strengths. The results are interpretable as physical quantities such as valences and local densities of states. The tight-binding approach does have less predictive power than techniques that use the local-density approximation (LDA), in which the electronic states are calculated self-consistently from first principles, but with electron correlations and exchange effects approximated by a local potential.[161] The LDA often provides a good description of ground-state properties, but is less accurate in representing the excited states. The tight-binding approach is more useful for many applications because of its simplicity.[162–166]

Both tight-binding and LDA models suffer qualitative failures in highly-correlated systems. These problems carry over to high-temperature superconductors, with La_2CuO_4 and $YBa_2Cu_3O_6$ predicted to be nonmagnetic metals rather than antiferromagnetic insulators.[142-145,150] Predictions for the highly-correlated copper d states may be in disagreement with photoemission measurements,[167] which indicate that the occupied d states are more strongly bound by $1 - 1.5$ eV. Also, electron-energy-loss spectroscopy measurements[168] indicate that the states nearest E_F are primarily of oxygen p character, with little or no Cu d admixture. These failures within the one-electron approximation are partially attributable to the neglect of many-body correlation effects.[169] It may ultimately be possible to treat the electronic states accurately using, for example, the variational quantum Monte Carlo method.[170]

We find in Chapter IV that a single tight-binding model, with fully transferable parameters, provides a good description of the electronic structure of the high-temperature superconductors, in the sense that the LDA results are satisfactorily reproduced. The fitted tight-binding parameters provide a basis for extrapolating to other related classes of materials. Some features of the one-electron description appear to be in at least qualitative agreement with photoemission, inverse photoemission, electron-energy-loss spectroscopy, and positron annihilation measurements of the high-temperature superconductors.

Numerical calculations were performed in double precision on a Digital Equipment Corporation VAX 11/782, a VAX 8650, and a VAX 8800. Matrix diagonalizations, matrix inversions, and numerical integrations were performed using software from the International Mathematical and Statistical Libraries (IMSL). Detailed codes are available from the author.

Electronic Energy Bands

The energy bands of the high-temperature superconductors are calculated in the one-electron approximation, using a semiempirical tight-binding model with valence p and s orbitals included for the O atoms and d and s orbitals for all the metal atoms. Valence p states were included for calculations with Al, Hg, Tl, Pb, and Bi. Atomic core levels were neglected in all cases, as were the localized f states. The effective atomic energy parameters ϵ_s, ϵ_p, and ϵ_d were fitted to the LDA energy bands of La_2CuO_4, $BaBiO_3$, and $BaPbO_3$, beginning with the nominal values from the table of Harrison.[165] Energy parameters not given in this table were extrapolated from the nearest atom for which a value is given. The parameters are referenced to a zero of energy at the ionization limit. We found it necessary to shift the Cu, Pb, and Bi energy parameters significantly from their tabulated values (which were originally applied to semiconductors and insulators[165,171]). We also shifted the energy parameters of the neighboring atoms to maintain the tabulated difference in energies of the atomic states, preserving the physical interpretation of these parameters as effective energies. The resulting atomic parameters are listed in Table 3.1.

The tight-binding Hamiltonian matrix has elements

$$H_{\alpha i,\beta j}(\vec{k}) = \sum_{l} \langle \alpha i | H | \beta j, l \rangle \exp\left[i\vec{k} \cdot (\vec{r}_{j,l} - \vec{r}_i) \right] , \qquad (3.1)$$

where α and β label orbitals, and the sum is over all atoms that are equivalent to atom j in the unit cell and that neighbor atom i. The diagonal elements of the Hamiltonian are the atomic energies in Table 3.1. The interatomic matrix elements $\langle \alpha i | H | \beta j, l \rangle$ are determined by the primitive tight-binding matrix elements and by the relative coordinate from atom i to atom j, l.[162,165] The

TABLE 3.1. Tight-binding parameters for high-temperature superconductors.

	ϵ_s (eV)	ϵ_p (eV)	ϵ_d (eV)	r_d (Å)
O	-29.0	-14.0	···	···
K	-4.2	···	-3.2	1.2
Ca	-5.4	···	-3.2	1.2
Cu[a]	-12.0	···	-14.0	0.95
Sr	-5.0	···	-6.8	1.6
Y	-5.5	···	-6.8	1.6
Ba	-4.5	···	-6.6	1.6
La	-4.9	···	-6.6	1.6
Tl	-14.8	-8.3	-23.0	1.0
Pb[b]	-18.0	-9.4	-29.0	1.0
Bi[c]	-21.2	-10.5	-35.0	1.0

[a] Parameters fitted to La_2CuO_4.
[b] Parameters fitted to $BaPbO_3$.
[c] Parameters fitted to $BaBiO_3$.

primitive tight-binding matrix elements between nearest-neighbor atoms are[165]

$$V_{ll'm} = \eta_{ll'm} \frac{\hbar^2}{m_e d^2} \quad (l, l' = s, p;\ m = \sigma, \pi) \tag{3.2}$$

and

$$V_{ldm} = \eta_{ldm} \frac{\hbar^2 r_d^{3/2}}{m_e d^{7/2}} \quad (l = s, p;\ m = \sigma, \pi)\ , \tag{3.3}$$

where m_e is the mass of the electron. The matrix element varies with the indicated inverse power of the interatomic separation, d, a result from scaling in the linear combination of atomic orbitals (LCAO) theory.[165] The strength of the interaction is given by the dimensionless variable $\eta_{ll'm}$, where l refers to the angular momentum quantum number (s, p, or d) of the first orbital, l' is the angular momentum quantum number of the second orbital, and m describes the total angular momentum of the interaction (σ or π bonding). $V_{ll'm}$ is unaffected under exchange of l and l' if the sum of the parities is even, but changes sign if the sum of the parities is odd.[162] The strengths $\eta_{ss\sigma}$, etc., were originally fitted from free-electron theory to the energy bands of silicon and germanium.[165,171] We have adjusted these parameters to better fit the LDA results for La_2CuO_4, $BaBiO_3$, and $BaPbO_3$. We obtain $\eta_{ss\sigma} = -1.1$, $\eta_{sp\sigma} = 0.9$, $\eta_{pp\sigma} = 1.5$, $\eta_{pp\pi} = -0.6$, $\eta_{sd\sigma} = -1.6$, $\eta_{pd\sigma} = -2.5$, and $\eta_{pd\pi} = 1.4$. A larger value $\eta_{sp\sigma} = 1.4$ is used for the Bi and Tl cuprate calculations, but the earlier calculations for $La_{2-x}Sr_xCuO_4$ and $YBa_2Cu_3O_7$ were insensitive to this value. The extent of the d-orbital interaction is characterized by the length r_d. The r_d parameter was fitted only for Cu.

The solution of the matrix form of the time-independent Schrödinger equation

$$H(\vec{k})\ \psi(\vec{k}, n) = E(\vec{k}, n)\ \psi(\vec{k}, n) \tag{3.4}$$

gives tight-binding wave functions $\psi(\vec{k},n)$ with components representing the atomic orbital basis of the model. The wave functions are normalized such that

$$\sum_{\alpha} |\psi^{\alpha}(\vec{k},n)|^2 = 1 \tag{3.5}$$

for the orbital components α. The wave functions and the energy eigenvalues are both functions of the wave vector $\vec{k}$. The energy eigenvalues are plotted as dispersion relations in $\vec{k}$ along particular symmetry lines of the Brillouin zone for each structure examined.[172]

The results for $La_{2-x}Sr_xCuO_4$ and $YBa_2Cu_3O_7$ did not require any second-neighbor interactions to reproduce the LDA energy bands. In particular, the oxygen-oxygen interactions were optimally zero. However, as described in Chapter IV, calculations for the Bi and Tl cuprates required second-neighbor Bi–Bi and Tl–Tl interactions in the rocksalt-like BiO and TlO layers to provide satisfactory agreement with the LDA results. In those cases, the same scaling and strengths were used for $V_{ll'm}$ as for the nearest-neighbor interactions, but no $d-d$ interactions were allowed.

Virtual Crystal Approximation

The doping with Sr in $La_{2-x}Sr_xCuO_4$, with Pb in $BaPb_{1-y}Bi_yO_3$, and with K in $Ba_{1-x}K_xBiO_3$ requires a modification of the energy parameters for the atoms in the solid solution. These substitutions are treated in the virtual crystal approximation,[173] in which the random distribution of dopants is assumed to give an average atom on a particular site. For example, the doping $La_{2-x}Sr_x$ is treated by replacing $\epsilon_s(\mathrm{La})$ with $(1-x/2)\epsilon_s(\mathrm{La})+(x/2)\epsilon_s(\mathrm{Sr})$, and by removing x electrons per chemical unit. This approximation gives a good description of

dimetal alloys in the range where the atomic energies are similar,[173] and we expect it to hold in the context of the high-temperature superconductors. In the particular case of $La_{2-x}Sr_xCuO_4$, the energy parameters ϵ_s and ϵ_d for La are almost identical to the corresponding parameters for Sr, so the only effect of doping with Sr is to add hole carriers to the system.

Density of States

The local density of states for both spins is calculated from

$$\rho(E) = -\frac{2}{\pi} Tr\ Im\ G_0(E)\ . \tag{3.6}$$

where Tr indicates a trace over those orbitals associated with a given site. The Green's function is given in the spectral representation by

$$G_0(E) = \sum_{\vec{k},n} w_{\vec{k}} \frac{\psi(\vec{k},n)\ \psi^{\dagger}(\vec{k},n)}{E - E(\vec{k},n) - i\delta}\ , \tag{3.7}$$

where $E(\vec{k},n)$ and $\psi(\vec{k},n)$ are the electronic energy eigenvalue and the wave function (in the tight-binding representation) for the n^{th} band and one of the N sample wave vectors $\vec{k}$ (with weight $w_{\vec{k}}$) within the irreducible part of the Brillouin zone.[174] For these calculations, $N = 64$ for the orthorhombic structures, $N = 24$ for the tetragonal and bct structures, and $N = 20$ for the cubic structures. A finite value $\delta = 0.2$ eV was used, smoothing the results with a Lorentzian lineshape. The total density of states is simply the sum of the local densities of states of each atom in the unit cell. The Fermi energy is calculated by integrating the total density of states up to the number of valence electrons for each material (which is consistent with an average of the highest occupied energy state across the sample wave vectors). The value of the density of states

at the Fermi energy, $\rho(E_F)$, is compared with those from other calculations; however, the most reliable use for $\rho(E_F)$ in this work is as a measure of change for various substitutions and vacancy effects, as detailed in Chapters V and VI.

Atomic Valence

The formal valence of an atom (also known as its oxidation state) is a well-defined quantity that provides a chemical prediction for the stoichiometry and bonding in compounds.[95] For example, the formal valences La^{3+}, Cu^{2-}, and O^{2-} correctly describe the stoichiometry in La_2CuO_4. In the context of this work, however, we are interested in the real charge that is associated with a particular atom bonded in the solid. If we consider the solid to form from originally neutral atoms, then charge transfer will occur between the atoms as a result of the bonding. The valence of each atom, defined to be the number of electrons transferred from the atom when it is bonded in the solid, is calculated from

$$\Delta n_i = n_i - 2 \sum_{\vec{k},\alpha,n}^{E(\vec{k},n)\leq E_F} w_{\vec{k}} \left|\psi_i^{\alpha}(\vec{k},n)\right|^2 , \qquad (3.8)$$

where n_i is the number of valence electrons on the free atom i, $\psi_i^{\alpha}(\vec{k},n)$ is the component of the wave function corresponding to the valence orbital α on this atom, and the sum [over all states with $E(\vec{k},n) \leq E_F$] is a weighted average over the N sample wave vectors $\vec{k}$. The Δn obtained is the real charge associated with all the valence basis states on a particular atom. This technique can also determine the relative occupancy of different orbitals on the same atom, such as the p_x, p_y, and p_z orbitals of oxygen.

CHAPTER IV

ELECTRONIC STRUCTURE

In this chapter we present the results of the tight-binding calculations for the electronic structure of the high-temperature superconductors. We have calculated the electronic energy bands, the local and total densities of states, and the atomic valences for the representative materials $La_{1.85}Sr_{0.15}CuO_4$, $YBa_2Cu_3O_7$, $Bi_2Sr_2CuO_6$, $Bi_2CaSr_2Cu_2O_8$, $Tl_2Ba_2CuO_6$, $Tl_2CaBa_2Cu_2O_8$, $Tl_2Ca_2Ba_2Cu_3O_{10}$, $TlCa_3Ba_2Cu_4O_{11}$, $BaPb_{0.75}Bi_{0.25}O_3$, and $Ba_{0.6}K_{0.4}BiO_3$. These results are compared with other theoretical work and with experiments that probe the electronic properties of the high-temperature superconductors. A summary of the similarities and differences in these materials is provided at the end of the chapter.

$La_{1.85}Sr_{0.15}CuO_4$

The bct crystal structure of $La_{1.85}Sr_{0.15}CuO_4$ is taken from experiment,[9] but the small orthorhombic distortion and the doubling of the unit cell are ignored for simplicity. The small displacements associated with the tilting of the CuO_6 octahedra and the buckling of the CuO_2 planes,[5] although fundamentally significant, would have an imperceptible effect in this calculation. The lattice parameters for the bct cell are $a = 3.782$ Å and $c = 13.249$ Å; we use the primitive unit cell with one formula unit per cell. The partial substitution of Sr for La is treated in the virtual crystal approximation as described in Chapter III.

The calculated energy bands for $La_{1.85}Sr_{0.15}CuO_4$ are shown in Fig. 4.1 along several symmetry lines in the Brillouin zone,[172] with the zero of energy

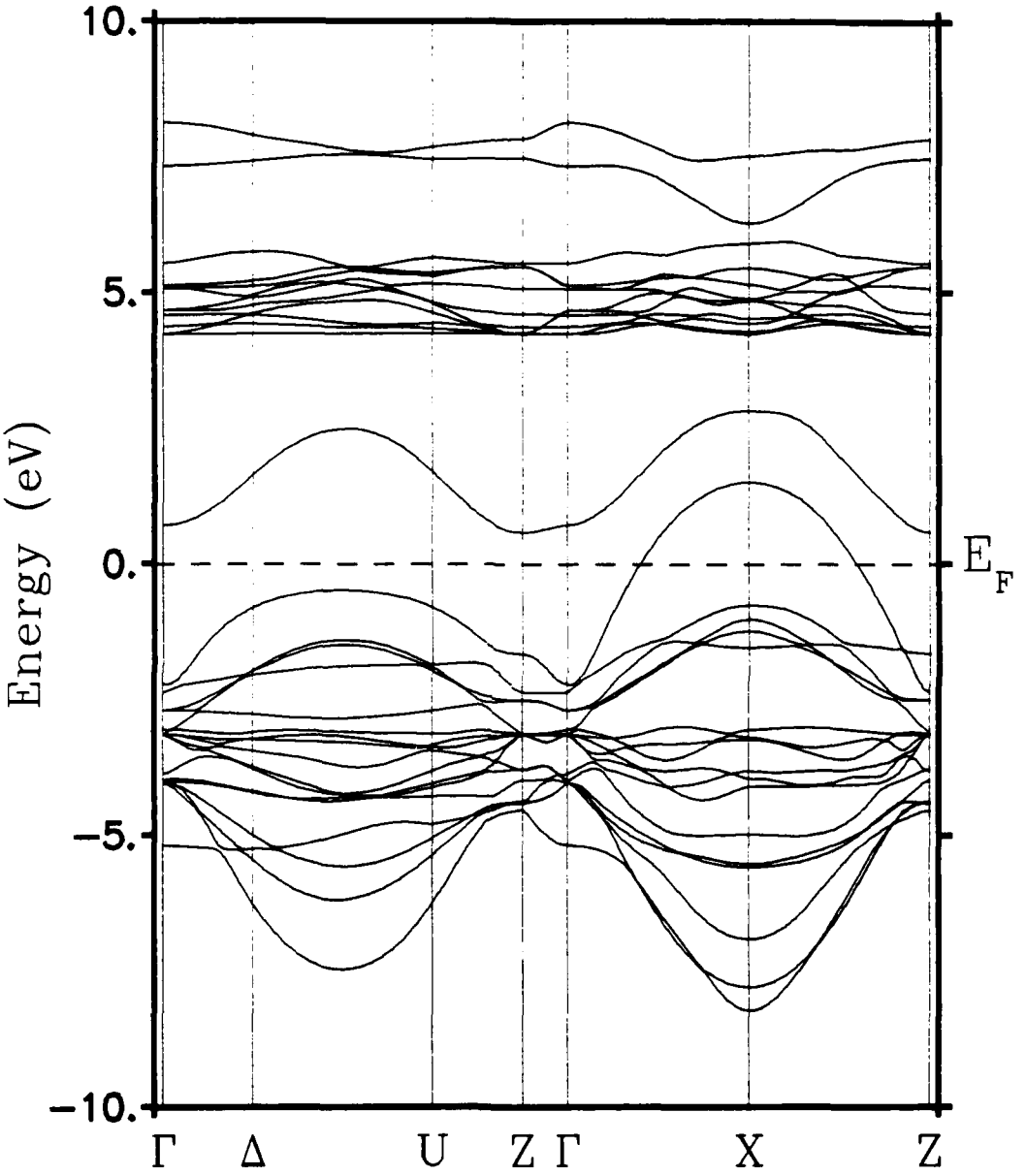

Fig. 4.1. Electronic energy bands for $La_{1.85}Sr_{0.15}CuO_4$.

shifted to E_F. Comparison with the LDA calculations[175–178] shows very similar structure. The principle bands within 10 eV below the Fermi energy are the seventeen bands contributed by Cu d and O p states. The valence bandwidth at the ΔU midpoint (along the [100] direction) is 7.0 eV, compared with 6.5 eV in Ref. 175. The bandwidth at X (along the [110] direction), the largest dispersion of the bands, is 9.7 eV, compared with 9.2 eV in Ref. 178, 9.4 eV in Ref. 175, 9.5 eV in Ref. 176, and 10.3 eV in Ref. 177. The single prominant Cu(d)–O(p) antibonding state protruding above E_F at X has an indirect overlap with the lowest-lying conduction band at Z of 0.9 eV, compared with 1.0 eV in Refs. 175 and 176, and 0.6 eV in Ref. 178. The relatively flat bands near 5 eV arise from the La/Sr d states, with the corresponding s bands about 2 eV higher in energy. The O s bands lie approximately 18 eV below E_F. The bands are found to have almost two-dimensional character,[175–178] with little variation along ΓZ in the k_z direction, perpendicular to the CuO_2 planes. There are certain details that are not reproduced in our calculation; for example, the highest occupied states along the symmetry line ΔU are consistently about 0.5 eV nearer E_F in the LDA models, and some degeneracies in the non-bonding oxygen p bands at Γ and at Z are broken in the self-consistent calculations. However, the level of agreement between the tight-binding bands and the LDA bands is very satisfactory, especially since the range of results in the LDA calculations (which ideally use the same Hamiltonian) includes the tight-binding bands. The parameters of the tight-binding model are thus considered properly fitted for $La_{1.85}Sr_{0.15}CuO_4$.

The local densities of states for $La_{1.85}Sr_{0.15}CuO_4$ are shown in Fig. 4.2, with O(1) and O(2) respectively labeling the in-plane and out-of-plane oxygen

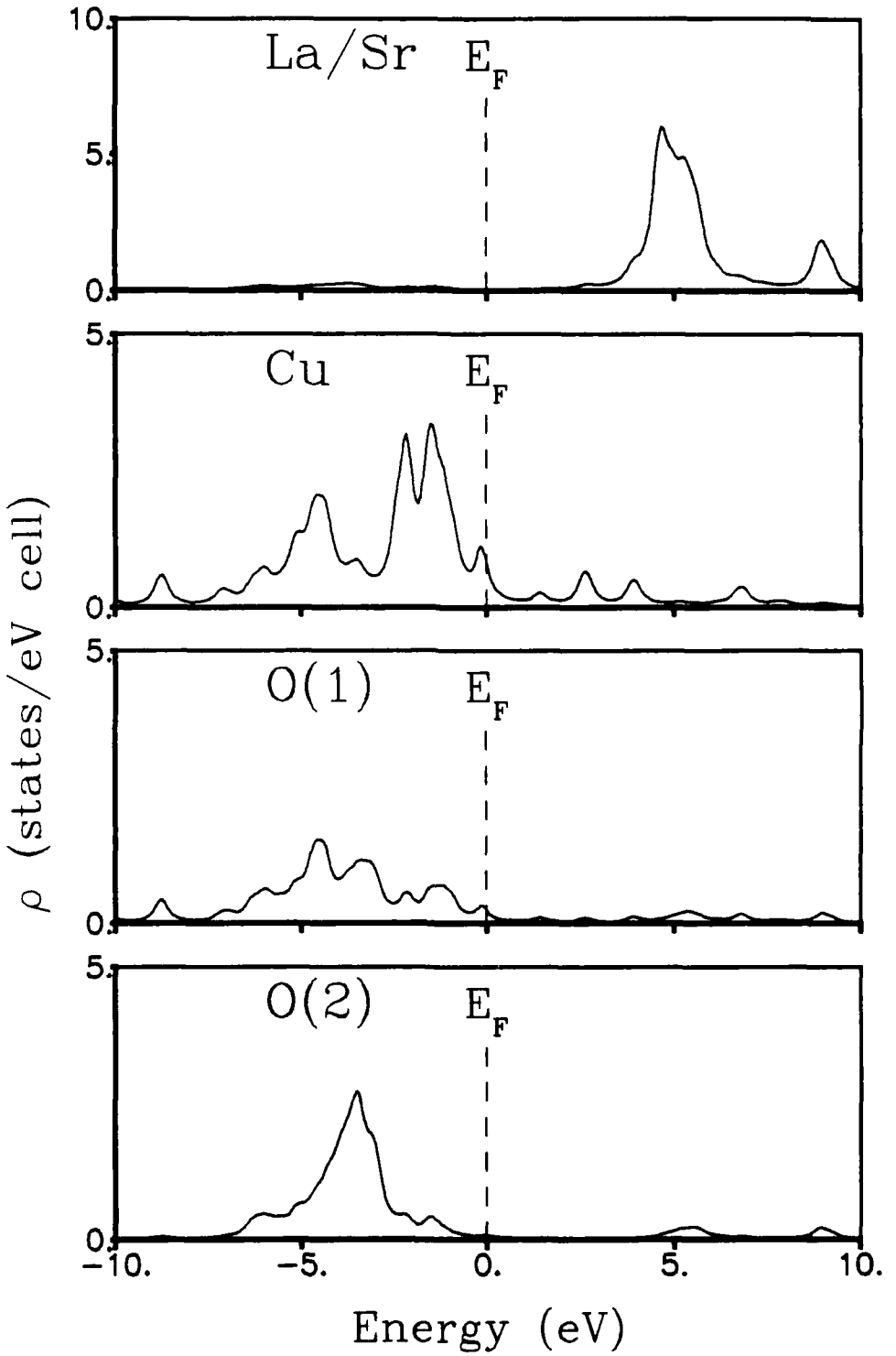

Fig. 4.2. Local densities of states for $La_{1.85}Sr_{0.15}CuO_4$.

sites. Since O(2) forms a more ionic bond to Cu, the p state peak for this site is narrower than for the O(1) site. The unoccupied La d bands peak near 5 eV with little dispersion. The Cu d and O p states, which have the same effective atomic energy in this model, are almost fully occupied, with some Cu–O(1) hybrid states dispersed above the Fermi energy, corresponding to the antibonding bands of Fig. 4.1. The total density of states at the Fermi energy, $\rho(E_F)$, is 1.9 states/eV cell, compared with the LDA values ranging from 1.1 states/eV cell[176] to 2.1 states/eV cell.[177] The metallic character arises from the Cu and O(1) sites, while the La and O(2) layers are insulating, in the sense that the local density of states at E_F is very small for these atoms.

The atomic valences for $La_{1.85}Sr_{0.15}CuO_4$ are listed in Table 4.1. As noted in Chapter III, this valence does not equal the formal valence associated with the atom, but rather the real charge that is distributed over the atomic basis states of the tight-binding model. The valence of O(2) is significantly larger in magnitude than that of O(1), reflecting the charge transfer associated with the ionic bond of the out-of-plane O(2) to the La ion. The lower charge on O(1) reflects the more covalent nature of the in-plane bond with Cu.

Photoemission measurements of $La_{2-x}Sr_xCuO_4$ reveal the occupied electronic states.[179–181] A low density of states at E_F is observed. The Cu(d)–O(p) hybrid bands are concentrated within 8 eV below the Fermi energy, but the peak in the emission intensity is more tightly bound by $1-2$ eV with respect to the calculated density of states.[180,181] This discrepancy occurs for both the tight-binding and the LDA models,[175–178] and may be related to correlation effects in the Cu d bands.[180]

Inverse photoemission[182–184] experiments and electron-energy-loss spec-

TABLE 4.1. Valences Δn for $La_{1.85}Sr_{0.15}CuO_4$ and $YBa_2Cu_3O_7$.

	La/Y	Sr/Ba	Cu(1)[a]	Cu(2)	O(1)	O(2)	O(3)	O(4)
$La_{1.85}Sr_{0.15}CuO_4$	2.12	1.12	1.08	···	-1.14	-1.51	···	···
$YBa_2Cu_3O_7$	1.77	1.44	1.34	0.98	-1.12	-1.09	-1.11	-1.21

[a] Cu site in $La_{1.85}Sr_{0.15}CuO_4$.

troscopy (EELS)[168,179] measurements probe the unoccupied states above E_F in $La_{2-x}Sr_xCuO_4$. The vacant La d bands were observed at 5.8 eV above the Fermi energy,[183] consistent with the tight-binding result ($\approx$ 5 eV) in Fig. 4.2. The LDA calculations placed these bands much lower, within 2 eV of E_F.[175] The La f bands (neglected in the tight-binding model) form a sharp peak near 8.7 eV.[183] The EELS data[168] indicate that only O p_x and p_y character is present at E_F, with no out-of-plane O p_z character observed. The extent of Cu d character at the Fermi energy has not been resolved, but the tight-binding and LDA results have some Cu(d)–O(p) admixture in the antibonding bands crossing E_F.

$YBa_2Cu_3O_7$

The orthorhombic crystal structure used for $YBa_2Cu_3O_7$ has lattice parameters a = 3.856 Å, b = 3.870 Å, and c = 11.666 Å.[18] For this calculation, we assume the oxygens are completely ordered in the chains along the b axis.[17] No adjustment of the tight-binding parameters was made for this calculation, so the results test the transferability of the parameters between materials. We choose the symmetry points of the orthorhombic Brillouin zone as shown in Fig. 4.3, with the path ΓXMY in the central plane of the Brillouin zone, and ZX′M′Y′ shifted along k_z to the zone boundary. The symmetry line ΓY is parallel to the CuO chains.

The energy bands for $YBa_2Cu_3O_7$ are shown in Fig. 4.4. The complex bands just below E_F arise from the 36 states in the Cu(d)–O(p) manifold. The bands are again two-dimensional, with little dispersion along ΓZ and very similar results along ΓXMY and ZX′M′Y′. Three antibonding Cu–O bands protrude above E_F, with one (associated with the CuO chain) having

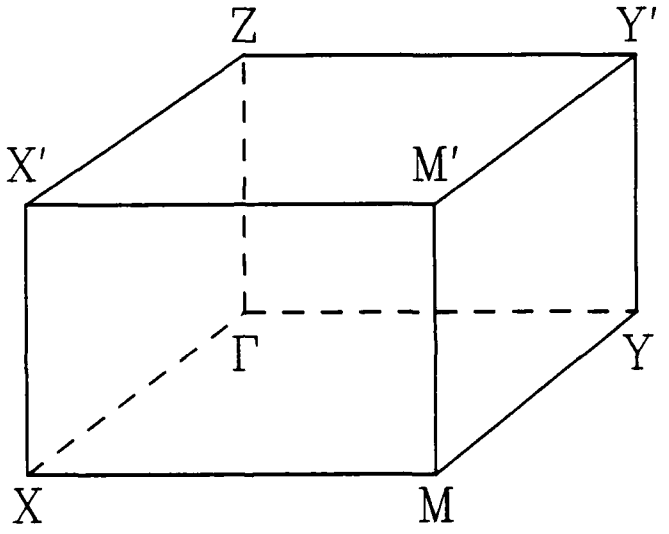

Fig. 4.3. Symmetry lines of the orthorhombic Brillouin zone for $YBa_2Cu_3O_7$.

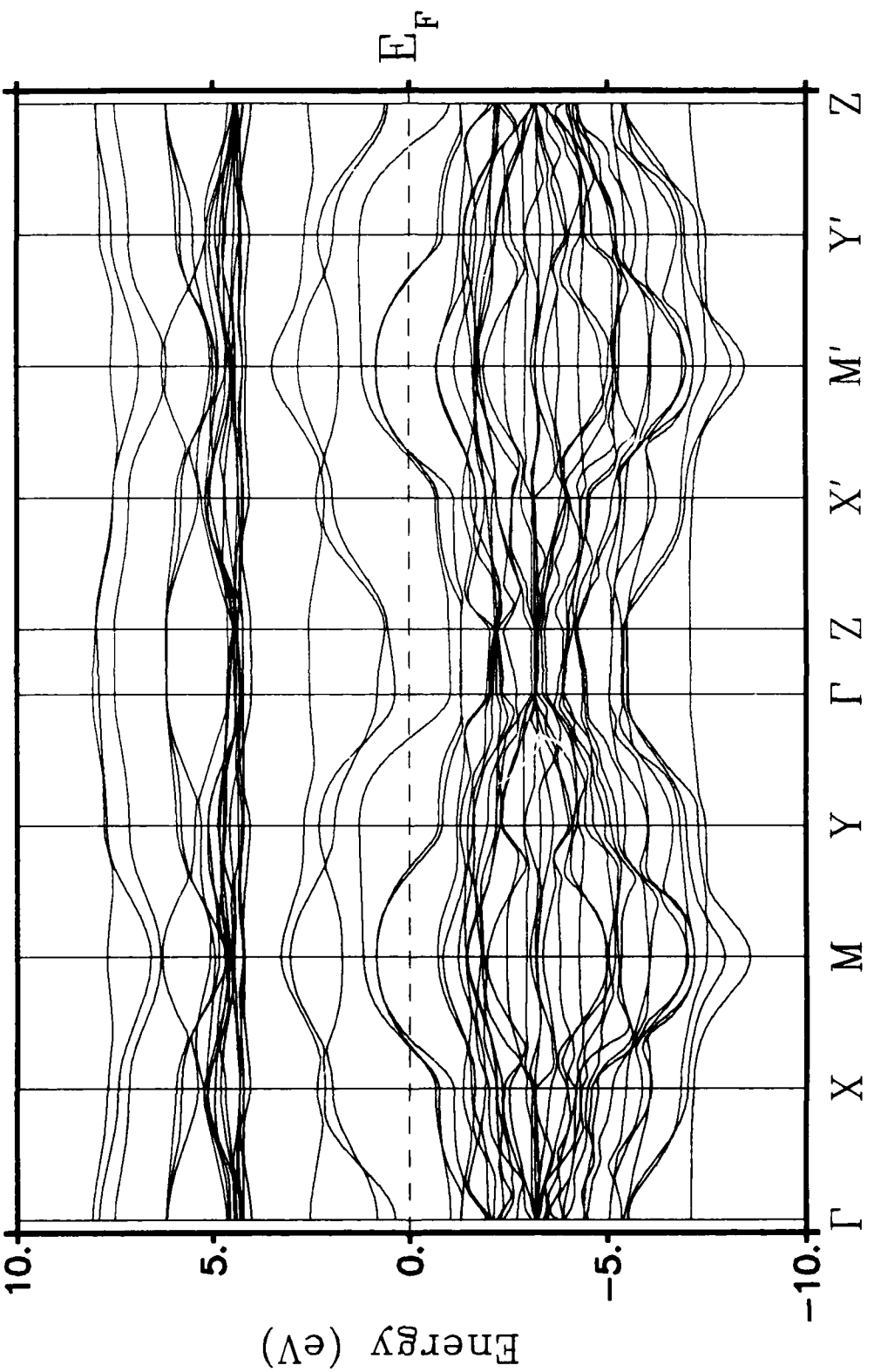

Fig. 4.4. Electronic energy bands for $YBa_2Cu_3O_7$.

little dispersion along MY, perpendicular to the CuO chains. The other two bands are associated with the CuO_2 planes, and have dispersion similar to the corresponding band in $La_{1.85}Sr_{0.15}CuO_4$. Satisfactory agreement is found with the LDA calculations.[185–188] For example, the valence bandwidth at M is 9.7 eV, compared with 7.3 eV in Ref. 185 and 8.9 eV in Ref. 187. The CuO chain band peaks 1.2 eV above E_F at Y, compared with 1.4 eV in Ref. 185, 1.7 eV in Ref. 187, and 2.1 eV in Ref. 188. For this material, the range of results is larger than for $La_{2-x}Sr_xCuO_4$; however, the overall structural features are in good agreement among the tight-binding and LDA calculations, indicating that the tight-binding parameters are transferable to $YBa_2Cu_3O_7$.

The local densities of states for the metal atoms in $YBa_2Cu_3O_7$ are shown in Fig. 4.5, with those of the oxygen sites given in Fig. 4.6. Cu(1) and O(1) refer to sites in the CuO chain: Cu(2), O(2), and O(3) to the CuO_2 plane sites: and O(4) to the out-of-plane oxygen in the BaO layer. The Y d and Ba d bands have narrow, unoccupied peaks above E_F. O(4) also has a sharp spectrum, related to the ionic bond formed with Ba. The Cu(2)–O(2,3) sites show broad features just below the Fermi energy characteristic of the $pd\sigma$ covalent bonds formed in the CuO_2 planes. The Cu(1)–O(1) chain sites have somewhat narrower peaks. The total density of states for $YBa_2Cu_3O_7$ is 3.2 states/eV cell, similar to the LDA results of 3.0 states/eV cell[185] and 3.4 states/eV cell.[187] The metallic contribution to $\rho(E_F)$ is primarily from the CuO_2 plane sites, but with an additional contribution from the CuO chains.

The valences Δn are given in Table 4.1. The valence for the plane Cu(2) site is close to that of Cu in $La_{1.85}Sr_{0.15}CuO_4$, but Cu(1) is more ionic. O(4) has the largest valence of the oxygens, reflecting the ionic bond formed with the

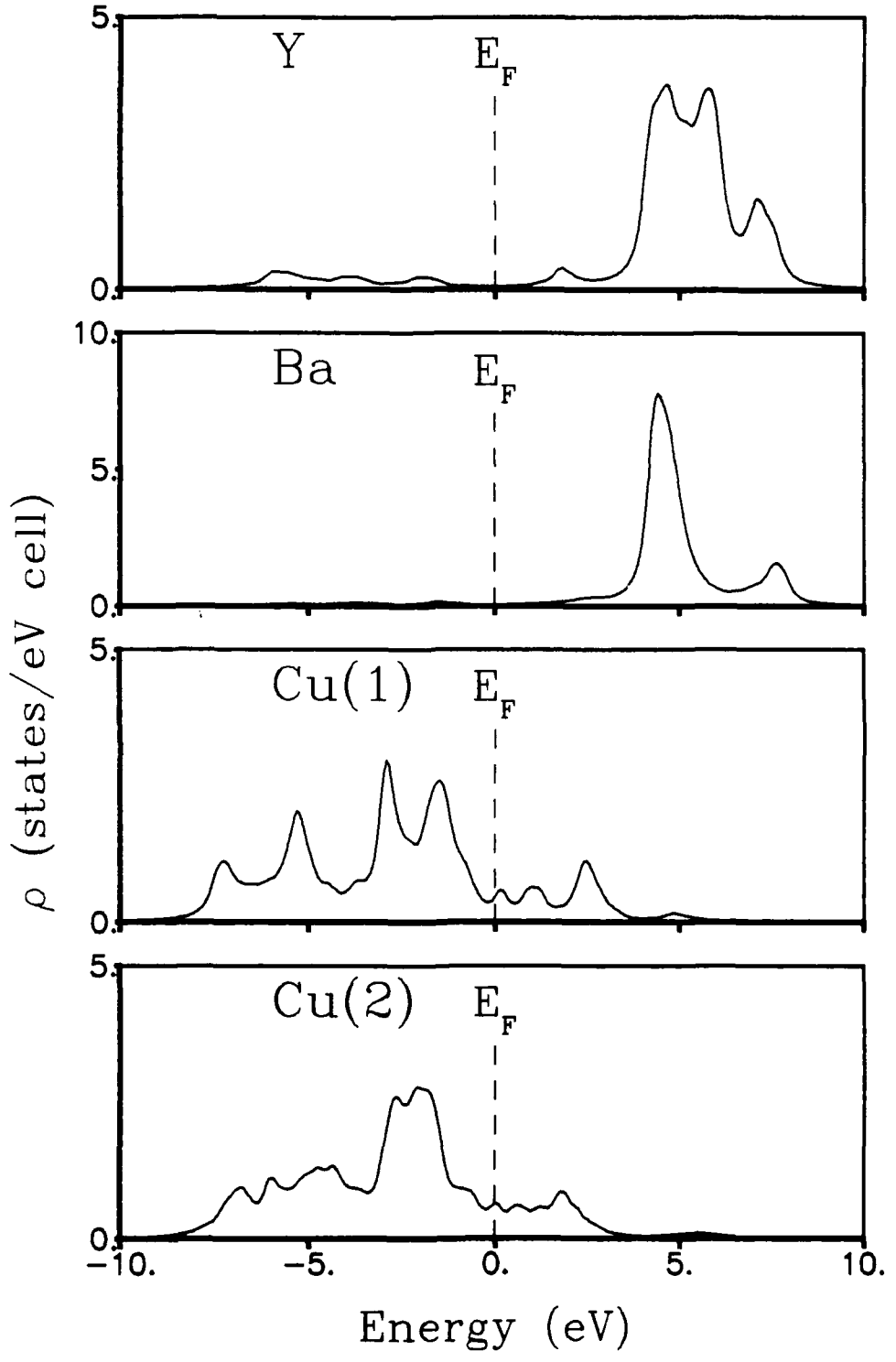

Fig. 4.5. Local densities of states for the metal atoms in $YBa_2Cu_3O_7$.

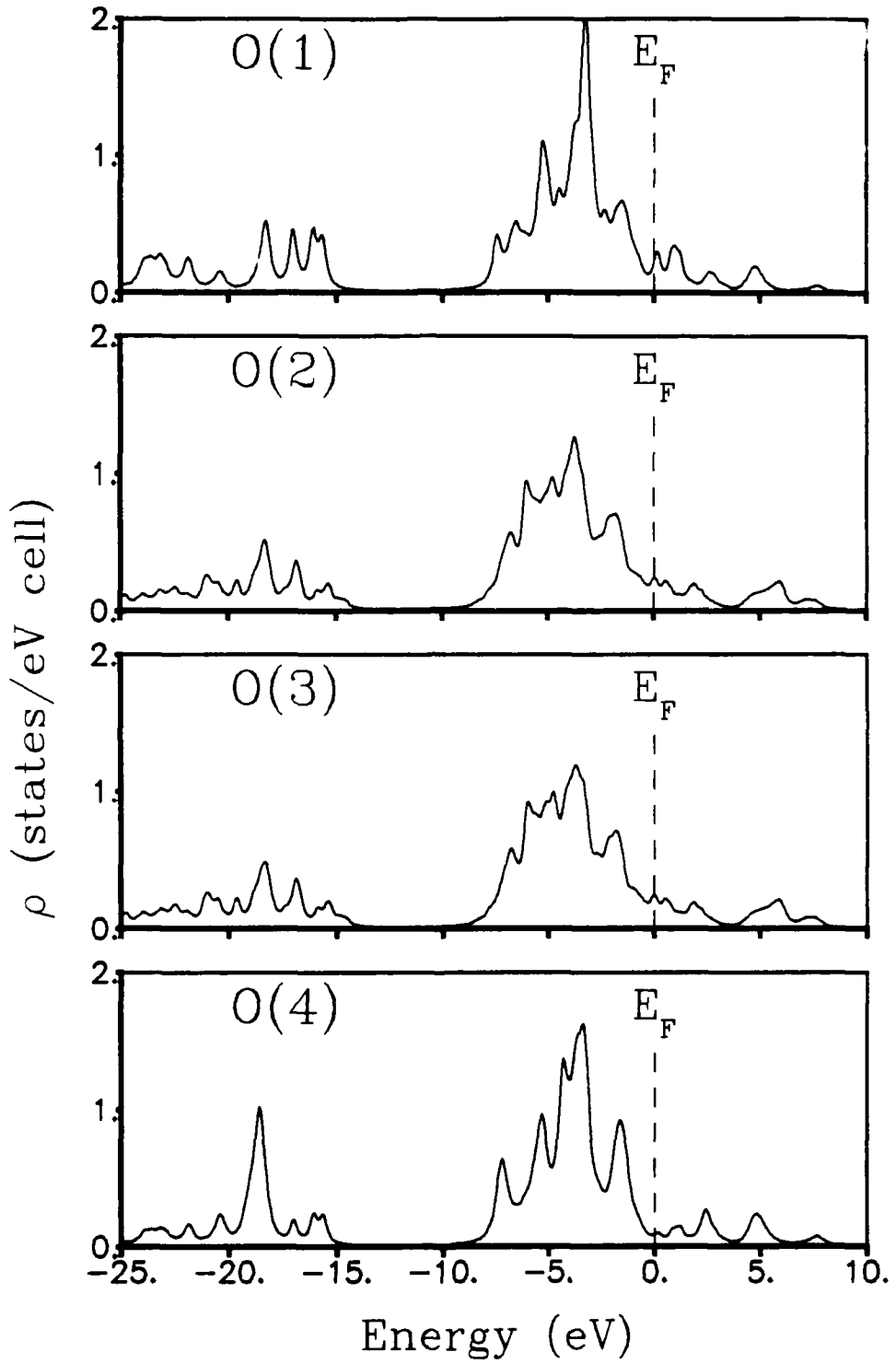

Fig. 4.6. Local densities of states for the oxygen atoms in $YBa_2Cu_3O_7$.

Ba ions.

The occupied electronic states of $YBa_2Cu_3O_7$ have been determined in photoemission experiments.[167,189–194] The peak of the Cu(d)–O(p) hybrid bands is more tightly bound by 1 – 1.5 eV with respect to the calculated density of states, again attributed to localization effects in the Cu d bands.[167] The oxygen s bands appear near -20 eV,[189,191] consistent with the local density of states results in Fig. 4.6. Angle-resolved photoemission measurements indicate a dispersion of $\approx$ 0.3 eV along the ΓM symmetry line for the uppermost antibonding Cu–O band,[194] smaller than the dispersion predicted by the tight-binding and LDA models. However, the angular dependence gives support to the use of band theory to describe the electronic states.

Inverse photoemission[195–197] and EELS[168,198–201] measurements reveal the unoccupied states in $YBa_2Cu_3O_7$. The Ba d and Y d bands were observed at 6.6 eV and 8.6 eV,[195] respectively, somewhat higher than the tight-binding results of $\approx$ 5 eV and $\approx$ 7 eV in Fig. 4.5. The Ba f bands are located at 13.4 eV, well-removed from the region of interest near the Fermi energy.[195] The EELS data[168,198] show O p_x and p_y character at E_F (again with no O p_z character), consistent with the observation of oxygen hole states above E_F in inverse photoemission data.[197] The amount of Cu d character at the Fermi energy has not been determined.

Another probe of the electronic structure is positron-annihilation spectroscopy. Interpretation of the results is often difficult because of trapping of the positrons at vacancies and defects rather than in specific electronic bands. However, angular correlation studies of $La_{2-x}Sr_xCuO_4$ and $YBa_2Cu_3O_7$ indicate that the core atomic states can be accurately studied,[202,203] and are found

to be localized as in band theory.

$Bi_2Sr_2CuO_6$

We have extended the original tight-binding model to the superconductors containing thallium, lead, and bismuth. In addition to the parameters previously fitted to La_2CuO_4, the valence s, p, and d energies for Tl, Pb, and Bi, and the $\eta_{sp\sigma}$, $\eta_{pp\sigma}$, and $\eta_{pp\pi}$ interatomic matrix element strengths are needed. (In the calculations for $La_{1.85}Sr_{0.15}CuO_4$ and $YBa_2Cu_3O_7$, no $pp\sigma$ or $pp\pi$ interactions occurred between nearest-neighbor atoms, and the results were insensitive to the value $\eta_{sp\sigma} = 0.9$ used for those materials.) To obtain the new parameters, we fitted the LDA energy bands of Mattheiss and Hamann[204] for $BaBiO_3$ and $BaPbO_3$. The energy parameters for Tl were extrapolated from those of Pb and Bi. The resulting atomic parameters are listed in Table 3.1; the interatomic strengths are $\eta_{sp\sigma} = 1.4$, $\eta_{pp\sigma} = 1.5$, and $\eta_{pp\pi} = -0.6$, as listed in Chapter III.

In order to find better agreement between the tight-binding and LDA bands for $Bi_2Sr_2CuO_6$ and $Bi_2CaSr_2Cu_2O_8$ (discussed in the next section), we have included the second-neighbor Bi–Bi interactions, using the same interatomic strengths and distance scaling as for nearest neighbors, but neglecting $d - d$ interactions. (To be precise, interactions between the large Bi atoms are included when the interatomic separation is less than 3.9 Å.) We regard these Bi–Bi interactions as justified by the large covalent radius of Bi and the relatively small lattice parameter $a \approx 3.81$ Å in these phases,[49,65] even though only nearest-neighbor interactions were needed for $La_{1.85}Sr_{0.15}CuO_4$ and $YBa_2Cu_3O_7$. We ignore the long-range structural modulation,[48–50,64–66] which should have only a minor effect on the electronic properties. The displacements of the atoms in

the BiO layers are also neglected.[48,55,66] Although this approximation allows direct comparison between the tight-binding results and the LDA calculations (which also used the idealized atomic positions), there may be significant effects in the electronic structure associated with the BiO disorder, particularly for the Bi p bands.

We use the bct crystal structure and idealized atomic positions[65] of $Bi_2Sr_2CuO_6$, with $a = 3.810$ Å and $c = 24.607$ Å. The energy bands are shown in Fig. 4.7 along the symmetry lines of the bct cell,[172] with D labeling the point at the Brillouin zone boundary in the [100] direction. The bands show two-dimensional structure, such as the symmetry of the bands along ΓX and ZX. A single Cu(d)–O(p) antibonding band crosses E_F along ΓX, peaking 1.5 eV above the Fermi energy at X, compared with 1.6 eV in the LDA calculation.[205] The Bi p states form dispersive bands up to ≈ 3 eV above E_F. For this idealized structure, two Bi p bands dip below the Fermi energy at D to a minimum of -0.7 eV. The LDA calculation finds the Bi p bands to cross below E_F to -0.1 eV.[205] The disorder in the BiO layers may decrease the dispersion and prevent these occupied electron pockets from forming.[66,205]

The local densities of states for the metal atoms in $Bi_2Sr_2CuO_6$ are shown in Fig. 4.8, with those for oxygen in Fig. 4.9. Oxygen site O(1) is in the CuO_2 plane, O(2) in the SrO layer, and O(3) in the BiO double layer. The Bi p bands give a small contribution to $\rho(E_F)$ from their dispersion to E_F, but the Sr d bands are unoccupied. The occupied Bi s bands peak near -10 eV, while the Bi d bands lie far below E_F near -24 eV. Cu and O(1) display broad features characteristic of the in-plane $pd\sigma$ bonds. O(2) has relatively narrow p bands, while O(3) shows significant mixing with the Bi s and p bands. This material

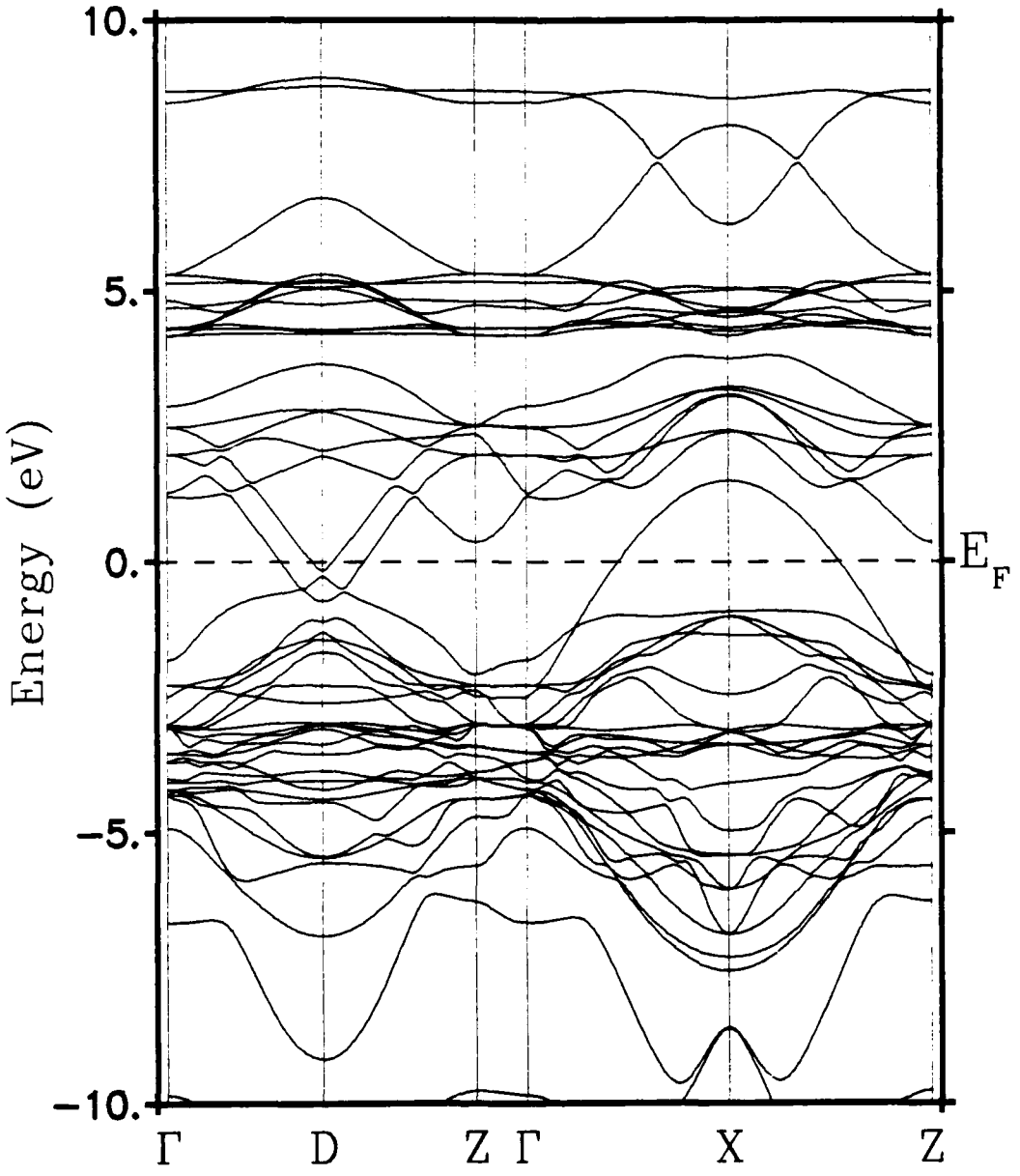

Fig. 4.7. Electronic energy bands for $Bi_2Sr_2CuO_6$.

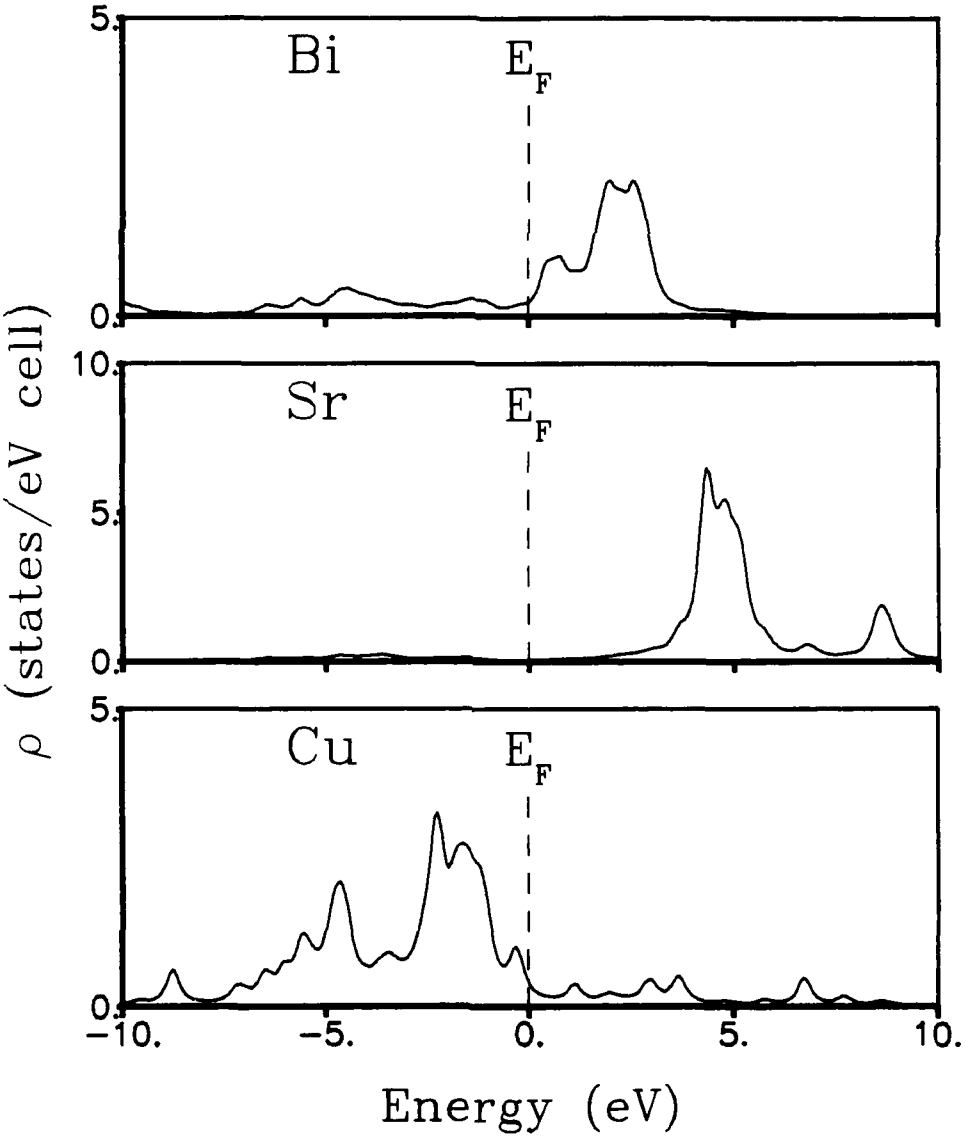

Fig. 4.8. Local densities of states for the metal atoms in $Bi_2Sr_2CuO_6$.

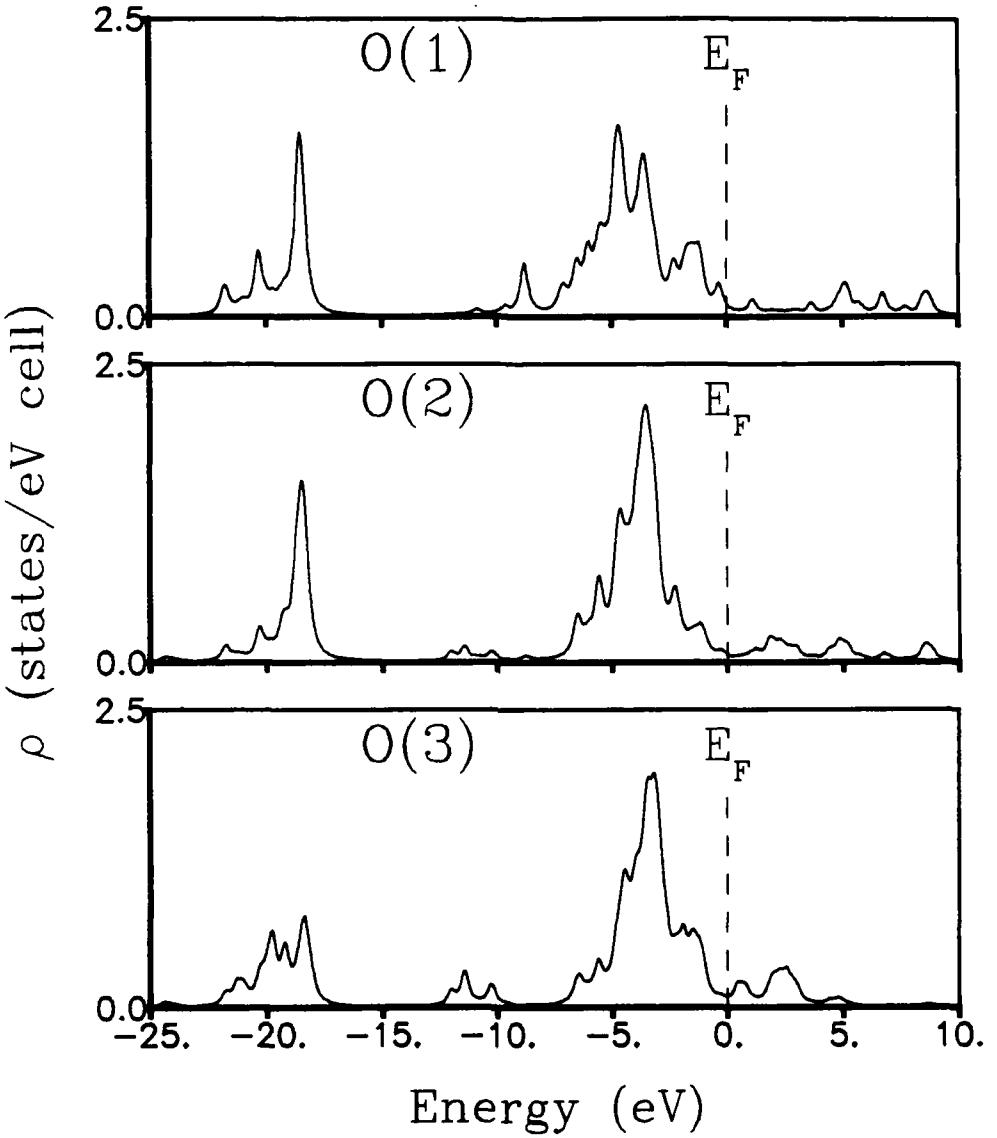

Fig. 4.9. Local densities of states for the oxygen atoms in $Bi_2Sr_2CuO_6$.

TABLE 4.2. Valences Δn for Bi–Ca–Sr–Cu–O superconductors.

	Bi	Ca	Sr	Cu	O(1)	O(2)	O(3)
$Bi_2Sr_2CuO_6$	1.83	···	1.15	0.87	-1.05	-1.18	-1.20
$Bi_2CaSr_2Cu_2O_8$	1.80	1.51	1.09	0.84	-1.09	-1.14	-1.18

has $\rho(E_F) = 1.6$ states/eV cell.

Table 4.2 lists the valences for $Bi_2Sr_2CuO_6$. The charges associated with Cu and O(1) are smaller than those of the CuO_2 plane sites of $La_{1.85}Sr_{0.15}CuO_4$ and of $YBa_2Cu_3O_7$ in Table 4.1. It is conceivable that the lower carrier density associated with the single CuO_2 layer accounts for the low superconducting transition temperature of 6 K in this phase, although the single CuO_2 layer of $La_{1.85}Sr_{0.15}CuO_4$ allows superconductivity up to 38 K. The BiO disorder may also contribute to the low T_c.[66]

$Bi_2CaSr_2Cu_2O_8$

The bct crystal structure and idealized atomic positions are used for $Bi_2CaSr_2Cu_2O_8$,[49] again neglecting the long-range structural modulation and the BiO disorder.[48-55] The lattice parameters are $a = 3.814$ Å and $c = 30.52$ Å for the bct cell.[49] The energy bands for $Bi_2CaSr_2Cu_2O_8$ along the symmetry lines of the Brillouin zone for the bct crystal structure[172] are shown in Fig. 4.10. These bands are quite similar to the results of several LDA calculations.[205-209] Strong two-dimensional character is observed, with little dispersion in the direction perpendicular to the copper-oxygen planes. The dispersive Cu(d)-O(p) bands have a width of about 12 eV at X, somewhat larger than the LDA bandwidths of 8.7 eV[205] and 9.5 eV.[206] Two $pd\sigma$ antibonding bands cross the Fermi energy from below to a peak of 1.6 eV at X, compared with 1.7 eV in Ref. 205, 2.2 eV in Refs. 207 and 209, 2.4 eV in Ref. 206, and 2.8 eV in Ref. 208. As in the LDA calculations, two Bi p bands disperse down to the Fermi energy, with one band crossing below E_F to -0.7 eV at D. This forms occupied electron pockets near the Brillouin zone boundary. However, this effect may be destroyed by the

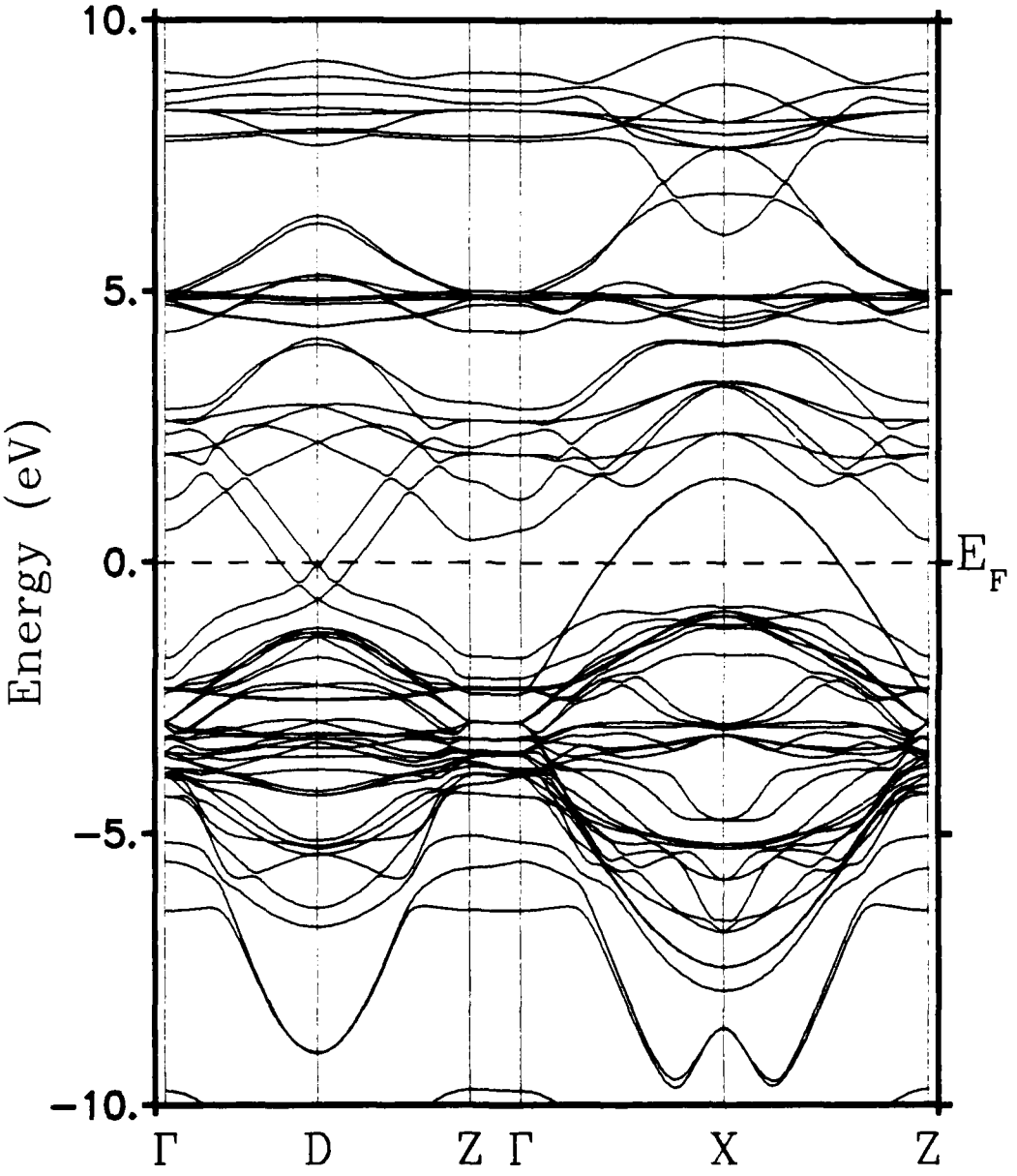

Fig. 4.10. Electronic energy bands for $Bi_2CaSr_2Cu_2O_8$.

disorder in the BiO layers.[55]

Figure 4.11 shows the local densities of states for Bi, Ca, Sr, and Cu, with the results for oxygen shown in Fig. 4.12. The notation for the oxygen sites is the same as for $Bi_2Sr_2CuO_6$ in the previous section. The Bi d bands lie approximately 24 eV below the Fermi energy, while the Bi p bands, centered slightly above E_F, interact strongly to produce a metallic contribution to $\rho(E_F)$. The Ca d and Sr d states are above E_F, and are quite ionic. The Cu and O(1) sites show strong interactions, related to the $pd\sigma$ bonds, resulting in the antibonding bands protruding above E_F in Fig. 4.10. The O(2) and O(3) sites show primarily p character just below the Fermi energy (with s bands far below E_F), but some p character is distributed above the Fermi energy because of mixing with the s and p orbitals of neighboring Bi. The density of states at the Fermi energy is 2.4 states/eV cell, comparable to the value $\rho(E_F) = 2.1$ states eV cell from Ref. 206. This gives a $\rho(E_F)$ larger than in $Bi_2Sr_2CuO_6$. However, the specific value of $\rho(E_F)$ is somewhat sensitive to the model,[205-209] and may be affected by the BiO disorder.

The atomic valences Δn are presented in Table 4.2. The valences are quite similar to those for $Bi_2Sr_2CuO_6$. The two adjacent CuO_2 planes, separated by the Ca ion, may support a larger carrier density in $Bi_2CaSr_2Cu_2O_8$ than in $Bi_2Sr_2CuO_6$. Combined with the larger $\rho(E_F)$, this may account for the higher transition temperature of 85 K in this phase.

Photoemission studies[210-216] of $Bi_2CaSr_2Cu_2O_8$ confirm the basic occupied electronic states of the tight-binding and LDA calculations[205-209] (with some discrepancies in detail). The spectral features near E_F are again observed to be more tightly bound by approximately 1.5 eV with respect to the calculated

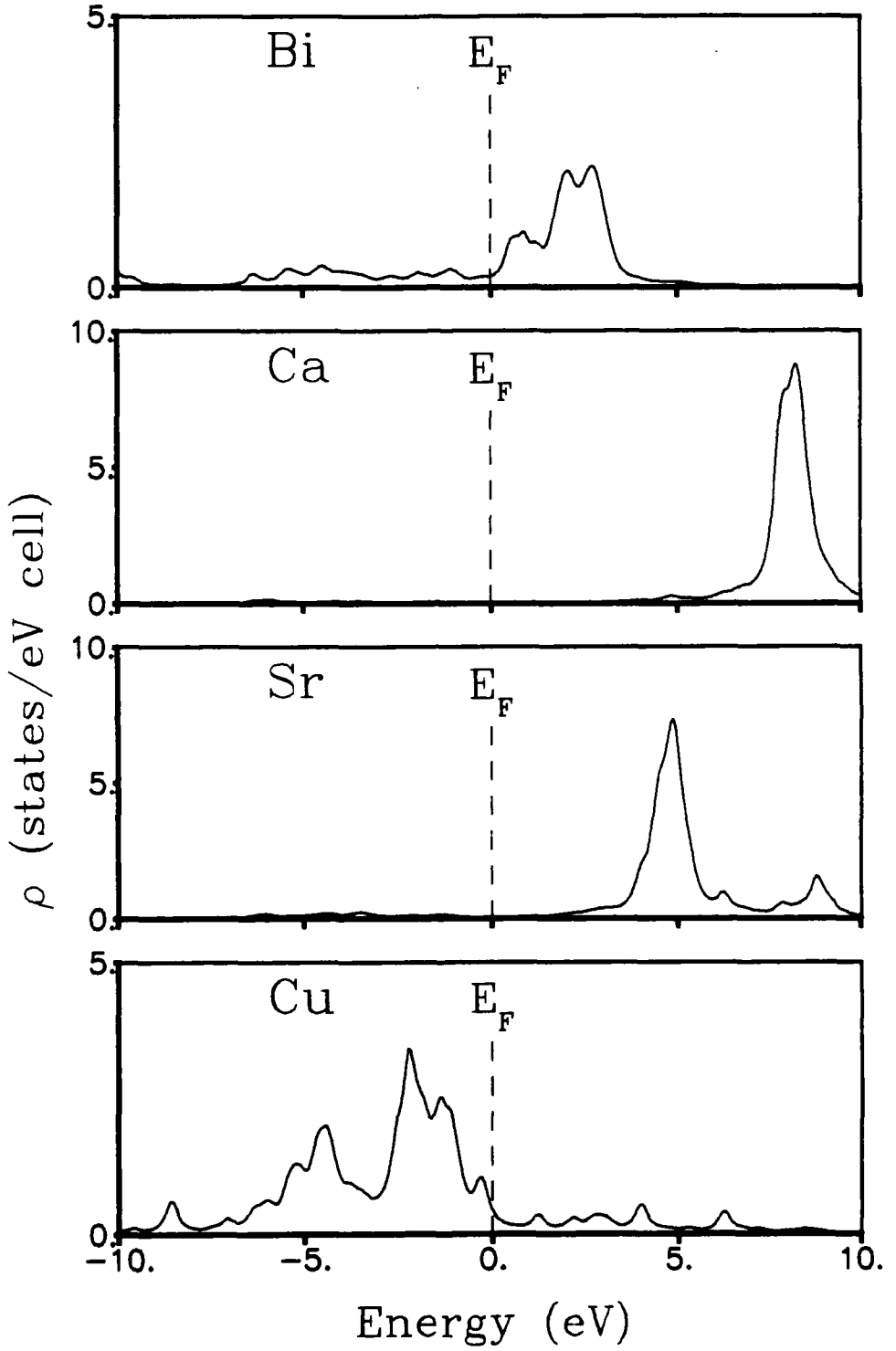

Fig. 4.11. Local densities of states for the metal atoms in $Bi_2CaSr_2Cu_2O_8$.

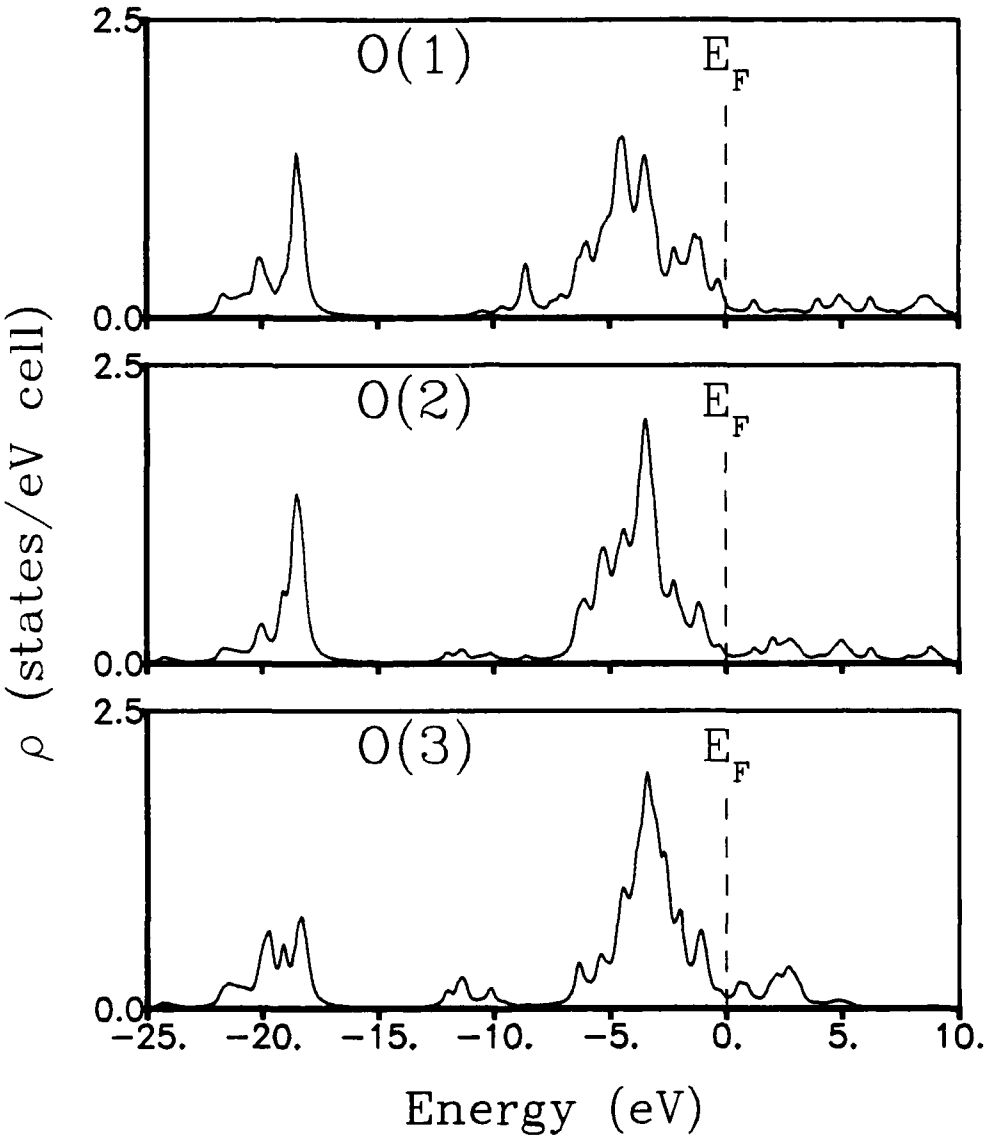

Fig. 4.12. Local densities of states for the oxygen atoms in $Bi_2CaSr_2Cu_2O_8$.

density of states. These copper-oxygen hybrid states form occupied bands extending from -8 eV to a clear cutoff at E_F.[210-216] The photoemission feature observed at a binding energy of $10 - 11$ eV corresponds to the occupied Bi s bands of the calculations,[210-213] while the O s spectra appear near -20 eV.[210] Some Bi p character has been observed at the Fermi energy.[213,216]

Angle-resolved resonant photoemission studies[217] indicate an energy band dispersion of 0.2 to 0.5 eV near the Fermi energy along the ΓX symmetry line in $Bi_2CaSr_2Cu_2O_8$. The hole carriers are observed only on the oxygen sites because of strong Coulomb repulsion on the copper sites.[217,212] Oxygen p states just above E_F are observed with resonant photoemission from the occupied oxygen s states.[217] These empty states have only p_x and p_y symmetry, so that the oxygen holes are well-confined in the CuO_2 planes.[212]

Inverse photoemission measurements[218] of $Bi_2CaSr_2Cu_2O_8$ reveal unoccupied states similar to the tight-binding density of states, although the empty Ca d and Sr d bands appear at higher energies above E_F than calculated. The Bi p states form a dispersive band centered ≈ 4 eV above E_F.[218]

$Tl_2Ba_2CuO_6$

We now consider the electronic structure of the thallium-containing superconductors. As noted above, the tight-binding energies ϵ_s, ϵ_p, and ϵ_d for Tl in Table 3.1 were extrapolated from the fitted parameters for Pb and Bi. Because of the similarity of the crystal structures for the Tl and Bi cuprates, we included the same second-neighbor Tl–Tl interactions that were required for the Bi atoms to properly model the electronic structures of the Bi cuprates. Since Tl and Bi have similar covalent radii and the same type of valence orbitals, we

expect their bonding properties to be similar in the tight-binding model. None of the Tl cuprates appear to have superlattice modulations as do the Bi cuprates. However, there are well-characterized displacements of the Tl and O atoms in the TlO layers, similar to the BiO disorder.[66,70-73] We have incorporated these displacements in the atomic substructure of each system. However, for this calculation we neglect any partial substitutions between the Tl and Ca sites,[66,70,72] and assume full occupation for these sites.

The bct crystal structure of $Tl_2Ba_2CuO_6$ has the lattice parameters a = 3.866 Å and c = 23.239 Å.[66] The single CuO_2 layer in the structure of this T_c = 83 K superconductor is strictly planar. The calculated electronic energy bands along the symmetry lines of the Brillouin zone[172] are shown in Fig. 4.13, with the zero of energy shifted to E_F. The bands are virtually dispersionless along ΓZ, perpendicular to the CuO_2 plane, and are dominated as usual by the $pd\sigma$ antibonding band of Cu(d)–O(p) near the Fermi energy. The $pd\sigma$ band peaks 1.6 eV above E_F at X. The LDA calculations[219,220] show this band peaking slightly higher in energy (2.2 eV in Ref. 219 and 2.8 eV in Ref. 220). The Tl–Tl in-plane interactions cause the Tl p bands to disperse by about 3 eV from Γ to D along the [100] direction in Fig. 4.13. These bands do not dip below the Fermi energy as do the Bi p bands in $Bi_2Sr_2CuO_6$ and $Bi_2CaSr_2Cu_2O_8$, but the Tl(s)–O(p) hybrid states do cross below E_F to about −0.5 eV at Γ, forming occupied electron pockets. A smaller dispersion below E_F to about −0.1 eV is seen in the LDA calculation for the Tl s bands.[219]

The local densities of states for the metal and the oxygen sites are shown in Figs. 4.14 and 4.15. The notation for the oxygen sites is similar to that for $Bi_2Sr_2CuO_6$: O(1) is in the CuO_2 plane, O(2) is in the BaO region separating

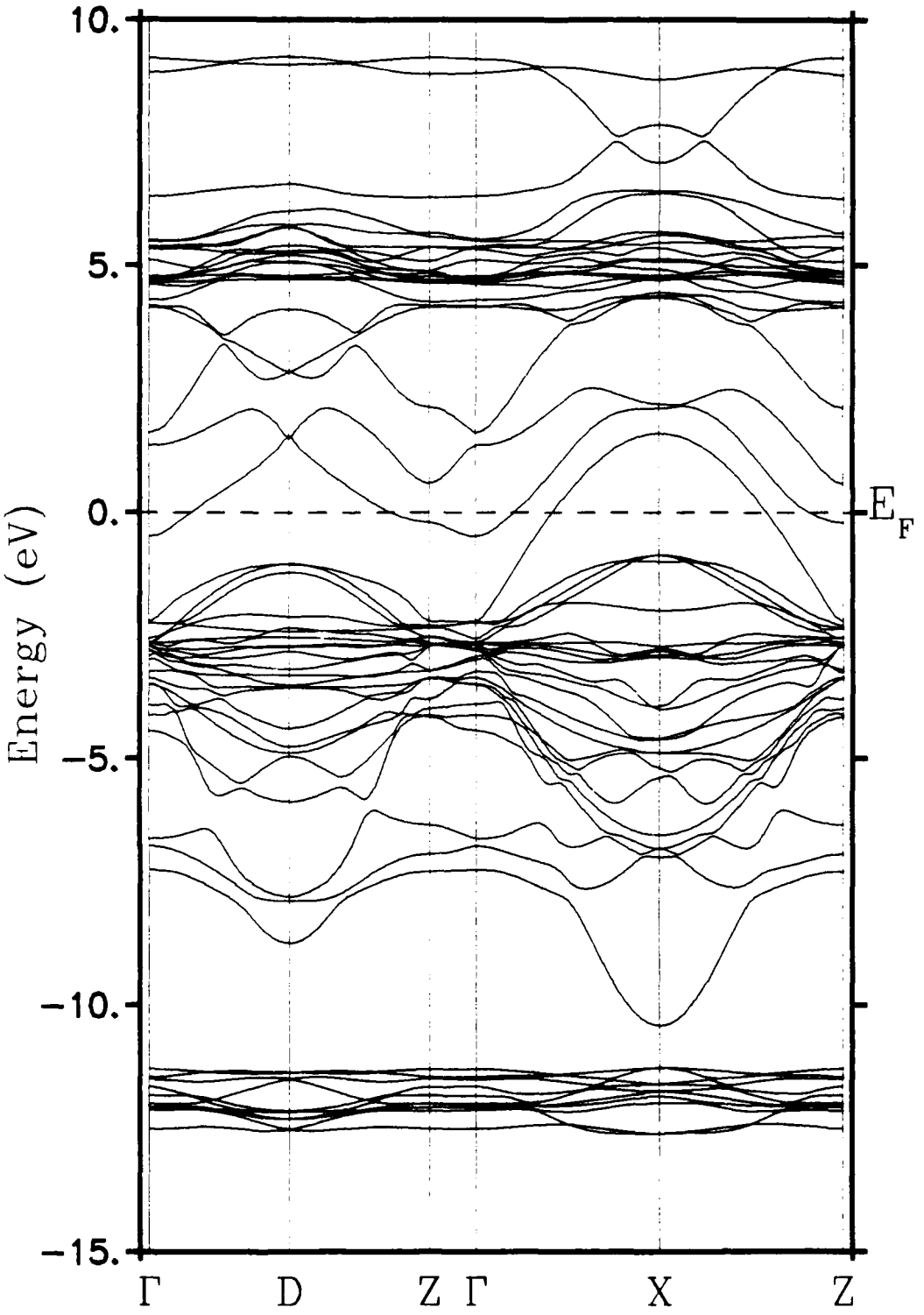

Fig. 4.13. Electronic energy bands for $Tl_2Ba_2CuO_6$.

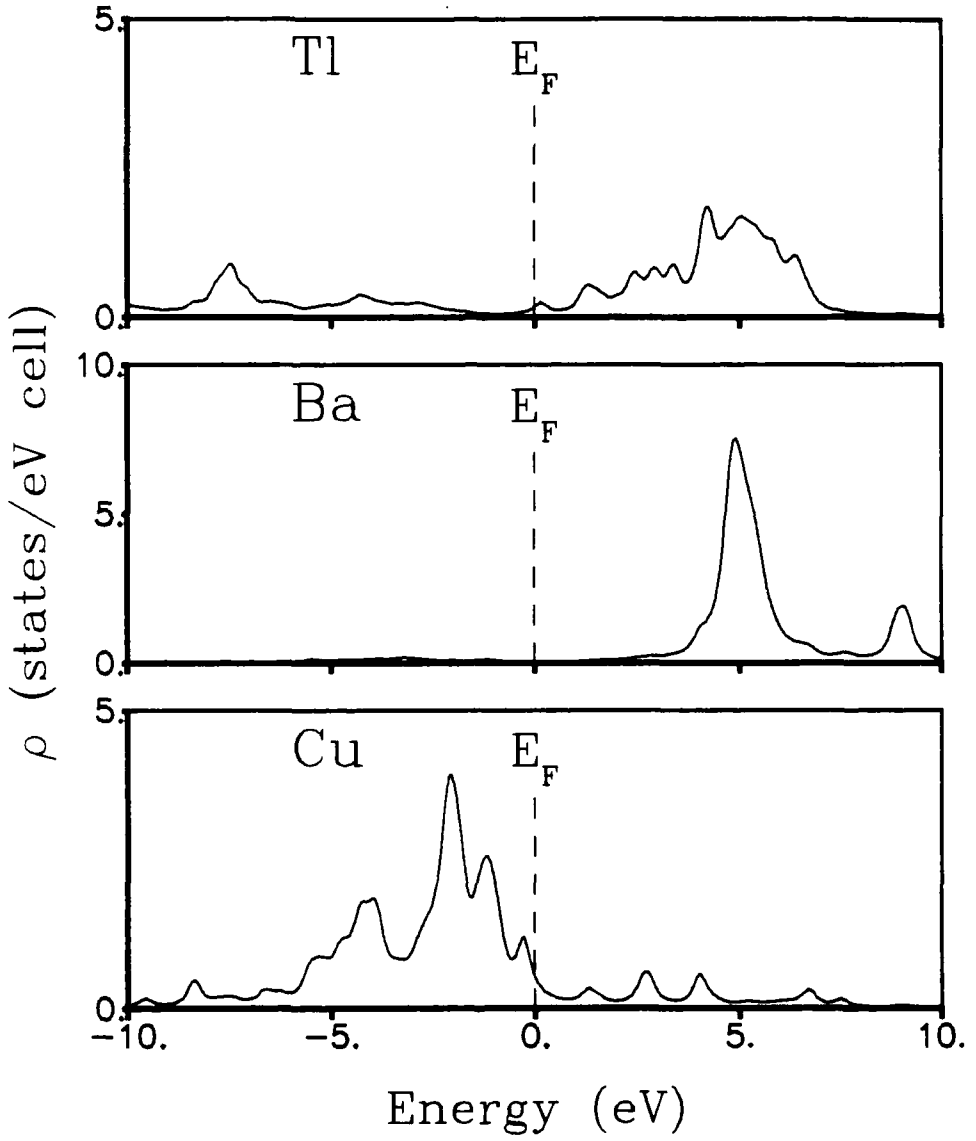

Fig. 4.14. Local densities of states for the metal atoms in $Tl_2Ba_2CuO_6$.

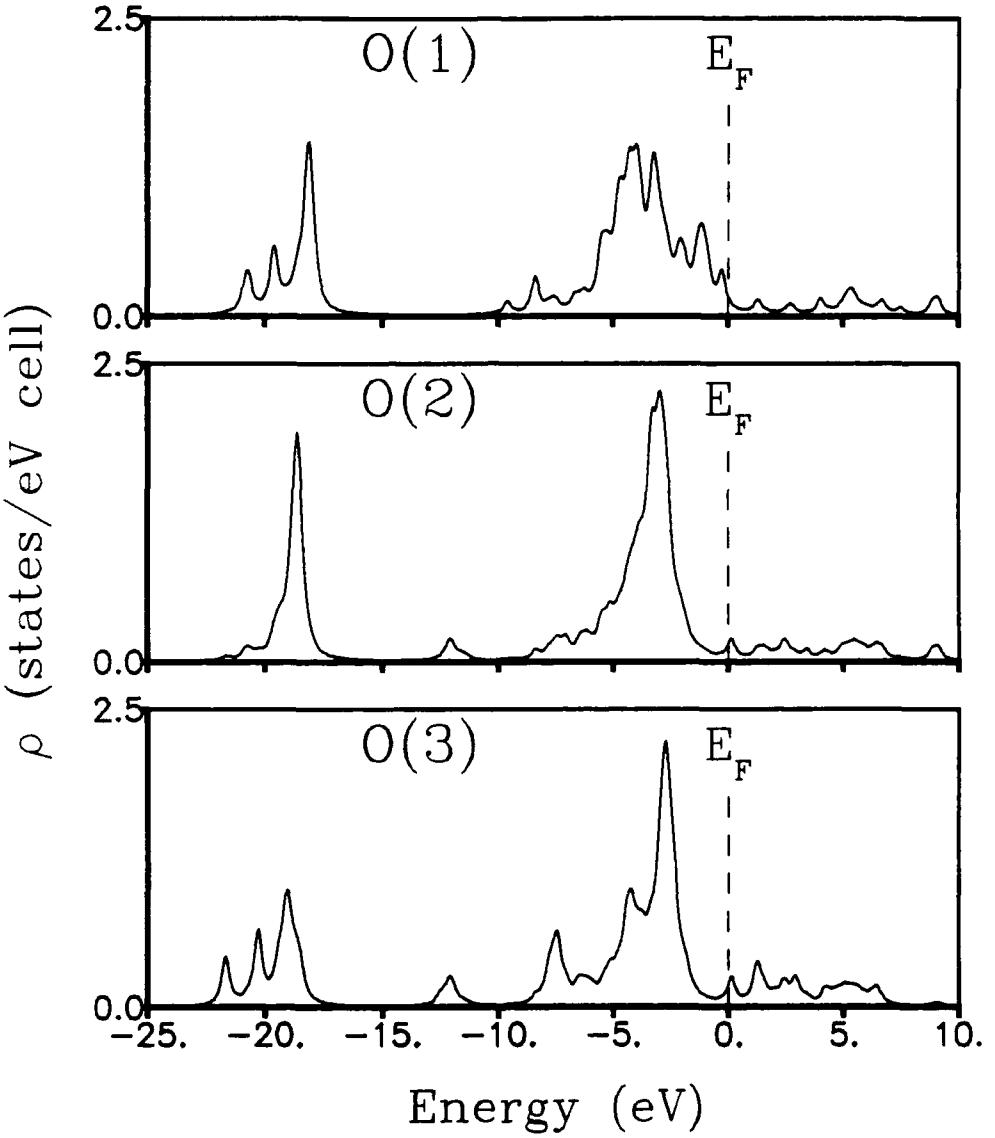

Fig. 4.15. Local densities of states for the oxygen atoms in $Tl_2Ba_2CuO_6$.

TABLE 4.3. Valences Δn for Tl-Ca-Ba-Cu-O superconductors.

	Tl	Ca[a]	Ba	Cu(1)[b]	Cu(2)	O(1)	O(2)	O(3)	O(4)
$Tl_2Ba_2CuO_6$	1.05	···	1.36	0.89	···	-1.10	-1.04	-0.72	···
$Tl_2CaBa_2Cu_2O_8$	1.05	1.45	1.37	0.86	···	-1.13	-1.03	-0.71	···
$Tl_2Ca_2Ba_2Cu_3O_{10}$	1.06	1.45	1.38	0.54	1.02	-1.27	-1.09	-1.08	-0.65
$TlCa_3Ba_2Cu_4O_{11}$	1.07	1.45	1.36	0.90	1.07	-1.12	-1.06	-1.10	-1.17

[a] Averaged over inner Ca(1) and outer Ca(2) sites for $TlCa_3Ba_2Cu_4O_{11}$.

[b] Cu site for $Tl_2Ba_2CuO_6$ and $Tl_2CaBa_2Cu_2O_8$.

the Cu and Tl layers, and O(3) is in the TlO layer. The dispersive Tl p bands range from 3 to 6 eV above E_F, while the s states give a metallic contribution to $\rho(E_F)$. Cu and O(1) show broad features below E_F arising from the in-plane bonding. In the present model, the total density of states at the Fermi energy is 2.0 states/eV cell.

The valences for $Tl_2Ba_2CuO_6$ are shown in Table 4.3. Notice that the valences for the Cu and O(1) sites are very close to the corresponding valences for the plane sites in $Bi_2Sr_2CuO_6$ and $Bi_2CaSr_2Cu_2O_8$ shown in Table 4.2. The charge associated with Tl is significantly smaller than that found on the Bi sites, even though both atoms are considered to have a formal valence of 3− in these materials. The Ba atoms appear more ionic than the corresponding Sr atoms in $Bi_2Sr_2CuO_6$ and $Bi_2CaSr_2Cu_2O_8$.

$Tl_2CaBa_2Cu_2O_8$

The lattice parameters for the bct crystal structure of $Tl_2CaBa_2Cu_2O_8$ are $a = 3.855$ Å and $c = 29.318$ Å.[70] The increase in the c axis is consistent with the inclusion of a $CaCuO_2$ layer into $Tl_2Ba_2CuO_6$, with a separation between copper layers of ≈ 3.2 Å. As noted above, the displacements of the oxygens in the TlO layers from their ideal positions are included in the tight-binding model. The energy bands calculated for $Tl_2CaBa_2Cu_2O_8$ are shown in Fig. 4.16. Two degenerate Cu(d)–O(p) states protrude above the Fermi energy to a peak of 1.6 eV at X, corresponding to the two adjacent CuO_2 planes in this material. The LDA calculations show similar bands peaking 2.2 eV[221] and 3.0 eV[220] above E_F. The width of the Cu–O manifold is ≈ 12 eV at X, somewhat larger than the bandwidth of 9 eV in the LDA results.[221] The unoccupied Tl p bands are again

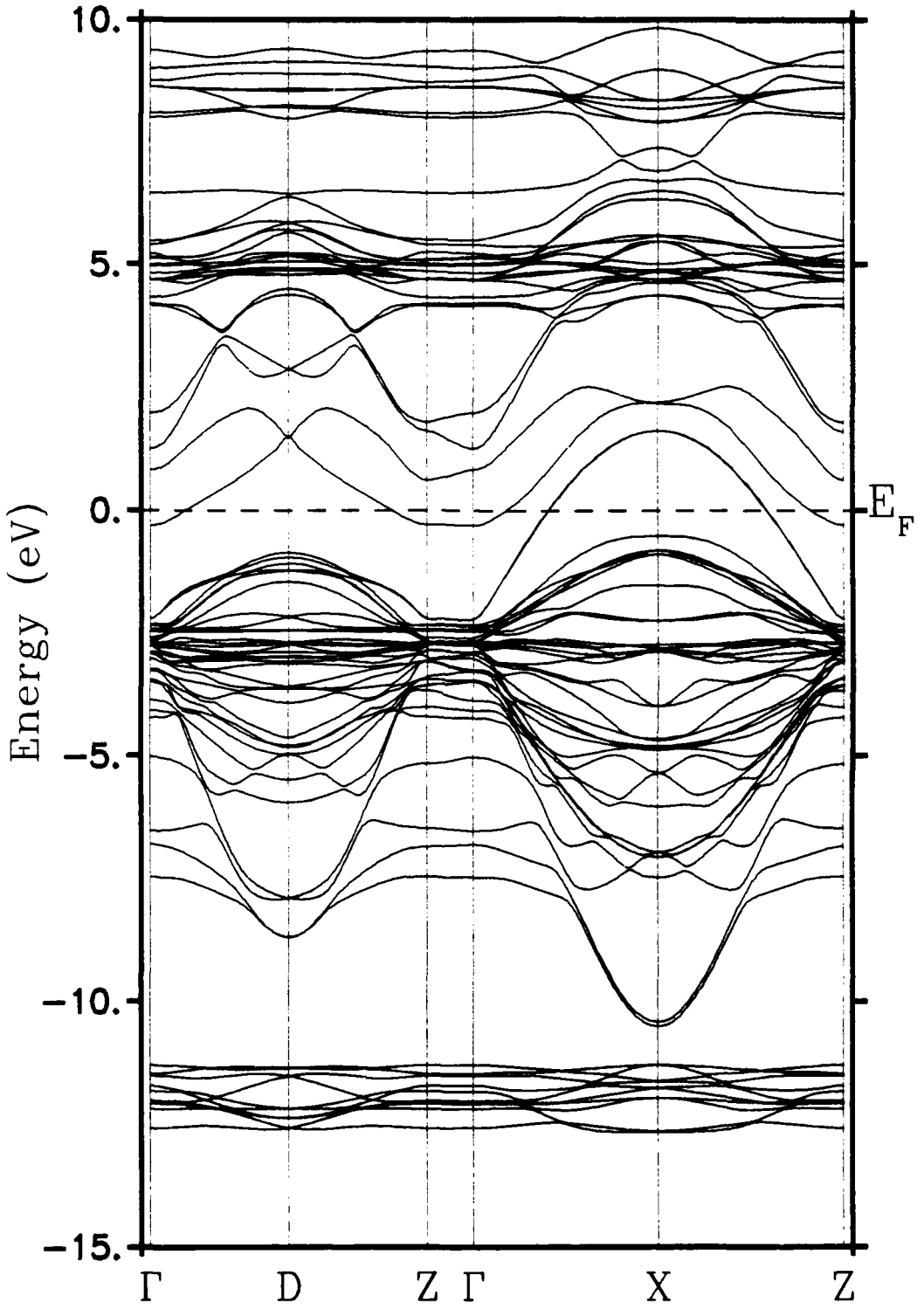

Fig. 4.16. Electronic energy bands for $Tl_2CaBa_2Cu_2O_8$.

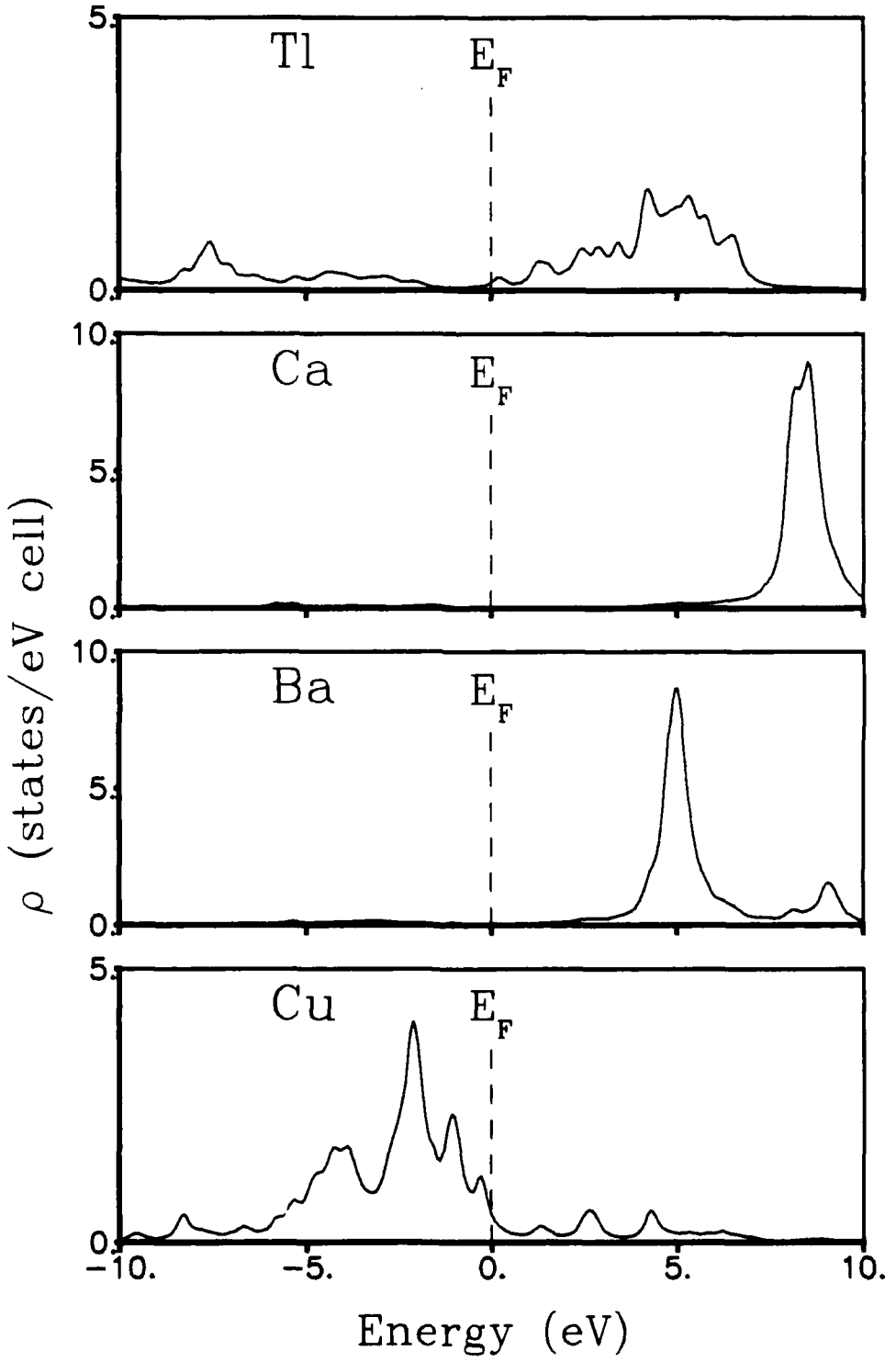

Fig. 4.17. Local densities of states for the metal atoms in $Tl_2CaBa_2Cu_2O_8$.

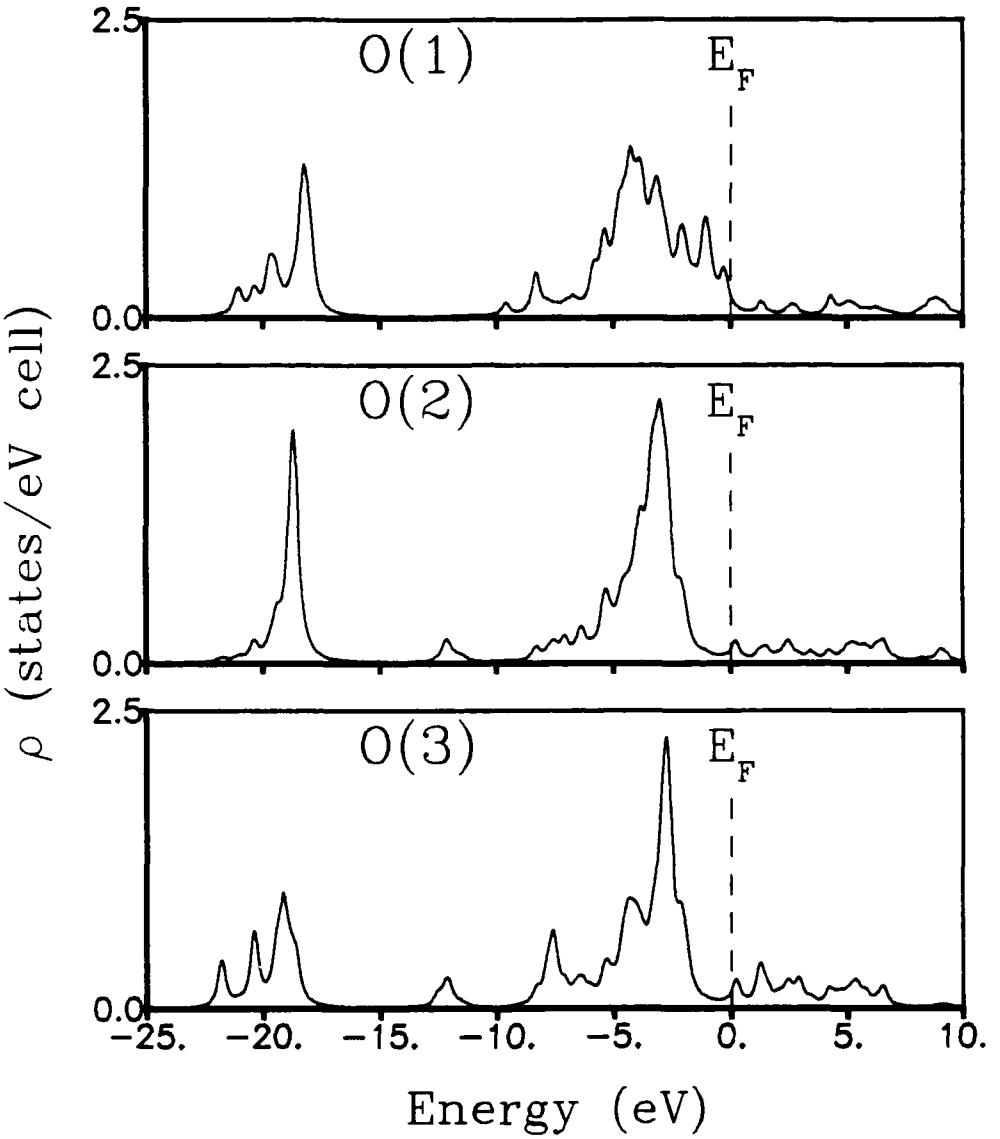

Fig. 4.18. Local densities of states for the oxygen atoms in $Tl_2CaBa_2Cu_2O_8$.

well-removed from the Fermi energy. The Tl(s)–O(p) hybrid bands disperse below the Fermi energy to -0.3 eV at the symmetry points Γ and Z, compared with an overlap of 0.1 to 0.2 eV in the LDA calculations.[220,221]

The local densities of states for Tl, Ca, Ba, and Cu are shown in Fig. 4.17, with those for oxygen presented in Fig. 4.18. The notation for the oxygen sites is the same as for $Tl_2Ba_2CuO_6$ in the previous section. The Tl d bands lie $\approx$ 12 eV below the Fermi energy, with Tl(s)–O(p) bonding states falling near -8 eV. The Ca d and Ba d states are unoccupied and insulating, with no contribution to $\rho(E_F)$. The Tl p bands above E_F interact somewhat weakly with the neighboring O(3) sites. The Cu and O(1) sites show strong $pd\sigma$ interactions, with the antibonding bands protruding above E_F at X in Fig. 4.16. The total density of states at the Fermi energy is 2.7 states/eV cell. The increase in $\rho(E_F)$ with respect to that for $Tl_2Ba_2CuO_6$ is attributed primarily to the extra CuO_2 plane in $Tl_2CaBa_2Cu_2O_8$.

The valences for $Tl_2CaBa_2Cu_2O_8$ are shown in Table 4.3, and are very similar to those for $Tl_2Ba_2CuO_6$. The most significant factor contributing to the higher T_c of 112 K in $Tl_2CaBa_2Cu_2O_8$ may be the increase in $\rho(E_F)$ associated with the double CuO_2 layers.

$Tl_2Ca_2Ba_2Cu_3O_{10}$

The triple CuO_2 layers of $Tl_2Ca_2Ba_2Cu_3O_{10}$ increase the c axis of the bct crystal structure to 35.88 Å, with a = 3.850 Å.[72] The increase in the c axis is again consistent with adding a $CaCuO_2$ layer to $Tl_2CaBa_2Cu_2O_8$. The displacements of the oxygens in the TlO layers are again included in the atomic substructure for the tight-binding model. The electronic energy bands

of $Tl_2Ca_2Ba_2Cu_3O_{10}$ are shown in Fig. 4.19. This 125 K superconductor has a triply-degenerate antibonding Cu(d)–O(p) band that crosses E_F along the ΓX symmetry line. This band peaks near 1.7 eV at X in the tight-binding results, compared with 2.5 eV[220] and 2.2 eV[221] in the LDA calculations. The Cu–O bandwidth at D (the point at the Brillouin zone boundary in the [100] direction) is 7.9 eV, somewhat larger than the LDA result of 5.8 eV.[221] Small electron pockets are again formed by Tl(s)–O(p) antibonding states that dip below E_F to -0.6 eV at the symmetry points Γ and Z. The LDA calculation[221] shows the occupied band dipping to -0.3 eV at Γ.

The local densities of states for the metal atoms of $Tl_2Ca_2Ba_2Cu_3O_{10}$ are shown in Fig. 4.20, with those for the oxygen atoms shown in Fig. 4.21. Two crystallographically distinct copper sites exist in this structure: Cu(1) lies in the center of the triple CuO_2 layers, and is separated by Ca ions from the outer CuO_2 planes with the Cu(2) site. The notation for the oxygen atoms places O(1) in the central CuO_2 plane, O(2) in the outer CuO_2 planes, O(3) in the BaO layer, and O(4) in the TlO layer. Cu(1) appears more ionic than Cu(2), with a narrower local density of states. O(3) and O(4) also have relatively narrow spectra, related to the ionic nature of the bonds formed with Ba and Tl. Tl p states form a broad band above E_F, with Tl s states contributing to $\rho(E_F)$. The total density of states at E_F for $Tl_2Ca_2Ba_2Cu_3O_{10}$ is 5.3 states/eV cell, considerably larger than $\rho(E_F)$ for the other Tl cuprates, but quite sensitive to small changes in E_F.

The atomic valences in Table 4.3 show that Cu(2), in the outer CuO_2 planes adjacent to the BaO layers, has a higher valence than that of Cu in $Tl_2Ba_2CuO_6$ and $Tl_2CaBa_2Cu_2O_8$. However, the central Cu(1) site shows a decreased valence

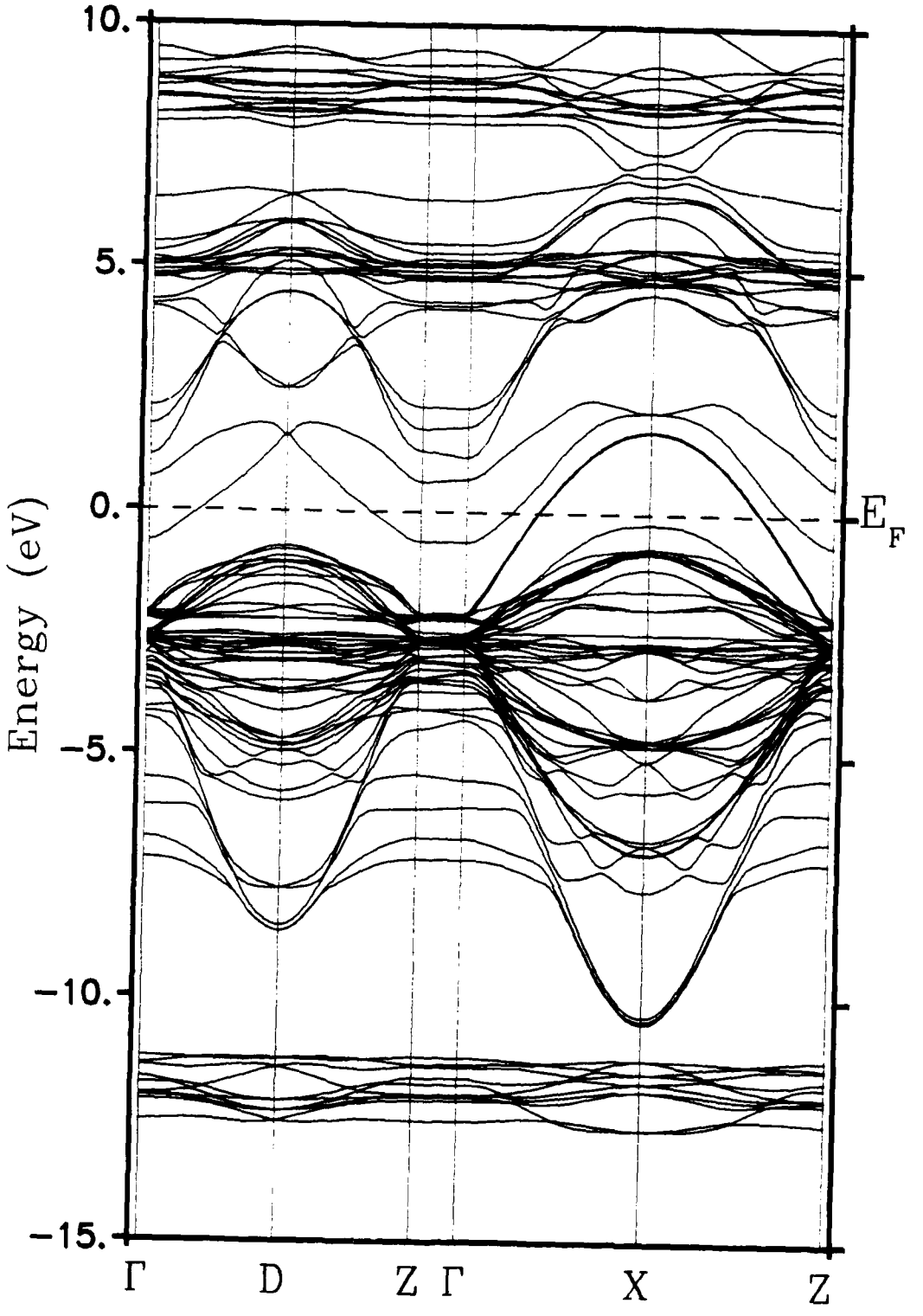

Fig. 4.19. Electronic energy bands for $Tl_2Ca_2Ba_2Cu_3O_{10}$.

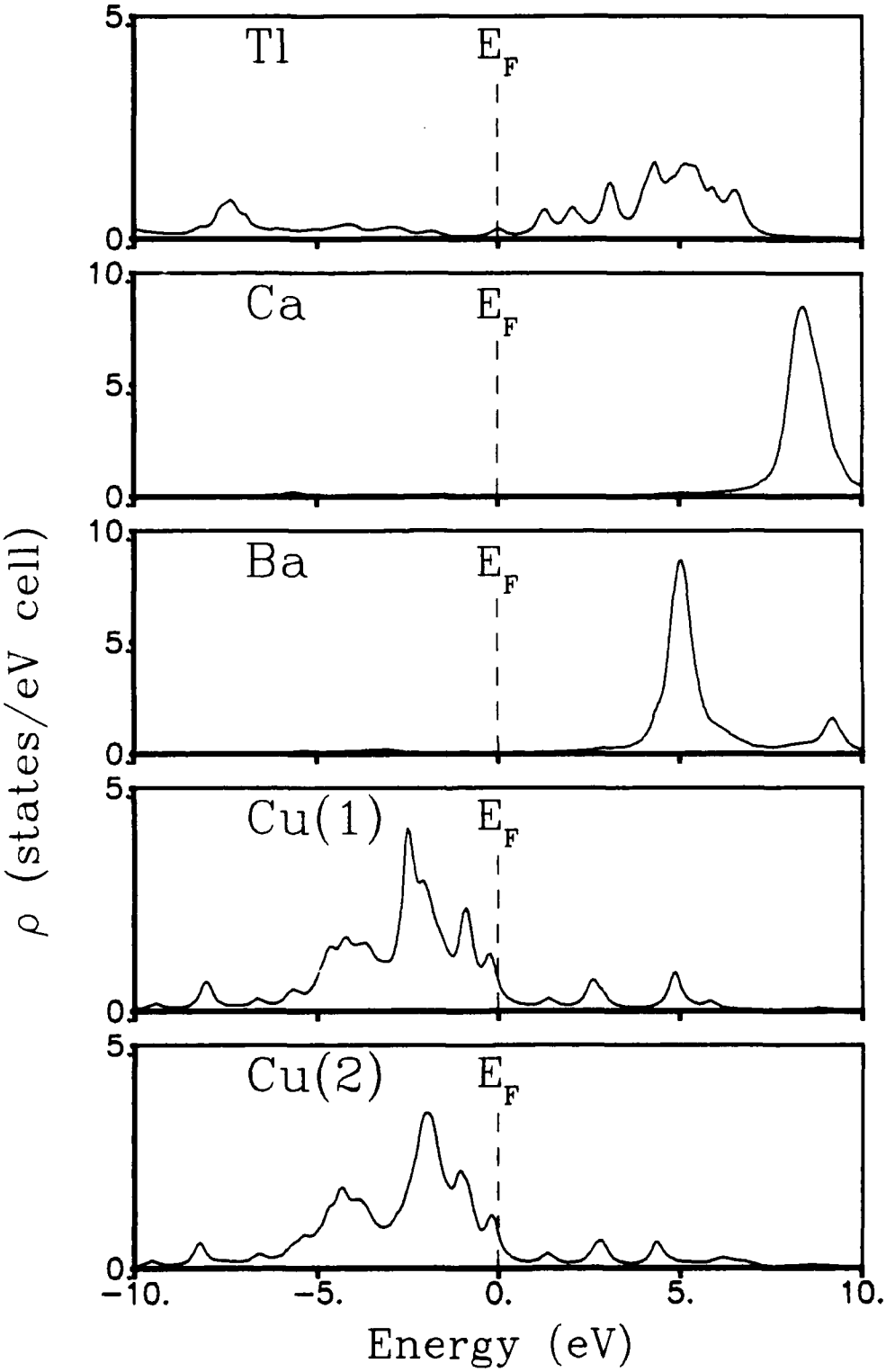

Fig. 4.20. Local densities of states for the metal atoms in $Tl_2Ca_2Ba_2Cu_3O_{10}$.

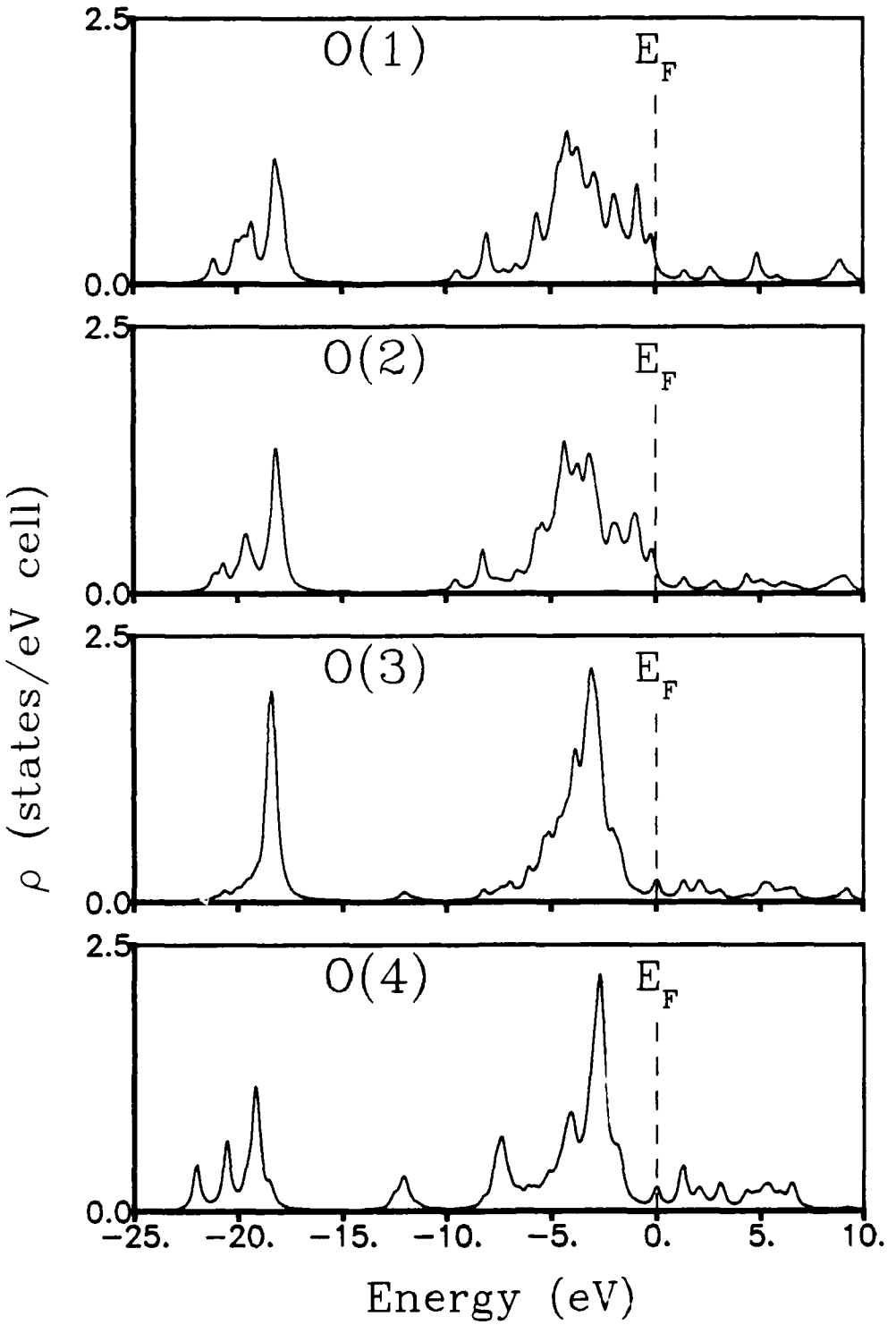

Fig. 4.21. Local densities of states for the oxygen atoms in $Tl_2Ca_2Ba_2Cu_3O_{10}$.

of only 0.54, while the O(1) site has substantially more negative charge than the O(2) site in the outer CuO_2 planes. The bonds in the central CuO_2 plane thus seem more ionic than in the outer CuO_2 planes. The prediction of a greatly reduced valence for the central Cu(1) atom in $Tl_2Ca_2Ba_2Cu_3O_{10}$ may be experimentally testable.

Photoemission and inverse photoemission studies of $Tl_2Ca_2Ba_2Cu_3O_{10}$ have revealed the occupied and vacant electronic states.[222] The occupied copper-oxygen bands within ≈ 8 eV below E_F are more tightly bound by about 1.5 eV than the calculated results. Tl may contribute some s character at E_F as found in the tight-binding and LDA results.[220-221] Unoccupied bands are observed at 3.7, 9.6, and 14 eV, associated with Tl p, Ba d, Ca d, and Ba f empty states.[222] These results are in reasonable agreement with the calculated densities of states (the Ba f states were ignored in the tight-binding model). Oxygen p holes are observed near E_F with resonant inverse photoemission.[222]

$TlCa_3Ba_2Cu_4O_{11}$

We next examine $TlCa_3Ba_2Cu_4O_{11}$ as a representative member of the Tl cuprates that contain only a single TlO layer per unit cell. This particular phase has $T_c = 122$ K, and has a simple tetragonal structure with $a = 3.85$ Å and $c = 19.01$ Å.[78,79] The atomic positions for $TlCa_3Ba_2Cu_4O_{11}$ were extrapolated from those of the analogous single TlO layer superconductor $TlCa_2Ba_2Cu_3O_9$ by inserting an additional $CaCuO_2$ layer.[76] Lacking other experimental data, the idealized atomic positions for the TlO layer have been used in this case. The electronic energy bands of $TlCa_3Ba_2Cu_4O_{11}$ are shown in Fig. 4.22 along the symmetry lines of the simple tetragonal Brillouin zone.[172] The point X lies

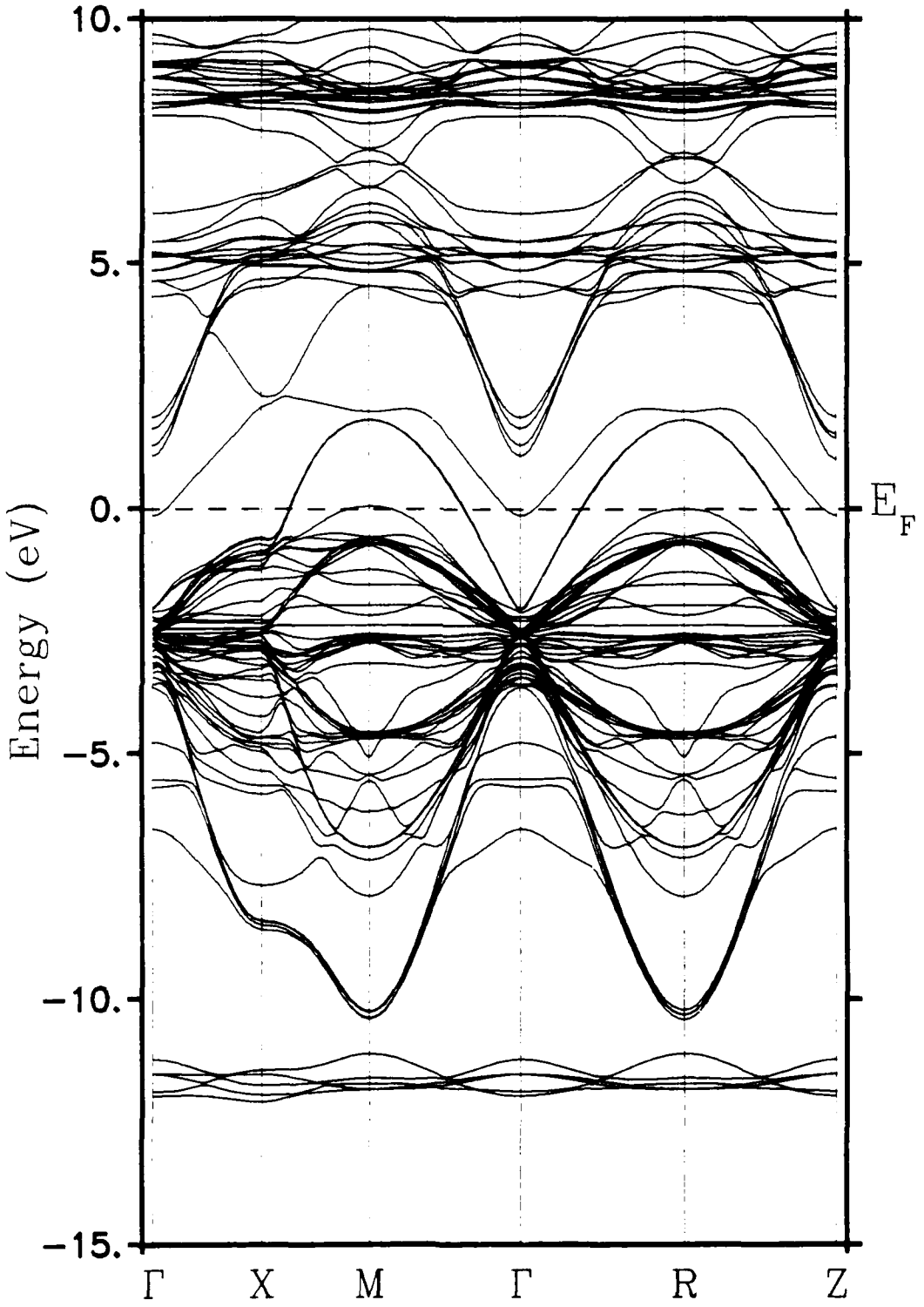

Fig. 4.22. Electronic energy bands for $TlCa_3Ba_2Cu_4O_{11}$.

along the [100] axis, and M lies at the Brillouin zone boundary along the [110] direction. The crystal structure contains four CuO_2 layers, separated by Ca ions, which contribute the Cu(d)-O(p) antibonding bands that form the hole conduction bands. These four degenerate bands peak 1.8 eV above E_F at M and R. The Cu-O bandwidth at M is 12.2 eV. These bands are essentially two dimensional, as demonstrated by the similarity of the dispersion along the symmetry lines ΓM and ZR. The TlO layer provides a single Tl(s)-O(p) band that just crosses below E_F at Γ and Z.

The local densities of states for the metal atoms are shown in Fig. 4.23, with those for oxygen shown in Fig. 4.24. Cu(1) labels the copper sites in the two inner CuO_2 planes, while Cu(2) labels the copper sites in the outer planes. Ca(1) lies in the center of the four-layer structure, while Ca(2) labels the two symmetric sites adjacent to the outer CuO_2 planes. The oxygen sites are labeled just as for $Tl_2Ca_2Ba_2Cu_3O_{10}$ in the previous section. The two inner copper-oxide planes are relatively isolated from the remaining structure by the two outer Cu(2)-O(2) layers, but the Cu(1) and Cu(2) spectra are similar. The Ca(1) and Ca(2) unoccupied d bands are almost identical. The O(3) and O(4) sites have quite narrow bands, indicating the ionic nature of their bonds with Ba and Tl. The total density of states at E_F within the tight-binding model is 7.5 states/eV cell, the largest value among the systems examined.

The results of the valence calculation for $TlCa_3Ba_2Cu_4O_{11}$ are listed in Table 4.3. The outer Cu(2) sites have the largest valence of all the Tl cuprate superconductors. The O(1) site again has slightly more negative charge than the oxygens in the outer CuO_2 planes. O(4) is significantly more ionic than the oxygens in the materials with double TlO layers.

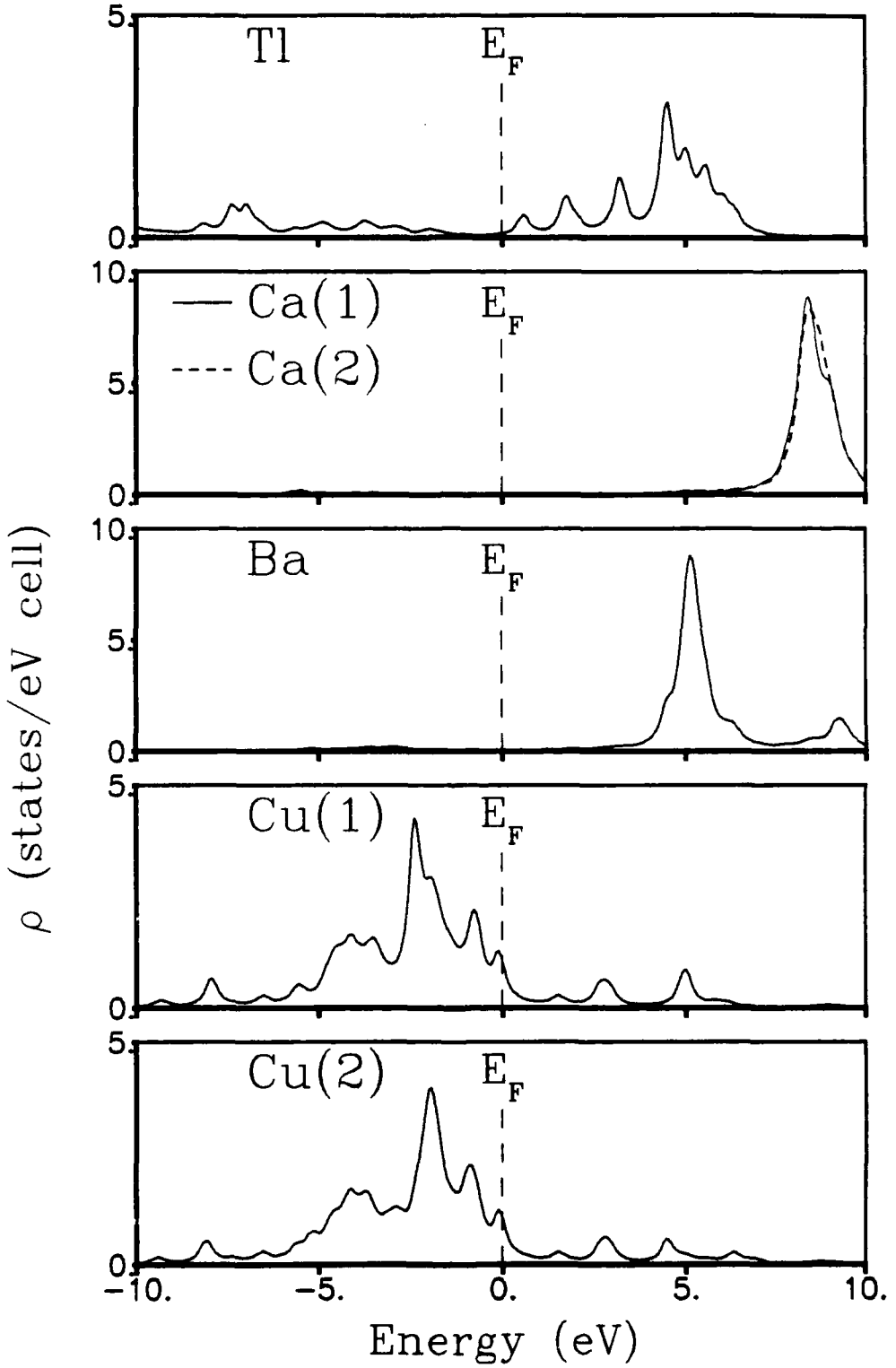

Fig. 4.23. Local densities of states for the metal atoms in $TlCa_3Ba_2Cu_4O_{11}$.

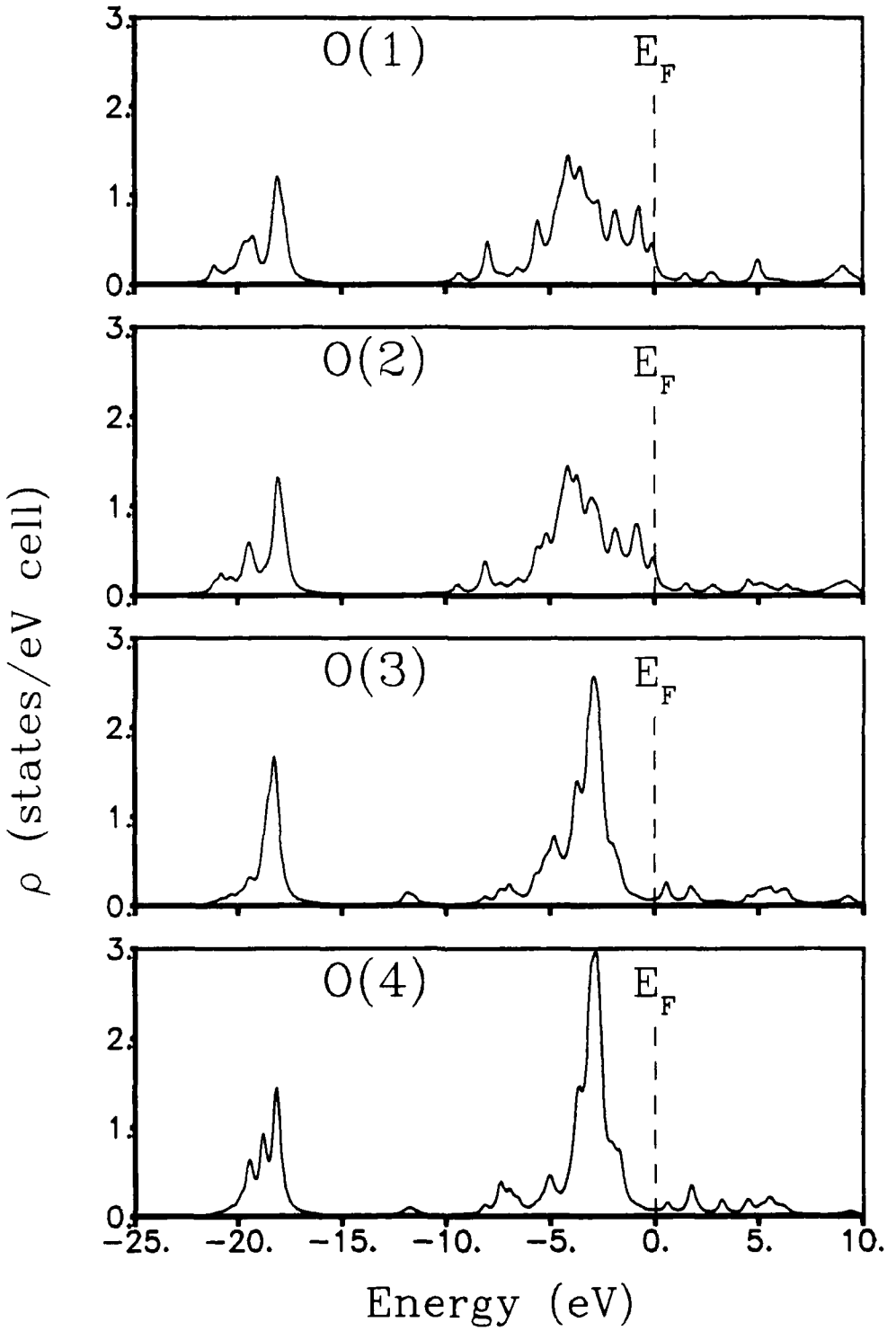

Fig. 4.24. Local densities of states for the oxygen atoms in $TlCa_3Ba_2Cu_4O_{11}$.

$BaPb_{0.75}Bi_{0.25}O_3$

Let us now examine the bismuth-oxide superconductors. The material $BaPb_{1-y}Bi_yO_3$ has T_c = 13 K for y = 0.25.[88] This phase was considered to have an unusually high T_c for an oxide prior to the discovery of the copper-oxide superconductors. This system is much simpler to examine than the cuprates, and is very similar to the high-temperature superconductor $Ba_{1-x}K_xBiO_3$ (described in the next section). The tight-binding energy parameters used for Bi and Pb are the same as those fitted to the LDA energy bands[204] of $BaBiO_3$ and $BaPbO_3$. The doping is treated in the virtual crystal approximation.

The tight-binding energy bands in Fig. 4.25 for $BaPb_{0.75}Bi_{0.25}O_3$ agree well with the previous LDA calculation[223] for $BaPb_{0.7}Bi_{0.3}O_3$, with both calculations using a model cubic structure with a_0 = 4.29 Å rather than the actual tetragonal structure.[90] The ten-band complex near the Fermi energy is composed of Pb/Bi(s)-O(p) hybrid states, with the highest antibonding band protruding above E_F to 3.0 eV at R, as in the LDA result.[223] The tight-binding bandwidth at R is 16 eV, slightly larger than the width of 14 eV in the LDA calculation. The density of states at the Fermi energy is 0.6 states/eV cell for the model structure, contributed by the Pb/Bi s and O p states. The LDA result is 0.3 states/eV cell.[223] The calculated valences for $BaPb_{0.75}Bi_{0.25}O_3$ are listed in Table 4.4; the effective valence of the Pb/Bi atom is 1.54.

A photoemission study of $BaPb_{0.75}Bi_{0.25}O_3$ shows that the valence bands down to −8 eV are derived from Pb/Bi(s)-O(p) hybrid states, with a contribution between −8 and −12 eV from the Pb and Bi s states.[224] The core-like Ba p states appear near −14 eV, with no Ba d or s states appearing at E_F.

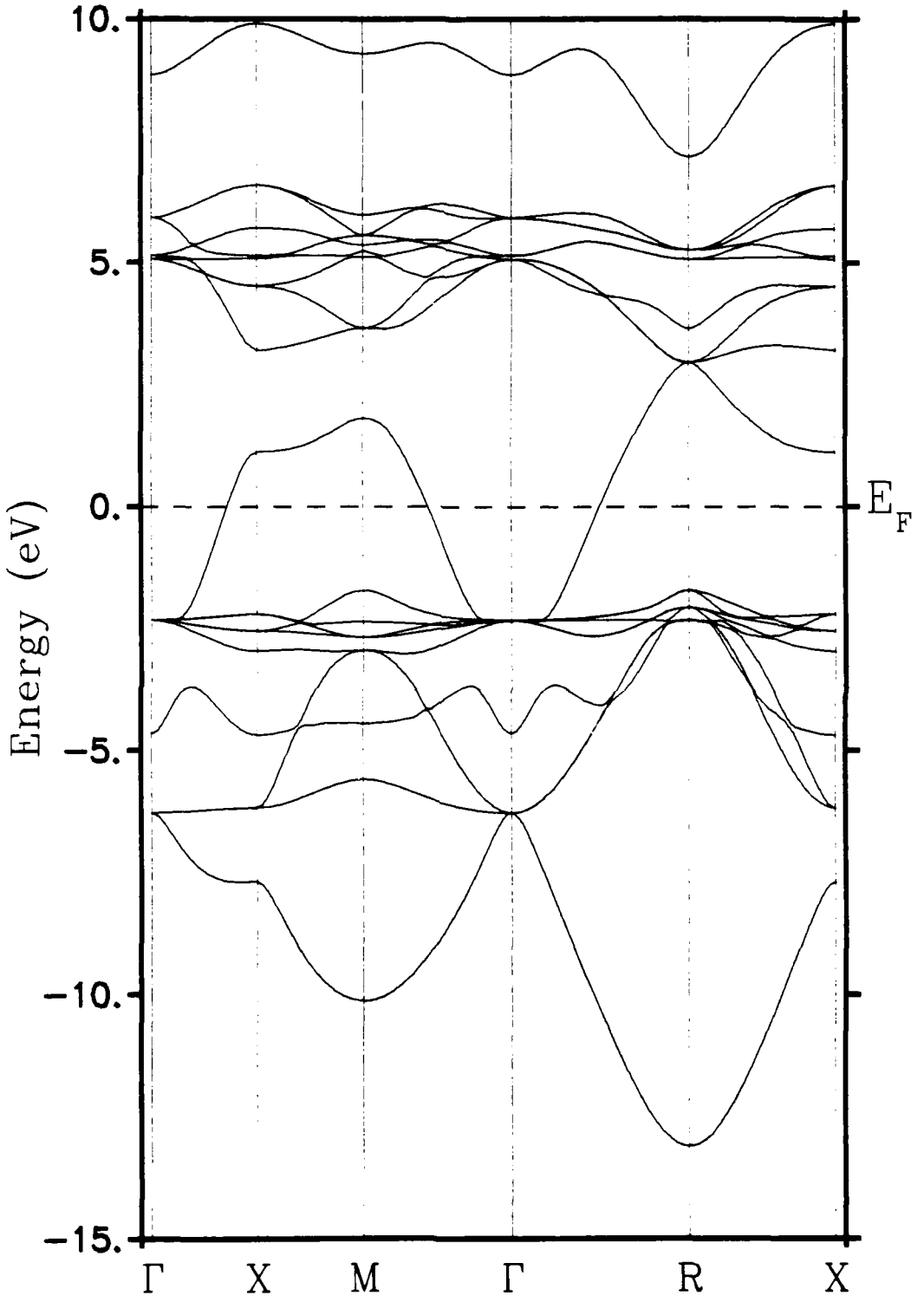

Fig. 4.25. Electronic energy bands for $BaPb_{0.75}Bi_{0.25}O_3$.

TABLE 4.4. Valences Δn for $BaPb_{0.75}Bi_{0.25}O_3$ and $Ba_{0.6}K_{0.4}BiO_3$.

	Ba	K	Bi	Pb	O
$BaPb_{0.75}Bi_{0.25}O_3$	1.49	···	2.29	1.29	-1.01
$Ba_{0.6}K_{0.4}BiO_3$	1.62	0.62	1.80	···	-1.01

$Ba_{0.6}K_{0.4}BiO_3$

The high-temperature superconductor $Ba_{1-x}K_xBiO_3$ has $T_c \approx 34$ K at $x = 0.4$.[93-95] The key to the higher T_c in this phase compared to $BaPb_{0.75}Bi_{0.25}O_3$ seems to be that the hole doping is performed on the Ba site rather than on the Bi site, so that the conduction bands are relatively undisturbed. The structure used for $Ba_{0.6}K_{0.4}BiO_3$ is strictly cubic,[93] with $a_0 = 4.293$ Å and an ideal perovskite atomic substructure. The doping is again treated in the virtual crystal approximation.

The energy bands in Fig. 4.26 are in good agreement with the recent LDA calculation[225] for $Ba_{0.5}K_{0.5}BiO_3$, and are quite similar to the bands for $BaPb_{0.75}Bi_{0.25}O_3$ in Fig. 4.25. The conduction band is formed from Bi(s)–O(p) antibonding states. The bandwidths at M and R are 12.9 and 17.0 eV, compared with 12.7 and 15.2 eV in the LDA results.[225] The larger bandwidth at R in the tight-binding calculation is partially attributed to the omission of the core-like Ba p states near -12 eV.[225] The unoccupied Bi p bands disperse from 2 to 5 eV above E_F, while the empty Ba d bands form a flat band at 6.3 eV.

The local densities of states for $Ba_{0.6}K_{0.4}BiO_3$ are shown in Fig. 4.27. The Bi s and O p states form broad spectra from -10 eV to the Fermi energy, and contribute the metallic $\rho(E_F) = 0.7$ states/eV/cell. The Ba/K d bands are ionic and insulating.

The valences for $Ba_{0.6}K_{0.4}BiO_3$ are listed in Table 4.4, with an effective Ba/K valence of 1.22. We find an increase of 0.26 holes per BiO_2 unit in $Ba_{0.6}K_{0.4}BiO_3$ with respect to the Pb/Bi oxide region of $BaPb_{0.75}Bi_{0.25}O_3$. The calculation also indicates that doping $Ba_{1-x}K_xBiO_3$ at $x = 0.4$ gives a carrier density of 0.22 holes per BiO_2 unit with respect to semiconducting $BaBiO_3$, while

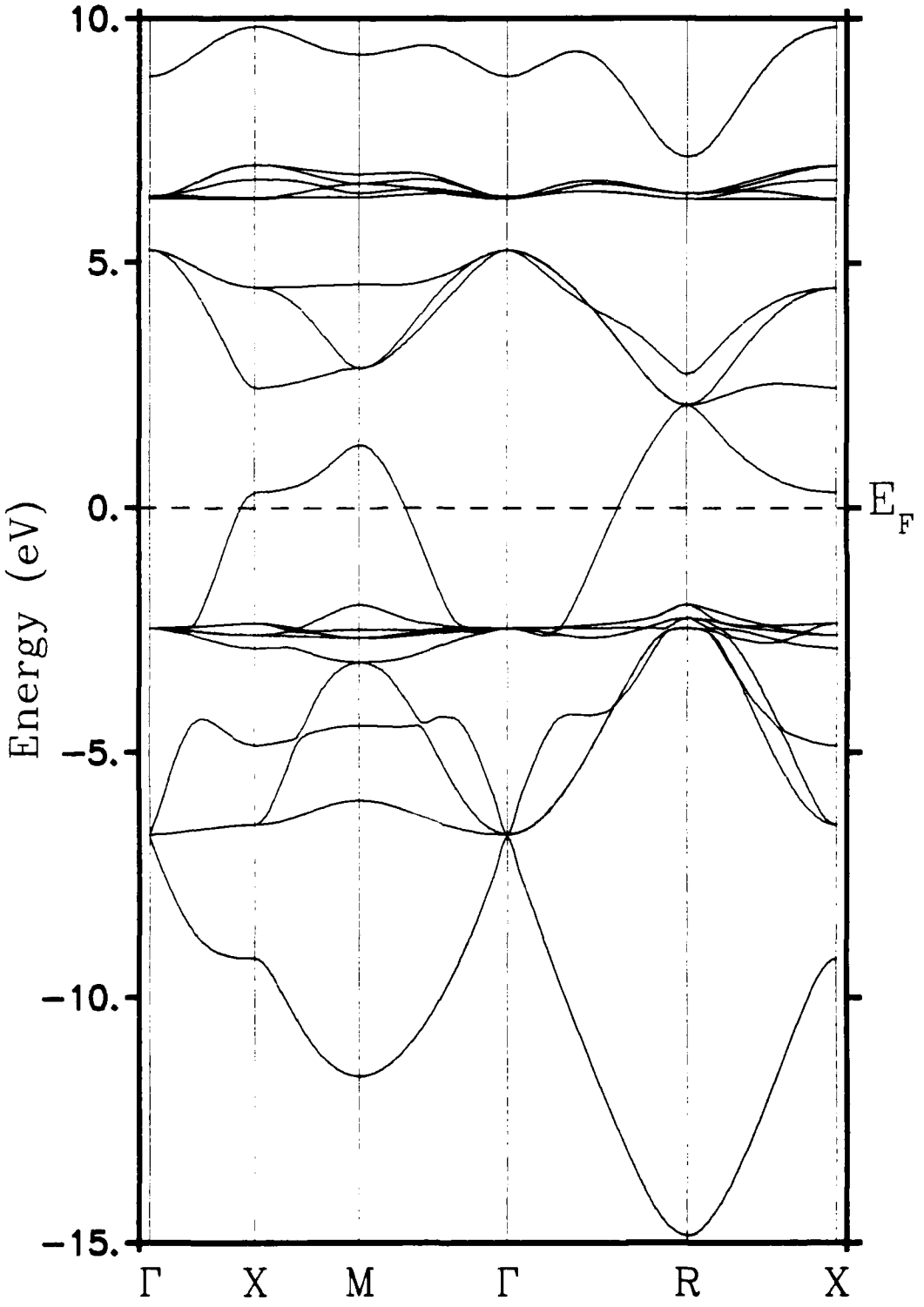

Fig. 4.26. Electronic energy bands for $Ba_{0.6}K_{0.4}BiO_3$.

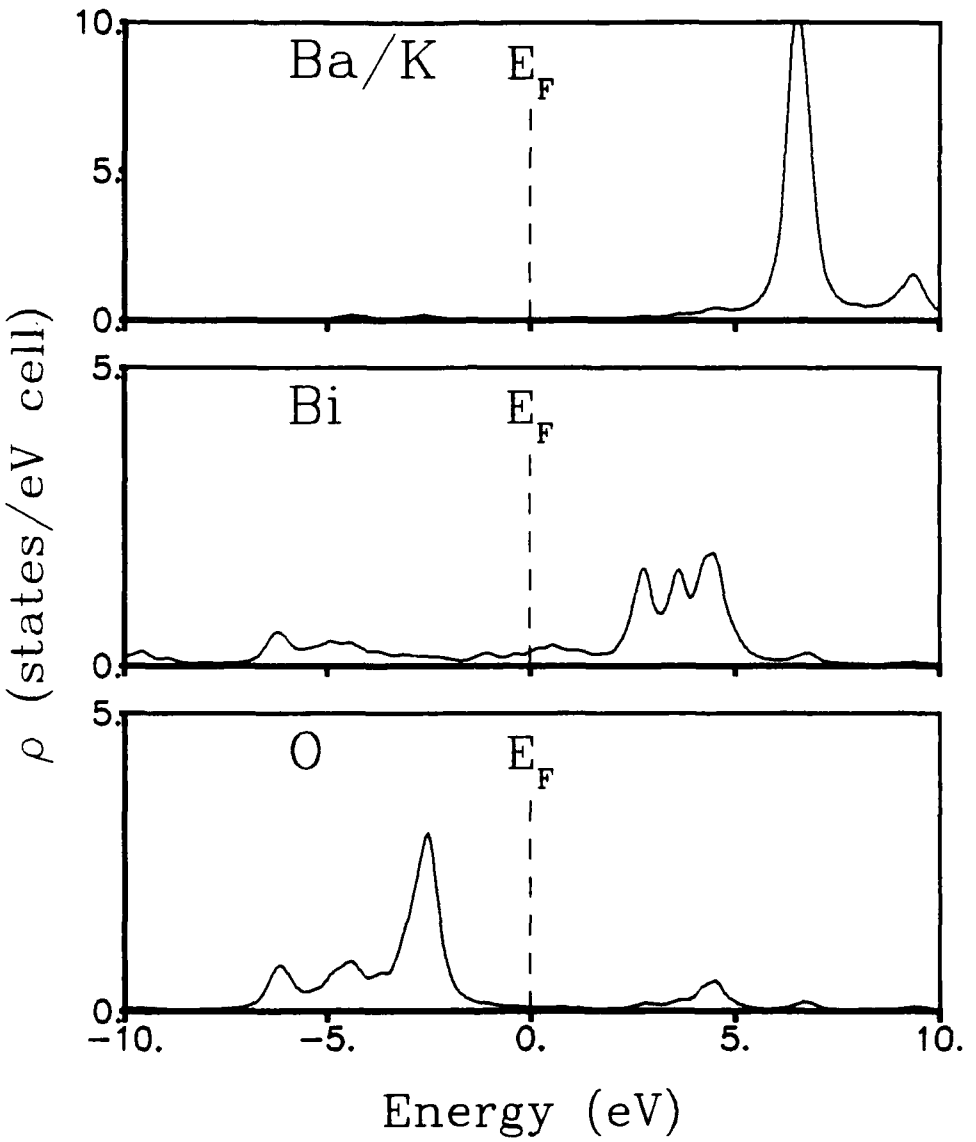

Fig. 4.27. Local densities of states for $Ba_{0.6}K_{0.4}BiO_3$.

the remaining 0.18 doped holes are localized, lowering the charge associated with the Ba/K site.

Photoemission studies[226,227] of $Ba_{0.6}K_{0.4}BiO_3$ show occupied states similar to the calculated bands. Oxygen p states dominate the structure near the Fermi energy, with O s core levels seen near -21 eV. Bi(s)–O(p) hybrid states are seen down to -13 eV. Inverse photoemission results[227] place the unoccupied Bi p bands near 4 eV and the Ba d bands near 7 eV, in agreement with the local densities of states for $Ba_{0.6}K_{0.4}BiO_3$ in Fig. 4.27.

Summary of Electronic Structure

We find that a single tight-binding model, with fully transferable parameters, provides a good description of the electronic structure of the high-temperature superconductors, in the sense that the results satisfactorily agree with the LDA calculations and with certain experimental details of the electronic states. The parameters fitted to La_2CuO_4, $BaPbO_3$, and $BaBiO_3$ provide sufficient input to extrapolate other parameters needed for the model.

All the copper-oxide superconductors have two-dimensional conduction bands arising from Cu(d)–O(p) antibonding states. The metal-oxide layers sandwiching the CuO_2 planes (such as LaO, BaO, and SrO) all display ionic and insulating behavior, in the sense that there is large charge transfer and the contribution to $\rho(E_F)$ is small. The copper-free bismuth-oxide superconductors $BaPb_{0.75}Bi_{0.25}O_3$ and $Ba_{0.6}K_{0.4}BiO_3$ have valence bands of antibonding Bi(s)–O(p) states, with cubic or almost-cubic band symmetry. These materials also have ionic BaO in their electronic structures.

CHAPTER V

ATOMIC SUBSTITUTION EFFECTS

In this chapter we report studies of the effect of various atomic substitutions on the electronic properties of the high-temperature superconductors. For the material $YBa_2Cu_3O_7$, we examined the following atomic substitutions: Al, Fe, Co, Ni, or Zn replacing Cu; Sr or La replacing Ba; and F or N replacing O. The phase $Bi_2CaSr_2Cu_2O_8$ was investigated for the substitution of Pb on the Bi site. Of the many phases of Tl cuprates, the representative material $Tl_2CaBa_2Cu_2O_8$ was examined for replacement of Tl with Hg or Pb. In each case, the change in the densities of states, the modified atomic valences, and the shift in the Fermi energy were calculated.

There have been many experimental studies of changes in the superconducting properties of $YBa_2Cu_3O_7$ induced by replacement of the original atomic species. The replacement of Y by any of the rare earth elements Nd, Sm, Eu, Gd, Dy, Ho, Er, Tm, Yb, or Lu had only a very small effect on T_c,[26,228–233] indicating a remarkable insensitivity of the relevant electronic and structural properties to the species on this site. (The rare earths Ce, Pr, and Tb do not form superconducting phases in $RBa_2Cu_3O_7$, perhaps because of the stable tetravalent state of these atoms.[26,95,234–236]) In particular, the magnetic moment of the substitutional atom does not appear to affect the superconducting transition temperature,[232,233] indicating that the Y site is electronically isolated from the superconducting region of this material.

Replacement of Ba by Sr was found to yield a depression of T_c that is linear in the Sr concentration, and which was attributed to lattice distortions

in the neighborhood of the Sr atom.[237,238] Substitution of La onto the Ba site leads to a more rapid decrease of T_c, with a sudden loss of superconductivity in $YBa_{2-x}La_xCu_3O_7$ for $x > 0.4$.[33,239,240] This effect was attributed to charge compensation for the donated electron of La by a reduction of the copper valence or by an increase in the oxygen content.[240] Further studies of the substitution of the rare earths Nd, Sm, Eu, Gd, and Dy for both Y and Ba indicate a strong suppression of T_c in $RBa_{2-x}R_xCu_3O_7$, with a loss of superconductivity for $x > 0.5$.[241]

Substitutions for copper lead to a particularly dramatic lowering of T_c. The substitution of Al onto the Cu(1) chain site in single crystal $YBa_2Cu_{3-x}Al_xO_7$ leads to a rapid decrease in T_c for $x > 0.1$, with complete loss of superconductivity for $x > 0.22$.[242] For the $3d$ transition metals, substitution in polycrystalline $YBa_2Cu_{3-x}M_xO_7$ for $x \leq 0.3$ yields a strong depression of the transition temperature.[243-247] Note particularly that nonmagnetic Zn suppresses T_c more than magnetic Fe or Co. Replacement of Cu by Ag also leads to a decreased transition temperature.[248,249]

The relative importance of the Cu(1) and Cu(2) sites for high-temperature superconductivity in $YBa_2Cu_3O_7$ has been examined by correlating the specific site for various metal substitutions with the effect on the superconducting properties. Neutron diffraction measurements place Fe substitutions on the Cu(1) site,[250-252] although other experiments indicate that Fe may also substitute on the Cu(2) site.[253] Doping with Co shows preferential substitution on the Cu(1) site,[251,254] along with an increase of the oxygen stoichiometry above 7.0. Both Fe and Co substitution allow superconductivity to persist (at a reduced T_c) up to relatively large dopant levels ($x \approx 0.4$ in $YBa_2Cu_{3-x}M_xO_7$), indicat-

ing that the Cu(1) chain site does not provide the primary states to support superconductivity.[250,254] However, Ni and Zn substitutions are found to occupy the Cu(2) sites in the copper-oxide planes.[251,255,256] The sharp depression in T_c with Zn substitution is thus directly attributable to disruption of the important CuO_2 plane region.

Replacement of oxygen with sulfur in $YBa_2Cu_3O_6S$ appears to enhance the Meissner effect, while leaving T_c unaffected near 90 K.[257] The substitutions of fluorine[258] and nitrogen[259] into $YBa_2Cu_3O_7$, presumably onto the oxygen sites, have produced conflicting and often irreproducible results.[260-264]

Substitution of Pb into $Bi_2CaSr_2Cu_2O_8$ has been found to increase the onset of superconductivity to 107 K.[50,60-62] This effect has been attributed to stabilization of the higher-T_c structure $Bi_2Ca_2Sr_2Cu_3O_{10}$,[50,61,6] but the p-type dopant nature of Pb replacing Bi may also play a role in the enhanced superconductivity.

The Tl cuprates display high-temperature superconductivity when Ba is completely replaced by Sr.[265-267] The phase with nominal composition $Tl_{0.75}Bi_{0.25}CaSr_2Cu_2O_7$ displays superconductivity at $T_c = 75$ K.[265] A slightly higher T_c near 85 K is obtained in the Pb-doped phase $Tl_{0.5}Pb_{0.5}CaSr_2Cu_2O_7$, while superconductivity at $T_c \approx 120$ K is observed for the material $Tl_{0.5}Pb_{0.5}Ca_2Sr_2Cu_3O_9$.[267] The phases with complete substitution of Sr for Ba require additional doping on the Tl site with Pb or Bi to stabilize the structure.

Method

Using the same tight-binding model for the electronic structure described in Chapter III, we consider the effects of atomic substitutions. For simplicity, we

employ a periodic substitution scheme, with the substitutional atom occupying the same location within each unit cell throughout the material. Systems that experimentally accommodate full atomic substitutions can be directly compared with these results. This technique does not address partial substitutions or defect ordering as a function of dopant fraction; however, the changes in the electronic properties calculated for the full atomic substitution provide an interpolative description of the model system at all dopant levels.

Starting with the fitted parameters in Table 2.1, the atomic energies for substitutional atoms are extrapolated from the solid state table of Ref. 165, maintaining the differences in atomic energies between elements. We extrapolate the energies ϵ_s, ϵ_p, and ϵ_d for Tl and Hg from the fitted Bi and Pb atomic energies. The resulting parameters are listed in Table 5.1. We neglect the small changes that occur in the lattice constants due to differences in the covalent radii of the substitutional atoms. Although such changes in the lattice parameters are observed, and may have a role in the superconductivity of these materials, they nevertheless have only a minor effect within the tight-binding model for the electronic structure of the material.

In the calculations for $BiPbCaSr_2Cu_2O_8$ and $Tl\mathit{M}CaBa_2Cu_2O_8$ (M = Hg or Pb), we include the same second-neighbor interactions (e.g., Pb–Pb) that were required to properly describe the electronic energy bands of $Bi_2Sr_2CuO_6$ and $Bi_2CaSr_2Cu_2O_8$ in Chapter IV. Since the covalent radii of Hg, Tl, Pb, and Bi are all nearly equal, we expect these atoms to have similar bonding characteristics within the same crystal structure.

The notation in labeling the substitutional atoms parallels the form for the undoped materials as given in Chapter IV. For example, Al(1) refers to

TABLE 5.1. Tight-binding parameters for atomic substitution calculations.

	ϵ_s (eV)	ϵ_p (eV)	ϵ_d (eV)	r_d (Å)
N	-23.0	-11.5	···	···
O	-29.0	-14.0	···	···
F	-36.0	-17.0	···	···
Al	-10.1	-4.9	···	···
Fe	-11.6	···	-10.4	0.95
Co	-11.7	···	-11.6	0.95
Ni	-11.9	···	-12.8	0.95
Cu	-12.0	···	-14.0	0.95
Zn	-13.5	···	-15.2	0.95
Sr	-5.0	···	-6.8	1.6
Ba	-4.5	···	-6.6	1.6
La	-4.9	···	-6.6	1.6
Hg	-11.6	-7.2	-17.0	1.0
Tl	-14.8	-8.3	-23.0	1.0
Pb	-18.0	-9.4	-29.0	1.0
Bi	-21.2	-10.5	-35.0	1.0

an aluminum atom that replaces the copper atom on the chain site Cu(1) in $YBa_2Cu_3O_7$, while Zn(2) refers to a zinc atom that replaces a plane site Cu(2).

$YBa_2Cu_2MO_7$, M = Al, Fe, Co, Ni, or Zn

The substitution of Al onto the Cu(1) site has a dramatic effect on the band structure of $YBa_2Cu_2AlO_7$, shown in Fig. 5.1, as compared with that of $YBa_2Cu_3O_7$ in Fig. 4.4. In particular, the conduction state associated with the Cu(d)–O(p) antibonding band of the one-dimensional chain is completely removed from the structure, indicating a complete loss of metallic conductivity for this region. However, the two-dimensional nature of the electronic energy bands is maintained, as demonstrated in Fig. 5.1 by the similarity of the two wave-vector paths ΓXMY and ZX′M′Y′, which trace the edge of the Brillouin zone in the Γ and Z planes. The total density of states of the Al-doped material is shown in Fig. 5.2. Note that the Al p bands lie about 6 eV above E_F, leading to weak interactions with the neighboring chain oxygens. The calculated valences in Table 5.2 show only minor changes in the CuO_2 plane regions, but Al(1) appears much more ionic than Cu(1) in $YBa_2Cu_3O_7$. Al(1) substitution thus leads to a localized destruction of conduction states within the one-dimensional chains, and substantially increases the ionic character of the chain region. The shift in the Fermi energy due to the Al(1) substitution, along with the total density of states at E_F, is given in Table 5.3. The Fermi energy shifts upwards, and the removal of the Cu(1)–O(1) chain band results in a decrease in $\rho(E_F)$.

For the transition-metal substitutions, we consider both Cu(1) and Cu(2) sites within $YBa_2Cu_3O_7$, and perform the calculation independently for each substitution site. The total densities of states for the replacement of Cu with

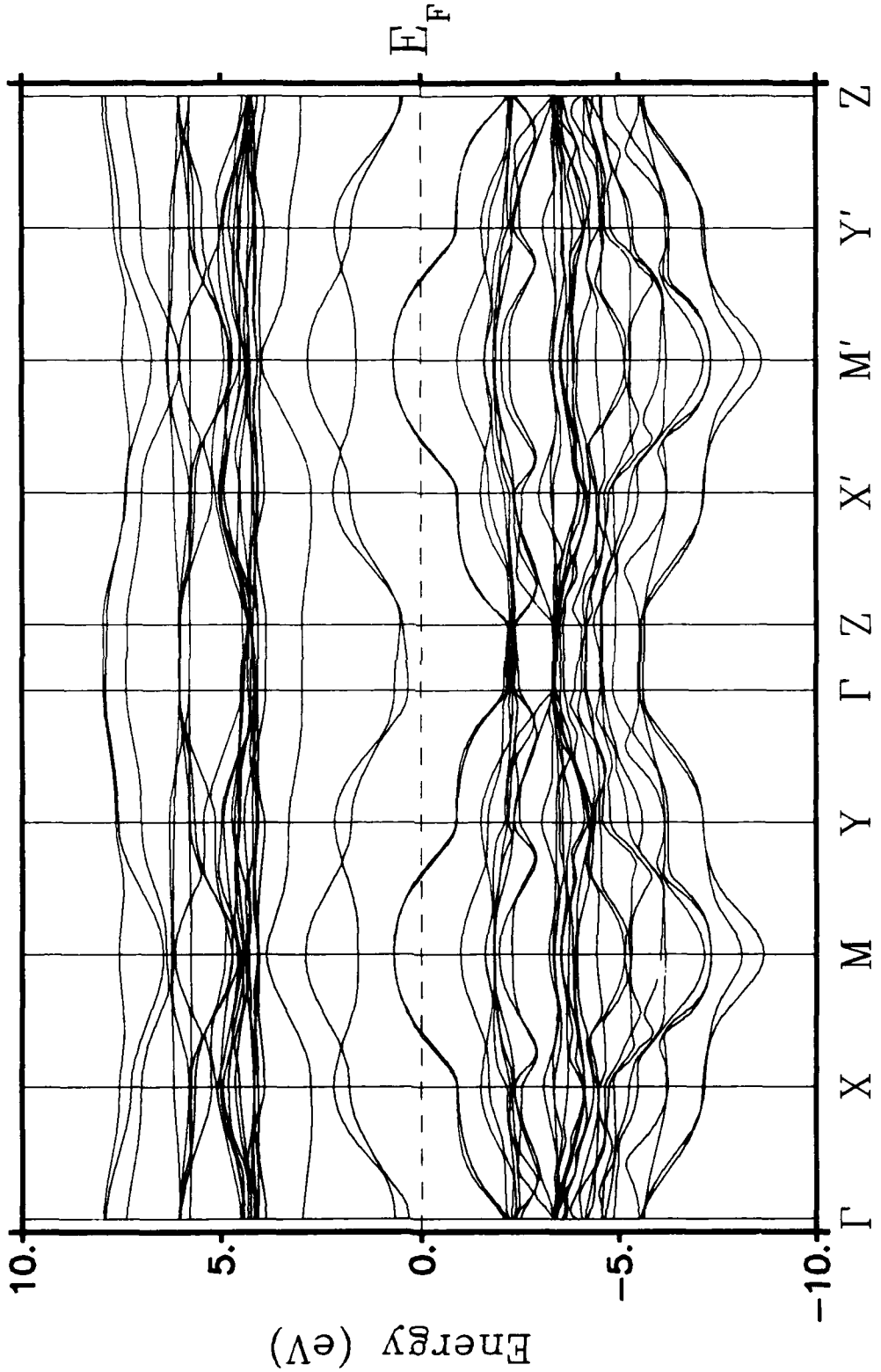

Fig. 5.1. Electronic energy bands for $YBa_2Cu_2AlO_7$.

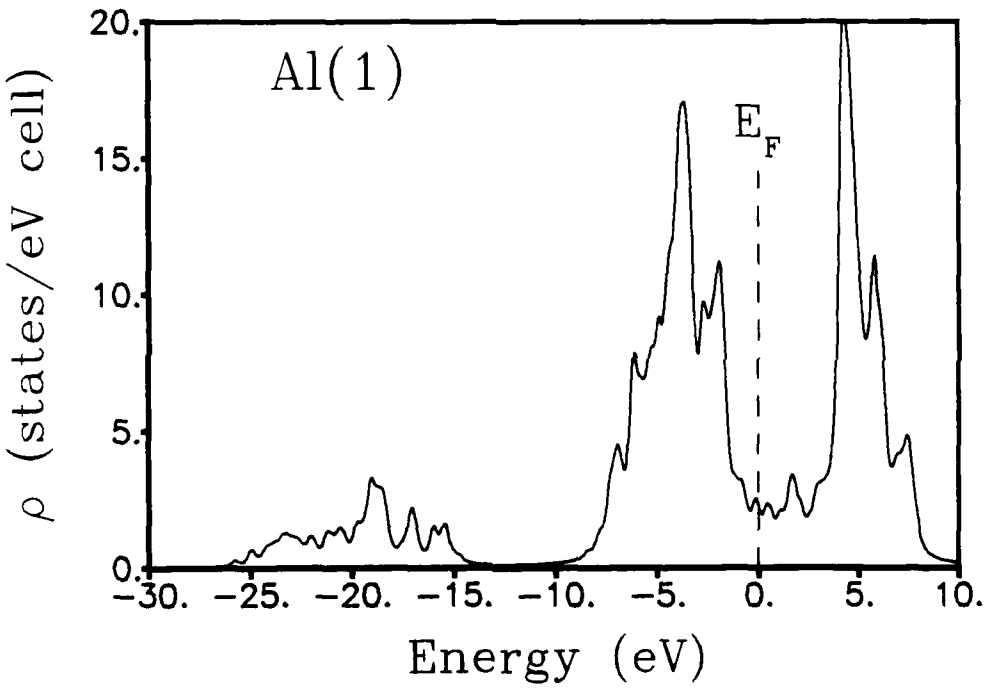

Fig. 5.2. Total density of states for $YBa_2Cu_2AlO_7$.

TABLE 5.2. Valences Δn for $YBa_2Cu_2MO_7$.

	Cu(1)	Cu(2)	M	O(1)	O(2)[a]	O(3)[a]	O(4)
Al(1)[b]	···	0.94	2.46	-1.59	-1.10	-1.11	-1.50
Fe(1)[b]	···	0.38	3.24	-1.13	-1.30	-1.31	-1.19
Fe(2)	0.67	0.36	2.85	-1.35	-1.15	-1.16	-1.30
Co(1)[b]	···	0.67	2.03	-1.10	-1.17	-1.17	-1.14
Co(2)	1.03	0.76	1.44	-1.18	-1.04	-1.06	-1.25
Ni(1)	···	0.99	1.12	-1.12	-1.07	-1.07	-1.18
Ni(2)[b]	1.31	0.96	0.82	-1.12	-1.04	-1.05	-1.23
Cu	1.34	0.98	···	-1.12	-1.09	-1.11	-1.21
Zn(1)	···	1.02	1.41	-1.33	-1.07	-1.07	-1.25
Zn(2)[b]	1.37	0.99	1.20	-1.11	-1.15	-1.17	-1.23

[a] Averaged over sites in unit cell.
[b] Experimentally-determined substitution site.

TABLE 5.3. Shift in E_F and density of states for $YBa_2Cu_2MO_7$.

M	ΔE_F (eV)	$\rho(E_F)$ (states/eV cell)
Al(1)[a]	0.15	2.4
Fe(1)[a]	0.79	6.3
Fe(2)	0.78	9.3
Co(1)[a]	0.22	7.5
Co(2)	0.16	6.3
Ni(1)	-0.12	4.2
Ni(2)[a]	-0.08	3.5
Cu	...	3.2
Zn(1)	0.16	3.0
Zn(2)[a]	0.08	3.3

[a] Experimentally-determined substitution site.

Fe, Co, Ni, or Zn are shown in Figs. 5.3–5.6. The results for Fe substitution in Fig. 5.3 show a large contribution from the Fe d bands at E_F, while the results for Co in Fig. 5.4 have Co d character at and below the Fermi energy. The Ni d and Zn d bands overlap the Cu(d)–O(p) bands below E_F. In general, substitutions on the Cu(1) site give sharper peaks in the density of states, arising from the d bands of the substitutional atom. The d peaks for Cu(1) substitutions also lie at slightly higher energies than those for substitutions on the Cu(2) site.

The valences for $YBa_2Cu_2MO_7$ are presented in Table 5.2, with the valences for M = Cu from Table 4.1 shown for comparison. The experimentally-determined substitution sites[250–256] are also indicated in Table 5.2. There is a strong dependence on the substitution site for both the metal and oxygen valences. Substitution on the Cu(1) site always results in a larger valence of the doped metal than for substitution on the Cu(2) site. The large dopant-metal valences for Fe and Co substitution may be due to the neglect of correlation effects within the d orbitals, which might alter the occupation of these bands. Both Fe(1,2) and Co(1,2) substitution give a substantial decrease in the valence of the copper atom on site Cu(2), but Ni or Zn substitution results in little change in the valence of the copper atom in the CuO_2 plane.

The density of states results for Fe and Co substitution in Table 5.3 show large changes in $\rho(E_F)$ for both Cu(1) and Cu(2) dopant sites. The Fermi energy is pinned near the peak of the Fe or Co d state energy, so that $\rho(E_F)$ is insensitive to small variations of the parameters ϵ_d(Fe) or ϵ_d(Co) in Table 5.1, but for the same reason ΔE_F is somewhat sensitive to these values. The Fermi energy shifts upwards for both Fe and Co substitution, with only a small dependence on the particular dopant site. These substitutions do disrupt the character of the

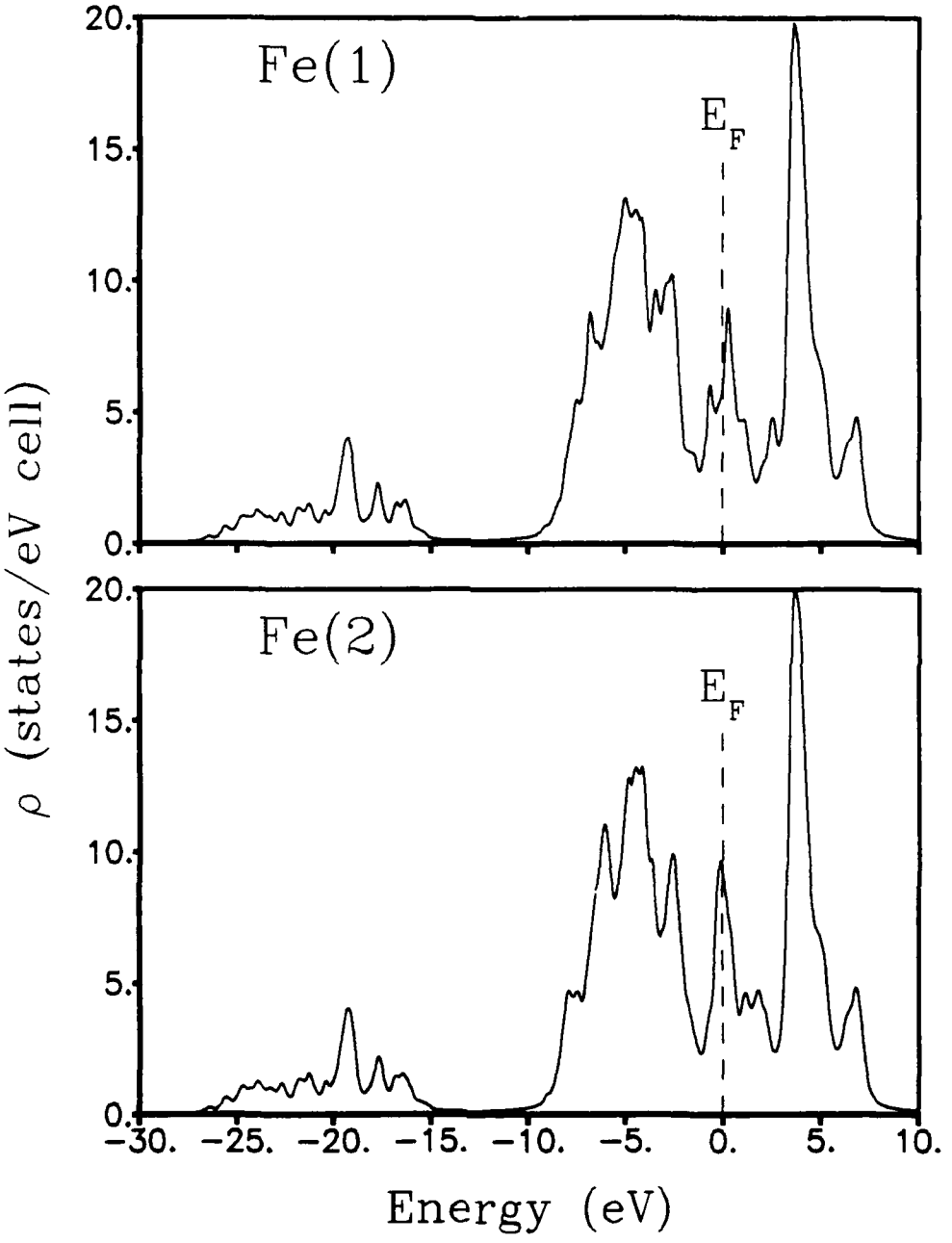

Fig. 5.3. Total densities of states for $YBa_2Cu_2FeO_7$.

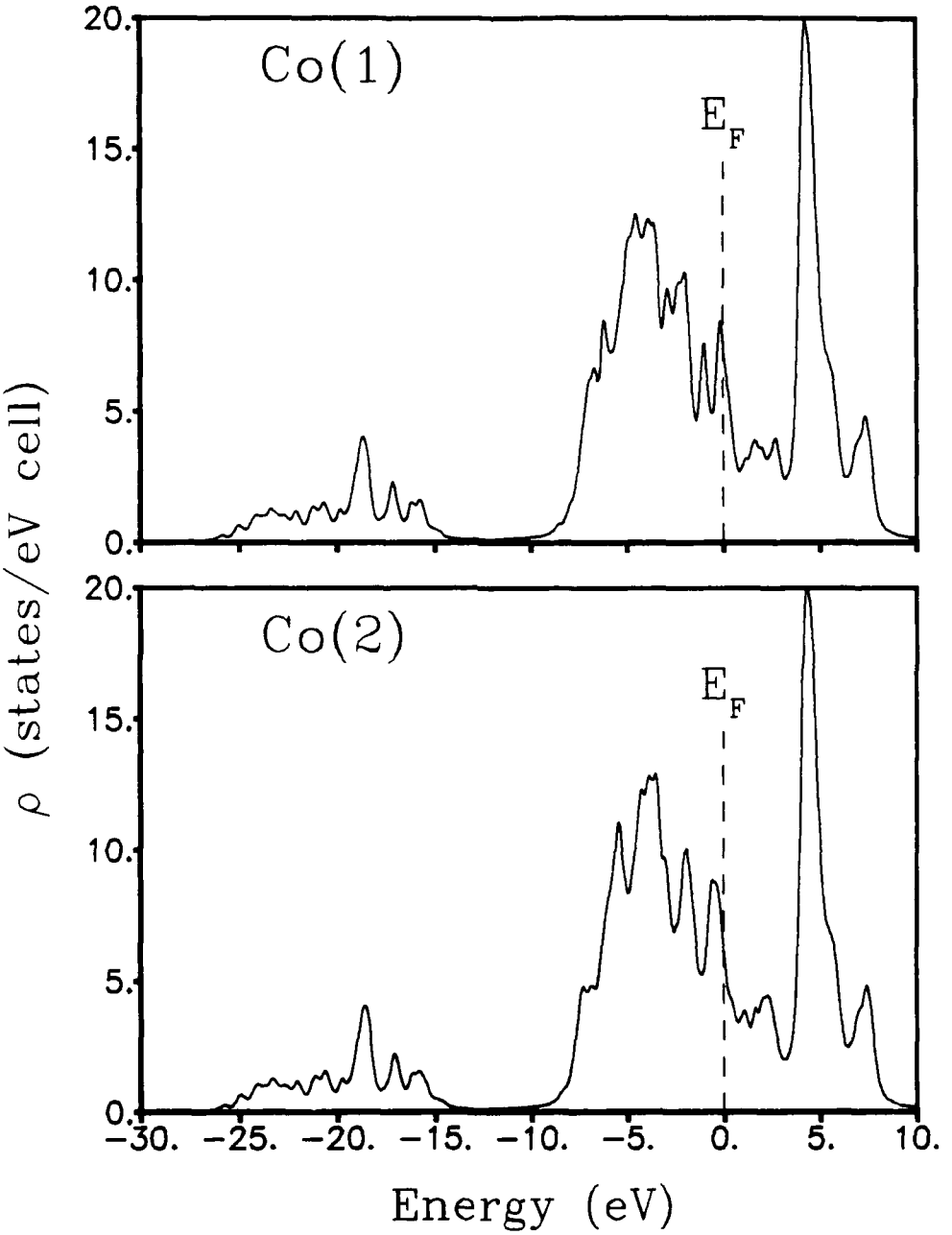

Fig. 5.4. Total densities of states for $YBa_2Cu_2CoO_7$.

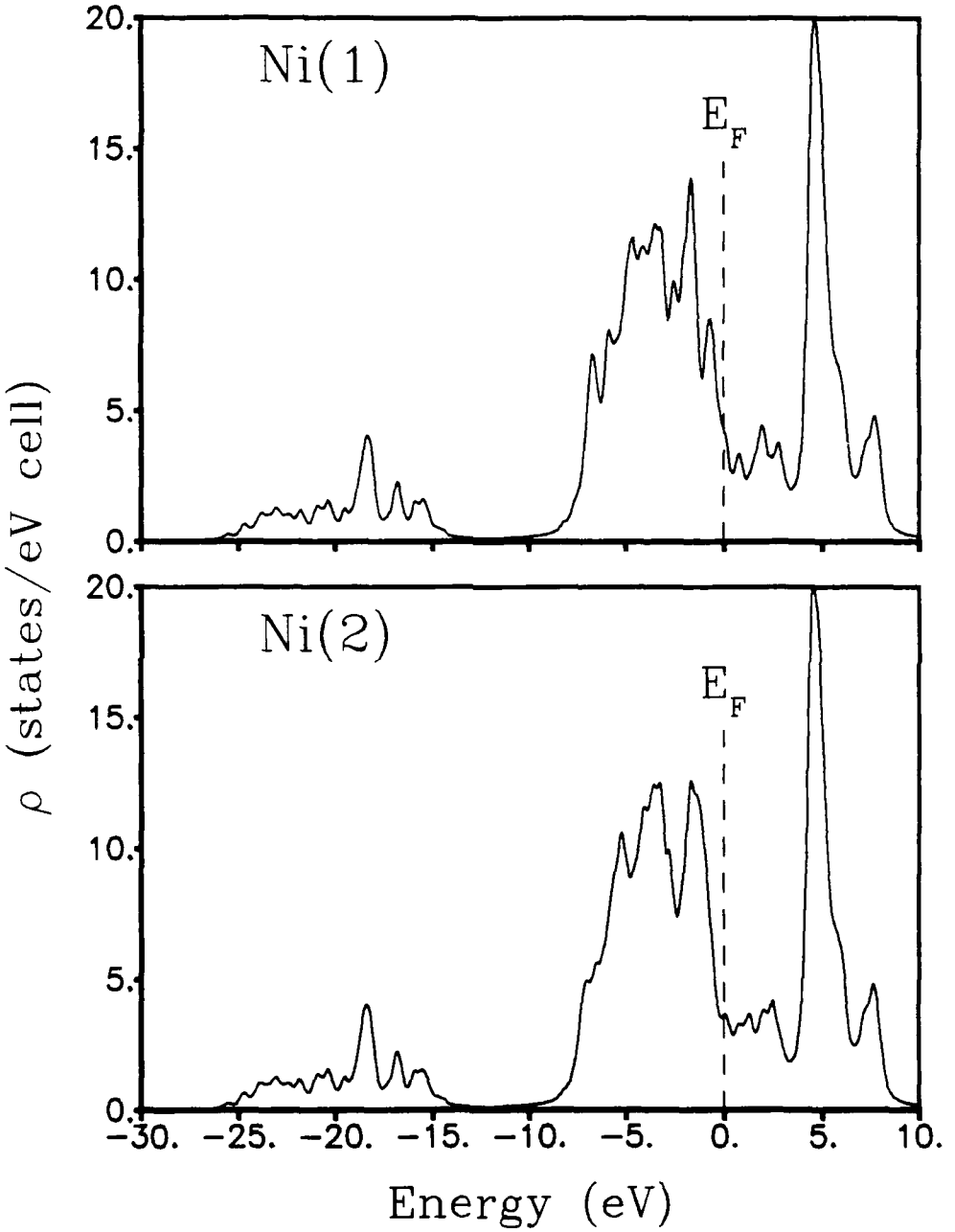

Fig. 5.5. Total densities of states for $YBa_2Cu_2NiO_7$.

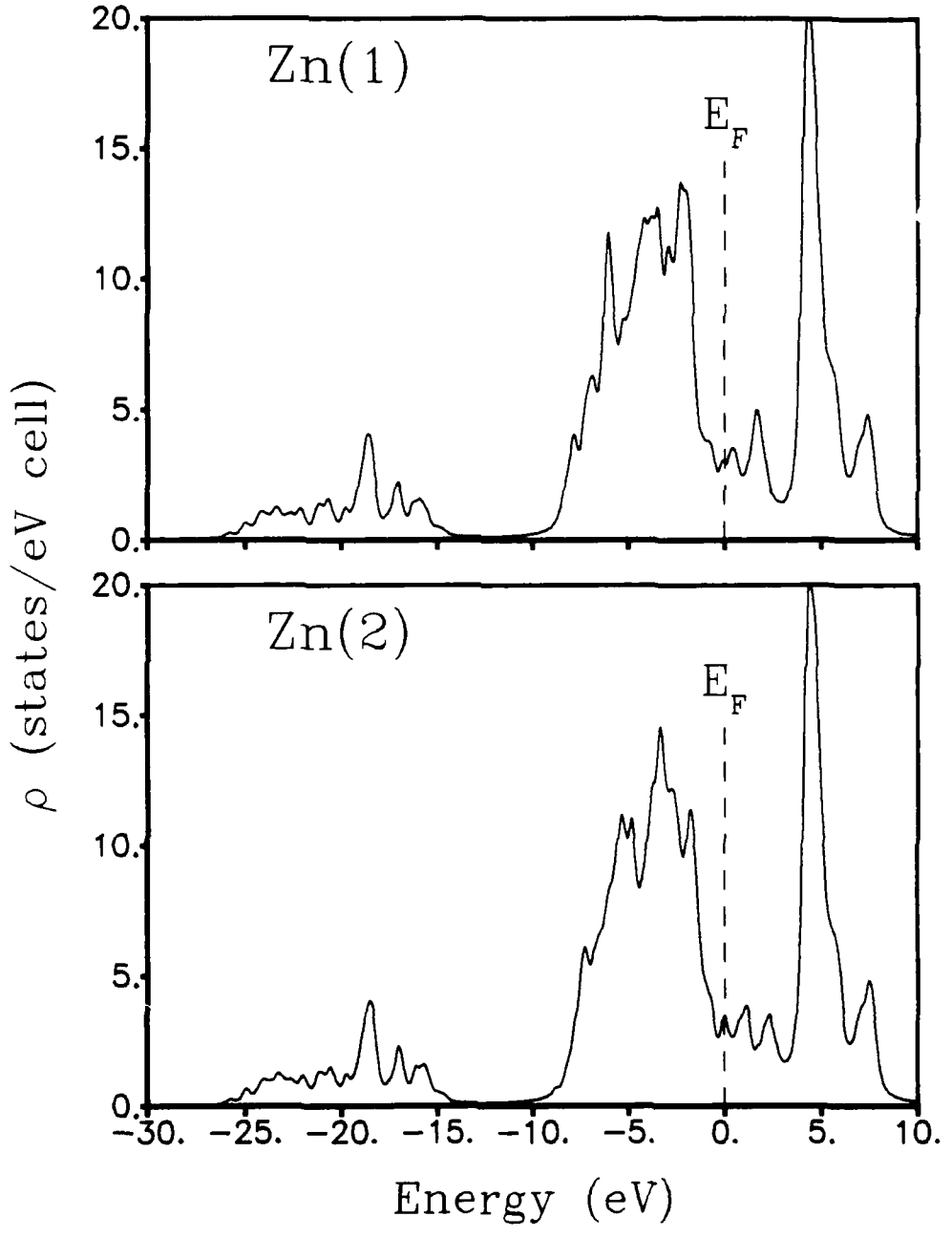

Fig. 5.6. Total densities of states for $YBa_2Cu_2ZnO_7$.

Cu(d)-O(p) antibonding band at E_F, even when located on the Cu(1) site, which may explain the decrease in T_c seen for Fe and Co substitution.[243,244,250-254] Replacement of Cu by Ni shows a smaller change in $\rho(E_F)$, as well as a slight lowering of the Fermi energy. This may explain the moderate decrease in T_c observed for this case,[243-245] even though Ni dopes the Cu(2) site.[251,256]

The shift in E_F in Table 5.3 is relatively site independent for all the transition-metal substitutions, indicating the dopant origin of the shift, while the density of states at E_F is strongly site dependent, except for the case of Zn. Substitution of Zn for Cu gives only small changes in the density of states at E_F, along with a slight increase in the Fermi energy, in contrast to the large decrease in T_c seen experimentally.[243,255] The lack of resonance of the Zn d states with the O p states leads to a smaller fraction of Zn d character at the Fermi energy for this case. Nevertheless, the present results indicate that the direct electronic effect of Zn should be less than that of, e.g., Fe. The Zn dopants on the Cu(2) site will interfere with the CuO_2 conduction bands, but additional calculations (perhaps including correlation effects) may be needed to properly describe this case.

$YBaMCu_3O_7$, M = Sr or La

Substitutions on the Ba site were examined in $YBaMCu_3O_7$ for M = Sr and M = La. For the case of Sr, little change is seen in direct electronic effects, as shown by the valences in Table 5.4. The shift in the Fermi energy is only -0.1 eV, as expected for the substitution of divalent Sr for divalent Ba. The total density of states at the Fermi energy is 3.2 states/eV cell, identical within the model to the result for $YBa_2Cu_3O_7$. This is consistent with the experimental

TABLE 5.4. Valences Δn for YBaMCu$_3$O$_7$.

	Y	Ba	M	Cu(1)	Cu(2)[a]	O(1)	O(2)[a]	O(3)[a]	O(4)[a]
M = Sr	1.77	1.44	1.41	1.34	0.98	-1.12	-1.09	-1.11	-1.20
M = Ba	1.77	1.44	···	1.34	0.98	-1.12	-1.09	-1.11	-1.21
M = La	1.76	1.44	2.43	1.30	0.71	-1.12	-1.19	-1.20	-1.23

[a] Averaged over sites in unit cell for M = Sr and La.

results and would support a purely structural effect for the observed decrease in the superconducting transition temperature of $YBa_{2-x}Sr_xCu_3O_7$.[237,238]

Substitution of La for Ba does change the atomic valences, as shown in Table 5.4, resulting in 0.46 fewer holes within each CuO_2 plane compared with the undoped material $YBa_2Cu_3O_7$. The additional electron of La raises the Fermi energy by $\Delta E_F = 0.31$ eV. There is also a slight decrease in $\rho(E_F)$ to 2.8 states/eV cell. We propose that the dominant effect of La substitution on the superconducting properties of $YBa_{2-x}La_xCu_3O_7$ is the destruction of the hole charge carriers within the CuO_2 planes.

$YBa_2Cu_3O_6L$, L = N or F

Substitution of N or F for O is complicated by the four crystallographically distinct oxygen sites, along with the many possible combinations for fractional or multiple-site substitutions. These atoms might also be accommodated in the structure at the normally-vacant sites that separate the CuO chains.[264] However, we find that sites O(2) and O(3) in the CuO_2 planes behave quite similarly in their electronic structure, as expected from the minor orthorhombic distortion of the structure.[17-21] We consider only single-site substitution of nitrogen or fluorine for oxygen, and neglect the possibility of interstitial sites or fractional occupations for the substitutional atom.

Table 5.5 gives the valences for the oxygen replacements, with the valences for $YBa_2Cu_3O_7$ listed for comparison. The largest valence effect occurs on the copper site nearest the substitutional atom. The substitutions N(1) and F(1) both lead to a significant decrease in the valence of copper on the Cu(1) site, while F(2) or F(4) substitutions cause a large decrease in the Cu(2) valence.

TABLE 5.5. Valences Δn for $YBa_2Cu_3O_6L$.

L	Cu(1)	Cu(2)[a]	O(1)	O(2)[a]	O(3)[a]	O(4)[a]
N(1)	1.18	0.97	-0.89	-1.06	-1.08	-1.25
N(2)	1.24	1.06	-1.13	-1.05	-1.05	-1.25
N(4)	1.30	0.98	-1.14	-1.08	-1.09	-1.14
O	1.34	0.98	-1.12	-1.09	-1.11	-1.21
F(1)	0.81	1.00	-0.67	-1.08	-1.07	-1.28
F(2)	1.36	0.73	-1.11	-0.86	-1.16	-1.23
F(4)	1.26	0.78	-1.15	-1.16	-1.18	-0.87

[a] Averaged over sites in unit cell.

TABLE 5.6. Shift in E_F and density of states for $YBa_2Cu_3O_6L$.

L	ΔE_F (eV)	$\rho(E_F)$ (states/eV cell)
N(1)	0.02	5.0
N(2)	-0.06	3.7
N(4)	-0.08	4.8
O	...	3.2
F(1)	0.11	3.5
F(2)	0.14	3.0
F(4)	0.25	2.8

The results for N(2) substitution do show a slight increase in the number of holes in the CuO_2 planes. However, we do not expect these small shifts to give a significant enhancement of the superconducting properties for $YBa_2Cu_3O_6N$.

Table 5.6 gives the shift in the Fermi energy and $\rho(E_F)$ for the replacement of oxygen. We note that N acts primarily to lower the Fermi energy, while F raises it; i.e., N acts as an acceptor and F as a donor when replacing oxygen. Fluorine is found to have a larger effect on E_F than nitrogen, but F substitution has little effect on $\rho(E_F)$. The N substitutions all show increases in $\rho(E_F)$ within the present model.

$BiPbCaSr_2Cu_2O_8$

We now consider the effect of periodic substitution of Pb for one Bi atom within the crystal structure of $Bi_2CaSr_2Cu_2O_8$. We again neglect the incommensurate structural modulation[48-50] and the disorder in the BiO layers[48-52,54] associated with this phase. Although Pb substitution may also stabilize a different crystal structure,[50,61,62] we confine this calculation to the same model structure that was used for $Bi_2CaSr_2Cu_2O_8$ in Chapter IV.

The electronic energy bands for $BiPbCaSr_2Cu_2O_8$ are shown in Fig. 5.7. The Fermi energy shifts by -0.19 eV compared with that of $Bi_2CaSr_2Cu_2O_8$, consistent with the removal of one electron per formula unit with Pb substitution. The Pb p bands lie well above E_F, while the remaining Bi p band crosses below E_F to only -0.3 eV at D, so that part of the electron reservoir is forced back into the remaining structure. However, the calculated valences in Table 5.7 show that the hole donated when Pb substitutes for Bi more than compensates for this addition of electrons, resulting in a net increase of 0.29 holes per CuO_2

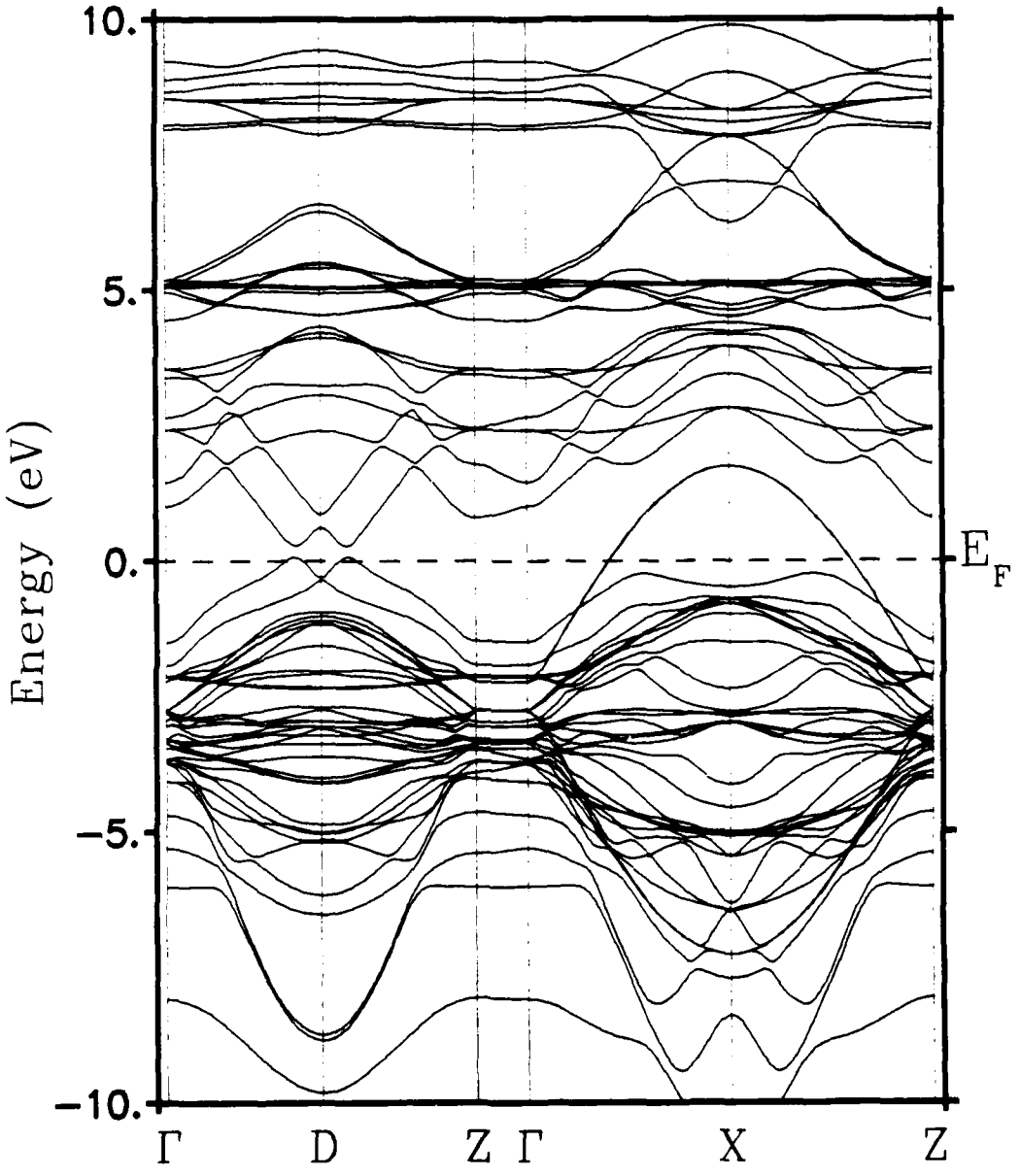

Fig. 5.7. Electronic energy bands for $BiPbCaSr_2Cu_2O_8$.

TABLE 5.7. Valences $\sum n$ for BiMCaSr$_2$Cu$_2$O$_8$.

	Bi	Pb	Ca	Sr[a]	Cu[a]	O(1)[a]	O(2)[a]	O(3)[a]
M = Bi	1.80	···	1.51	1.09	0.84	-1.09	-1.14	-1.18
M = Pb	1.79	1.23	1.51	1.09	1.01	-1.03	-1.14	-1.17

[a] Averaged over sites in unit cell for M = Pb.

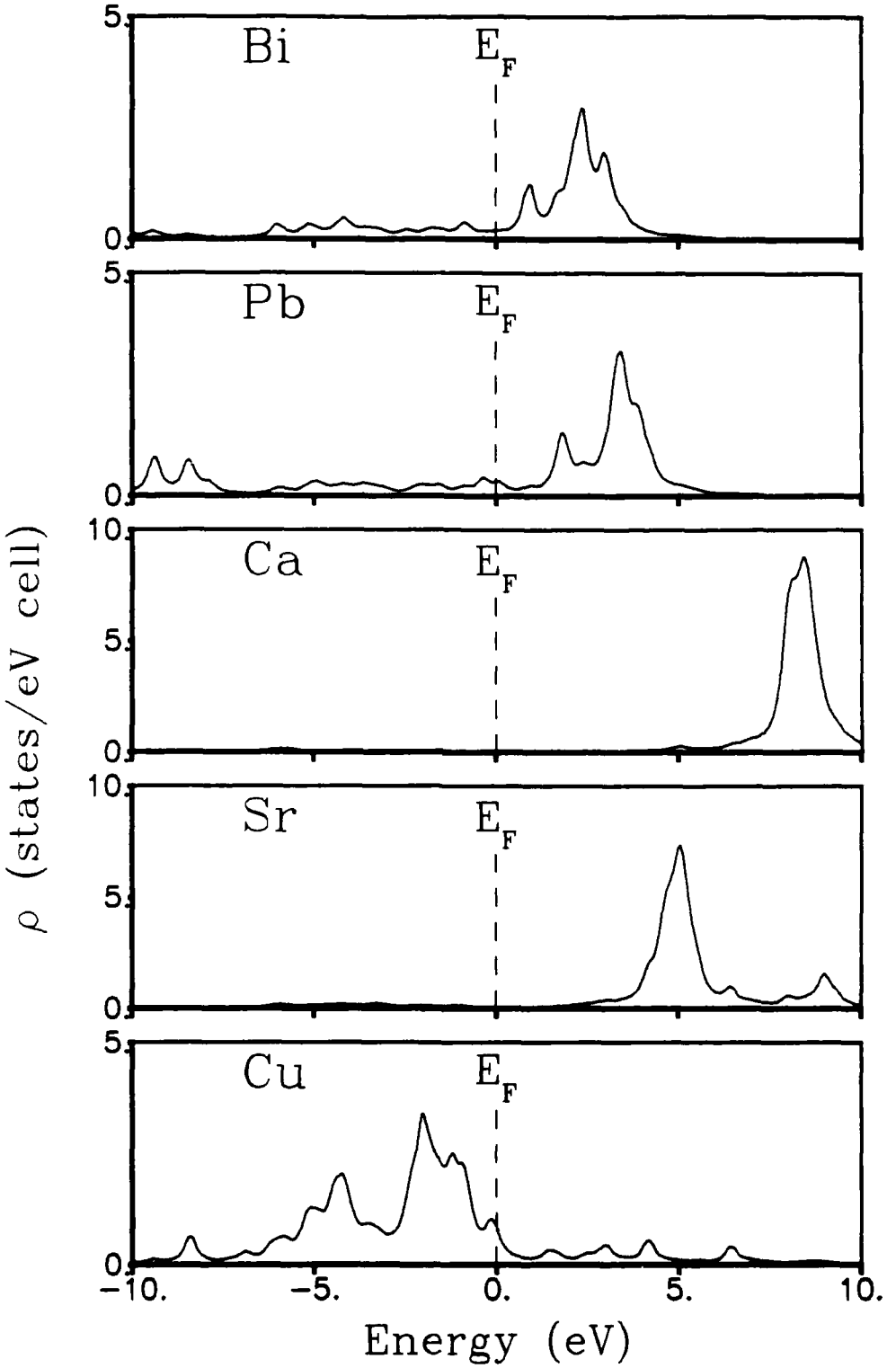

Fig. 5.8. Local densities of states for the metal atoms in $BiPbCaSr_2Cu_2O_8$.

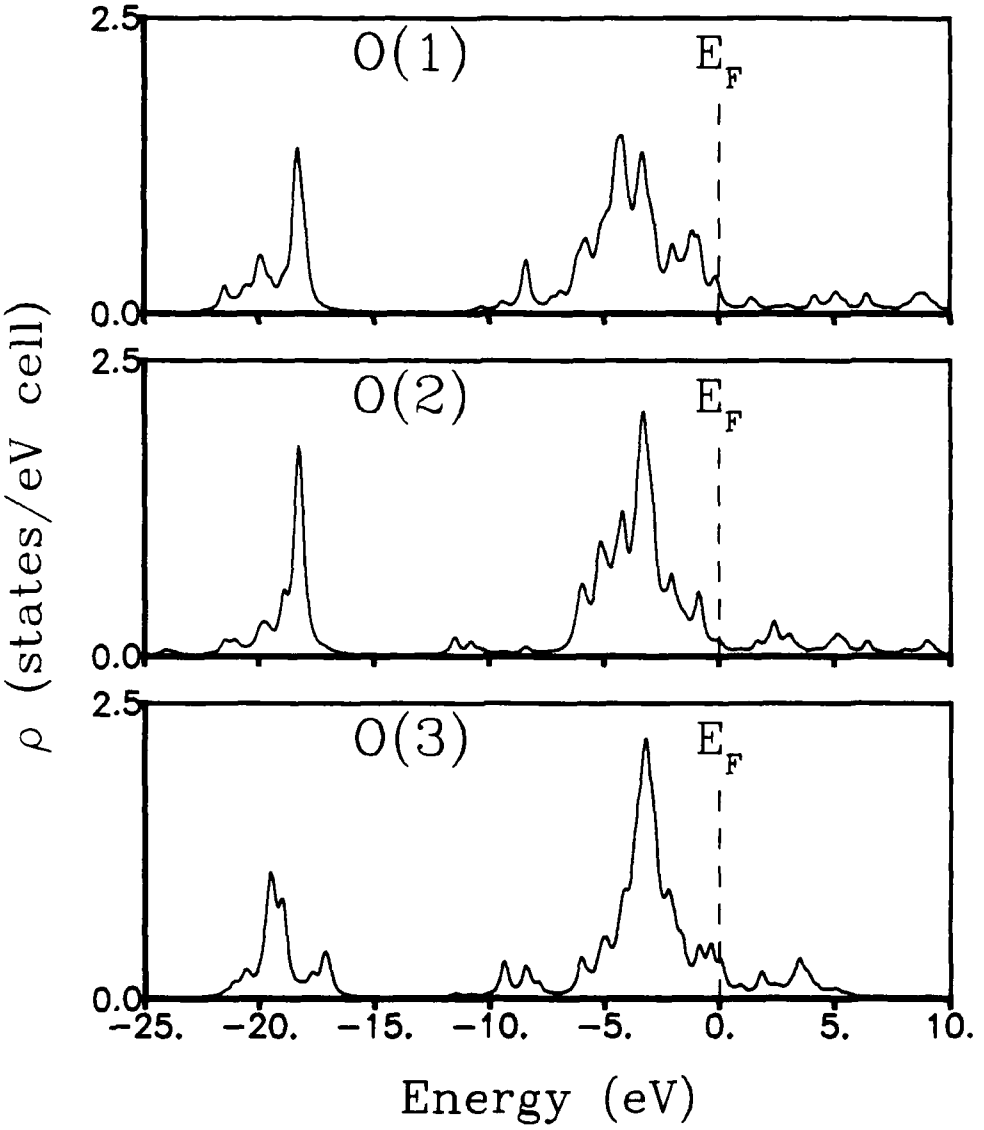

Fig. 5.9. Local densities of states for the oxygen atoms in $BiPbCaSr_2Cu_2O_8$.

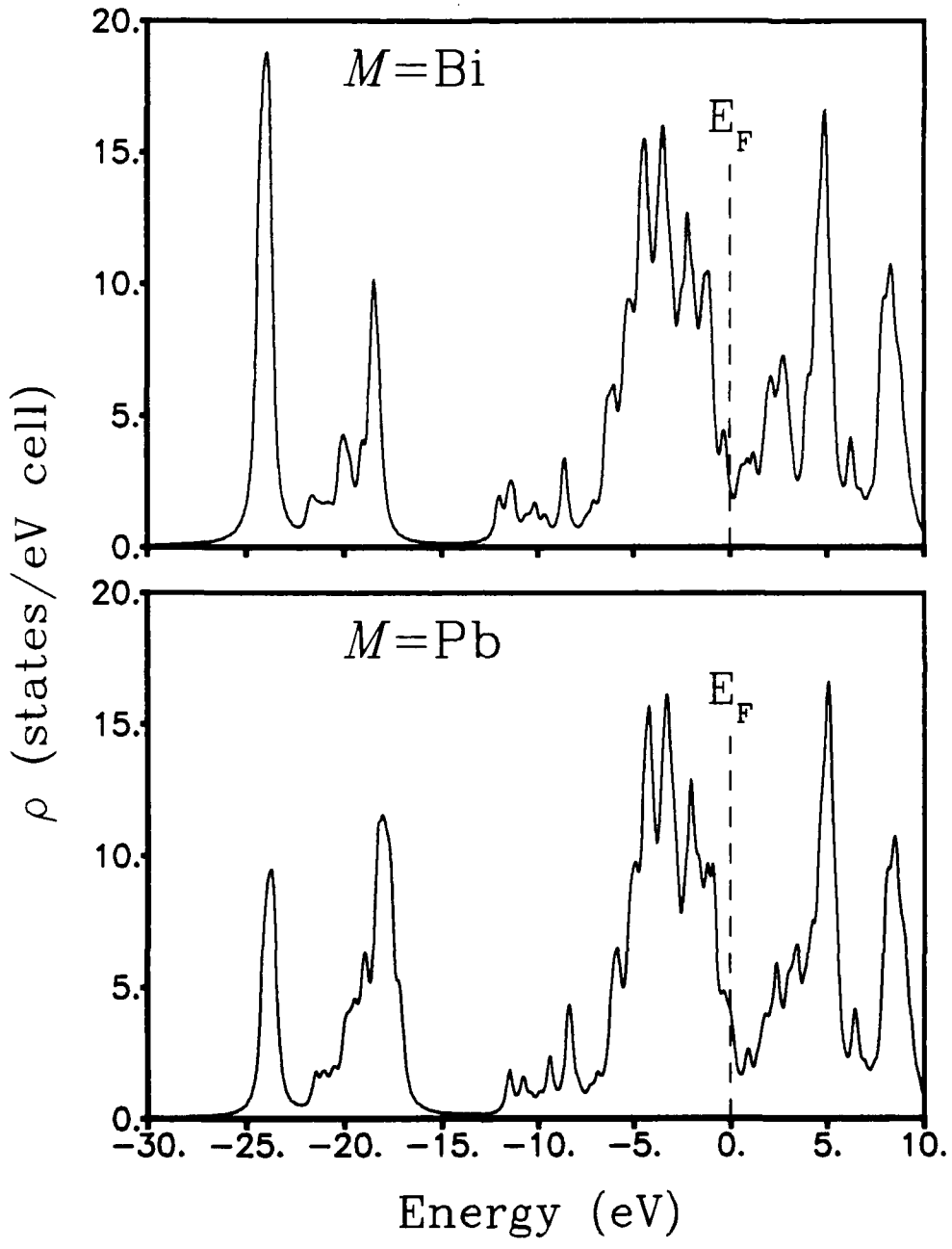

Fig. 5.10. Total densities of states for $BiMCaSr_2Cu_2O_8$.

layer in each unit cell.

The local densities of states for $BiPbCaSr_2Cu_2O_8$ are shown in Figs. 5.8 and 5.9. The results are very similar to those for $Bi_2CaSr_2Cu_2O_8$ in Figs. 4.11 and 4.12, with an overall shift in the Fermi energy of $\Delta E_F = -0.19$ eV and an upward shift of the Pb local density of states with respect to Bi. The total densities of states for $Bi_2CaSr_2Cu_2O_8$ and $BiPbCaSr_2Cu_2O_8$ are shown in Fig. 5.10. Within the present model, the density of states at the Fermi energy increases with Pb doping, from 2.4 states/eV cell to 4.1 states/eV cell. We propose that the primary effect of Pb substitution is to increase the carrier density within the superconducting copper-oxide regions.

$TlMCaBa_2Cu_2O_8$, M = Hg or Pb

Let us now consider the modification of the electronic structure when Tl is partially replaced by Hg or Pb, focusing on the representative material $Tl_2CaBa_2Cu_2O_8$. The electronic energy bands for $TlHgCaBa_2Cu_2O_8$ are shown in Fig. 5.11. Only the hole conduction bands cross E_F in this material, with the Tl s and Hg s states remaining unoccupied. The local density of states for Hg is shown in Fig. 5.12, with the d states at about -6 eV. The local densities of states for the other atoms in $TlHgCaBa_2Cu_2O_8$ are very similar to those in Figs. 4.17 and 4.18, but with a shift in the Fermi energy of $\Delta E_F = -0.23$ eV. The valences given in Table 5.8 indicate that Hg is much less ionic than Tl in this material. The added hole of Hg leads to a lowering of E_F, and in the present model there is an increase in $\rho(E_F)$ from 2.7 states/eV cell to 4.2 states eV cell. As can be seen in Table 5.8, there is a positive shift in the valence of both Cu and O(1) in the charge-carrying CuO_2 planes, indicating that hole carriers are

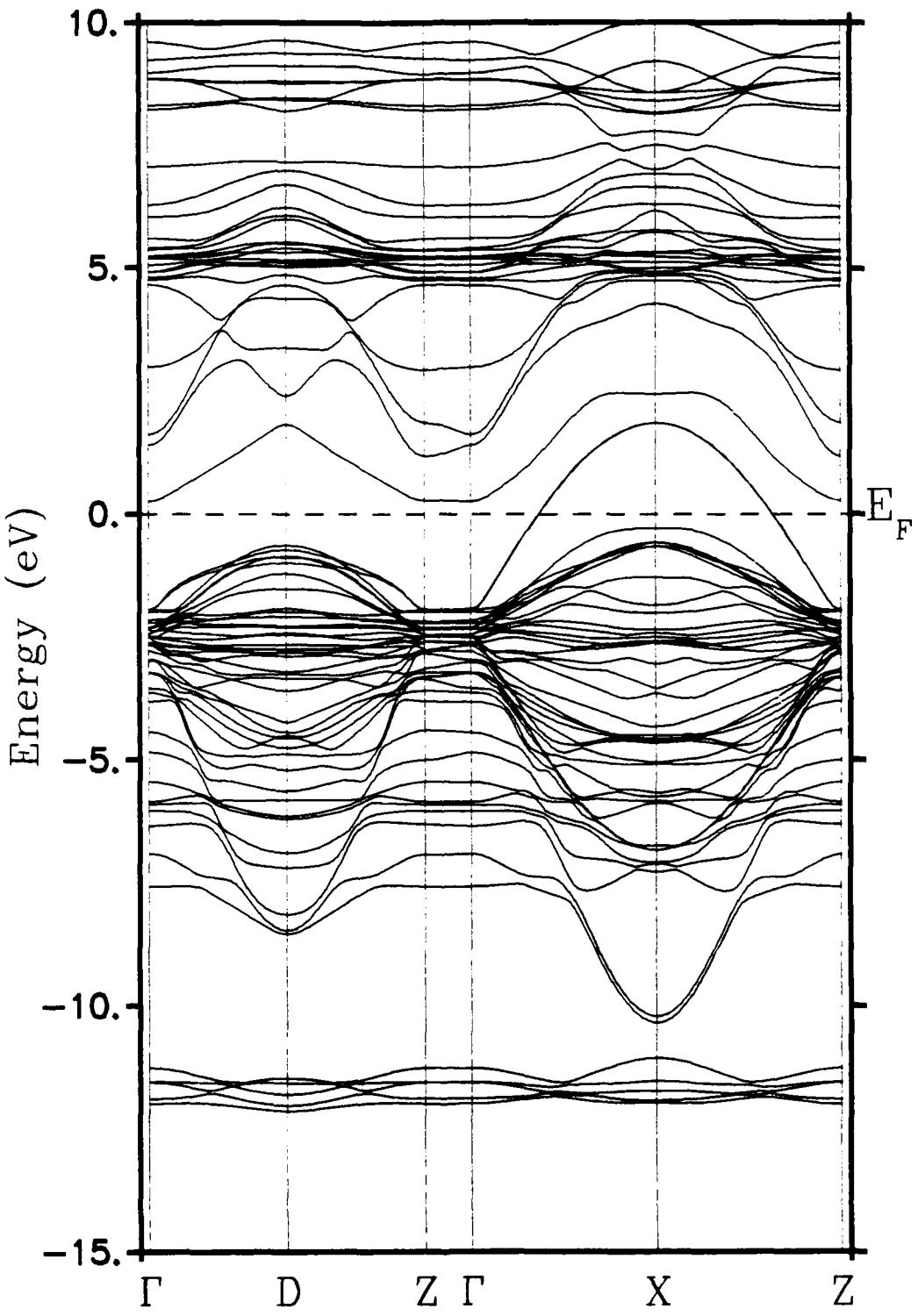

Fig. 5.11. Electronic energy bands for $TlHgCaBa_2Cu_2O_8$.

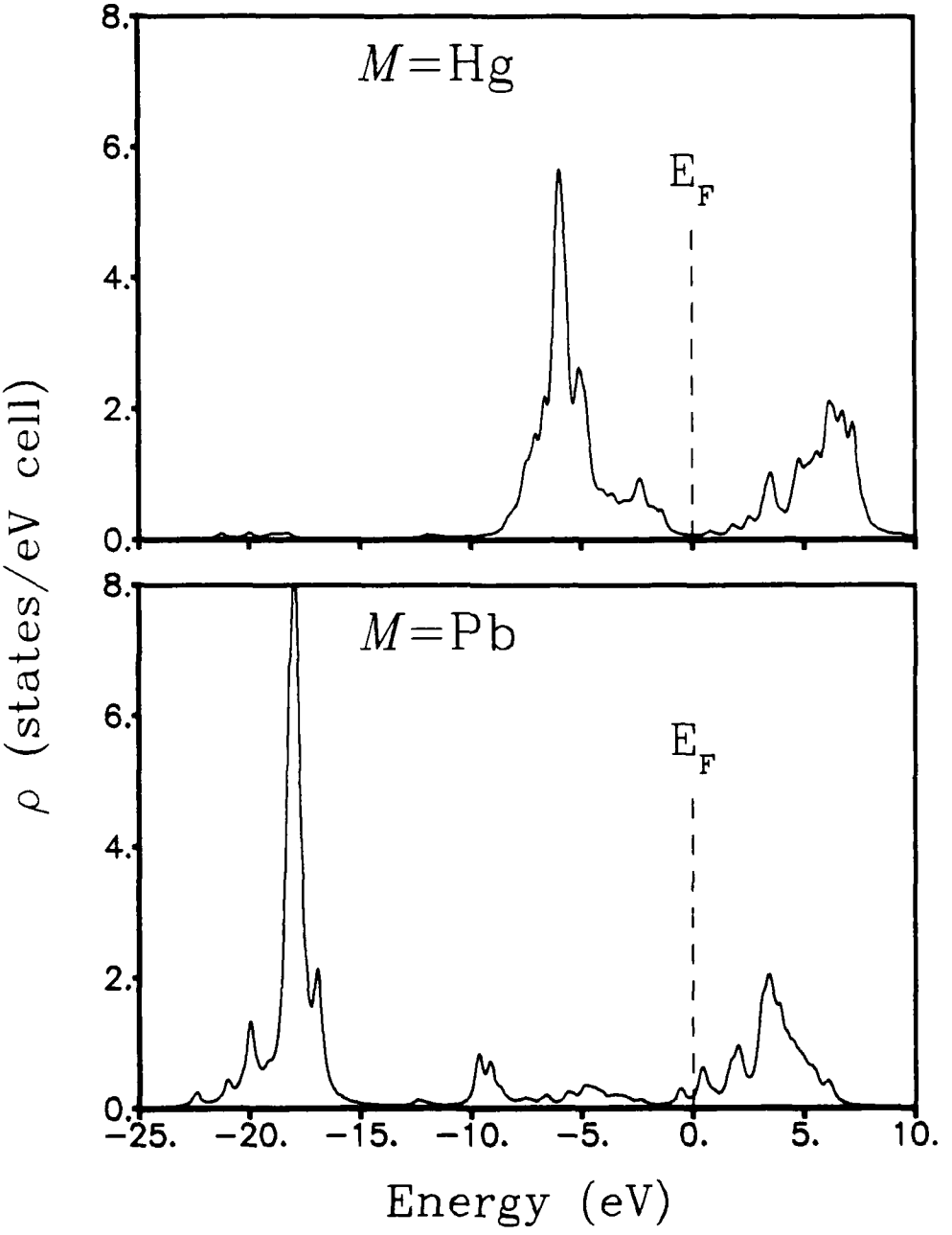

Fig. 5.12. Local densities of states for Hg and Pb in TlMCaBa$_2$Cu$_2$O$_8$.

TABLE 5.8. Valences Δn for TlMCaBa$_2$Cu$_2$O$_8$.

	Tl	M	Ca	Ba[a]	Cu[a]	O(1)[a]	O(2)[a]	O(3)[a]
M = Hg	1.02	0.50	1.45	1.38	1.14	-1.03	-1.10	-0.83
M = Tl	1.05	···	1.45	1.37	0.86	-1.13	-1.03	-0.71
M = Pb	1.06	1.46	1.45	1.37	0.66	-1.21	-0.98	-0.62

[a] Averaged over sites in unit cell for M = Hg and Pb.

doped into the superconducting region by Hg substitution.

A similar calculation for Pb replacing Tl finds that Pb raises the Fermi energy by $\Delta E_F = 0.19$ eV. The valences of Table 5.8 for $TlPbCaBa_2Cu_2O_8$ demonstrate that doping with Pb significantly decreases the valences of the Cu and O(1) sites in the CuO_2 planes. The local density of states for Pb is shown in Fig. 5.12. The Pb d states lie about 18 eV below E_F, while the dispersive p states are unoccupied. The total density of states at the Fermi energy is lower for this case: $\rho(E_F) = 1.9$ states/eV cell.

Summary of Substitution Effects

In summary, calculations for the replacement of Cu, Ba, and O with other elements have been performed for the system $YBa_2Cu_3O_7$. The results are in reasonable agreement with expected chemical trends. The suppression of T_c by Al substitution on the Cu(1) site is associated with the destruction of the conduction band within the CuO chain and a more ionic character for Al and O within the chain. The substitutions of the transition metals Fe, Co, Ni, and Zn for Cu also give results that are compatible with experiment, except in the case of Zn. However, the experimentally-observed changes in superconducting properties may result from structural changes that are not considered here. Substitutions on the Cu(2) site disrupt the CuO_2 plane conduction bands more than do substitutions on the Cu(1) site. Results for the replacement of Ba by Sr give support for a purely structural suppression of T_c, while we suggest that La substitution leads to destruction of the hole charge carriers by the donor electrons, resulting in suppression of superconductivity. The results for F and N substitutions on the oxygen sites show that the electronic

structure of $YBa_2Cu_3O_7$ may be affected by such replacements, but no obvious enhancements of the superconducting properties are found.

Substitution of Pb for Bi in $BiMCaSr_2Cu_2O_8$ gives an increase in the hole carriers within the CuO_2 planes, assuming an isostructural form for $BiPbCaSr_2Cu_2O_8$ and $Bi_2CaSr_2Cu_2O_8$. The most obvious effect of doping with Hg or Pb in $TlMCaBa_2Cu_2O_8$ is the shift in the Fermi energy, with Hg creating holes and Pb destroying them.

CHAPTER VI

VACANCY EFFECTS

Using the tight-binding model of Chapter III, we now consider the electronic effects of isolated oxygen vacancies in $La_{1.85}Sr_{0.15}CuO_{4-y}$ and $YBa_2Cu_3O_{7-y}$, and of lanthanum vacancies in $La_{2-x}CuO_4$. We neglect local strains and the small changes in the lattice constants that occur as vacancies are introduced. For simplicity, we use the bct structure[9] for $La_{1.85}Sr_{0.15}CuO_4$, neglecting the small orthorhombic distortion. For $YBa_2Cu_3O_7$, the observed orthorhombic structure[18] is used. The change in the density of states is computed with a Green's function method.

As described in Chapter II, oxygen vacancies have a significant effect on the electronic properties of $La_{2-x}Sr_xCuO_{4-y}$ and $YBa_2Cu_3O_{7-y}$. In the simplest picture of a rigid-band model, the removal of oxygen is expected to add electrons, giving the opposite effect of doping with holes. Indeed, both $La_{2-x}Sr_xCuO_{4-y}$ and $YBa_2Cu_3O_{7-y}$ exhibit a depression in T_c with increasing oxygen vacancies.[3,6,7,26,27] However, the lead cuprates $Pb_2A_{1-x}Ca_xSr_2Cu_3O_{8\pm y}$ (A = Y or a rare earth element) show little change in electronic properties as oxygen is added to or removed from the Cu layer intercalated between the PbO layers,[83] while the electron-doped materials such as $Nd_{2-x}Ce_xCuO_{4-y}$ have improved superconducting properties with the introduction of oxygen vacancies.[86]

The magnetic properties of these materials are also strongly affected by oxygen vacancies.[142,150] Electronic structure calculations within the local-density approximation for La_2CuO_{4-y} have been interpreted as indicating that oxy-

gen vacancies may lead to antiferromagnetism through narrowing of the valence bands in the neighborhood of E_F,[268] although the LDA may be inadequate for a proper treatment of magnetic effects.[269] LDA calculations for $YBa_2Cu_3O_6$ do not properly describe the antiferromagnetism in this material.[270,271]

Green's Function Technique

The unperturbed Green's function from (3.7) is

$$G_0(E) = \sum_{\vec{k},n} w_{\vec{k}} \frac{\psi(\vec{k},n)\,\psi^{\dagger}(\vec{k},n)}{E - E(\vec{k},n) - i\delta} . \tag{6.1}$$

In the tight-binding representation, the Green's function is a $N \times N$ matrix, $\bar{G}_0(E)$, over the N basis states of the system. For a perturbing potential $\bar{V}$, the total density of states $\rho(E)$ is changed by[272,273]

$$\Delta\rho(E) = \frac{2}{\pi} \frac{\partial\eta(E)}{\partial E} , \tag{6.2}$$

where $\eta(E)$ is the phase shift

$$\eta(E) \equiv - Im \text{ Log det } [\bar{1} - \bar{V}\bar{G}_0(E)] . \tag{6.3}$$

Here $\bar{1}$ is the $N \times N$ identity matrix. Now suppose the perturbing potential $\bar{V}$ acts only on a particular $n \times n$ subspace of states in the system, e.g., the n states associated with an isolated atomic vacancy. Using the subspace Hamiltonian technique,[274] we partition the Green's function such that the perturbation $\bar{V}$ has nonzero elements only in the $n \times n$ subspace. The determinant of (6.3) is then

$$\det [\bar{1} - \bar{V}\bar{G}_0(E)] = \det \left[\begin{pmatrix} 1 & 0 \\ 0 & 1 \end{pmatrix} - \begin{pmatrix} V & 0 \\ 0 & 0 \end{pmatrix} \begin{pmatrix} G_0^{sub} & G^{12} \\ G^{21} & G^{22} \end{pmatrix} \right] , \tag{6.4}$$

and thus

$$\det\,[\bar{1} - \bar{V}\bar{G}_0(E)] = \det\,[1 - VG_0^{\rm sub}(E)]\,. \tag{6.5}$$

The matrices 1, V, and $G_0^{\rm sub}(E)$ are thus reduced in size to $n \times n$ for the n states in the perturbation subspace, substantially reducing the numerical effort for the problem.

For the particular case of an atomic vacancy calculation, the perturbing potential V may be approximated[275] by letting the diagonal elements of V approach $-\infty$, so that for a full atomic vacancy the perturbed states are completely unoccupied. The elements of the identity matrix may then be neglected, so that (6.5) reduces to

$$\begin{aligned} \det\,[\bar{1} - \bar{V}\bar{G}_0(E)] &\approx \det\,[-VG_0^{\rm sub}(E)] \\ &\approx \det\,(-V)\,\det\,G_0^{\rm sub}(E)\,. \end{aligned} \tag{6.6}$$

Within this approximation the perturbation V is independent of the energy, so substituting (6.6) into (6.2) and (6.3) yields the change in the total density of states

$$\begin{aligned} \Delta\rho(E) &= -\frac{2}{\pi}\,\frac{\partial}{\partial E}\,Im\ \mathrm{Log}\ \det\,G_0^{\rm sub}(E) \\ &= -\frac{2}{\pi}\,\frac{\partial}{\partial E}\,\arctan\!\left(\frac{Im\ \det\,G_0^{\rm sub}(E)}{Re\ \det\,G_0^{\rm sub}(E)}\right)\,. \end{aligned} \tag{6.7}$$

The second form in (6.7) is used for the calculations. The principal value of the arctangent is used, but with shifts of $\pm 2\pi$ added to preserve continuity in the physical result. The energy derivative is calculated numerically. For the full vacancy result, a simple check of the calculation is that the integral of $\Delta\rho(E)$ gives the number of states (for both spins) associated with the vacancy site:

$$\int_{-\infty}^{+\infty} \Delta\rho(E)\,\mathrm{d}E = 2n\,. \tag{6.8}$$

The modified total density of states for y atomic vacancies is given by

$$\rho(E) = \rho_0(E) + y\Delta\rho(E) , \tag{6.9}$$

with the unperturbed total density of states $\rho_0(E)$ given by (3.6). The Fermi energy is calculated by integrating $\rho(E)$ up to the number of valence electrons for a given concentration of vacancies. This calculation neglects the interaction between vacancies, and is strictly valid only for a small fraction of vacancies. However, for $y = 1$ we have performed an independent calculation with one oxygen vacancy per formula unit for $La_{1.85}Sr_{0.15}CuO_3$ and for $YBa_2Cu_3O_6$, and the change in the density of states is approximately the same.[276]

Oxygen Vacancies in $La_{1.85}Sr_{0.15}CuO_{4-y}$

We consider both oxygen sites in $La_{1.85}Sr_{0.15}CuO_4$, with O(1) in the CuO_2 plane and O(2) in the LaO layer. The perturbation affects only the 4×4 subspace associated with the s, p_x, p_y, and p_z states of the oxygen atom. Figure 6.1 shows the change in the density of states $\Delta\rho(E)$ for a single oxygen vacancy in $La_{1.85}Sr_{0.15}CuO_{4-y}$. Notice that $\Delta\rho$ has more structure near the Fermi energy for the O(1) site than for the O(2) site, because of the strong $pd\sigma$ interactions of O(1) p orbitals with copper d orbitals. For both sites, $\Delta\rho$ is negative at the unperturbed Fermi energy. The larger magnitude at E_F^0 for the O(1) site is consistent with the observation of substantial in-plane O p_x and p_y character at the Fermi energy.[168] Figure 6.2 shows the resulting total density of states for y oxygen vacancies per formula unit on the O(1) site. A substantial decrease is seen in the total density of states within 2 eV below E_F as y increases. As shown in Table 6.1, the density of states at E_F is smaller than the $y = 0.0$ value

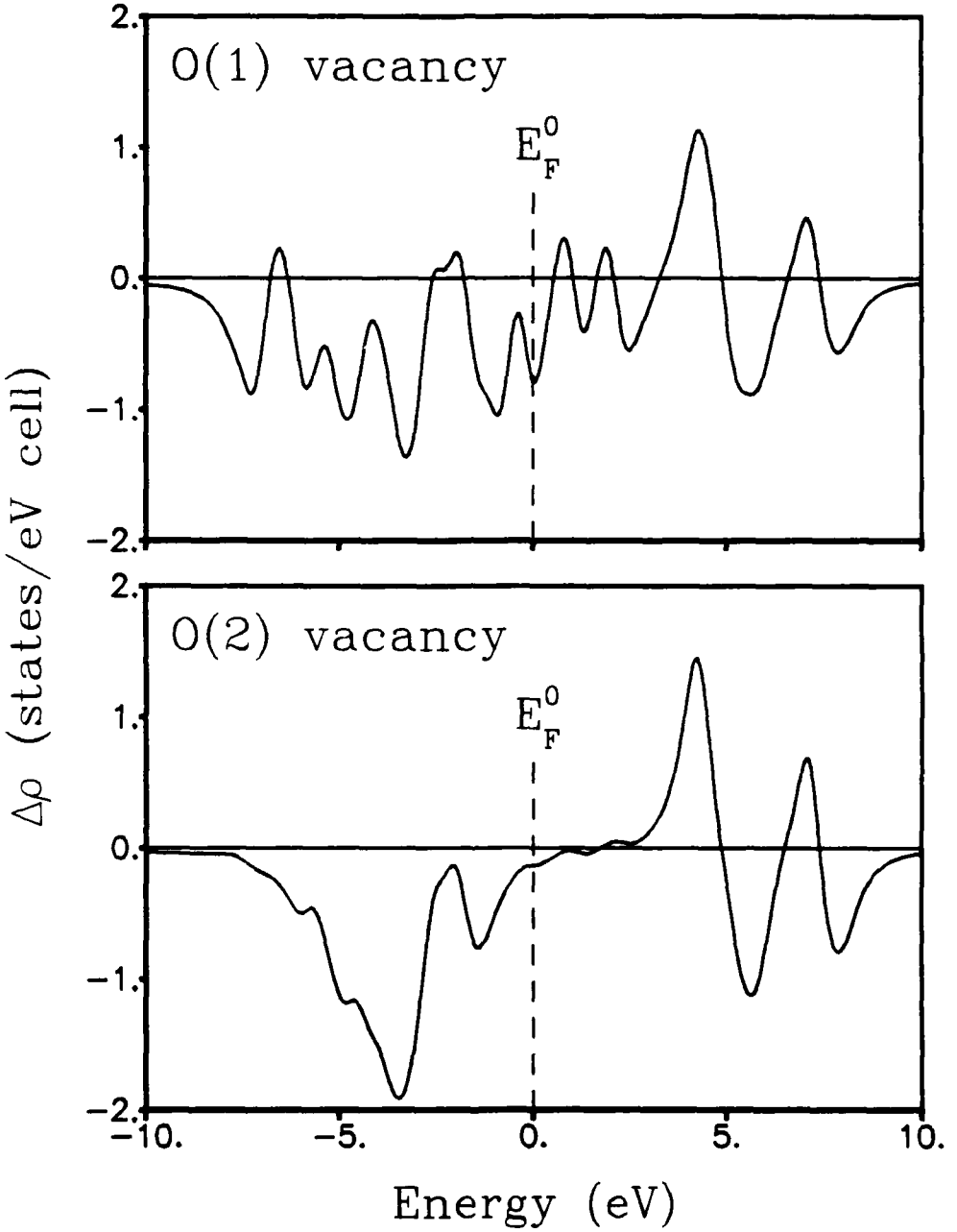

Fig. 6.1. Change in density of states for an isolated oxygen vacancy in $La_{1.85}Sr_{0.15}CuO_{4-y}$. Oxygen site O(1) is in the CuO_2 plane, and O(2) is in the La/Sr layer.

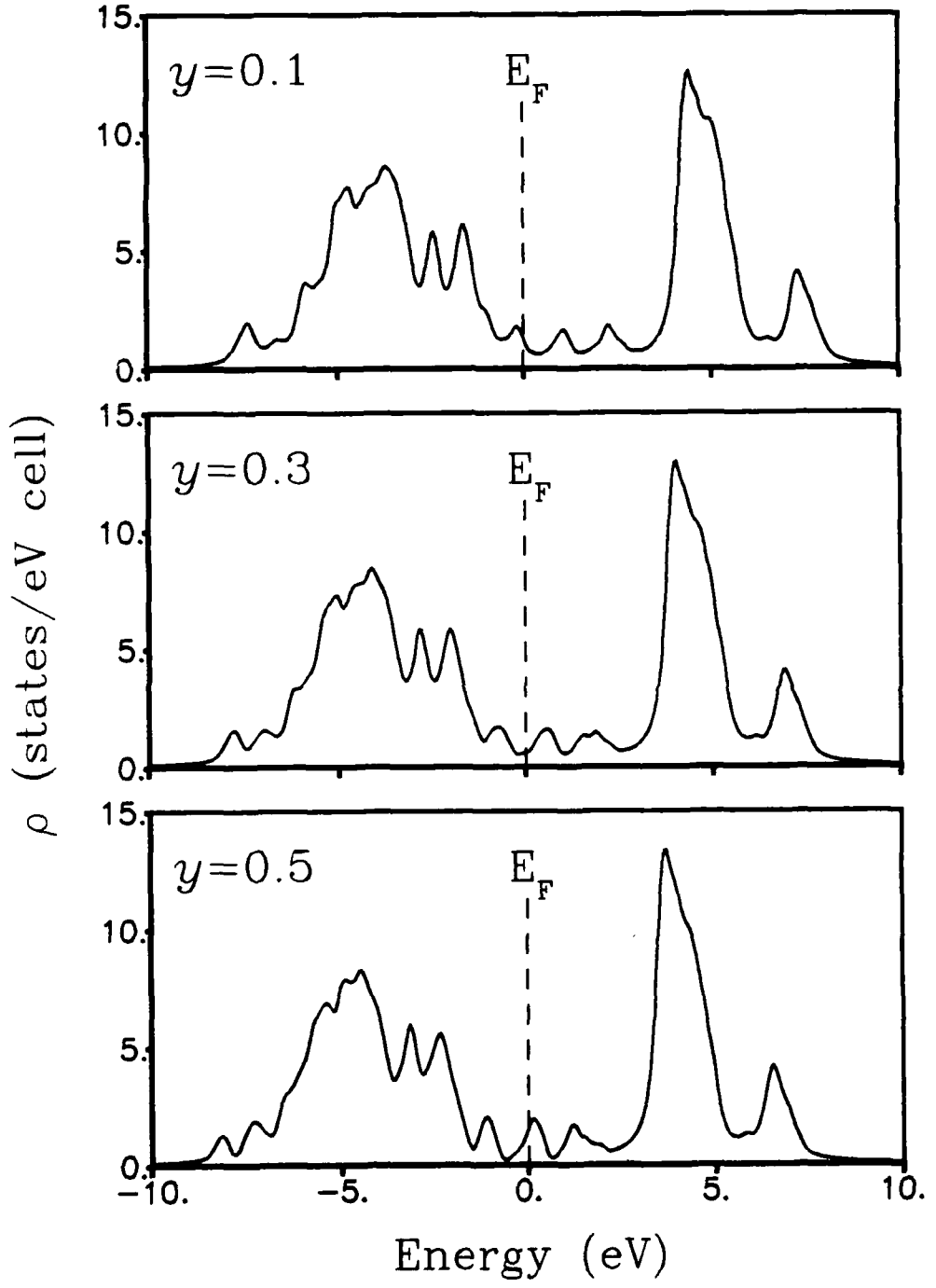

Fig. 6.2. Density of states for y oxygen vacancies on the O(1) plane site in $La_{1.85}Sr_{0.15}CuO_{4-y}$.

TABLE 6.1. Shift in E_F and density of states for y oxygen vacancies per formula unit on site O(1) in $La_{1.85}Sr_{0.15}CuO_{4-y}$.

y	ΔE_F (eV)	$\rho(E_F)$ (states/eV cell)
0.0	0.00	1.9
0.1	0.07	1.3
0.2	0.20	0.7
0.3	0.44	0.6
0.4	0.65	1.0
0.5	0.76	1.5
0.6	0.83	2.0
0.7	0.88	2.3
0.8	0.93	2.3
0.9	0.97	2.3
1.0	1.01	2.3

TABLE 6.2. Shift in E_F and density of states for y oxygen vacancies per formula unit on site O(2) in $La_{1.85}Sr_{0.15}CuO_{4-y}$.

y	ΔE_F (eV)	$\rho(E_F)$ (states/eV cell)
0.0	0.00	1.9
0.1	0.12	1.3
0.2	0.31	0.7
0.3	0.60	0.6
0.4	0.87	0.9
0.5	1.03	1.4
0.6	1.14	1.8
0.7	1.26	1.5
0.8	1.41	0.9
0.9	1.66	0.6
1.0	1.94	0.8

for $y \leq 0.5$, and E_F monotonically increases with y. The O(1) vacancies thus behave as donors, filling the hole states near the Fermi energy.

For vacancies on the O(2) site, Table 6.2 indicates that $\rho(E_F)$ is smaller than the $y = 0.0$ value for all $y > 0$. The Fermi energy increases somewhat faster for O(2) vacancies than for O(1) vacancies, since the more ionic nature of the Cu–O(2) and the La–O(2) bonds leaves most of the O(2) character below E_F. These O(2) vacancies are again electron donors.

Lanthanum Vacancies in $La_{2-x}CuO_4$

The perturbation subspace for a La vacancy contains the six states (one s and five d) associated with lanthanum. The change in the density of states of $La_{2-x}CuO_4$ for a single La vacancy is shown in Fig. 6.3. Little change is seen at E_F^0, because of the ionic and insulating nature of the LaO layer. The large contribution near ≈ 5 eV arises from the unoccupied La d bands. The total density of states for x lanthanum vacancies per formula unit is shown in Fig. 6.4. The density of states near E_F is relatively unchanged, with only a rigid shift of the bands observed with increasing x. As shown in Table 6.3, E_F is lowered as La vacancies are introduced. Lanthanum vacancies thus donate holes to the material, just as divalent Sr does when substituted for trivalent La. This may explain the enhancement of superconductivity[11,12] observed in some samples of La_2CuO_4, in that deficiencies of La within the undoped material can provide the required hole carriers. In our calculations, there is an increase in $\rho(E_F)$ for $x \leq 0.3$.

A recent set of experiments has shown that excess oxygen can be incorporated into the structure of La_2CuO_{4+y} while maintaining full La

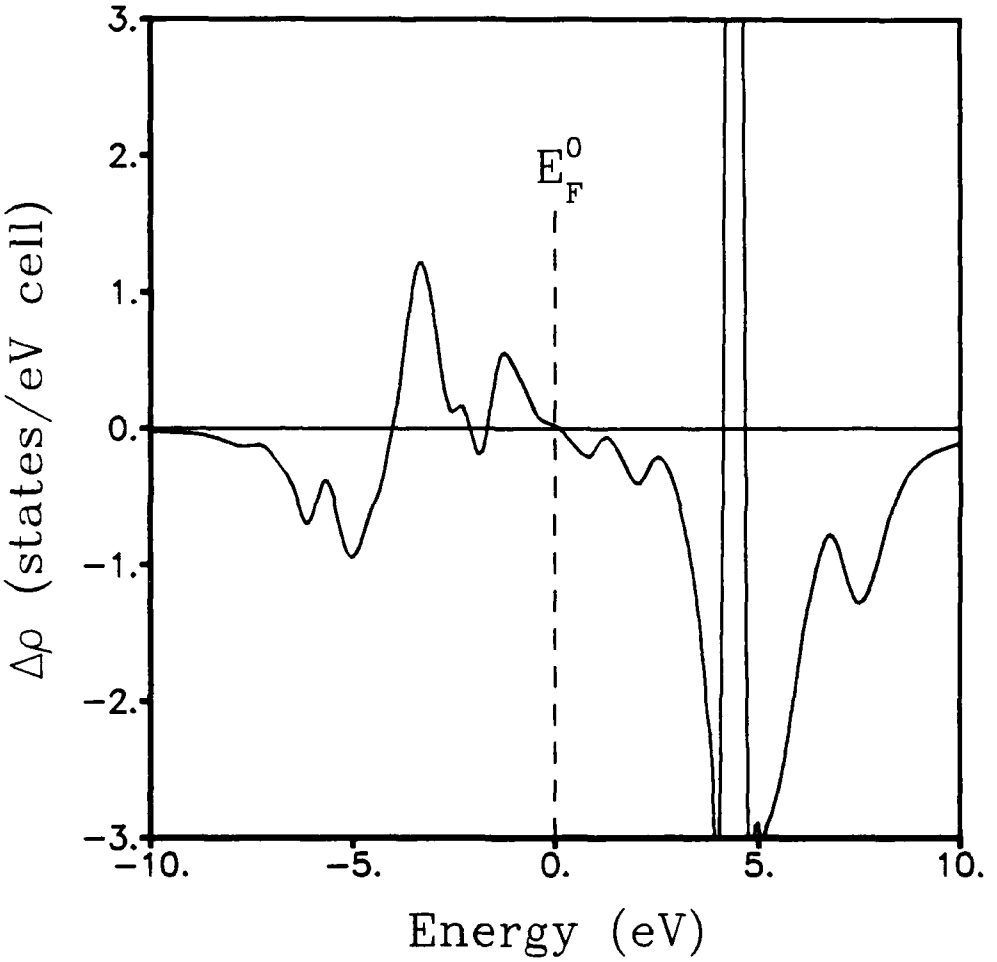

Fig. 6.3. Change in density of states for a lanthanum vacancy in $La_{2-x}CuO_4$.

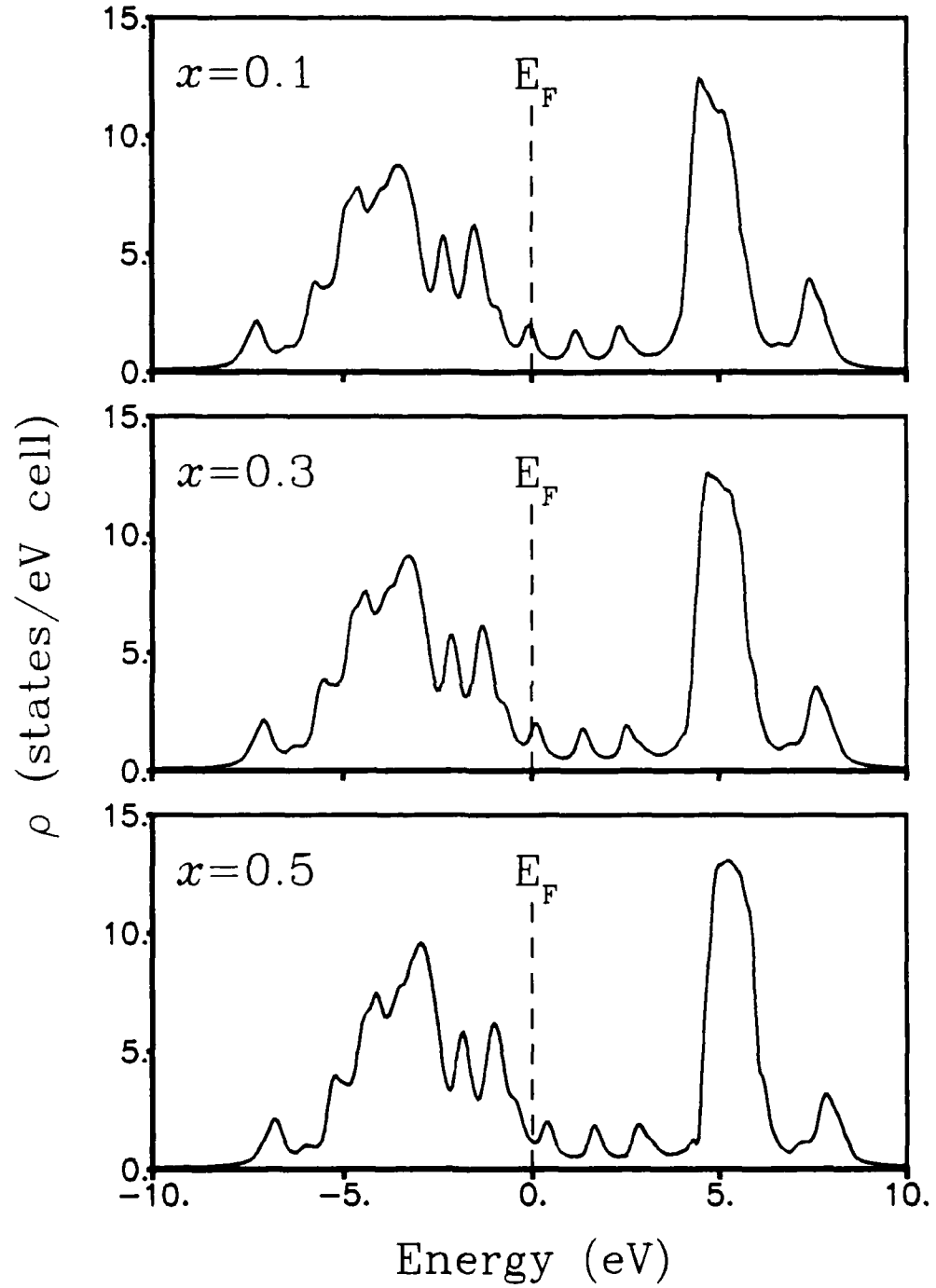

Fig. 6.4. Density of states for x lanthanum vacancies in $La_{2-x}CuO_4$.

TABLE 6.3. Shift in E_F and density of states for x lanthanum vacancies per formula unit in $La_{2-x}CuO_4$.

x	ΔE_F (eV)	$\rho(E_F)$ (states/eV cell)
0.0	0.00	1.4
0.1	-0.11	1.9
0.2	-0.20	1.9
0.3	-0.29	1.7
0.4	-0.42	1.2
0.5	-0.56	1.2
0.6	-0.69	1.5
0.7	-0.79	2.0
0.8	-0.86	2.4
0.9	-0.92	2.9
1.0	-0.98	3.2

stoichiometry.[277–279] The excess oxygen ($y \approx 0.1$) appears to cluster in the superoxide ion O_2^- within the material.[278] This oxygen-rich material forms a second orthorhombic phase below 320 K (with a slightly larger c lattice constant), separating from the non-superconducting phase of stoichiometric La_2CuO_4.[279] The oxygen-rich phase exhibits bulk superconductivity at $T_c = 34$ K in 30% of the sample volume for $y = 0.13$.[278] These experiments indicate that doping with oxygen does in fact lead to bulk superconductivity in La_2CuO_4. However, to test the results of our calculations, further experiments that introduce La vacancies while fixing the oxygen stoichiometry are needed.

Oxygen Vacancies in $YBa_2Cu_3O_{7-y}$

We now consider the electronic effects of oxygen vacancies in $YBa_2Cu_3O_7$. We examine only the oxygen chain site $O(1)$, which is experimentally determined to be the primary site for the introduction of oxygen vacancies.[24] The perturbation subspace is again 4×4 for oxygen vacancies.

The change in the density of states of $YBa_2Cu_3O_{7-y}$ for an isolated oxygen vacancy introduced on the O(1) site is shown in Fig. 6.5. The largest contributions to $\Delta\rho(E)$ are well-removed from the Fermi energy, but a negative contribution is found at E_F^0. Figure 6.6 shows the resulting densities of states for y oxygen vacancies per formula unit. We find peaks in the density of states that correspond to valence band photoemission results for $y \leq 0.3$, although the experimental binding energies are about 0.5 eV higher.[167,180,189,191] As the number of oxygen vacancies y increases, $\rho(E_F)$ decreases monotonically, consistent with a calculation within the LDA for $YBa_2Cu_3O_6$.[280] Table 6.4 shows the calculated shifts in E_F and $\rho(E_F)$ for $0.0 \leq y \leq 1.0$. The removal of

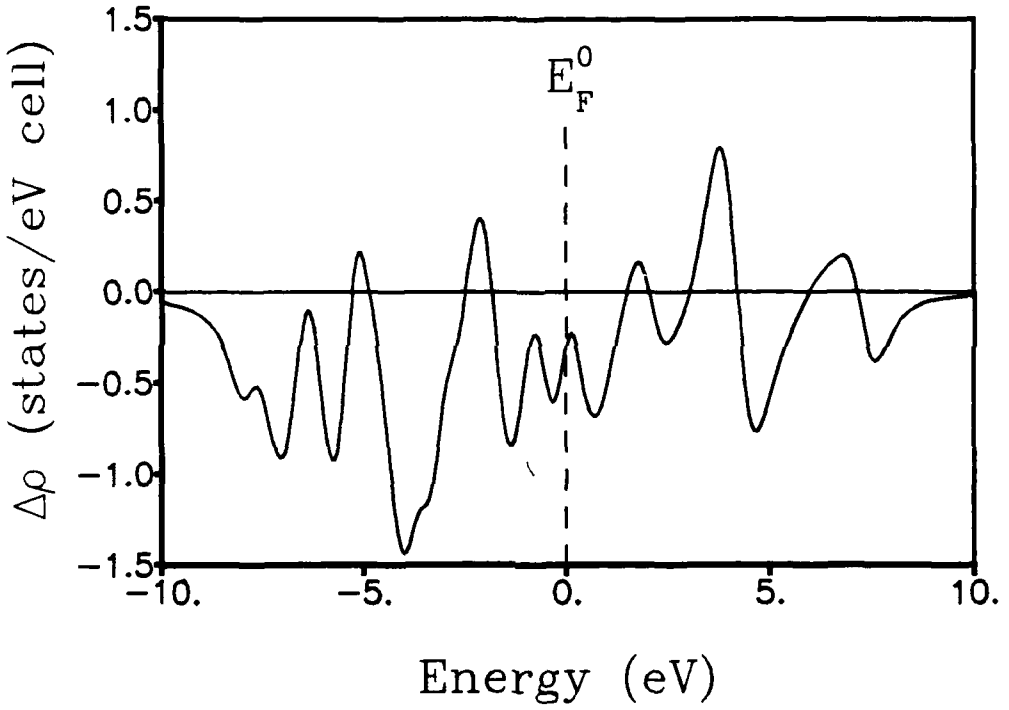

Fig. 6.5. Change in density of states for a single oxygen vacancy on the O(1) chain site in $YBa_2Cu_3O_{7-y}$.

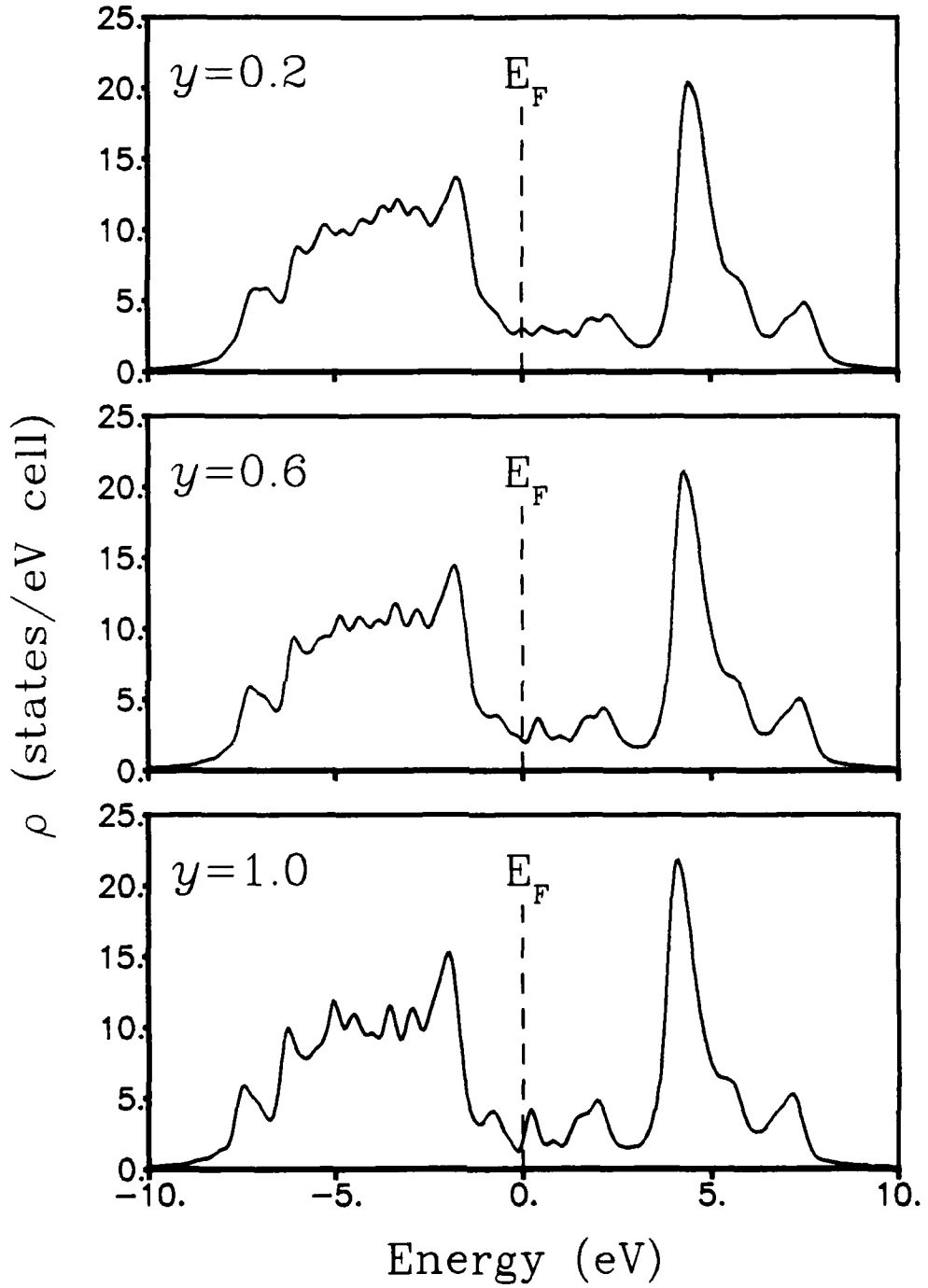

Fig. 6.6. Density of states for y oxygen vacancies on the O(1) chain site in $YBa_2Cu_3O_{7-y}$.

TABLE 6.4. Shift in E_F and density of states for y oxygen vacancies per formula unit on site O(1) in $YBa_2Cu_3O_{7-y}$.

y	ΔE_F (eV)	$\rho(E_F)$ (states/eV cell)
0.0	0.00	3.2
0.1	0.01	3.1
0.2	0.03	3.0
0.3	0.05	2.8
0.4	0.07	2.7
0.5	0.10	2.4
0.6	0.13	2.2
0.7	0.16	2.0
0.8	0.21	1.8
0.9	0.26	1.6
1.0	0.31	1.5

oxygen monotonically raises the Fermi level, so the present calculation confirms the expectation that oxygen vacancies act as electron donors in this system. The decrease in the density of states at E_F is consistent with shifts of the valence bands seen experimentally in photoemission studies of oxygen-deficient $YBa_2Cu_3O_{7-y}$.[194]

Within this model, we do not find a plateau in $\rho(E_F)$ with respect to y that might correspond to the change in T_c with oxygen vacancies.[26,27] However, we note that we have neglected ordering of the oxygen vacancies, which may play a role in this effect.[28,29] Also, recent experiments show that the electrons added with oxygen vacancies first localize on the CuO chains, with additional vacancies causing charge transfer from the chains to the CuO_2 planes.[32,281] The details of this charge transfer may be responsible for the plateau in T_c with oxygen vacancy concentration.[282] Oxygen-deficient $YBa_2Cu_3O_{7-y}$ has been shown to be single phase for $0.0 \leq y \leq 1.0$, so that a single T_c is associated with each oxygen stoichiometry.[283]

Summary of Vacancy Effects

Using the tight-binding model of Chapter III, we have calculated the electronic effects of oxygen vacancies in $La_{1.85}Sr_{0.15}CuO_{4-y}$ and $YBa_2Cu_3O_{7-y}$, and of lanthanum vacancies in $La_{2-x}CuO_4$. We find that oxygen vacancies act as electron donors in both systems, raising the Fermi energy and decreasing $\rho(E_F)$ for $y \leq 0.5$. The concentration of holes is thus decreased, consistent with the observations that oxygen vacancies degrade the superconductivity and metallic conductivity in these materials.

Lanthanum vacancies in $La_{2-x}CuO_4$ donate holes, lowering the Fermi

energy and increasing $\rho(E_F)$ for $x \leq 0.3$. Small concentrations of La vacancies may thus have the same effect electronically as divalent metal dopants such as Sr, leading to enhancement of superconductivity in nominally stoichiometric La_2CuO_4.

CHAPTER VII

EXCITONIC MECHANISM FOR SUPERCONDUCTIVITY

Although many mechanisms have been proposed to explain high-T_c superconductivity, no theory has yet successfully described the properties of these materials.[284] In this chapter we examine a specific version of the generic excitonic mechanism for superconductivity originally proposed by Little,[285] and elaborated by Ginzburg[286] and by Allender, Bray, and Bardeen.[287] Our mechanism requires a specific structural and electronic configuration, namely metallic planes (containing the charge carriers) adjacent to insulating metal-oxide layers such as LaO, BaO, or NdO. The insulating layers must support virtual excitations from oxygen p states, below the Fermi energy, to metal d states, above E_F. The effective pairing potential of the charge carriers is mediated by the interaction of the carriers with these excitations.

One advantage of the present mechanism is its applicability to both the copper-oxide and the bismuth-oxide superconductors, since no specific magnetic properties are required. For example, the systems $Ba_{1-x}K_xBiO_3$ and $BaPb_{1-y}Bi_yO_3$ are diamagnetic,[160] while both the hole-doped and the electron-doped cuprates generally display antiferromagnetic order in their nonsuperconducting stoichiometries.[85,142–145,150,157–159] It is thus unlikely that a magnetic mechanism for high-temperature superconductivity could apply to both the copper-oxide and the bismuth-oxide materials. Also, as found below, the exciton-mediated pairing potential is independent of the sign of the charge carriers, so that the present mechanism can describe both the n-type and p-type cuprates. Other excitonic mechanisms (with substantial differences from each

other and from the present mechanism) have been recently proposed to describe the high-temperature superconductors.[288-296]

Electronic and Structural Requirements

The present excitonic mechanism for high-temperature superconductivity was suggested by our electronic structure calculations for $La_{1.85}Sr_{0.15}CuO_4$ and for $YBa_2Cu_3O_7$, presented in Chapter IV, and strengthened by subsequent calculations for the other high-T_c materials. In every material examined, there are metallic layers, such as the CuO_2 planes in all the cuprates and the BiO_2 layers in $Ba_{0.6}K_{0.4}BiO_3$ and $BaPb_{0.75}Bi_{0.25}O_3$. Surrounding these metallic regions are metal-oxide layers such as LaO, BaO, SrO, PrO, NdO, or SmO. In Fig. 7.1 we show the local densities of states for these metal-oxide layers found in the results of Chapter IV for the hole-doped superconductors. The dashed curve peaking below E_F shows the local density of states for the oxygen atom in the metal-oxide layer [e.g., O(4) in $YBa_2Cu_3O_7$]. The region within ≈ 8 eV below E_F is primarily composed of O p states. The solid curve peaking above E_F gives $\rho(E)$ for the metal atom in this layer, with the largest peak arising from the unoccupied d states. In every case, these layers are insulating, in the sense that $\rho(E_F)$ is very small. Similar local densities of states have been calculated for the NdO layers in the electron-doped material $Nd_{2-x}Ce_xCuO_4$.[297] The atomic valences presented in Chapter IV show that the metal-oxide layer is also quite ionic in each material, with significant charge transfer between the metal and oxygen atom.

These ionic and insulating layers thus can support electronic excitations from the occupied oxygen p states to the vacant metal d states, with character-

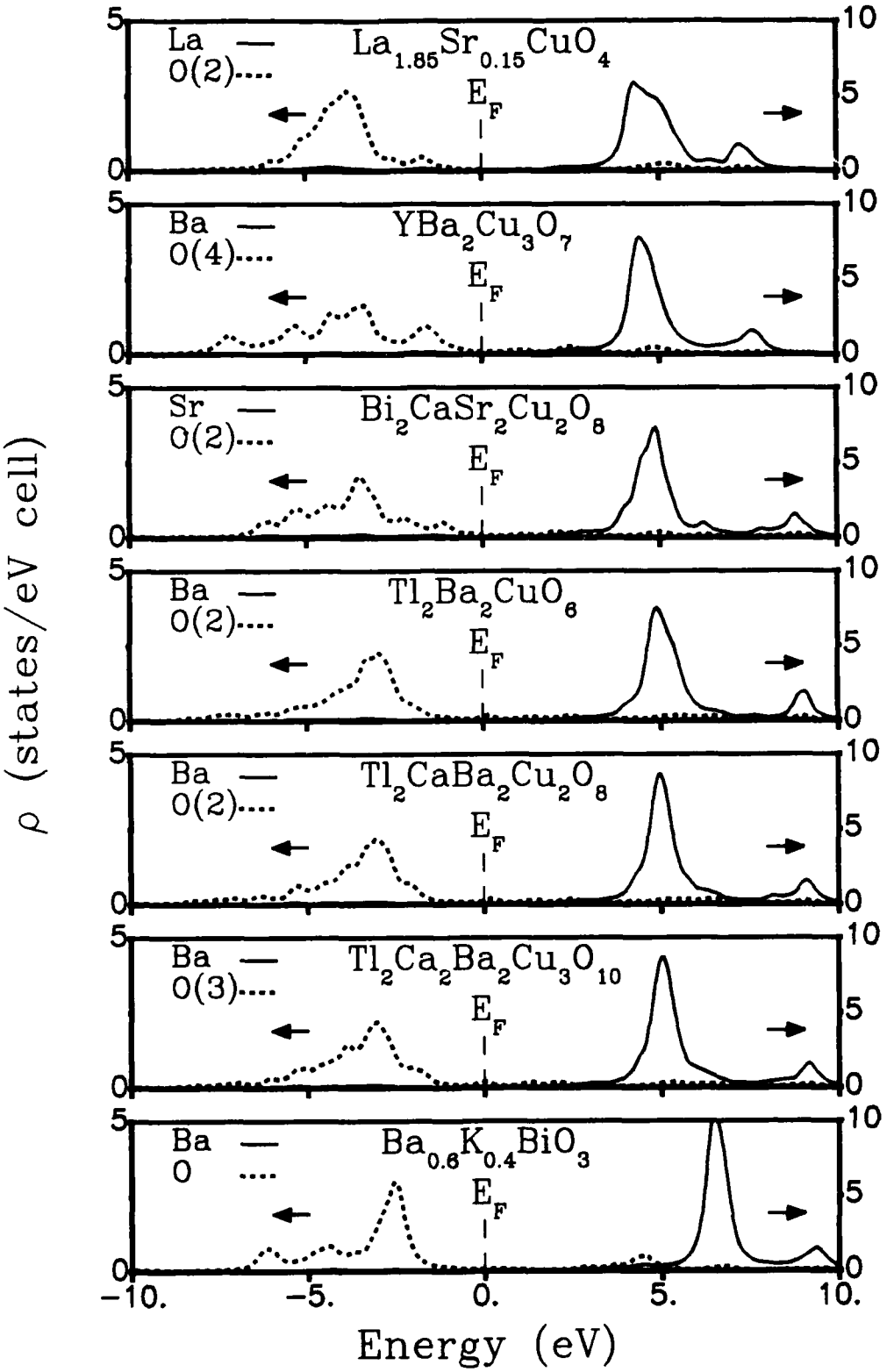

Fig. 7.1. Local densities of states for oxygen (dashed curves) and metal atoms (solid curves) in the insulating layers.

istic excitational energies of $5 - 10$ eV. The possibility of these band excitations forming bound electron-hole pairs (excitons) is described in the next section. As in Refs. 285-287, the excitations are spatially separated from the charge carriers. However, the insulating layers must lie in close proximity to the metallic planes (as in the sandwich structures of the high-temperature superconductors) to produce a pairing potential sufficient for superconductivity.

Formation of the Exciton

One approach is to treat an exciton within an insulating metal-oxide layer as a Frenkel-like, tightly-bound charge transfer exciton, using the Green's function method that was applied in the atomic vacancy calculations in Chapter VI. We model the exciton as a state that is split off from the one-electron band structure by a perturbation V_{eh} given by the electron-hole Coulomb interaction

$$V_{eh} = -\frac{e^2}{\epsilon d_0} , \tag{7.1}$$

where d_0 is the metal-oxygen bond length and ϵ is a dielectric constant that characterizes the region between the metal and oxygen atoms. Since the metal d states are initially unoccupied, there is no additional electron-electron repulsive term U as might be associated with occupied metal states.

Beginning with the unperturbed Green's function $G_0(E)$ in (3.7), we consider the perturbation to act only on the subspace of states associated with the metal site, so that the perturbed Green's function $G(E)$ is obtained from the one-electron Dyson's equation

$$G(E) = G_0^{\rm sub}(E) - G_0^{\rm sub}(E)VG(E) , \tag{7.2}$$

where all the matrices are 5×5 (representing the five d states on the metal site), and V is a diagonal matrix with elements V_{eh} applied to the d states of the metal site. We invert (7.2) to the form

$$G(E) = [1 - G_0^{\rm sub}(E)V]^{-1} G_0^{\rm sub}(E) \tag{7.3}$$

for the numerical calculations. The density of states for the exciton is then found from (3.6)

$$\rho(E) = -\frac{2}{\pi} Tr\ Im\ G(E)\ , \tag{7.4}$$

where the trace includes only the d states on the metal site.

The Frenkel exciton states are calculated for the representative materials $La_{1.85}Sr_{0.15}CuO_4$ and $YBa_2Cu_3O_7$. From the crystal structures of these materials,[9,18] the metal-oxygen bond lengths are 2.73 Å for La–O(2) and 2.76 Å for Ba–O(4). A simple estimate for the static dielectric constant ϵ is obtained from the relation[298]

$$\epsilon = 1 + \frac{\omega_p^2}{\omega_g^2}\ , \tag{7.5}$$

where ω_p is the bulk plasma frequency and $\hbar\omega_g$ is the energy gap of the insulating region. From the local densities of states in Fig. 7.1, the energy gap in the metal-oxide layer is ≈ 8.3 eV for $La_{1.85}Sr_{0.15}CuO_4$ and ≈ 7.8 eV for $YBa_2Cu_3O_7$. Using an estimate $\hbar\omega_p \approx 10$ eV, the electron-hole interaction in (7.1) is $V_{eh} = -2.1$ eV for the LaO exciton and $V_{eh} = -2.0$ eV for the BaO exciton. The resulting exciton states are shown as the solid curves in Fig. 7.2, with the local densities of states for the oxygen atoms again shown by the dashed curve for reference. Although the Green's function $G_0(E)$ in (3.7) is broadened by a Lorentzian lineshape with $\delta = 0.2$ eV, the exciton states in Fig. 7.2 have a larger width of

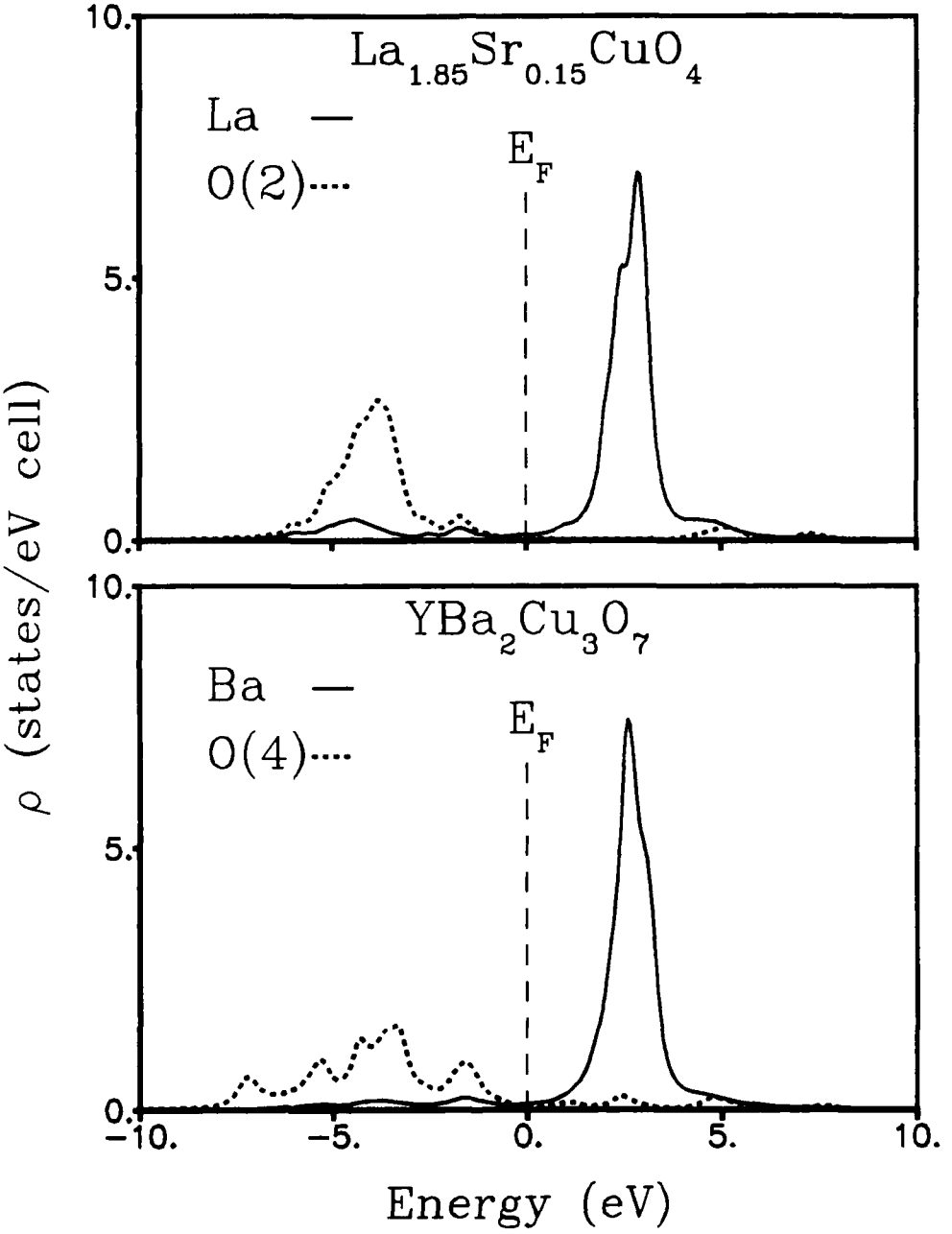

Fig. 7.2. Densities of states for a tightly-bound Frenkel exciton in $La_{1.85}Sr_{0.15}CuO_4$ and $YBa_2Cu_3O_7$.

order 1 eV, related to the bandwidth of the unoccupied d orbitals that form the final state of the charge transfer exciton.

These exciton states should be observable in electron-energy-loss spectroscopy (EELS) or other spectroscopies that create holes and excited electrons. Recent EELS measurements on $YBa_2Cu_3O_{7-y}$ show a rather sharp peak approximately 4 eV above the Fermi energy, which has been attributed to a BaO exciton.[299] The agreement with the exciton state in Fig. 7.2 is somewhat fortuitous considering the approximations made for the binding interaction V_{eh}, but this experimental observation appears to confirm that real excitons can be formed in the insulating layers of the high-temperature superconductors.

Two-Dimensional Exciton States

A more sophisticated treatment of the exciton states is needed to properly evaluate the matrix elements for the interaction between the excitons and the charge carriers. Rather than limiting the exciton to the tightly-bound Frenkel states of the previous section, we now allow the exciton to form on arbitrary metal and oxygen sites within the insulating layers, and then proceed to calculate the dominant contributions to the effective pairing interaction of the charge carriers.

The crystal environment of the insulating metal-oxide layers is essentially planar, with each metal or oxygen atom four-fold coordinated with its nearest in-plane neighbors. Neglecting the displacements along the c axis of the metal and oxygen atoms in one layer, we model each layer as a two-dimensional system. This model is valid for the cubic bismuth-oxide systems and for the hole-doped cuprates, which have small c-axis displacements in the insulating

layers [e.g., 0.57 Å for La–O(2) in $La_{1.85}Sr_{0.15}CuO_4$ (Ref. 9)], but is more approximate for the electron-doped systems such as $Nd_{2-x}Ce_xCuO_4$, which have a three-dimensional bonding coordination for the metal and oxygen atoms in the insulating regions.[86]

The eigenstates $\Phi(r,\phi)$ for the two-dimensional Coulomb potential may be found from the Schrödinger equation

$$\left\{ -\frac{\hbar^2}{2m_{\rm eff}}\left[\frac{1}{r}\frac{\partial}{\partial r}\left(r\frac{\partial}{\partial r}\right) - \frac{1}{r^2}\frac{\partial^2}{\partial\phi^2}\right] - \frac{e^2}{\epsilon_2 r}\right\}\Phi(r,\phi) = E\Phi(r,\phi)\,, \qquad (7.6)$$

where $m_{\rm eff}$ is the reduced effective mass of the electron-hole pair, ϵ_2 is the dielectric constant characterizing the insulating region, and (r,ϕ) are the polar coordinates. Separating variables by

$$\Phi(r,\phi) = R(r)\,\frac{e^{\pm im\phi}}{\sqrt{2\pi}} \qquad (7.7)$$

gives the radial equation

$$\left[\frac{d^2}{dr^2} + \frac{1}{r}\frac{d}{dr} - \frac{m^2}{r^2} + \frac{2m_{\rm eff}e^2}{\hbar^2\epsilon_2 r} + \frac{2m_{\rm eff}E}{\hbar^2}\right]R(r) = 0\,. \qquad (7.8)$$

where $m = 0,\ 1,\ 2,\ \ldots$. This equation has a straightforward solution for the bound states with $E < 0$.

We first find the energy eigenvalues E for (7.8). Defining the length scale $a \equiv \hbar^2\epsilon_2/4m_{\rm eff}e^2$ and substituting $u(r) = \sqrt{r}\ R(r)$ gives the modified radial equation

$$\left[\frac{d^2}{dr^2} - \frac{(m^2-\frac{1}{4})}{r^2} + \frac{1}{2ar} + \frac{2m_{\rm eff}E}{\hbar^2}\right]u(r) = 0\,. \qquad (7.9)$$

Changing variables with

$$\rho = 2\left(-\frac{2m_{\rm eff}E}{\hbar^2}\right)^{1/2} r \qquad (7.10)$$

and defining

$$\lambda \equiv \left(-\frac{\hbar^2}{2m_{\text{eff}}E}\right)^{1/2} \frac{1}{2a} \tag{7.11}$$

gives the differential equation

$$\left[\frac{d^2}{d\rho^2} - \frac{(m^2-\frac{1}{4})}{\rho^2} + \frac{\lambda}{2\rho} - \frac{1}{4}\right] u(\rho) = 0 . \tag{7.12}$$

The asymptotic solution to (7.12) is

$$\lim_{\rho\to\infty} u(\rho) \propto e^{-\rho/2} \tag{7.13}$$

for the bound states. We thus seek a general solution of the form

$$u(\rho) = e^{-\rho/2} f(\rho) , \tag{7.14}$$

where $f(\rho)$ satisfies

$$\left[\frac{d^2}{d\rho^2} - \frac{d}{d\rho} - \frac{(m+\frac{1}{2})(m-\frac{1}{2})}{\rho^2} - \frac{\lambda}{2\rho}\right] f(\rho) = 0 . \tag{7.15}$$

Assuming a polynomial form

$$f(\rho) = \rho^{m+\frac{1}{2}} \sum_{k=0}^{\infty} c_k \rho^k \tag{7.16}$$

and substituting into (7.15) gives

$$\left[\rho\frac{d^2}{d\rho^2} + (2m-1-\rho)\frac{d}{d\rho} + \left(\frac{\lambda-1}{2} - m\right)\right] \sum_{k=0}^{\infty} c_k \rho^k = 0 . \tag{7.17}$$

Solving for the recurrence relation of the coefficients gives

$$c_{k+1} = \left[\frac{k+m-(\frac{\lambda-1}{2})}{(k+1)(k-2m-1)}\right] c_k . \tag{7.18}$$

For finite solutions the series in (7.16) must terminate at some $k_{\max}$, so that (7.18) requires

$$\lambda \;=\; 2(k_{\max} + m) + 1 \; . \tag{7.19}$$

Since $k_{\max}$, $m \;=\; 0,\; 1,\; 2,\; \ldots$, then λ may only have odd integral values. Renaming λ as the principal quantum number n gives the energy eigenvalues from (7.11)

$$E_n \;=\; -4 \left(\frac{m_{\rm eff} e^4}{2\hbar^2 \epsilon_2^2} \right) \frac{1}{n^2} \; , \quad n = 1,\; 3,\; 5,\; \ldots . \tag{7.20}$$

The two-dimensional Coulomb potential thus gives binding energies four times larger than the three-dimensional case.

To solve for the eigenstates, we note that (7.17) is in the form of the differential equation for the associated Laguerre polynomials

$$\left[z \frac{d^2}{dz^2} \;+ (p + 1 - z) \frac{d}{dz} \;+\; (q - p) \right] L_q^p(z) \;=\; 0 \; ,$$

$$L_q^p(z) \;\equiv\; \frac{d^p}{dz^p} \left[e^z \; \frac{d^q}{dz^q} (z^q e^{-z}) \right] \; . \tag{7.21}$$

Comparing with (7.17) gives $p = 2m$ and $q = m + (n-1)/2$. The properly normalized radial wave function satifying (7.8) is thus found to be

$$R_{n,m}(r) \;=\; 2 \left\{ \frac{\left(\frac{n-1}{2} - m\right)!}{\left[\left(\frac{n-1}{2} + m\right)!\right]^3} \right\}^{1/2} \left(\frac{r}{na} \right)^m \exp\left(-\frac{r}{2na} \right) L^{2m}_{m+(n-1)/2} \left(\frac{r}{na} \right)$$

$$n \;=\; 1,\; 3,\; 5,\; \ldots$$

$$m \;=\; 0,\; 1,\; 2,\; \ldots,\; (n-1)/2 \; . \tag{7.22}$$

For these two-dimensional wave functions, the principal peak of the radial probability density occurs at a distance $r_n = an^2 = \frac{1}{4}(\hbar^2 \epsilon_2 / m_{\rm eff} e^2) n^2$, which is

four times smaller than the equivalent "Bohr radius" for the three-dimensional Coulomb potential.

To complete this treatment of the excitons, we examine the parameters for the model. The electron in the exciton is transferred into an unoccupied metal d state, and is regarded as localized because of the large effective mass for the relatively flat d bands. The hole in the exciton is found on some linear combination of oxygen sites neighboring the metal atom. The oxygen p bands are more dispersive than the metal d bands, so that the reduced effective mass $m_{\rm eff}$ is essentially the mass of the hole, which we take to be simply m_e. (Notice that only the ratio $\epsilon_2/m_{\rm eff}$ occurs in r_n above.) The exciton wave functions found above thus describe the hole, with the origin located on the metal site containing the electron in a localized d orbital. The probability distribution gives an envelope function for the hole, weighting the possible occupation of the neighboring oxygen sites.

Figure 7.3 shows the radial probability distribution, $rR_{1,0}^2$, for a range of dielectric constants ϵ_2, using the crystal structure of $La_{1.85}Sr_{0.15}CuO_4$. Even for a dielectric screening as large as $\epsilon_2 = 20$, the peak of the probability distribution occurs inside the first unit cell, indicated by the La–O(2) bond length (2.73 Å) in Fig. 7.3. The s-like exciton ground state thus gives equal occupation weight to the four nearest-neighbor oxygen sites in the LaO layer, with negligible weight on more distant neighbors. Since the first excited state has $n = 3$, the distribution for all but the ground state will be significantly spread to more distant neighbors. As described in the next section, the exciton transition density is negligible for all but nearest-neighbor atoms, so we conclude that only the ground state of the exciton will contribute to the effective pairing interaction between the carriers

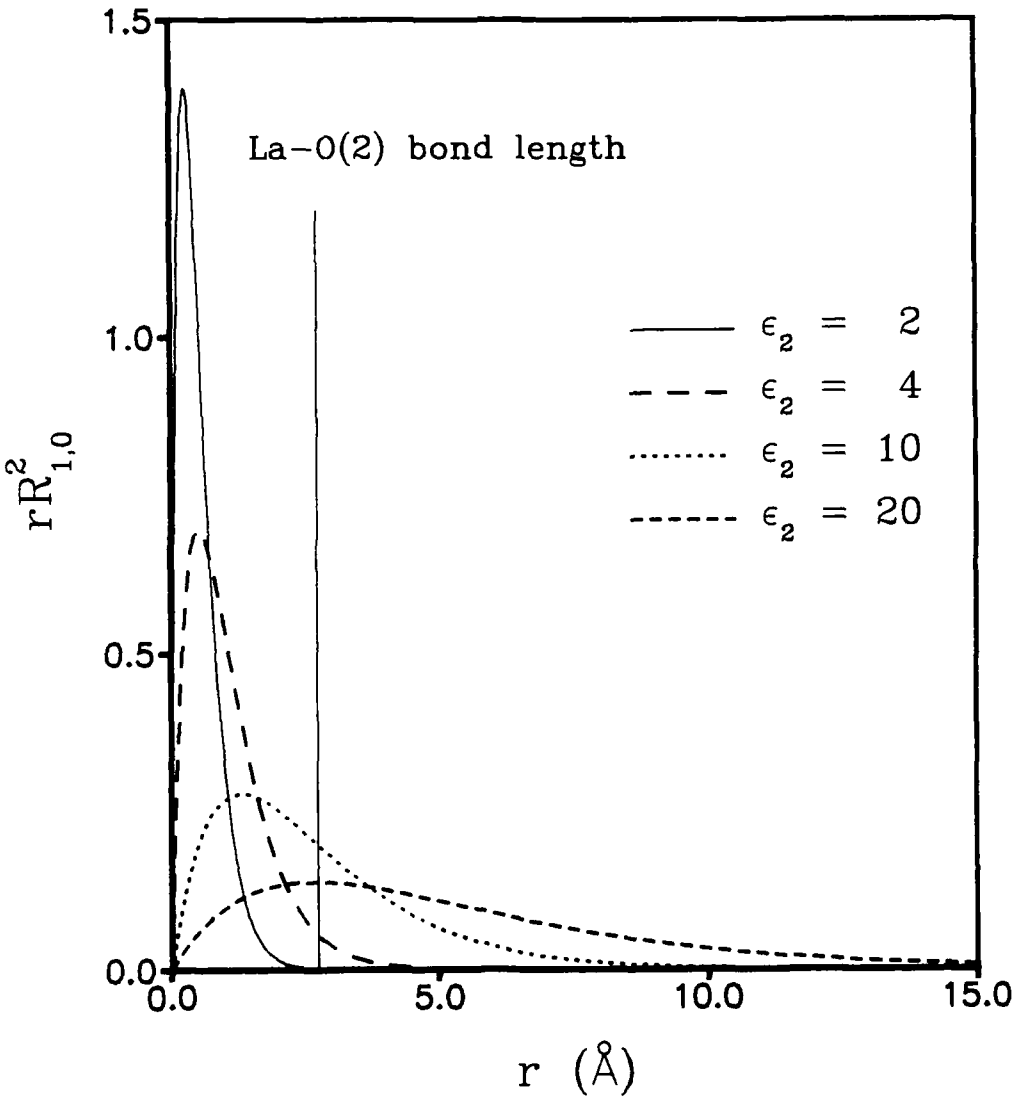

Fig. 7.3. Radial probability distribution for two-dimensional excitons in $La_{1.85}Sr_{0.15}CuO_4$.

in the adjacent metallic plane.

Interaction Hamiltonian and Matrix Elements

To calculate the effective interaction between the charge carriers in the metallic plane, we begin with the second-quantized Hamiltonian[300]

$$\hat{H}_{\text{met-ins}} = \frac{1}{2} \int d\vec{x} d\vec{x}' \; \hat{\psi}^{\dagger}_{\text{met}}(\vec{x}) \hat{\psi}^{\dagger}_{\text{ins}}(\vec{x}') V(\vec{x}, \vec{x}') \hat{\psi}_{\text{ins}}(\vec{x}') \hat{\psi}_{\text{met}}(\vec{x}) \; . \tag{7.23}$$

Here $V(\vec{x}, \vec{x}')$ is limited to interactions which occur between an electron at $\vec{x}$ in the metallic plane and one in the insulating layer at $\vec{x}'$. Specifically, the Coulomb repulsion between charge carriers within the metallic planes has been excluded, as well as interactions between charges in the insulating region. The field operators in (7.23) are given in the metallic region by the standard expressions

$$\begin{aligned} \hat{\psi}_{\text{met}}(\vec{x}) &= \sum_{\vec{k}_1, n} \Phi_{\vec{k}_1, n}(\vec{x}) \hat{a}_{\vec{k}_1, n} \\ \hat{\psi}^{\dagger}_{\text{met}}(\vec{x}) &= \sum_{\vec{k}_1, n} \Phi^{*}_{\vec{k}_1, n}(\vec{x}) \hat{a}^{\dagger}_{\vec{k}_1, n} \; , \end{aligned} \tag{7.24}$$

where $\hat{a}^{\dagger}_{\vec{k}_1, n}$ and $\hat{a}_{\vec{k}_1, n}$ are, respectively, the creation and annihilation operators for an electron with momentum $\vec{k}_1$ in the n^{th} band. The basis states can be written as Bloch sums

$$\Phi_{\vec{k}_1, n}(\vec{x}) = \frac{1}{\sqrt{N}} \sum_{\vec{R}_1} \phi_n(\vec{x} - \vec{R}_1) e^{i \vec{k}_1 \cdot \vec{R}_1} \; . \tag{7.25}$$

The basis states are normalized over the N unit cells:

$$\int d\vec{x} \; |\Phi_{\vec{k}_1, n}(\vec{x})|^2 = 1 \; . \tag{7.26}$$

In the following, we approximate the $\phi_n(\vec{x})$ in (7.25) by the atomic orbitals associated with a metallic plane.

The operators in (7.23) that act on the insulating region are written as

$$\begin{aligned}\hat{\psi}_{\rm ins}(\vec{x}') &= \sum_{\vec{k}}\left[\sum_{m'}\chi^{\alpha}_{\vec{k}-\vec{q},m'}(\vec{x}')\,\hat{c}_{\vec{k}-\vec{q},m'} + \sum_{m}\chi^{\beta}_{\vec{k},m}(\vec{x}')\,\hat{c}_{\vec{k},m}\right] \\ \hat{\psi}^{\dagger}_{\rm ins}(\vec{x}') &= \sum_{\vec{k}}\left[\sum_{m'}\chi^{\alpha\,*}_{\vec{k}+\vec{q},m'}(\vec{x}')\,\hat{c}^{\dagger}_{\vec{k}+\vec{q},m'} + \sum_{m}\chi^{\beta\,*}_{\vec{k},m}(\vec{x}')\,\hat{c}^{\dagger}_{\vec{k},m}\right] .\end{aligned} \tag{7.27}$$

The operators $\hat{c}^{\dagger}$ and $\hat{c}$ act only in the insulating layer, creating or destroying electrons in the basis states

$$\begin{aligned}\chi^{\alpha}_{\vec{k}-\vec{q},m'}(\vec{x}') &= \frac{1}{\sqrt{N}}\sum_{\vec{R}}\alpha_{m'}(\vec{x}'-\vec{R})e^{i(\vec{k}-\vec{q})\cdot\vec{R}} \\ \chi^{\beta}_{\vec{k},m}(\vec{x}') &= \frac{1}{\sqrt{N}}\sum_{\vec{R}}\beta_{m}(\vec{x}'-\vec{R})e^{i\vec{k}\cdot\vec{R}} ,\end{aligned} \tag{7.28}$$

where $\alpha_{m'}(\vec{x}')$ represents one of the five d atomic orbitals associated with the metal atom in the insulating layer, and $\beta_m(\vec{x}')$ represents one of the linear combinations of p orbitals on the neighboring oxygen atoms. The momentum $\vec{q}$ introduced explicitly in (7.27) and (7.28) will be found below to be the momentum of the exciton.

The operators in the metallic plane anticommute with those acting in the insulating layer. We can thus examine the product of field operators in (7.23) for each region. We limit the calculation to the material $La_{1.85}Sr_{0.15}CuO_4$. As mentioned in Chapter IV, EELS data indicate that the conduction bands have primarily oxygen p_x and p_y character within the CuO_2 planes.[168] We consider only the σ-bonded O p band as a carrier state, so that $\phi_n(\vec{x}) = \phi(\vec{x})$ is simply

an oxygen p orbital. The operator product in the metallic region is then

$$\hat{\psi}^{\dagger}_{\rm met}(\vec{x})\hat{\psi}_{\rm met}(\vec{x}) = \frac{1}{N}\sum_{\vec{k}_1,\vec{k}'_1}\sum_{\vec{R}_1,\vec{R}'_1}\phi^*(\vec{x}-\vec{R}'_1)\phi(\vec{x}-\vec{R}_1) \times e^{i(\vec{k}_1\cdot\vec{R}_1-\vec{k}'_1\cdot\vec{R}'_1)}\,\hat{a}^{\dagger}_{\vec{k}'_1}\hat{a}_{\vec{k}_1}\,. \tag{7.29}$$

Neglecting the overlap of atomic orbitals on different sites reduces (7.29) to

$$\hat{\psi}^{\dagger}_{\rm met}(\vec{x})\hat{\psi}_{\rm met}(\vec{x}) = \frac{1}{N}\sum_{\vec{k}_1,\vec{k}'_1}\sum_{\vec{R}_1}|\phi(\vec{x}-\vec{R}_1)|^2\, e^{i(\vec{k}_1-\vec{k}'_1)\cdot\vec{R}_1}\,\hat{a}^{\dagger}_{\vec{k}'_1}\hat{a}_{\vec{k}_1}\,. \tag{7.30}$$

The product of operators in the insulating region is

$$\hat{\psi}^{\dagger}_{\rm ins}(\vec{x}')\hat{\psi}_{\rm ins}(\vec{x}') = \frac{1}{N}\sum_{\vec{k},\vec{k}'}\sum_{m,m'}\sum_{\vec{R},\vec{R}'} \left\{\alpha^*_{m'}(\vec{x}'-\vec{R}')\beta_m(\vec{x}'-\vec{R})e^{i[\vec{k}\cdot\vec{R}-(\vec{k}'+\vec{q})\cdot\vec{R}']}\,\hat{c}^{\dagger}_{\vec{k}'+\vec{q},m'}\hat{c}_{\vec{k},m} - \beta^*_m(\vec{x}'-\vec{R})\alpha_{m'}(\vec{x}'-\vec{R}')e^{i[(\vec{k}-\vec{q})\cdot\vec{R}'-\vec{k}'\cdot\vec{R}]}\,\hat{c}^{\dagger}_{\vec{k}',m}\hat{c}_{\vec{k}-\vec{q},m'}\right\}. \tag{7.31}$$

Here we have dropped the terms with initial and final states on the same atom (i.e., $\alpha^*\alpha$ and $\beta^*\beta$), since these terms do not lead to the creation or destruction of a metal-oxide exciton. The integrated transition density for the exciton is

$$\int d\vec{x}'\;\alpha^*_{m'}(\vec{x}')\beta_m(\vec{x}')\,. \tag{7.32}$$

The oxygen p and lanthanum d states are treated as hydrogenic wave functions with the Thomas-Fermi scaling[301] $Z_{\rm effective} = Z^{1/3}$. Within this approximation, all but nearest neighbors will give a negligible result for (7.32). The exciton states are therefore limited to one unit cell, requiring $\vec{R}' = \vec{R}$ in (7.31). As found in the previous section, the envelope function for the exciton ground state gives equal weight to the nearest neighbors. Since the LaO layers are essentially

planar, we expect the out-of-plane O p_z orbitals to have small transition densities with the La d orbitals, so they are excluded from the combinations making up $\mathcal{Z}_m(\vec{x}')$. There are thus 40 types of excitons, arising from the five lanthanum d orbitals and the eight linear combinations of p_x and p_y orbitals on each of four adjacent oxygen sites. The sums over m and m' in (7.31) can then be relabeled to sum over the types of excitons (a = 1, 2, ..., 40), giving

$$\begin{aligned}\hat{\psi}^{\dagger}_{\rm ins}(\vec{x}')\hat{\psi}_{\rm ins}(\vec{x}') &= \frac{1}{N}\sum_{\vec{k},\vec{k}',\mathrm{a}}\sum_{\vec{R}} e^{i(\vec{k}-\vec{k}'-\vec{q})\cdot\vec{R}} \\ &\times\Big\{\alpha^{*}_{\mathrm{a}}(\vec{x}'-\vec{R})\mathcal{Z}_{\mathrm{a}}(\vec{x}'-\vec{R})\;\hat{c}^{\dagger}_{\vec{k}'+\vec{q},\mathrm{a}}\hat{c}_{\vec{k},\mathrm{a}} \\ &+\mathcal{Z}^{*}_{\mathrm{a}}(\vec{x}'-\vec{R})\alpha_{\mathrm{a}}(\vec{x}'-\vec{R})\;\hat{c}^{\dagger}_{\vec{k}',\mathrm{a}}\hat{c}_{\vec{k}-\vec{q},\mathrm{a}}\Big\}\,.\end{aligned} \tag{7.33}$$

To this point, $\vec{q}$ is arbitrary, so we may set $\vec{k}' = \vec{k}$ and sum over $\vec{k}$ and $\vec{q}$. We define the exciton operators

$$\begin{aligned}\hat{b}^{\dagger}_{\vec{q},\mathrm{a}} &\equiv \frac{1}{N}\sum_{\vec{k}}\hat{c}^{\dagger}_{\vec{k}+\vec{q},\mathrm{a}}\hat{c}_{\vec{k},\mathrm{a}} \\ \hat{b}_{-\vec{q},\mathrm{a}} &\equiv \frac{1}{N}\sum_{\vec{k}}\hat{c}^{\dagger}_{\vec{k},\mathrm{a}}\hat{c}_{\vec{k}-\vec{q},\mathrm{a}}\,,\end{aligned} \tag{7.34}$$

where $\hat{b}^{\dagger}_{\vec{q},\mathrm{a}}$ creates an exciton of momentum $\vec{q}$ and type a in the insulating region, and $\hat{b}_{-\vec{q},\mathrm{a}}$ destroys an exciton of momentum $-\vec{q}$ and type a. We then write (7.33) as

$$\begin{aligned}\hat{\psi}^{\dagger}_{\rm ins}(\vec{x}')\hat{\psi}_{\rm ins}(\vec{x}') &= \sum_{\vec{q},\mathrm{a}}\sum_{\vec{R}} e^{-i\vec{q}\cdot\vec{R}}\Big\{\alpha^{*}_{\mathrm{a}}(\vec{x}'-\vec{R})\mathcal{Z}_{\mathrm{a}}(\vec{x}'-\vec{R})\;\hat{b}^{\dagger}_{\vec{q},\mathrm{a}} \\ &\qquad -\mathcal{Z}^{*}_{\mathrm{a}}(\vec{x}'-\vec{R})\alpha_{\mathrm{a}}(\vec{x}'-\vec{R})\;\hat{b}_{-\vec{q},\mathrm{a}}\Big\}\,.\end{aligned} \tag{7.35}$$

The interaction Hamiltonian in (7.23) may now be written as

$$\begin{aligned}\hat{H}_{\text{met-ins}} &= \frac{1}{2} \sum_{\vec{k}_1,\vec{k}_1'} \sum_{\vec{q},\mathrm{a}} \sum_{\vec{R}_1,\vec{R}} e^{i[(\vec{k}_1-\vec{k}_1')\cdot\vec{R}_1-\vec{q}\cdot\vec{R}]} \\ &\times \frac{1}{N}\int d\vec{x}d\vec{x}' \; |\phi(\vec{x}-\vec{R}_1)|^2 \; V(\vec{x},\vec{x}') \; \hat{a}^\dagger_{\vec{k}_1'} \hat{a}_{\vec{k}_1} \\ &\times \left\{ \alpha^*_{\mathrm{a}}(\vec{x}'-\vec{R})\beta_{\mathrm{a}}(\vec{x}'-\vec{R}) \; \hat{b}^\dagger_{\vec{q},\mathrm{a}} \; + \; \beta^*_{\mathrm{a}}(\vec{x}'-\vec{R})\alpha_{\mathrm{a}}(\vec{x}'-\vec{R}) \; \hat{b}_{-\vec{q},\mathrm{a}} \right\} .\end{aligned} \tag{7.36}$$

To proceed further, we limit the form of the interaction to $V(\vec{x},\vec{x}') = V(\vec{x}-\vec{x}')$. We then use the change of variables

$$\begin{aligned}\vec{x}_0 &= \vec{x} - \vec{R}_1 \\ \vec{x}_0' &= \vec{x}' - \vec{R}_1 \\ \vec{l} &= \vec{R} - \vec{R}_1 \; ,\end{aligned} \tag{7.37}$$

so that $\vec{x}_0 - \vec{x}_0' = \vec{x} - \vec{x}'$. Substituting into (7.36), we find

$$\begin{aligned}\hat{H}_{\text{met-ins}} &= \frac{1}{2} \sum_{\vec{k}_1,\vec{k}_1'} \sum_{\vec{q},\mathrm{a}} \sum_{\vec{R}_1,\vec{l}} e^{i[(\vec{k}_1-\vec{k}_1')-\vec{q}]\cdot\vec{R}_1} \; e^{-i\vec{q}\cdot\vec{l}} \\ &\times \frac{1}{N}\int d\vec{x}_0 d\vec{x}_0' \; |\phi(\vec{x}_0)|^2 \; V(\vec{x}_0-\vec{x}_0') \; \hat{a}^\dagger_{\vec{k}_1'} \hat{a}_{\vec{k}_1} \\ &\times \left\{ \alpha^*_{\mathrm{a}}(\vec{x}_0'-\vec{l})\beta_{\mathrm{a}}(\vec{x}_0'-\vec{l}) \; \hat{b}^\dagger_{\vec{q},\mathrm{a}} \; + \; \beta^*_{\mathrm{a}}(\vec{x}_0'-\vec{l})\alpha_{\mathrm{a}}(\vec{x}_0'-\vec{l}) \; \hat{b}_{-\vec{q},\mathrm{a}} \right\} .\end{aligned} \tag{7.38}$$

The sum over $\vec{R}_1$ gives $N\delta_{\vec{k}_1-\vec{k}_1'+\vec{K},\vec{q}}$, where $\vec{K}$ is any reciprocal lattice vector. If we neglect Umklapp processes, then $\vec{K} = 0$ and $\vec{k}_1' = \vec{k}_1 - \vec{q}$. The final Hamiltonian is then

$$\hat{H}_{\text{met-ins}} = \frac{1}{2} \sum_{\vec{k}_1} \sum_{\vec{q},\mathrm{a}} \hat{a}^\dagger_{\vec{k}_1-\vec{q}} \; \hat{a}_{\vec{k}_1} \left[M_{\mathrm{a}}(\vec{q}) \; \hat{b}^\dagger_{\vec{q},\mathrm{a}} \; + \; M^*_{\mathrm{a}}(-\vec{q}) \; \hat{b}_{-\vec{q},\mathrm{a}} \right] . \tag{7.39}$$

The carrier-exciton interaction matrix element is given by

$$M_{\mathrm{a}}(\vec{q}) = \sum_{\vec{l}} e^{-i\vec{q}\cdot\vec{l}} \int d\vec{x}d\vec{x}' \; |\phi(\vec{x})|^2 V(\vec{x}-\vec{x}')\alpha^*_{\mathrm{a}}(\vec{x}'-\vec{l})\beta_{\mathrm{a}}(\vec{x}'-\vec{l}) \; . \tag{7.40}$$

In (7.40) the sum over excitons centered at different lattice points $\vec{l}$ is limited to third-neighbor unit cells with respect to the electron at $\vec{x}$ in the metallic plane, assuming that interactions with more distant excitons will be fully screened. The interaction $V(\vec{x}-\vec{x}')$ is taken to be the Coulomb interaction

$$V(\vec{x}-\vec{x}') \;=\; \frac{e^2}{\epsilon_1|\vec{x}-\vec{x}'|}\;, \tag{7.41}$$

where ϵ_1 is the effective dielectric constant that characterizes the region between the metallic and insulating layers. A bulk static dielectric constant of ≈ 20 has been reported[302] for insulating La_2CuO_4, which may be used as a crude estimate for ϵ_1.

The interaction Hamiltonian (7.39) is now in precisely the form given by the left side of the Feynman diagram in Fig. 7.4. The exchange of the exciton with four-momentum $q=(\vec{q},q_0)$ between the two carriers leads to the exciton-mediated effective interaction[303]

$$V_{\rm ex}(\vec{q},q_0) \;=\; 2\sum_{\rm a}\frac{|M_{\rm a}(\vec{q})|^2\;\hbar\omega_{\vec{q},{\rm a}}}{q_0^2-(\hbar\omega_{\vec{q},{\rm a}})^2}\;. \tag{7.42}$$

For energy transfer $q_0 \ll \hbar\omega_{\vec{q},{\rm a}}$, and for characteristic excitational energies $\hbar\omega_{\vec{q},{\rm a}} \approx \hbar\omega_0$, (7.42) reduces to

$$V_{\rm ex}(\vec{q}) \;=\; -2\sum_{\rm a}\frac{|M_{\rm a}(\vec{q})|^2}{\hbar\omega_0}\;. \tag{7.43}$$

This is exactly the form originally given by Little for a generic exciton coupling mechanism,[285] but here evaluated specifically for the oxygen p to metal d excitons of the high-temperature superconductors. A significant addition in this development is that the transition densities in (7.32) can be large because of the nearest-neighbor orbital overlap, so that a substantial $V_{\rm ex}(\vec{q})$ can be found

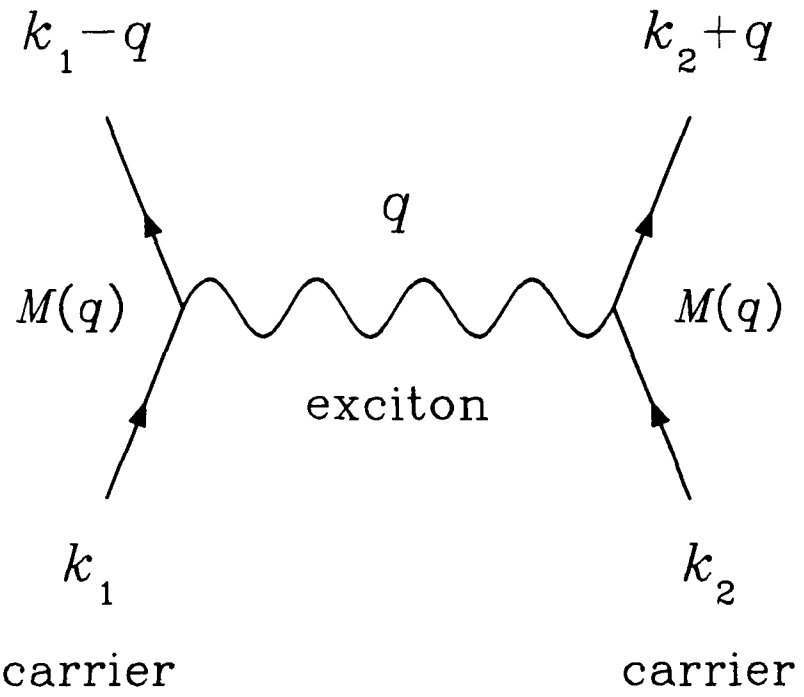

Fig. 7.4. Feynman diagram for excitonic interaction.

even for large excitational energies $\hbar\omega_0$. We also see that the exciton-mediated pairing potential is independent of the sign of the charge carriers because of the factor $|M_a(\vec{q})|^2$ in (7.43), so the present mechanism can be applied to both n-type and p-type carriers.

The six-dimensional integral of (7.40) was evaluated using Gaussian quadratures, with a factor $1-\exp(-\lambda|\vec{x}-\vec{x}'|^2)$ applied to (7.41) to avoid the divergence at $\vec{x}=\vec{x}'$. A value $\lambda = 10$ Å^{-2} was used, creating a correlation screening radius of ≈ 0.3 Å about each charge. The results were unchanged for larger values of λ (corresponding to shorter screening lengths). The results for $V_{ex}(\vec{q})$ are given in Table 7.1 for $\vec{q}$ parallel to the CuO_2 planes, using the parameters $\epsilon_1 = 20$ and $\hbar\omega_0 = 7$ eV. The largest contributions occur for $\vec{q}=0$, as expected from the Coulomb-like interaction between the carrier and the exciton.

For the crystal structure of $La_{1.85}Sr_{0.15}CuO_4$, there are two identical LaO layers sandwiching the CuO_2 plane, so that $M_a(\vec{q})$ in (7.40) must also include a factor $2\cos(q_z d_z)$ for the coherent sum over these two layers, where d_z is the distance in the z direction between the metallic and insulating layers (e.g., 1.9 Å between the CuO_2 and LaO layers). The resulting $V_{ex}(\vec{q})$ is then simply $4[\cos(q_z d_z)]^2$ times the values in Table 7.1. We note that in the materials with multiple CuO_2 layers per unit cell (such as $Tl_2Ca_2Ba_2Cu_3O_{10}$), there is only a single insulating metal-oxide layer adjacent to the outer CuO_2 plane, so that no summation occurs for excitons in different insulating layers.

The $V_{ex}(\vec{q})$ found within this model may be used to further develop the details of this mechanism for high-temperature superconductivity. For example, a crude estimate for the transition temperature can be made using the expression

TABLE 7.1. Exciton-mediated effective interaction $V_{ex}(\vec{q})$ for $La_{1.85}Sr_{0.15}CuO_4$, in eV.

$q_x =$	0	$\pi/6a$	$\pi/4a$	$\pi/3a$	$\pi/2a$	$2\pi/3a$	$3\pi/4a$	$5\pi/6a$	π/a
$q_y = 0$	-1.00	-0.84	-0.67	-0.49	-0.19	-0.05	-0.02	-0.01	0.00
$q_y = \pi/6a$	-0.88	-0.73	-0.58	-0.41	-0.15	-0.03	-0.01	0.00	0.00
$q_y = \pi/4a$	-0.74	-0.61	-0.47	-0.33	-0.11	-0.02	-0.01	0.00	0.00
$q_y = \pi/3a$	-0.58	-0.47	-0.36	-0.24	-0.07	-0.01	0.00	0.00	0.00
$q_y = \pi/2a$	-0.27	-0.20	-0.14	-0.08	-0.01	0.00	0.00	0.00	0.00
$q_y = 2\pi/3a$	-0.08	-0.05	-0.03	-0.01	-0.01	-0.02	-0.02	-0.01	0.00
$q_y = 3\pi/4a$	-0.04	-0.02	-0.01	-0.01	-0.03	-0.04	-0.04	-0.02	0.00
$q_y = 5\pi/6a$	-0.02	-0.01	-0.01	-0.01	-0.05	-0.06	-0.05	-0.03	0.00
$q_y = \pi/a$	-0.02	-0.01	-0.02	-0.03	-0.07	-0.08	-0.06	-0.03	0.00

of Emery and Reiter[304]

$$T_c \sim E_F \, e^{-1/\lambda_{ex}} , \tag{7.44}$$

where $\lambda_{ex} \equiv N(0)V_{ex}$. This expression is appropriate for nonretarded electronic interactions.[304] For $N(0) \approx 0.5$ states/eV cell, an average $V_{ex}(\vec{q})$ of roughly -1 eV (including the q_z dependence times the results listed in Table 7.1), and an estimate of $E_F = 0.15$ eV for $La_{1.85}Sr_{0.15}CuO_4$,[304] we obtain $T_c \sim$ 200 K. This is certainly not a quantitative result, but simply indicates that the excitonic mechanism described above can provide the pairing necessary for superconductivity within a physically reasonable range of parameters.

Summary of the Excitonic Mechanism

The specific structural and electronic configuration required for this excitonic mechanism of high-temperature superconductivity has been observed in all currently-known high-T_c materials, including the hole-doped cuprates such as $La_{1.85}Sr_{0.15}CuO_4$, $YBa_2Cu_3O_7$, $Bi_2CaSr_2Cu_2O_8$, and $Tl_2Ca_2Ba_2Cu_3O_{10}$; the electron-doped cuprates such as $Nd_{2-x}Ce_xCuO_4$; and the copper-free system $Ba_{1-x}K_xBiO_3$. In every case, metallic layers are found in close proximity to insulating layers, so that excitons within the insulating region can interact with carriers in the metallic region. Excitons in the predicted energy range have apparently been observed in the BaO layers of $YBa_2Cu_3O_{7-y}$.[299]

For reasonable estimates of the physical parameters, this mechanism provides a pairing interaction sufficient to give high-T_c superconductivity. No specific magnetic properties are required for this mechanism. We predict that high-temperature superconductivity will not be seen in materials such as $Ca_{1-x}K_xCuO_2$ or $Ca_{1-x}Y_xCuO_2$, since these structures, although containing

CuO_2 planes, have no insulating metal-oxide layers to support the excitons.[82] Quantitative predictions within this theory will require a comprehensive treatment of the superconductivity, including the effects of anisotropy and large excitational energies associated with the excitons.

CHAPTER VIII

CONCLUSION

The characterization of high-temperature superconductors is a significant experimental and theoretical challenge. The present research has concentrated on a theoretical model for the electronic properties of these materials. We have also proposed an excitonic mechanism that is applicable to all currently-known high-temperature superconductors.

In Chapter III we developed the semiempirical tight-binding model which was used to calculate the electronic energy bands, the local and total densities of states, and the atomic valences for each of the materials. The results of the calculations were presented in Chapter IV for the copper-oxide superconductors $La_{1.85}Sr_{0.15}CuO_4$, $YBa_2Cu_3O_7$, $Bi_2Sr_2CuO_6$, $Bi_2CaSr_2Cu_2O_8$, $Tl_2Ba_2CuO_6$, $Tl_2CaBa_2Cu_2O_8$, $Tl_2Ca_2Ba_2Cu_3O_{10}$, and $TlCa_3Ba_2Cu_4O_{11}$, and for the bismuth oxides $BaPb_{0.75}Bi_{0.25}O_3$ and $Ba_{0.6}K_{0.4}BiO_3$. We find that a single tight-binding model, with fully transferable parameters, provides a good description of the electronic structure for each of these high-temperature superconductors.

All the copper-oxide superconductors have two-dimensional conduction bands arising from Cu(d)–O(p) antibonding states. The metal-oxide layers sandwiching the CuO_2 planes (such as LaO, BaO, and SrO) all display ionic and insulating behavior. The copper-free bismuth-oxide superconductors $BaPb_{0.75}Bi_{0.25}O_3$ and $Ba_{0.6}K_{0.4}BiO_3$ have valence bands of antibonding Bi(s)–O(p) states, with cubic or almost-cubic symmetry. These materials also have ionic and insulating layers of BaO in their structure. Although all of these systems have very different crystal and magnetic structures, the common fea-

tures in the electronic structures provide support for a single mechanism of high-temperature superconductivity.

Chapter V reported the study of atomic substitutions in $YBa_2Cu_3O_7$, $Bi_2CaSr_2Cu_2O_8$, and $Tl_2CaBa_2Cu_2O_8$. There is reasonable agreement with expected chemical trends and with experimentally-observed changes in the superconducting properties. The results for substitution of Al, Fe, Co, Ni, and Zn for Cu in $YBa_2Cu_3O_7$ show that substitutions on the Cu(2) site disrupt the CuO_2 plane conduction bands more than do substitutions on the Cu(1) site. Results for the replacement of Ba by Sr in $YBa_2Cu_3O_7$ support a purely structural effect for the suppression of T_c. We find that La substitution for Ba leads to destruction of hole charge carriers by the donated electrons, resulting in direct suppression of superconductivity. Substitution of F or N on the oxygen sites shows that the electronic structure of $YBa_2Cu_3O_7$ may be slightly affected by such replacements, but no obvious changes in the superconducting properties are correlated with these results.

Substitution of Pb for Bi in $BiMCaSr_2Cu_2O_8$ gives an increase in the number of hole carriers within the CuO_2 planes, assuming the same idealized structure for $BiPbCaSr_2Cu_2O_8$ and $Bi_2CaSr_2Cu_2O_8$. The observed enhancement of T_c with Pb substitution in the bismuth cuprates has to date been correlated with the stabilization of the higher-T_c phase $Bi_2Ca_2Sr_2Cu_3O_{10}$, making a direct comparison with these results somewhat difficult. The strongest effect of doping with Hg or Pb in $TlMCaBa_2Cu_2O_8$ is the shift in the Fermi energy, with Hg creating holes and Pb destroying them.

Chapter VI presented the results for the electronic effects of oxygen vacancies in $La_{1.85}Sr_{0.15}CuO_{4-y}$ and $YBa_2Cu_3O_{7-y}$, and of lanthanum vacancies in

$La_{2-x}CuO_4$. The modification of the density of states and the shift in the Fermi energy were calculated for each case. Oxygen vacancies act as electron donors in both systems, raising the Fermi energy and decreasing $\rho(E_F)$ for $y \leq 0.5$. The concentration of holes is thus decreased for the oxygen-defect systems, consistent with the observations that oxygen vacancies degrade the superconductivity and metallic conductivity in these materials. Lanthanum vacancies in $La_{2-x}CuO_4$ donate holes, lowering the Fermi energy and increasing $\rho(E_F)$ for $x \leq 0.3$. Small concentrations of La vacancies may thus have the same effect electronically as divalent metal dopants or excess oxygen, leading to enhancement of superconductivity in nominally stoichiometric La_2CuO_4.

Chapter VII presented a specific mechanism for high-temperature superconductivity which requires tightly-bound excitons in the insulating metal-oxide layers adjacent to the superconducting planes. Excitons with energies in the predicted range appear to have been observed in the BaO layers of $YBa_2Cu_3O_{7-y}$. No specific magnetic structure for the metallic region is needed for this mechanism, making it equally applicable to the copper oxides and the bismuth oxides. The required structural and electronic configuration has been observed in all currently-known high-T_c materials, including the hole-doped cuprates such as $La_{1.85}Sr_{0.15}CuO_4$, $YBa_2Cu_3O_7$, $Bi_2CaSr_2Cu_2O_8$, and $Tl_2Ca_2Ba_2Cu_3O_{10}$; the electron-doped cuprates such as $Nd_{2-x}Ce_xCuO_4$; and the copper-free system $Ba_{1-x}K_xBiO_3$. In every case, metallic layers are found adjacent to insulating layers, so that carriers in the metallic region can experience a net attractive interaction mediated by the excitons. A rough estimate with reasonable values of the physical parameters gives $T_c \sim 200$ K. This mechanism predicts that high-temperature superconductivity will not be seen in systems such as

$Ca_{1-x}K_xCuO_2$ or $Ca_{1-x}Y_xCuO_2$, since these layered CuO_2 structures do not have the insulating metal-oxide layers necessary to support the excitons.

REFERENCES

[1] J. G. Bednorz and K. A. Müller, Z. Phys. B **64**, 189 (1986).

[2] S. Uchida, H. Takagi, K. Kitazawa, and S. Tanaka, Jpn. J. Appl. Phys. **26**, L1 (1987); H. Takagi, S. Uchida, K. Kitazawa, and S. Tanaka, Jpn. J. Appl. Phys. **26**, L123 (1987).

[3] R. J. Cava, R. B. Van Dover, B. Batlogg, and E. A. Rietman, Phys. Rev. Lett. **58**, 408 (1987); R. B. Van Dover, R. J. Cava, B. Batlogg, and E. A. Rietman, Phys. Rev. B **35**, 5337 (1987).

[4] J. M. Tarascon, L. H. Greene, W. R. McKinnon, G. W. Hull, and T. H. Geballe, Science **235**, 1373 (1987).

[5] R. J. Cava, A. Santoro, D. W. Johnson, Jr., and W. W. Rhodes, Phys. Rev. B **35**, 6716 (1987); R. M. Fleming, B. Batlogg, R. J. Cava, and E. A. Rietman, Phys. Rev. B **35**, 7191 (1987).

[6] L. C. Smedskjaer, J. L. Routbort, B. K. Flandermeyer, S. J. Rothman, D. G. Legnini, and J. E. Baker, Phys. Rev. B **36**, 3903 (1987).

[7] M. W. Shafer, T. Penney, and B. L. Olson, Phys. Rev. B **36**, 4047 (1987).

[8] J. B. Torrance, Y. Tokura, A. I. Nazzal, A. Bezinge, T. C. Huang, and S. S. P. Parkin, Phys. Rev. Lett. **61**, 1127 (1988).

[9] J. D. Jorgensen, H.-B. Schüttler, D. G. Hinks, D. W. Capone, II, K. Zhang, M. B. Brodsky, and D. J. Scalapino, Phys. Rev. Lett. **58**, 1024 (1987).

[10] E. F. Skelton, W. T. Elam, D. U. Gubser, V. Letourneau, M. S. Osofsky, S. B. Qadri, L. E. Toth, and S. A. Wolf, Phys. Rev. B **36**, 5713 (1987); S. C. Moss, K. Forster, J. D. Axe, H. You, D. Hohlwein, D. E. Cox, P. H. Hor, R. L. Meng, and C. W. Chu, Phys. Rev. B **35**, 7195 (1987); S. A. Shaheen, N. Jisrawi, Y. H. Lee, Y. Z. Zhang, M. Croft, W. L. McLean, H. Zhen, L. Rebelsky, and S. Horn, Phys. Rev. B **36**, 7214 (1987).

[11] P. M. Grant, S. S. P. Parkin, V. Y. Lee, E. M. Engler, M. L. Ramirez, J. E. Vazquez, G. Lim, R. D. Jacowitz, and R. L. Greene, Phys. Rev. Lett. **58**, 2482 (1987).

[12] S. M. Fine, M. Greenblatt, S. Simizu, and S. A. Friedberg, Phys. Rev. B **36**, 5716 (1987).

[13] M. K. Wu, J. R. Ashburn, C. J. Torng, P. H. Hor, R. L. Meng, L. Gao, Z. J. Huang, Y. Q. Wang, and C. W. Chu, Phys. Rev. Lett. **58**, 908 (1987).

[14] R. J. Cava, B. Batlogg, R. B. van Dover, D. W. Murphy, S. Sunshine, T. Siegrist, J. P. Remeika, E. A. Rietman, S. M. Zahurak, and G. P. Espinosa, Phys. Rev. Lett. **58**, 1676 (1987).

[15] R. M. Hazen, L. W. Finger, R. J. Angel, C. T. Prewitt, N. L. Ross, H. K. Mao, C. G. Hadidiacos, P. H. Hor, R. L. Meng, and C. W. Chu, Phys. Rev. B **35**, 7238 (1987).

[16] P. M. Grant, R. B. Beyers, E. M. Engler, G. Lim, S. S. P. Parkin, M. L. Ramirez, V. Y. Lee, A. Nazzal, J. E. Vazquez, and R. J. Savoy, Phys. Rev. B **35**, 7242 (1987).

[17] M. A. Beno, L. Soderholm, D. W. Capone, II, D. G. Hinks, J. D. Jorgensen, J. D. Grace, I. K. Schuller, C. U. Segre, and K. Zhang, Appl. Phys. Lett. **51**, 57 (1987).

[18] T. Siegrist, S. Sunshine, D. W. Murphy, R. J. Cava, and S. M. Zahurak, Phys. Rev. B **35**, 7137 (1987).

[19] Y. LePage, W. R. McKinnon, J. M. Tarascon, L. H. Greene, G. W. Hull, and D. M. Hwang, Phys. Rev. B **35**, 7245 (1987).

[20] J. E. Greedan, A. H. O'Reilly, and C. V. Stager, Phys. Rev. B **35**, 8770 (1987).

[21] J. J. Capponi, C. Chaillout, A. W. Hewat, P. Lejay, M. Marezio, N. Nguyen, B. Raveau, J. L. Soubeyroux, J. L. Tholence, and R. Tournier, Europhys. Lett. **3**, 1301 (1987).

[22] C. H. Chen, D. J. Werder, S. H. Liou, J. R. Kwo, and M. Hong, Phys. Rev. B **35**, 8767 (1987).

[23] J. D. Jorgensen, M. A. Beno, D. G. Hinks, L. Soderholm, K. J. Volin, R. L. Hitterman, J. D. Grace, I. K. Schuller, C. U. Segre, K. Zhang, and M. S. Kleefisch, Phys. Rev. B **36**, 3608 (1987); J. D. Jorgensen, B. W. Veal, W. K. Kwok, G. W. Crabtree, A. Umezawa, L. J. Nowicki, and A. P. Paulikas, Phys. Rev. B **36**, 5731 (1987).

[24] F. Beech, S. Miraglia, A. Santoro, and R. S. Roth. Phys. Rev. B **35**, 8778 (1987).

[25] W. K. Kwok, G. W. Crabtree, A. Umezawa, B. W. Veal, J. D. Jorgensen, S. K. Malik, L. J. Nowicki, A. P. Paulikas, and L. Nunez, Phys. Rev. B **37**, 106 (1988).

[26] J. M. Tarascon, W. R. McKinnon, L. H. Greene, G. W. Hull, and E. M. Vogel, Phys. Rev. B **36**, 226 (1987).

[27] R. J. Cava, B. Batlogg, C. H. Chen, E. A. Rietman, S. M. Zahurak, and D. Werder, Phys. Rev. B **36**, 5719 (1987).

[28] D. J. Werder, C. H. Chen, R. J. Cava, and B. Batlogg, Phys. Rev. B **37**, 2317 (1988); R. M. Fleming, L. F. Schneemeyer, P. K. Gallagher, B. Batlogg, L. W. Rupp, and J. V. Waszczak, Phys. Rev. B **37**, 7920 (1988); C. H. Chen, D. J. Werder, L. F. Schneemeyer, P. K. Gallagher, and J. V. Waszczak, Phys. Rev. B **38**, 2888 (1988).

[29] C. Chaillout, M. A. Alario-Franco, J. J. Capponi, J. Chenavas, J. L. Hodeau, and M. Marezio, Phys. Rev. B **36**, 7118 (1987); C. Chaillout, M. A. Alario-Franco, J. J. Capponi, J. Chenavas, P. Strobel, and M. Marezio, Solid State Commun. **65**, 283 (1988).

[30] S. I. Park, C. C. Tsuei, and K. N. Tu, Phys. Rev. B **37**, 2305 (1988).

[31] J. W. Halley and H. B. Shore, Phys. Rev. B **37**, 525 (1988).

[32] Y. Tokura, J. B. Torrance, T. C. Huang, and A. I. Nazzal, Phys. Rev. B **38**, 7156 (1988).

[33] R. J. Cava, B. Batlogg, R. M. Fleming, S. A. Sunshine, A. Ramirez, E. A. Rietman, S. M. Zahurak, and R. B. van Dover, Phys. Rev. B **37**, 5912 (1988).

[34] J. B. Torrance, presented at the International Superconductor Applications Convention, San Francisco, 1989 (unpublished).

[35] J. M. Tranquada, S. M. Heald, A. R. Moodenbaugh, and Y. Xu, Phys. Rev. B **38**, 8893 (1988).

[36] J. Narayan, V. N. Shukla, S. J. Lukasiewicz, N. Biunno, R. Singh, A. F. Schreiner, and S. J. Pennycook, Appl. Phys. Lett. **51**, 940 (1987).

[37] H. W. Zandbergen, R. Gronsky, K. Wang, and G. Thomas, Nature **331**, 596 (1988).

[38] A. F. Marshall, R. W. Barton, K. Char, A. Kapitulnik, B. Oh, R. H. Hammond, and S. S. Laderman, Phys. Rev. B **37**, 9353 (1988); K. Char, M. Lee, R. W. Barton, A. F. Marshall, I. Bozovic, R. H. Hammond, M. R. Beasley, T. H. Geballe, A. Kapitulnik, and S. S. Laderman, Phys. Rev. B **38**, 834 (1988).

[39] J. Kwo, M. Hong, R. M. Fleming, A. F. Hebard, M. L. Mandich, A. M. DeSantolo, B. A. Davidson, P. Marsh, and N. D. Hobbins, Appl. Phys. Lett. **52**, 1625 (1988); M. L. Mandich, A. M. DeSantolo, R. M. Fleming,

P. Marsh, S. Nakahara, S. Sunshine, J. Kwo, M. Hong, T. Boone, T. Y. Kometani, and L. Martinez-Miranda, Phys. Rev. B **38**, 5031 (1988).

[40] P. Marsh, R. M. Fleming, M. L. Mandich, A. M. DeSantolo, J. Kwo, M. Hong, and L. J. Martinez-Miranda, Nature **334**, 141 (1988).

[41] P. Bordet, C. Chaillout, J. Chenavas, J. L. Hodeau, M. Marezio, J. Karpinski, and E. Kaldis, Nature **334**, 596 (1988); J. Karpinski, E. Kaldis, E. Jilek, S. Rusiecki, and B. Bucher, Nature **336**, 660 (1988).

[42] D. E. Morris, J. H. Nickel, J. Y. T. Wei, N. G. Asmar, J. S. Scott, U. M. Scheven, C. T. Hultgren, A. G. Markelz, J. E. Post, P. J. Heaney, D. R. Veblen, and R. M. Hazen, Phys. Rev. B **39**, 7347 (1989).

[43] C. Michel, J. Provost, F. Deslandes, B. Raveau, J. Beille, R. Cabanel, P. Lejay, A. Sulpice, J. L. Tholence, R. Tournier, B. Chevallier, G. Demazeau, and J. Etourneau, Z. Phys. B **68**, 417 (1987).

[44] C. Michel, M. Hervieu, M. M. Borel, A. Grandin, F. Deslandes, J. Provost, and B. Raveau, Z. Phys. B **68**, 421 (1987).

[45] H. Maeda, Y. Tanaka, M. Fukutomi, and T. Asano, Jpn. J. Appl. Phys. **27**, L209 (1988).

[46] C. W. Chu, J. Bechtold, L. Gao, P. H. Hor, Z. J. Huang, R. L. Meng, Y. Y. Sun, Y. Q. Wang, and Y. Y. Xue, Phys. Rev. Lett. **60**, 941 (1988).

[47] R. M. Hazen, C. T. Prewitt, R. J. Angel, N. L. Ross, L. W. Finger, C. G. Hadidiacos, D. R. Veblen, P. J. Heaney, P. H. Hor, R. L. Meng, Y. Y. Sun, Y. Q. Wang, Y. Y. Xue, Z. J. Huang, L. Gao, J. Bechtold, and C. W. Chu, Phys. Rev. Lett. **60**, 1174 (1988).

[48] M. A. Subramanian, C. C. Torardi, J. C. Calabrese, J. Gopalakrishnan, K. J. Morrissey, T. R. Askew, R. B. Flippen, U. Chowdhry, and A. W. Sleight, Science **239**, 1015 (1988).

[49] J. M. Tarascon, Y. LePage, P. Barboux, B. G. Bagley, L. H. Greene, W. R. McKinnon, G. W. Hull, M. Giroud, and D. M. Hwang, Phys. Rev. B **37**, 9382 (1988).

[50] S. A. Sunshine, T. Siegrist, L. F. Schneemeyer, D. W. Murphy, R. J. Cava, B. Batlogg, R. B. van Dover, R. M. Fleming, S. H. Glarum, S. Nakahara, R. Farrow, J. J. Krajewski, S. M. Zahurak, J. V. Waszczak, J. H. Marshall, P. Marsh, L. W. Rupp, Jr., and W. F. Peck, Phys. Rev. B **38**, 893 (1988); R. J. Cava, B. Batlogg, S. A. Sunshine, T. Siegrist, R. M. Fleming, K. Rabe, L. F. Schneemeyer, D. W. Murphy, R. B. van Dover, P. K. Gallagher, S. H. Glarum, S. Nakahara, R. C. Farrow, J. J. Krajewski, S. M. Zahurak, J. V.

Waszczak, J. H. Marshall, P. Marsh, L. W. Rupp, Jr., W. F. Peck, and E. A. Rietman, Physica C **153-155**, 560 (1988).

[51] T. M. Shaw, S. A. Shivashankar, S. J. La Placa, J. J. Cuomo, T. R. McGuire, R. A. Roy, K. H. Kelleher, and D. S. Yee, Phys. Rev. B **37**, 9856 (1988).

[52] P. Bordet, J. J. Capponi, C. Chaillout, J. Chenavas, A. W. Hewat, E. A. Hewat, J. L. Hodeau, M. Marezio, J. L. Tholence, and D. Tranqui, Physica C **153-155**, 623 (1988).

[53] C. H. Chen, D. J. Werder, S. H. Liou, H. S. Chen, and M. Hong, Phys. Rev. B **37**, 9834 (1988).

[54] E. A. Hewat, M. Dupuy, P. Bordet, J. J. Capponi, C. Chaillout, J. L. Hodeau, and M. Marezio, Nature **333**, 53 (1988).

[55] Y. Gao, P. Lee, P. Coppens, M. A. Subramanian, and A. W. Sleight, Science **241**, 954 (1988).

[56] H. W. Zandbergen, P. Groen, G. Van Tendeloo, J. Van Landuyt, and S. Amelinckx, Solid State Commun. **66**, 397 (1988).

[57] M. D. Kirk, C. B. Eom, B. Oh, S. R. Spielman, M. R. Beasley, A. Kapitulnik, T. H. Geballe, and C. F. Quate, Appl. Phys. Lett. **52**, 2071 (1988); M. D. Kirk, J. Nogami, A. A. Baski, D. B. Mitzi, A. Kapitulnik, T. H. Geballe, and C. F. Quate, Science **242**, 1673 (1988).

[58] B. G. Bagley, J. M. Tarascon, L. H. Greene, P. Barboux, P. A. Morris, G. W. Hull, M. Giroud, D. M. Hwang, Y. LePage, and W. R. McKinnon, presented at the Fall Meeting of the Materials Research Society, Boston, 1988 (unpublished).

[59] J. M. Tarascon, Y. LePage, L. H. Greene, B. G. Bagley, P. Barboux, D. M. Hwang, G. W. Hull, W. R. McKinnon, and M. Giroud, Phys. Rev. B **38**, 2504 (1988).

[60] S. M. Green, C. Jiang, Y. Mei, H. L. Luo, and C. Politis, Phys. Rev. B **38**, 5016 (1988).

[61] E. Chavira, R. Escudero, D. Ríos-Jara, and L. M. León, Phys. Rev. B **38**, 9272 (1988).

[62] R. Ramesh, G. Thomas, S. Green, C. Jiang, Y. Mei, M. L. Rudee, and H. L. Luo, Phys. Rev. B **38**, 7070 (1988).

[63] H. W. Zandbergen, Y. K. Huang, M. J. V. Menken, J. N. Li, K. Kadowaki, A. A. Menovsky, G. van Tendeloo, and S. Amelinckx, Nature **332**, 620 (1988).

[64] J. M. Tarascon, W. R. McKinnon, P. Barboux, D. M. Hwang, B. G. Bagley, L. H. Greene, G. W. Hull, Y. LePage, N. Stoffel, and M. Giroud, Phys. Rev. B **38**, 8885 (1988).

[65] J. B. Torrance, Y. Tokura, S. J. LaPlaca, T. C. Huang, R. J. Savoy, and A. I. Nazzal, Solid State Commun. **66**, 703 (1988).

[66] C. C. Torardi, M. A. Subramanian, J. C. Calabrese, J. Gopalakrishnan, E. M. McCarron, K. J. Morrissey, T. R. Askew, R. B. Flippen, U. Chowdhry, and A. W. Sleight, Phys. Rev. B **38**, 225 (1988).

[67] Z. Z. Sheng and A. M. Hermann, Nature **332**, 55 (1988); Z. Z. Sheng, A. M. Hermann, A. El Ali, C. Almasan, J. Estrada, T. Datta, and R. J. Matson, Phys. Rev. Lett. **60**, 937 (1988).

[68] Z. Z. Sheng and A. M. Hermann, Nature **332**, 138 (1988); Z. Z. Sheng and A. M. Hermann, in *Proceedings of the World Congress on Superconductivity*, edited by C. G. Burnam and R. D. Kane (World Scientific, Singapore, 1988), p. 365.

[69] L. Gao, Z. J. Huang, R. L. Meng, P. H. Hor, J. Bechtold, Y. Y. Sun, C. W. Chu, Z. Z. Sheng, and A. M. Hermann, Nature **332**, 623 (1988).

[70] M. A. Subramanian, J. C. Calabrese, C. C. Torardi, J. Gopalakrishnan, T. R. Askew, R. B. Flippen, K. J. Morrissey, U. Chowdhry, and A. W. Sleight, Nature **332**, 420 (1988).

[71] R. M. Hazen, L. W. Finger, R. J. Angel, C. T. Prewitt, N. L. Ross, C. G. Hadidiacos, P. J. Heaney, D. R. Veblen, Z. Z. Sheng, A. El Ali, and A. M. Hermann, Phys. Rev. Lett. **60**, 1657 (1988).

[72] C. C. Torardi, M. A. Subramanian, J. C. Calabrese, J. Gopalakrishnan, K. J. Morrissey, T. R. Askew, R. B. Flippen, U. Chowdhry, and A. W. Sleight, Science **240**, 631 (1988).

[73] S. S. P. Parkin, V. Y. Lee, E. M. Engler, A. I. Nazzal, T. C. Huang, G. Gorman, R. Savoy, and R. Beyers, Phys. Rev. Lett. **60**, 2539 (1988).

[74] D. E. Cox, C. C. Torardi, M. A. Subramanian, J. Gopalakrishnan, and A. W. Sleight, Phys. Rev. B **38**, 6624 (1988).

[75] W. Dmowksi, B. H. Toby, T. Egami, M. A. Subramanian, J. Gopalakrishnan, and A. W. Sleight, Phys. Rev. Lett. **61**, 2608 (1988).

[76] S. S. P. Parkin, V. Y. Lee, A. I. Nazzal, R. Savoy, R. Beyers, and S. J. La Placa, Phys. Rev. Lett. **61**, 750 (1988).

[77] R. Beyers, S. S. P. Parkin, V. Y. Lee, A. I. Nazzal, R. Savoy, G. Gorman, T. C. Huang, and S. La Placa, Appl. Phys. Lett. **53**, 432 (1988).

[78] H. Ihara, R. Sugise, M. Hirabayashi, N. Terada, M. Jo, K. Hayashi, A. Negishi, M. Tokumoto, Y. Kimura, and T. Shimomura, Nature **334**, 510 (1988); R. Sugise, M. Hirabayashi, N. Terada, M. Jo, T. Shimomura, and H. Ihara, Physica C **157**, 131 (1989).

[79] P. Haldar, K. Chen, B. Maheswaran, A. Roig-Janicki, N. K. Jaggi, R. S. Markiewicz, and B. C. Giessen, Science **241**, 1198 (1988).

[80] S. S. P. Parkin, V. Y. Lee, A. I. Nazzal, R. Savoy, T. C. Huang, G. Gorman, and R. Beyers, Phys. Rev. B **38**, 6531 (1988).

[81] A. W. Sleight, presented at the International Superconductor Applications Convention, San Francisco, 1989 (unpublished).

[82] T. Siegrist, S. M. Zahurak, D. W. Murphy, and R. S. Roth, Nature **334**, 231 (1988); S. Sunshine (private communication).

[83] R. J. Cava, B. Batlogg, J. J. Krajewski, L. W. Rupp, L. F. Schneemeyer, T. Siegrist, R. B. van Dover, P. Marsh, W. F. Peck, Jr., P. K. Gallagher, S. H. Glarum, J. H. Marshall, R. C. Farrow, J. V. Waszczak, R. Hull, and P. Trevor, Nature **336**, 211 (1988).

[84] A. M. Hermann, presented at the International Superconductor Applications Convention, San Francisco, 1989 (unpublished).

[85] A. W. Sleight, in *Chemistry of High-Temperature Superconductors*, edited by D. L. Nelson, M. S. Whittingham, and T. F. George, ACS Symposium Series **351** (American Chemical Society, Washington, DC, 1987), p. 2; G. M. Luke, B. J. Sternlieb, Y. J. Uemura, J. H. Brewer, R. Kadono, R. F. Kiefl, S. R. Kreitzman, T. M. Riseman, J. Gopalakrishnan, A. W. Sleight, M. A. Subramanian, S. Uchida, H. Takagi, and Y. Tokura, Nature **338**, 49 (1989).

[86] Y. Tokura, H. Takagi, and S. Uchida, Nature **337**, 345 (1989); H. Takagi, S. Uchida, and Y. Tokura, Phys. Rev. Lett. **62**, 1197 (1989).

[87] K. Kitazawa, presented at the International Superconductor Applications Convention, San Francisco, 1989 (unpublished).

[88] A. W. Sleight, J. L. Gillson, and P. E. Bierstedt, Solid State Commun. **17**, 27 (1975).

[89] R. D. Shannon and P. E. Bierstedt, J. Amer. Cer. Soc. **53**, 635 (1970).

[90] D. E. Cox and A. W. Sleight, Solid State Commun. **19**, 969 (1976).

[91] C. W. Chu, S. Huang, and A. W. Sleight, Solid State Commun. **18**, 977 (1976).

[92] L. F. Mattheiss, E. M. Gyorgy, and D. W. Johnson, Jr., Phys. Rev. B **37**, 3745 (1988).

[93] R. J. Cava, B. Batlogg, J. J. Krajewski, R. Farrow, L. W. Rupp, Jr., A. E. White, K. Short, W. F. Peck, and T. Kometani, Nature **332**, 814 (1988).

[94] D. G. Hinks, B. Dabrowski, J. D. Jorgensen, A. W. Mitchell, D. R. Richards, S. Pei, and D. Shi, Nature **333**, 836 (1988).

[95] A. W. Sleight, Science **242**, 1519 (1988); N. Jones, R. Flippen, and A. W. Sleight (unpublished).

[96] L. F. Schneemeyer, J. K. Thomas, T. Siegrist, B. Batlogg, L. W. Rupp, R. L. Opila, R. J. Cava, and D. W. Murphy, Nature **335**, 421 (1988).

[97] R. M. Fleming, P. Marsh, R. J. Cava, and J. J. Krajewski, Phys. Rev. B **38**, 7026 (1988).

[98] J. Bardeen, L. N. Cooper, and J. R. Schrieffer, Phys. Rev. **106**, 162 (1957); J. Bardeen, L. N. Cooper, and J. R. Schrieffer, Phys. Rev. **108**, 1175 (1957).

[99] C. W. Chu, P. H. Hor, R. L. Meng, L. Gao, and Z. J. Huang, Science **235**, 567 (1987).

[100] P. H. Hor, L. Gao, R. L. Meng, Z. J. Huang, Y. Q. Wang, K. Forster, J. Vassilious, C. W. Chu, M. K. Wu, J. R. Ashburn, and C. J. Torng, Phys. Rev. Lett. **58**, 911 (1987).

[101] N. P. Ong, Z. Z. Wang, J. Clayhold, J. M. Tarascon, L. H. Greene, and W. R. McKinnon, Phys. Rev. B **35**, 8807 (1987).

[102] S. Uchida, H. Takagi, H. Yanagisawa, K. Kishio, K. Kitazawa, K. Fueki, and S. Tanaka, Jpn. J. Appl. Phys. **26**, L445 (1987).

[103] Z. Z. Wang, J. Clayhold, N. P. Ong, J. M. Tarascon, L. H. Greene, W. R. McKinnon, and G. W. Hull, Phys. Rev. B **36**, 7222 (1987).

[104] H. Takagi, H. Eisaki, S. Uchida, A. Maeda, S. Tajima, K. Uchinokura, and S. Tanaka, Nature **332**, 236 (1988).

[105] J. Clayhold, N. P. Ong, P. H. Hor, and C. W. Chu, Phys. Rev. B **38**, 7016 (1988).

[106] B. Batlogg, Physica **126B**, 275 (1984).

[107] B. Dabrowski, D. G. Hinks, J. D. Jorgensen, R. K. Kalia, P. Vashishta, D. R. Richards, D. T. Marx, and A. W. Mitchell, Physica C **156**, 24 (1988).

[108] S-W. Cheong, Z. Fisk, R. S. Kwok, J. P. Remeika, J. D. Thompson, and G. Gruner, Phys. Rev. B **37**, 5916 (1988).

[109] S. W. Tozer, A. W. Kleinsasser, T. Penney, D. Kaiser, and F. Holtzberg, Phys. Rev. Lett. **59**, 1768 (1987); T. Penney, S. von Molnár, D. Kaiser, F. Holtzberg, and A. W. Kleinsasser, Phys. Rev. B **38**, 2918 (1988).

[110] S. J. Hagen, T. W. Jing, Z. Z. Wang, J. Horvath, and N. P. Ong, Phys. Rev. B **37**, 7928 (1988).

[111] S. Martin, A. T. Fiory, R. M. Fleming, L. F. Schneemeyer, and J. V. Waszczak, Phys. Rev. Lett. **60**, 2194 (1988).

[112] C. E. Gough, M. S. Colclough, E. M. Forgan, R. G. Jordan, M. Keene, C. M. Muirhead, A. I. M. Rae, N. Thomas, J. S. Abell, and S. Sutton, Nature **326**, 855 (1987).

[113] P. L. Gammel, D. J. Bishop, G. J. Dolan, J. R. Kwo, C. A. Murray, L. F. Schneemeyer, and J. V. Waszczak, Phys. Rev. Lett. **59**, 2592 (1987).

[114] D. Estève, J. M. Martinis, C. Urbina, M. H. Devoret, G. Collin, P. Monod, M. Ribault, and A. Revcolevschi, Europhys. Lett. **3**, 1237 (1987).

[115] J. S. Tsai, Y. Kubo, and J. Tabuchi, Phys. Rev. Lett. **58**, 1979 (1987).

[116] J. Niemeyer, M. R. Dietrich, and C. Politis, Z. Phys. B **67**, 155 (1987).

[117] D. R. Harshman, G. Aeppli, E. J. Ansaldo, B. Batlogg, J. H. Brewer, J. F. Carolan, R. J. Cava, M. Celio, A. C. D. Chaklader, W. N. Hardy, S. R. Kreitzman, G. M. Luke, D. R. Noakes, and M. Senba, Phys. Rev. B **36**, 2386 (1987); D. R. Harshman, L. F. Schneemeyer, J. V. Waszczak, G. Aeppli, R. J. Cava, B. Batlogg, L. W. Rupp, E. J. Ansaldo, and D. Ll. Williams, Phys. Rev. B **39**, 851 (1989).

[118] L. Krusin-Elbaum, R. L. Greene, F. Holtzberg, A. P. Malozemoff, and Y. Yeshurun, Phys. Rev. Lett. **62**, 217 (1989).

[119] W. Eidelloth, F. S. Barnes, Z. Z. Sheng, and A. M. Hermann, Phys. Rev. B (submitted); A. M. Hermann (private communication).

[120] For a review, see G. A. Thomas, R. N. Bhatt, A. Millis, R. Cava, and E. Rietman, Jpn. J. Appl. Phys. **26**, Suppl. 26-3, 1001 (1987).

[121] H. F. C. Hoevers, P. J. M. van Bentum, L. E. C. van de Leemput, H. van Kempen, A. J. G. Schellingerhout, and D. van der Marel, Physica C **152**, 105 (1988).

[122] G. A. Thomas, J. Orenstein, D. H. Rapkine, M. Capizzi, A. J. Millis, R. N. Bhatt, L. F. Schneemeyer, and J. V. Waszczak, Phys. Rev. Lett. **61**, 1313 (1988).

[123] B. Batlogg, J. P. Remeika, R. C. Dynes, H. Barz, A. S. Cooper, and J. P. Garno, in *Superconductivity in d- and f-Band Metals*, edited by W. Buckel and W. Weber (Kernforschungszentrum Karlsruhe GmbH, Karlsruhe, 1982), p. 401.

[124] Z. Schlesinger, R. T. Collins, B. A. Scott, and J. A. Calise, Phys. Rev. B **38**, 9284 (1988).

[125] S. Vieira, M. A. Ramos, M. Vallet-Regí, and J. M. Gonzalez-Calbet, Phys. Rev. B **38**, 9295 (1988).

[126] M. Lee, D. B. Mitzi, A. Kapitulnik, and M. R. Beasley, Phys. Rev. B **39**, 801 (1989).

[127] M. Reedyk, D. A. Bonn, J. D. Garrett, J. E. Greedan, C. V. Stager, T. Timusk, K. Kamarás, and D. B. Tanner, Phys. Rev. B **38**, 11981 (1988).

[128] J.-M. Imer, F. Patthey, B. Dardel, W.-D. Schneider, Y. Baer, Y. Petroff, and A. Zettl, Phys. Rev. Lett. **62**, 336 (1989).

[129] A. Junod, A. Bezinge, and J. Muller, Physica C **152**, 50 (1988).

[130] B. Batlogg, T. T. M. Palstra, L. F. Schneemeyer, R. B. van Dover, and R. J. Cava, Physica C **153-155**, 1062 (1988).

[131] T. T. M. Palstra, B. Batlogg, L. F. Schneemeyer, R. B. van Dover, and J. V. Waszczak, Phys. Rev. B **38**, 5102 (1988); T. T. M. Palstra, B. Batlogg, L. F. Schneemeyer, and J. V. Waszczak, Phys. Rev. Lett. **61**, 1662 (1988).

[132] P. L. Gammel, L. F. Schneemeyer, J. V. Waszczak, and D. J. Bishop, Phys. Rev. Lett. **61**, 1666 (1988).

[133] B. Batlogg, G. Kourouklis, W. Weber, R. J. Cava, A. Jayaraman, A. E. White, K. T. Short, L. W. Rupp, and E. A. Rietman, Phys. Rev. Lett. **59**, 912 (1987).

[134] T. A. Faltens, W. K. Ham, S. W. Keller, K. J. Leary, J. N. Michaels, A. M. Stacy, H.-C. zur Loye, D. E. Morris, T. W. Barbee, III, L. C. Bourne, M. L. Cohen, S. Hoen, and A. Zettl, Phys. Rev. Lett. **59**, 915 (1987).

[135] B. Batlogg, R. J. Cava, A. Jayaraman, R. B. van Dover, G. A. Kourouklis, S. Sunshine, D. W. Murphy, L. W. Rupp, H. S. Chen, A. White, K. T. Short, A. M. Mujsce, and E. A. Rietman, Phys. Rev. Lett. **58**, 2333 (1987).

[136] L. C. Bourne, M. F. Crommie, A. Zettl, H.-C. zur Loye, S. W. Keller, K. J. Leary, A. M. Stacy, K. J. Chang, M. L. Cohen, and D. E. Morris, Phys. Rev. Lett. **58**, 2337 (1987).

[137] K. J. Leary, H.-C. zur Loye, S. W. Keller, T. A. Faltens, W. K. Ham, J. N. Michaels, and A. M. Stacy, Phys. Rev. Lett. **59**, 1236 (1987).

[138] D. E. Morris, R. M. Kuroda, A. G. Markelz, J. H. Nickel, and J. Y. T. Wei, Phys. Rev. B **37**, 5936 (1988).

[139] H. Katayama-Yoshida, T. Hirooka, A. Oyamada, Y. Okabe, T. Takahashi, T. Sasaki, A. Ochiai, T. Suzuki, A. J. Mascarenhas, J. I. Pankove, T. F. Ciszek, S. K. Deb, R. B. Goldfarb, and Y. Li, Physica C **156**, 481 (1988).

[140] B. Batlogg, R. J. Cava, L. W. Rupp, Jr., A. M. Mujsce, J. J. Krajewski, J. P. Remeika, W. F. Peck, Jr., A. S. Cooper, and G. P. Espinosa, Phys. Rev. Lett. **61**, 1670 (1988).

[141] D. G. Hinks, D. R. Richards, B. Dabrowski, D. T. Marx, and A. W. Mitchell, Nature **335**, 419 (1988).

[142] D. Vaknin, S. K. Sinha, D. E. Moncton, D. C. Johnston, J. M. Newsam, C. R. Safinya, and H. E. King, Jr., Phys. Rev. Lett. **58**, 2802 (1987); D. C. Johnston, J. P. Stokes, D. P. Goshorn, and J. T. Lewandowski, Phys. Rev. B **36**, 4007 (1987).

[143] S. Mitsuda, G. Shirane, S. K. Sinha, D. C. Johnston, M. S. Alvarez, D. Vaknin, and D. E. Moncton, Phys. Rev. B **36**, 822 (1987).

[144] T. Freltoft, J. E. Fischer, G. Shirane, D. E. Moncton, S. K. Sinha, D. Vaknin, J. P. Remeika, A. S. Cooper, and D. Harshman, Phys. Rev. B **36**, 826 (1987).

[145] Y. J. Uemura, W. J. Kossler, X. H. Yu, J. R. Kempton, H. E. Schone, D. Opie, C. E. Stronach, D. C. Johnston, M. S. Alvarez, and D. P. Goshorn, Phys. Rev. Lett. **59**, 1045 (1987).

[146] T. Thio, T. R. Thurston, N. W. Preyer, P. J. Picone, M. A. Kastner, H. P. Jenssen, D. R. Gabbe, C. Y. Chen, R. J. Birgeneau, and A. Aharony, Phys. Rev. B **38**, 905 (1988).

[147] G. Shirane, Y. Endoh, R. J. Birgeneau, M. A. Kastner, Y. Hidaka, M. Oda, M. Suzuki, and T. Murakami, Phys. Rev. Lett. **59**, 1613 (1987).

[148] R. J. Birgeneau, D. R. Gabbe, H. P. Jenssen, M. A. Kastner, P. J. Picone, T. R. Thurston, G. Shirane, Y. Endoh, M. Sato, K. Yamada, Y. Hidaka, M. Oda, Y. Enomoto, M. Suzuki, and T. Murakami, Phys. Rev. B **38**, 6614 (1988).

[149] A. Weidinger, Ch. Niedermayer, A. Golnik, R. Simon, E. Recknagel, J. I. Budnick, B. Chamberland, and C. Baines, Phys. Rev. Lett. **62**, 102 (1989).

[150] J. M. Tranquada, D. E. Cox, W. Kunnmann, H. Moudden, G. Shirane, M. Suenaga, P. Zolliker, D. Vaknin, S. K. Sinha, M. S. Alvarez, A. J. Jacobson, and D. C. Johnston, Phys. Rev. Lett. **60**, 156 (1988); J. M. Tranquada, A. H. Moudden, A. I. Goldman, P. Zolliker, D. E. Cox, G. Shirane, S. K. Sinha, D. Vaknin, D. C. Johnston, M. S. Alvarez, A. J. Jacobson, J. T. Lewandowski, and J. M. Newsam, Phys. Rev. B **38**, 2477 (1988).

[151] J. H. Brewer, E. J. Ansaldo, J. F. Carolan, A. C. D. Chaklader, W. N. Hardy, D. R. Harshman, M. E. Hayden, M. Ishikawa, N. Kaplan, R. Keitel, J. Kempton, R. F. Kiefl, W. J. Kossler, S. R. Kreitzman, A. Kulpa, Y. Kuno, G. M. Luke, H. Miyatake, K. Nagamine, Y. Nakazawa, N. Nishida, K. Nishiyama, S. Ohkuma, T. M. Riseman, G. Roehmer, P. Schleger, D. Shimada, C. E. Stronach, T. Takabatake, Y. J. Uemura, Y. Watanabe, D. Ll. Williams, T. Yamazaki, and B. Yang, Phys. Rev. Lett. **60**, 1073 (1988).

[152] P. F. Miceli, J. M. Tarascon, L. H. Greene, P. Barboux, M. Giroud, D. A. Neumann, J. J. Rhyne, L. F. Schneemeyer, and J. V. Waszczak, Phys. Rev. B **38**, 9209 (1988).

[153] M. Sato, S. Shamoto, J. M. Tranquada, G. Shirane, and B. Keimer, Phys. Rev. Lett. **61**, 1317 (1988).

[154] R. Yoshizaki, Y. Saito, Y. Abe, and H. Ikeda, Physica C **152**, 408 (1988).

[155] A. Manthiram and J. B. Goodenough, Appl. Phys. Lett. **53**, 420 (1988).

[156] M. A. Subramanian, A. R. Strzelecki, J. Gopalakrishnan, and A. W. Sleight, J. Solid State Chem. **77**, 196 (1988).

[157] Y. J. Uemura *et al.*, J. Phys. (Paris) (in press); B. X. Yang, R. F. Kiefl, J. H. Brewer, J. F. Carolan, W. N. Hardy, R. Kadono, J. R. Kempton, S. R. Kreitzman, G. M. Luke, T. M. Riseman, D. Ll. Williams, Y. J. Uemura, B. Sternlieb, M. A. Subramanian, A. R. Strzelecki, J. Gopalakrishnan, and A. W. Sleight, Phys. Rev. B **39**, 847 (1989).

[158] N. Nishida, H. Miyatake, S. Okuma, T. Tamegai, Y. Iye, R. Yoshizaki, K. Nishiyama, and K. Nagamine, Physica C **156**, 625 (1988).

[159] J. Mizuki, Y. Kubo, T. Manako, Y. Shimakawa, H. Igarashi, J. M. Tranquada, Y. Fujii, L. Rebelsky, and G. Shirane, Physica C **156**, 781 (1988).

[160] Y. J. Uemura, B. J. Sternlieb, D. E. Cox, J. H. Brewer, R. Kadono, J. R. Kempton, R. F. Kiefl, S. R. Kreitzman, G. M. Luke, P. Mulhern, T. Riseman, D. L. Williams, W. J. Kossler, X. H. Yu, C. E. Stronach, M. A. Subramanian, J. Gopalakrishnan, and A. W. Sleight, Nature **335**, 151 (1988).

[161] E. Wigner, Phys. Rev. **46**, 1002 (1934).

[162] J. C. Slater and G. F. Koster, Phys. Rev. **94**, 1498 (1954).

[163] G. Leman and J. Friedel, J. Appl. Phys. **33**, 281 (1962).

[164] D. J. Chadi and M. L. Cohen, Phys. Stat. Sol. (b) **68**, 405 (1975).

[165] W. A. Harrison, *Electronic Structure and the Properties of Solids* (Freeman, San Francisco, 1980).

[166] The tight-binding approach has also been applied to high-temperature superconductors by W. Weber, Phys. Rev. Lett. **58**, 1371 (1987); by D. A. Papaconstantopoulos, W. E. Pickett, and M. J. DeWeert, Phys. Rev. Lett. **61**, 211 (1988); by W. A. Harrison, in *Novel Superconductivity*, edited by S. A. Wolf and V. Z. Kresin (Plenum, New York, 1987), p. 507, and Phys. Rev. B **38**, 270 (1988); by R. Combescot and J. Labbe, Phys. Rev. B **38**, 262 (1988); by J. Zaanen, A. T. Paxton, O. Jepsen, and O. K. Andersen, Phys. Rev. Lett. **60**, 2685 (1988); and by A. K. McMahan, R. M. Martin, and S. Satpathy, Phys. Rev. B **38**, 6650 (1988). In addition, see Refs. 175, 185, 206, and 219.

[167] P. D. Johnson, S. L. Qiu, L. Jiang, M. W. Ruckman, M. Strongin, S. L. Hulbert, R. F. Garrett, B. Sinković, N. V. Smith, R. J. Cava, C. S. Jee, D. Nichols, E. Kaczanowicz, R. E. Salomon, and J. E. Crow, Phys. Rev. B **35**, 8811 (1987).

[168] N. Nücker, J. Fink, J. C. Fuggle, P. J. Durham, and W. M. Temmerman, Phys. Rev. B **37**, 5158 (1988).

[169] M. S. Hybertsen and S. G. Louie, Phys. Rev. Lett. **58**, 1551 (1987) and references therein.

[170] S. Fahy, X. W. Wang, and S. G. Louie, in *Proceedings of the Nineteenth International Conference on the Physics of Semiconductors* (Warsaw, August 1988, in press).

[171] S. Froyen and W. A. Harrison, Phys. Rev. B **20**, 2420 (1979).

[172] A. W. Luehrmann, Adv. Phys. **17**, 1 (1968).

[173] J. S. Faulkner, in *Progress in Materials Science*, edited by J. W. Christian, P. Haasen, and T. B. Massalski (Pergamon, Oxford, 1982), Vol. 27, p. 1.

[174] D. J. Chadi and M. L. Cohen, Phys. Rev. B **8**, 5747 (1973); D. J. Chadi, Phys. Rev. B **16**, 1746 (1977).

[175] L. F. Mattheiss, Phys. Rev. Lett. **58**, 1028 (1987).

[176] J. Yu, A. J. Freeman, and J.-H. Xu., Phys. Rev. Lett. **58**, 1035 (1987).

[177] T. Oguchi, Jpn. J. Appl. Phys. **26**, L417 (1987).

[178] K. Takegahara, H. Harima, and A. Yanase, Jpn. J. Appl. Phys. **26**, L352 (1987).

[179] N. Nücker, J. Fink, B. Renker, D. Ewert, C. Politis, P. J. W. Weijs, and J. C. Fuggle, Z. Phys. B **67**, 9 (1987).

[180] A. Fujimori, E. Takayama-Muromachi, Y. Uchida, and B. Okai, Phys. Rev. B **35**, 8814 (1987).

[181] T. Takahashi, F. Maeda, H. Katayama-Yoshida, Y. Okabe, T. Suzuki, A. Fujimori, S. Hosoya, S. Shamoto, and M. Sato, Phys. Rev. B **37**, 9788 (1988).

[182] B. Reihl, T. Riesterer, J. G. Bednorz, and K. A. Müller, Phys. Rev. B **35**, 8804 (1987).

[183] Y. Gao, T. J. Wagener, J. H. Weaver, A. J. Arko, B. Flandermeyer, and D. W. Capone II, Phys. Rev. B **36**, 3971 (1987).

[184] J. C. Fuggle, P. J. W. Weijs, R. Schoorl, G. A. Sawatzky, J. Fink, N. Nücker, P. J. Durham, and W. M. Temmerman, Phys. Rev. B **37**, 123 (1988).

[185] L. F. Mattheiss and D. R. Hamann, Solid State Commun. **63**, 395 (1987).

[186] T. Fujiwara and Y. Hatsugai, Jpn. J. Appl. Phys. **26**, L716 (1987).

[187] S. Massidda, J. Yu, A. J. Freeman, and D. D. Koelling, Phys. Lett. A **122**, 198 (1987).

[188] F. Herman, R. V. Kasowski, and W. Y. Hsu, Phys. Rev. B **36**, 6904 (1987).

[189] R. L. Kurtz, R. L. Stockbauer, D. Mueller, A. Shih, L. E. Toth, M. Osofsky, and S. A. Wolf, Phys. Rev. B **35**, 8818 (1987).

[190] P. Steiner, V. Kinsinger, I. Sander, B. Siegwart, S. Hüfner, and C. Politis, Z. Phys. B **67**, 19 (1987).

[191] M. Onellion, Y. Chang, D. W. Niles, R. Joynt, G. Margaritondo, N. G. Stoffel, and J. M. Tarascon, Phys. Rev. B **36**, 819 (1987).

[192] F. C. Brown, T. -C. Chiang, T. A. Friedmann, D. M. Ginsberg, G. N. Kwawer, T. Miller, and M. G. Mason, J. Low Temp. Phys. **69**, 151 (1987); A. Samsavar, T. Miller, T. -C. Chiang, B. G. Pazol, T. A. Friedmann, and D. M. Ginsberg, Phys. Rev. B **37**, 5164 (1988).

[193] K. -L. Tsang, C. H. Zhang, T. A. Callcott, L. R. Canfield, D. L. Ederer, J. E. Blendell, C. W. Clark, N. Wassdahl, J. E. Rubensson, G. Bray, N. Mortensson, J. Nordgren, R. Nyholm, and S. Cramm, Phys. Rev. B **37**, 2293 (1988).

[194] N. G. Stoffel, J. M. Tarascon, Y. Chang, M. Onellion, D. W. Niles, and G. Margaritondo, Phys. Rev. B **36**, 3986 (1987); N. G. Stoffel, Y. Chang, M. K. Kelly, L. Dottl, M. Onellion, P. A. Morris, W. A. Bonner, and G. Margaritondo, Phys. Rev. B **37**, 7952 (1988).

[195] T. J. Wagener, Y. Gao, J. H. Weaver, A. J. Arko, B. Flandermeyer, and D. W. Capone II, Phys. Rev. B **36**, 3899 (1987).

[196] J. A. Yarmoff, D. R. Clarke, W. Drube, U. O. Karlsson, A. Teleb-Ibrahimi, and F. J. Himpsel, Phys. Rev. B **36**, 3967 (1987).

[197] A. J. Viescas, J. M. Tranquada, A. R. Moodenbaugh, and P. D. Johnson, Phys. Rev. B **37**, 3738 (1988).

[198] P. E. Batson and M. F. Chisholm, Phys. Rev. B **37**, 635 (1988).

[199] J. Yuan, L. M. Brown, and W. Y. Liang, J. Phys. C **21**, 517 (1988).

[200] M. Tang, Y. Chang, M. Onellion, J. Seuntjens, D. C. Larbalestier, G. Margaritondo, N. G. Stoffel, and J. M. Tarascon, Phys. Rev. B **37**, 1611 (1988).

[201] C. H. Chen, L. F. Schneemeyer, S. H. Liou, M. Hong, J. Kwo, H. S. Chen, and J. V. Waszczak, Phys. Rev. B **37**, 9780 (1988).

[202] A. L. Wachs, P. E. A. Turchi, Y. C. Jean, K. H. Wetzler, R. H. Howell, M. J. Fluss, D. R. Harshman, J. P. Remeika, A. S. Cooper, and R. M. Fleming, Phys. Rev. B **38**, 913 (1988).

[203] M. J. Fluss, A. L. Wachs, P. E. A. Turchi, R. H. Howell, Y. C. Jean, J. Kyle, H. Nakanishi, C. W. Chu, R. L. Meng, H. P. Hor, and J. Z. Huang, in *Proceedings of the World Congress on Superconductivity*, edited by C. G. Burnham and R. D. Kane (World Scientific, Singapore, 1988), p. 357.

[204] L. F. Mattheiss and D. R. Hamann, Phys. Rev. B **28**, 4227 (1983).

[205] P. A. Sterne and C. S. Wang, J. Phys. C **21**, L949 (1988).

[206] M. S. Hybertsen and L. F. Mattheiss, Phys. Rev. Lett. **60**, 1661 (1988); L. F. Mattheiss and D. R. Hamann, Phys. Rev. B **38**, 5012 (1988).

[207] H. Krakauer and W. E. Pickett, Phys. Rev. Lett. **60**, 1665 (1988).

[208] F. Herman, R. V. Kasowski, and W. Y. Hsu, Phys. Rev. B **38**, 204 (1988).

[209] S. Massidda, J. Yu, and A. J. Freeman, Physica C **152**, 251 (1988).

[210] H. M. Meyer III, D. M. Hill, J. H. Weaver, D. L. Nelson, and C. F. Gallo, Phys. Rev. B **38**, 7144 (1988).

[211] M. Onellion, M. Tang, Y. Chang, G. Margaritondo, J. M. Tarascon, P. A. Morris, W. A. Bonner, and N. G. Stoffel, Phys. Rev. B **38**, 881 (1988); R. Zanoni, Y. Chang, M. Tang, Y. Hwu, M. Onellion, G. Margaritondo, P. A. Morris, W. A. Bonner, J. M. Tarascon, and N. G. Stoffel, Phys. Rev. B **38**, 11832 (1988).

[212] F. J. Himpsel, G. V. Chandrashekhar, A. Teleb-Ibrahimi, A. B. McLean, and M. W. Shafer, in *High-T_c Superconducting Thin Films, Devices, and Characterization*, edited by G. Margaritondo, M. Onellion, and R. Joynt, AIP Conference Series (American Institute of Physics, New York, in press); F. J. Himpsel, G. V. Chandrashekhar, A. B. McLean, and M. W. Shafer, Phys. Rev. B **38**, 11946 (1988).

[213] P. A. P. Lindberg, Z.-X. Shen, I. Lindau, W. E. Spicer, C. B. Eom, and T. H. Geballe, Appl. Phys. Lett. **53**, 529 (1988); Z.-X. Shen, P. A. P. Lindberg, I. Lindau, W. E. Spicer, C. B. Eom, and T. H. Geballe, Phys. Rev. B **38**, 7152 (1988); Z.-X. Shen, P. A. P. Lindberg, B. O. Wells, D. B. Mitzi, I. Lindau, W. E. Spicer, and A. Kapitulnik, Phys. Rev. B **38**, 11820 (1988); Z.-X. Shen, P. A. P. Lindberg, P. Soukiassian, C. B. Eom, I. Lindau, W. E. Spicer, and T. H. Geballe, Phys. Rev. B **39**, 823 (1989).

[214] E. G. Michel, J. Alvarez, M. C. Asensio, R. Miranda, J. Ibáñez, G. Peral, J. L. Vicent, F. García, E. Morán, and M. A. Alario-Franco, Phys. Rev. B **38**, 5146 (1988).

[215] S. Kohiki, T. Wada, S. Kawashima, H. Takagi, S. Uchida, and S. Tanaka, Phys. Rev. B **38**, 7051 (1988); and Phys. Rev. B **38**, 8868 (1988).

[216] F. U. Hillebrecht, J. Fraxedas, L. Ley, H. J. Trodahl, J. Zaanen, W. Braun, M. Mast, H. Petersen, M. Schaible, L. C. Bourne, P. Pinsukanjana, and A. Zettl, Phys. Rev. B **39**, 236 (1989).

[217] T. Takahashi, H. Matsuyama, H. Katayama-Yoshida, Y. Okabe, S. Hosoya, K. Seki, H. Fujimoto, M. Sato, and H. Inokuchi, Nature **334**, 691 (1988).

[218] T. J. Wagener, Y. Hu, Y. Gao, M. B. Jost, J. H. Weaver, N. D. Spencer, and K. C. Goretta, Phys. Rev. B **39**, 2928 (1989); J. H. Weaver, H. M. Meyer III, T. J. Wagener, D. M. Hill, and Y. Hu, in *High-T_c Superconducting Thin Films, Devices, and Characterization*, edited by G. Margaritondo, M. Onellion, and R. Joynt, AIP Conference Series (American Institute of Physics, New York, in press).

[219] D. R. Hamann and L. F. Mattheiss, Phys. Rev. B **38**, 5138 (1988).

[220] R. V. Kasowski, W. Y. Hsu, and F. Herman, Phys. Rev. B **38**, 6470 (1988).

[221] J. Yu, S. Massidda, and A. J. Freeman, Physica C **152**, 273 (1988).

[222] H. M. Meyer III, T. J. Wagener, J. H. Weaver, and D. S. Ginley, Phys. Rev. B **39**, 7343 (1989).

[223] L. F. Mattheiss and D. R. Hamann, Phys. Rev. B **26**, 2686 (1982).

[224] G. K. Wertheim, J. P. Remeika, and D. N. E. Buchanan, Phys. Rev. B **26**, 2120 (1982).

[225] L. F. Mattheiss and D. R. Hamann, Phys. Rev. Lett. **60**, 2681 (1988).

[226] M. W. Ruckman, D. Di Marzio, Y. Jeon, G. Liang, J. Chen, M. Croft, and M. S. Hegde, Phys. Rev. B **39**, 7359 (1989).

[227] T. J. Wagener, H. M. Meyer III, D. M. Hill, Y. Hu, M. B. Jost, J. H. Weaver, and D. G. Hinks, Phys. Rev. B (submitted).

[228] D. W. Murphy, S. Sunshine, R. B. van Dover, R. J. Cava, B. Batlogg, S. M. Zahurak, and L. F. Schneemeyer, Phys. Rev. Lett. **58**, 1888 (1987).

[229] P. H. Hor, R. L. Meng, Y. Q. Wang, L. Gao, Z. J. Huang, J. Bechtold, K. Forster, and C. W. Chu, Phys. Rev. Lett. **58**, 1891 (1987).

[230] K. Kitazawa, K. Kishio, H. Takagi, T. Hasegawa, S. Kanbe, S. Uchida, S. Tanaka, and K. Fueki, Jpn. J. Appl. Phys. **26**, L339 (1987).

[231] A. R. Moodenba ,n, M. Suenaga, T. Asano, R. N. Shelton, H. C. Ku, R. W. McCallum, and P. Klavins, Phys. Rev. Lett. **58**, 1885 (1987).

[232] S. E. Brown, J. D. Thompson, J. O. Willis, R. M. Aikin, E. Zirngiebl, J. L. Smith, Z. Fisk, and R. B. Schwarz, Phys. Rev. B **36**, 2298 (1987).

[233] F. Zuo, B. R. Patton, D. L. Cox, S. I. Lee, Y. Song, J. P. Golben, X. D. Chen, S. Y. Lee, Y. Cao, Y. Lu, J. R. Gaines, J. C. Garland, and A. J. Epstein, Phys. Rev. B **36**, 3603 (1987).

[234] Y. Le Page, T. Siegrist, S. A. Sunshine, L. F. Schneemeyer, D. W. Murphy, S. M. Zahurak, J. V. Waszczak, W. R. McKinnon, J. M. Tarascon, G. W. Hull, and L. H. Greene, Phys. Rev. B **36**, 3617 (1987).

[235] A. P. Gonçalves, I. C. Santos, E. B. Lopes, R. T. Henriques, M. Almeida, and M. O. Figueiredo, Phys. Rev. B **37**, 7476 (1988).

[236] A. Matsuda, K. Kinoshita, T. Ishii, H. Shibata, T. Watanabe, and T. Yamada, Phys. Rev. B **38**, 2910 (1988).

[237] T. Wada, S. Adachi, T. Mihara, and R. Inaba, Jpn. J. Appl. Phys. **26**, L706 (1987).

[238] B. W. Veal, W. K. Kwok, A. Umezawa, G. W. Crabtree, J. D. Jorgensen, J. W. Downey, L. J. Nowicki, A. W. Mitchell, A. P. Paulikas, and C. H. Sowers, Appl. Phys. Lett. **51**, 279 (1987).

[239] C. U. Segre, B. Dabrowski, D. G. Hinks, K. Zhang, J. D. Jorgensen, M. A. Beno, and I. K. Schuller, Nature **329**, 227 (1987).

[240] R. J. Cava, B. Batlogg, A. P. Ramirez, D. Werder, C. H. Chen, E. A. Rietman, and S. M. Zahurak, in *High-Temperature Superconductors*, edited by M. B. Brodsky, R. C. Dynes, K. Kitazawa, and H. L. Tuller, MRS Symposium Proceedings **99** (Materials Research Society, Pittsburgh, 1988), p. 1[illegible].

[241] K. Zhang, B. Dabrowski, C. U. Segre, D. G. Hinks, I. K. Schuller, J. D. Jorgensen, and M. Slaski, J. Phys. C **20**, L935 (1987).

[242] T. Siegrist, L. F. Schneemeyer, J. V. Waszczak, N. P. Singh, R. L. Opila, B. Batlogg, L. W. Rupp, and D. W. Murphy, Phys. Rev. B **36**, 8365 (1987).

[243] G. Xiao, F. H. Streitz, A. Gavrin, Y. W. Du, and C. L. Chien, Phys. Rev. B **35**, 8782 (1987).

[244] Y. Maeno, T. Tomita, M. Kyogoku, S. Awaji, Y. Aoki, K. Hoshino, A. Minami, and T. Fujita, Nature **328**, 512 (1987).

[245] Y. Maeno, T. Nojima, Y. Aoki, M. Kato, K. Hoshino, A. Minami, and T. Fujita, Jpn. J. Appl. Phys. **26**, L774 (1987).

[246] J. M. Tarascon, L. H. Greene, P. Barboux, W. R. McKinnon, G. W. Hull, T. P. Orlando, K. A. Delin, S. Foner, and E. J. McNiff, Jr., Phys. Rev. B **36**, 8393 (1987).

[247] P. Mandal, A. Poddar, P. Choudhury, A. N. Das, and B. Ghosh, J. Phys. C **20**, L953 (1987).

[248] Y. Saito, T. Noji, A. Endo, N. Higuchi, K. Fujimoto, T. Oikawa, A. Hattori, and K. Furuse, Jpn. J. Appl. Phys. **26**, L832 (1987).

[249] K. K. Pan, H. Mathias, C. M. Rey, W. G. Moulton, H. K. Ng, L. R. Testardi, and Y. L. Wang, Phys. Lett. A **125**, 147 (1987).

[250] C. W. Kimball, J. L. Matykiewicz, J. Giapintzakis, H. Lee, B. D. Dunlap, M. Slaski, F. Y. Fradin, C. Segre, and J. D. Jorgensen, in *High-Temperature Superconductors*, edited by M. B. Brodsky, R. C. Dynes, K. Kitazawa, and H. L. Tuller, MRS Symposium Proceedings **99** (Materials Research Society, Pittsburgh, 1988), p. 107.

[251] J. M. Tarascon, P. Barboux, P. F. Miceli, L. H. Greene, G. W. Hull, M. Eibschutz, and S. A. Sunshine, Phys. Rev. B **37**, 7458 (1988).

[252] G. Roth, G. Heger, B. Renker, J. Pannetier, V. Caignaert, M. Hervieu, and B. Raveau, Z. Phys. B **71**, 43 (1988).

[253] P. Boolchand, C. Blue, K. Elgaid, I. Zitkovsky, D. McDaniel, W. Huff, B. Goodman, G. Lemon, D. E. Farrell, and B. S. Chandrasekhar, Phys. Rev. B **38**, 11313 (1988).

[254] P. F. Miceli, J. M. Tarascon, L. H. Greene, P. Barboux, F. J. Rotella, and J. D. Jorgensen, Phys. Rev. B **37**, 5932 (1988).

[255] G. Xiao, M. Z. Cieplak, A. Gavrin, F. H. Streitz, A. Bakhshai, and C. L. Chien, Phys. Rev. Lett. **60**, 1446 (1988): G. Xiao, M. Z. Cieplak, D. Musser, A. Gavrin, F. H. Streitz, C. L. Chien, J. J. Rhyne, and J. A. Gotaas, Nature **332**, 238 (1988).

[256] J. Clayhold, S. Hagen, Z. Z. Wang, N. P. Ong, J. M. Tarascon, and P. Barboux, Phys. Rev. B **39**, 777 (1989).

[257] I. Felner, I. Nowik, and Y. Yeshurun, Phys. Rev. B **36**, 3923 (1987); I. Felner and B. Barbara, Phys. Rev. B **37**, 5820 (1988).

[258] S. R. Ovshinsky, R. T. Young, D. D. Allred, G. DeMaggio, and G. A. Van der Leeden, Phys. Rev. Lett. **58**, 2579 (1987).

[259] D. N. Matthews, A. Bailey, R. A. Vaile, G. J. Russell, and K. N. R. Taylor, Nature **328**, 786 (1987).

[260] R. N. Bhargava, S. P. Herko, and W. N. Osborne, Phys. Rev. Lett. **59**, 1468 (1987); and Phys. Rev. Lett. **60**, 1455 (1988).

[261] P. K. Davies, J. A. Stuart, D. White, C. Lee, P. M. Chaikin, M. J. Naughton, R. C. Yu, and R. L. Ehrenkaufer, Solid State Commun. **64**, 1441 (1987).

[262] H. H. Wang, A. M. Kini, H.-C. I. Kao, E. H. Appelman, A. R. Thompson, R. E. Botto, K. D. Carlson, J. M. Williams, M. Y. Chen, J. A. Schlueter, B. D. Gates, S. L. Hallenbeck, and A. M. Despotes, Inorg. Chem. **27**, 8 (1988).

[263] N. P. Bansal, A. L. Sandkuhl, and D. E. Farrell, Appl. Phys. Lett. **52**, 838 (1988).

[264] J. R. LaGraff, E. C. Behrman, J. A. T. Taylor, F. J. Rotella, J. D. Jorgensen, L. Q. Wang, and P. G. Mattocks, Phys. Rev. B **39**, 347 (1989).

[265] P. Haldar, S. Sridhar, A. Roig-Janicki, W. Kennedy, D. H. Wu, C. Zahopoulos, and B. C. Giessen, J. Superconductivity **1**, 211 (1988).

[266] Z. Z. Sheng, A. M. Hermann, D. C. Vier, S. Schultz, S. B. Oseroff, D. J. George, and R. M. Hazen, Phys. Rev. B **38**, 7074 (1988).

[267] M. A. Subramanian, C. C. Torardi, J. Gopalakrishnan, P. L. Gai, J. C. Calabrese, T. R. Askew, R. B. Flippen, and A. W. Sleight, Science **242**, 249 (1988).

[268] R. V. Kasowski, W. Y. Hsu, and F. Herman, Phys. Rev. B **36**, 7248 (1987).

[269] P. A. Sterne and C. S. Wang, Phys. Rev. B **37**, 7472 (1988).

[270] W. M. Temmerman, Z. Szotek, and G. Y. Guo, J. Phys. C **21**, L867 (1988).

[271] W. E. Pickett, Rev. Mod. Phys. **61**, 433 (1989).

[272] B. S. DeWitt, Phys. Rev. **103**, 1565 (1956).

[273] G. L. Toulouse, Solid State Commun. **4**, 593 (1966).

[274] R. E. Allen and M. Menon, Phys. Rev. B **33**, 5611 (1986).

[275] M. Lannoo and P. Lenglart, J. Phys. Chem. Solids **30**, 2409 (1969).

[276] B. A. Richert and R. E. Allen, in *Proceedings of the 18th International Conference on Low Temperature Physics, Part II*, edited by Y. Nagaoka [Jpn. J. Appl. Phys. **26**, Suppl. 26-3, 989 (1987)]; B. A. Richert and R. E. Allen (unpublished).

[277] J. E. Schirber, E. L. Venturini, B. Morosin, J. F. Kwak, D. S. Ginley, and R. J. Baughman, in *High-Temperature Superconductors*, edited by M. B. Brodsky, R. C. Dynes, K. Kitazawa, and H. L. Tuller, MRS Symposium Proceedings **99** (Materials Research Society, Pittsburgh, 1988), p. 479.

[278] J. E. Schirber, B. Morosin, R. M. Merrill, P. F. Hlava, E. L. Venturini, J. F. Kwak, P. J. Nigrey, R. J. Baughman, and D. S. Ginley, Physica C **152**,

121 (1988); J. W. Rogers, Jr., N. D. Shinn, J. E. Schirber, E. L. Venturini, D. S. Ginley, and B. Morosin, Phys. Rev. B **38**, 5021 (1988).

[279] J. D. Jorgensen, B. Dabrowski, S. Pei, D. G. Hinks, L. Soderholm, B. Morosin, J. E. Shirber, E. L. Venturini, and D. S. Ginley, Phys. Rev. B **38**, 11337 (1988).

[280] F. Herman, R. V. Kasowski, and W. Y. Hsu, Phys. Rev. B **36**, 6904 (1987).

[281] R. J. Cava, B. Batlogg, K. M. Rabe, E. A. Rietman, P. K. Gallagher, and L. W. Rupp, Jr., Physica C **156**, 523 (1988).

[282] W. W. Warren, Jr., R. E. Walstedt, G. F. Brennert, R. J. Cava, B. Batlogg, and L. W. Rupp, Phys. Rev. B **39**, 831 (1989).

[283] A. J. Jacobson, J. M. Newsam, D. C. Johnston, D. P. Goshorn, J. T. Lewandowski, and M. S. Alvarez, Phys. Rev. B **39**, 254 (1989).

[284] For reviews of current theories, see T. M. Rice, Z. Phys. B **67**, 141 (1987); P. Fulde, Physica C **153-155**, 1769 (1988); *Novel Superconductivity*, edited by S. A. Wolf and V. Z. Kresin (Plenum, New York, 1987); *Theories of High-Temperature Superconductivity*, edited by J. W. Halley (Addison-Wesley, New York, 1988); *Mechanisms of High-Temperature Superconductivity*, edited by H. Kamimura and A. Oshiyama (Springer-Verlag, Berlin, 1989); *Towards the Theoretical Understanding of High-T_c Superconductors*, edited by S. Lundqvist, E. Tosatti, M. P. Tosi, and Y. Lu (World Scientific, Singapore, 1988); and W. A. Little, Science **242**, 1390 (1988).

[285] W. A. Little, Phys. Rev. **134**, A1416 (1964); D. Davis, H. Gutfreund, and W. A. Little, Phys. Rev. B **13**, 4766 (1976).

[286] V. L. Ginzburg, Usp. Fiz. Nauk **101**, 185 (1970) [Sov. Phys. Usp. **13**, 335 (1970)].

[287] D. Allender, J. Bray, and J. Bardeen, Phys. Rev. B **7**, 1020 (1973); Phys. Rev. B **8**, 4433 (1973).

[288] C. M. Varma, S. Schmitt-Rink, and E. Abrahams, Solid State Commun. **62**, 681 (1987); and in *Novel Superconductivity*, edited by S. A. Wolf and V. Z. Kresin (Plenum, New York, 1987).

[289] F. Marsiglio and J. P. Carbotte, Phys. Rev. B **36**, 3937 (1987); F. Marsiglio, R. Akis, and J. P. Carbotte, Solid State Commun. **64**, 905 (1987); F. Marsiglio and J. P. Carbotte, Phys. Rev. B **39**, 2726 (1989).

[290] W. Y. Ching, Y. Xu, G.-L. Zhao, K. W. Wong, and F. Zandiehnadem, Phys. Rev. Lett. **59**, 1333 (1987); K. W. Wong and W. Y. Ching, Physica C **152**, 397 (1988).

[291] W. Y. Liang, J. Phys. C **20**, L571 (1987).

[292] W. Weber, Z. Phys. B **70**, 323 (1988).

[293] M. Tachiki and S. Takahashi, Phys. Rev. B **38**, 218 (1988).

[294] W. A. Little, J. P. Collman, G. T. Yee, M. J. Holcomb, J. T. McDevitt, and G. E. Brown, J. Am. Chem. Soc. **110**, 1301 (1988).

[295] M. D. Nuñez Regueiro and A. A. Aligia, Phys. Rev. Lett. **61**, 1889 (1988).

[296] Z. Tesanović, A. R. Bishop, and R. L. Martin, Solid State Commun. **68**, 337 (1988).

[297] S. Massidda, N. Hamada, J. Yu, and A. J. Freeman, Physica C **157**, 571 (1989).

[298] C. Kittel, *Introduction to Solid State Physics*, Sixth Edition (Wiley, New York, 1986), p. 315.

[299] J. Fink, presented at the March Meeting of the American Physical Society, St. Louis, 1989 (unpublished).

[300] A. L. Fetter and J. D. Walecka, *Quantum Theory of Many-Particle Systems* (McGraw-Hill, New York, 1971), p. 19.

[301] B. H. Bransden and C. J. Joachain, *Physics of Atoms and Molecules* (Longman, London, 1983), p. 318.

[302] C. Y. Chen, R. J. Birgeneau, D. R. Gabbe, H. P. Jenssen, M. A. Kastner P. J. Picone, and N. W. Preyer, presented at the March Meeting of the American Physical Society, St. Louis, 1989 (unpublished).

[303] J. Bardeen, *Encyclopedia of Physics*, Vol. 15, edited by S. Flügge (Springer-Verlag, Berlin, 1956), p. 352.

[304] V. J. Emery and G. Reiter, Phys. Rev. B **38**, 4547 (1988).

VITA

Brent Armand Richert [redacted] in 1979, and received an appointment to the United States Air Force Academy in Colorado Springs, Colorado. In 1983 he graduated with a B.S. in Physics and Mathematics, and received a commission in the U. S. Air Force. He worked as a research physicist at the Air Force Weapons Laboratory in Albuquerque, New Mexico from 1983 to 1986, modeling several atomic and molecular systems for potential laser applications. He concurrently earned a M.S. in Physics from the University of New Mexico in 1985, with a research project in lattice gauge theory. In 1986 he received a fellowship from the Air Force Institute of Technology, and began his Ph.D. work at Texas A&M University. [redacted]